Interactions between host metabolism, immune regulation, and the gut microbiota in diet-associated obesity and metabolic dysfunction

Andersen, Daniel

Publication date:
2017

Document Version
Publisher's PDF, also known as Version of record

Interactions between host metabolism, immune regulation, and the gut microbiota in diet-associated obesity and metabolic dysfunction

PhD thesis

Daniel Andersen

Submitted: January 4th 2017

DTU Bioengineering
Department of Biotechnology and Biomedicine

Notes to the printed thesis

The results of this thesis were presented for public examination and debate on March 13, 2017 at the Technical University of Denmark.

The evaluation committee consisted of:

- Dr. Maximilian Zeyda, Medical University of Vienna
- Professor Hanne Frøkiær, Dept. of Veterinary Disease Biology, University of Copenhagen
- Associate Professor Katharina Lahl, DTU Vet (chairperson)

Only minor changes were made to the originally submitted thesis before printing.

Preface

This thesis entitled *Interactions between host metabolism, immune regulation, and the gut microbiota in diet-associated obesity and metabolic dysfunction* has been submitted to the PhD school at The Department of Biotechnology and Biomedicine at The Technical University of Denmark in order to obtain the PhD degree.

The work presented in this thesis has been carried out in the labs of Associate Professor Lars Hellgren and Associate Professor Susanne Brix at DTU Bioengineering.

I would like to thank Lasse and Susanne for having me in their labs and providing excellent guidance and interesting discussions during the course of my studies. I also wish to thank past and present members of their labs for providing a nice working environment with a stimulating scientific atmosphere.

During my PhD fellowship, I have participated in successful collaborative projects, resulting in several publications presented in this thesis.
My PhD fellowship is part of the Gut, Grain and Greens Centre (3G) supported by the Innovation Fund Denmark, and I have therefore been part of a close collaboration with Professor Tine Rask Licht and Li Zhang at DTU Food, which I have really enjoyed. I would like to thank Li and Tine for their great contribution.
Furthermore, I wish to thank Niels Banhos Danneskiold-Samsøe from Karsten Kristiansen's lab at the Department of Biology, University of Copenhagen for his tireless efforts and scientific eagerness.

Also, I would like to thank all past and present members of the Systems Metabolic Lipidology and Disease Systems Immunology groups at DTU.

Finally, I wish to thank my family for all their support, which was highly needed when handing in two PhD's while having two little kids.

Daniel Andersen
M.Sc. Molecular Biomedicine
January 4th 2017

Table of contents

Summary

The increase in the prevalence of obesity and obesity-associated complications such as the metabolic syndrome is becoming a global challenge. Dietary habits and nutrient consumption modulates host homeostasis, which manifests in various diet-induced complications marked by changes in host metabolism and immune regulation, which are intricately linked. In addition, diet effectively shapes the gut microbiota composition and activity, which in turn interacts with the host to modulate host metabolism and immune regulation.

In the three studies included in this PhD thesis, we have explored the impact of specific dietary components on host metabolic function, immune regulation and gut microbiota composition and activity.

In the first study, we have characterized the effect of a combined high-fat and gliadin-rich diet, since dietary gliadin has been reported to be associated with intestinal inflammation and permeability. The combination of gliadin with an obesogenic diet allowed us to investigate the long-term effects of a single dietary component on host function of obese mice, resulting in identification of notable changes in host metabolic and immune function, as well as in the gut microbiota composition.

In the second study, the effect of a safflower-based high-fat diet on host homeostasis is evaluated, and we show that intake of this *n*-6 polyunsaturated fatty acid-rich diet exerts only minor host metabolic and inflammatory changes even after 40 weeks intake. Although potentially pro-inflammatory *n*-6 polyunsaturated fatty acids are effectively contributing to the liver phospholipids and glucose intolerance manifested after 5 weeks intake, body weight gain, insulin resistance and adipose tissue inflammation are delayed and detectable only after 40 weeks feeding.

In the last study, we evaluated the effect of short-term fasting of obese mice. By applying a co-abundance cluster analysis that identifies fasting-induced changes in urine metabolites, gut microbiome and liver lipid composition; we identified defining factors that integrate with the host response to propagate a fasting-induced metabolic shift.

The use of multivariate analyses allows for a better understanding of the interplay between diet, host metabolic regulation, immune function and gut microbiota composition and activity. These studies indicate new directions in which to focus further studies to increase our knowledge of host-diet-microbiome interactions.

Resumé på dansk

Den stigende forekomst af fedme og fedme-relaterede sygdomme såsom det metaboliske syndrom er et globalt problem. Ændrede kostvaner har stor indflydelse på kroppens homeostase og er ophav til forskellige kostrelaterede komplikationer, og påvirker både stofskiftet og immunregulering. Endvidere har kostens sammensætning stor betydning for tarmfloraens sammensætning og funktion, hvilket igen har indflydelse på både stofskifte og immunregulering.

De tre studier, som præsenteres i denne PhD-afhandling fokuserer alle på at forstå effekten af specifikke komponenter i kosten på kroppens stofskifte, immunregulering og tarmfloraens sammensætning og funktion.

I det første studie har vi karakteriseret effekten af en kombineret høj-fedt og gliadin-rig diæt, da gliadin gennem kosten er blevet sat i sammenhæng med tarminflammation og øget tarm-permeabilitet. Kombinationen af gliadin med en fedme-fremmende diæt muliggjorde en længerevarende undersøgelse af en enkel kostkomponents indflydelse på fede mus, og vi identificerede klare ændringer i både stofskifte, immunregulering og tarmfloraens sammensætning.

I det andet studie undersøgte vi effekten af en tidselolie-baseret høj-fedt diæt på musenes homeostase. Her fandt vi, at indtaget af denne type høj-fedt diæt kun fører til små ændringer i musenes stofskifte og inflammation. På trods af effektivt bidrag af de potentielt pro-inflammatoriske n-6 flerumættede fedtsyrer til leverens fosfolipid-sammensætning og tidligt forekommende glukose-intolerance allerede efter 5 uger, optræder vægtøgning, insulinresistens of fedtvævsinflammation først sent efter 40 uger.

I det sidste forsøg evaluerede vi effekten af faste på mus fodret med høj-fedt-diæt. Ved hjælp af omfattende bioinformatisk analyse af faste-inducerede ændringer i urin-metabolitter, tarmfloraen og leverens lipidsammensætning. Gennem disse analyser har vi fundet frem til faktorer med vigtige funktioner i samspillet mellem kroppens reaktioner på faste-inducerede stofskifteændringer.

Brugen af multivariate analyser muliggør en bedre forståelse af den komplekse sammenhæng mellem kost, stofskifte, immunregulering samt sammensætning og aktivitet af tarmfloraen. Med disse studier har vi fundet vigtig ny viden og indikationer af nye retninger for fremtidige studier, som kan øge vores forståelse af det komplekse forhold mellem krop, kost og tarmflora.

Outline of thesis

In this thesis I will present the main findings of my PhD project, which has centered on furthering our understanding of the complex interplay between host metabolism, immune regulation and the gut microbiota through dietary intervention studies in mice.

I will start by giving an introduction to relevant topics, namely diet-dependent regulation of host metabolism, mainly focusing on the relationship between high fat diet-induced obesity and its major complication, the establishment of the metabolic syndrome. Then, since a substantial part of my focus has been on the immunological aspects of metabolic disease, I will attempt to thoroughly describe the current, and drastically increasing, knowledge on the role of the immune system in metabolic disease, and, finally, focus on the relation between three factors that are shaped by diet; host metabolism, immune response and gut microbiota, and their possible interplay.

My studies focus on host metabolism, immune response and gut microbiota composition after intake of gliadin in combination with a high fat diet (Project I, “Gliadin Study”), and after long-term intake of a safflower oil-based high fat diet (Project II, “Safflower Study”). The “Gliadin Study” generated data on metabolic regulation and gut microbiota composition in two different feeding states, fed and fasted. As the fasted mice were intended for a gut permeability assay that did not succeed, fasted mice were excluded from the final manuscript. While the data from high-fat diet fed mice were used to characterize the effect of the feeding state on metabolic and inflammatory regulation, gut microbiome composition and the urine metabolome, the fasted mice were used for in-depth, multivariate analyses of the host response to short-term fasting (Project III, “Fasting study”).

The data obtained from these studies are presented in three manuscripts (listed below), followed by a brief collective discussion.

- Manuscript I: Effects of Gliadin consumption on the Intestinal Microbiota and Metabolic Homeostasis in Mice Fed a High-fat Diet

- Manuscript II: A safflower oil-based high fat/high-sucrose diet modulates the gut microbiota and liver phospholipid profiles associated with early glucose intolerance in the absence of tissue inflammation

- Manuscript III: Systems level analysis connects intestinal *Porphyromonadaceae*, *Il33* and butyric acid to *Ucp1* induction in visceral adipose tissue during short-term fasting

Abbreviations

AA	Arachidonic acid
ACC	Acetyl CoA-carboxylase
BCFA	Branched-chain fatty acid
BMI	Body mass index
cDC	Conventional dendritic cell
CYP7a1	Cholesterol 7α-hydroxylase
DAG	Diacyl glycerol
DAMP	Danger-associated molecular patterns
DC	Dendritic cell
DHA	Docosahexaenoic acid
EPA	Eicosapentaenoic acid
FXR	Farnesoid X receptor
γδ T cells	Gamma-delta T cells
GLP-1	Glucagon-like peptide-1
GPCR	G-protein coupled receptor
HDL	High-density lipoproteins
HFD	High-fat diet
IFNγ	Interferon γ
IGN	Intestinal gluconeogenesis
IL	Interleukin
ILC	Innate lymphoid cell
iNOS	Inducible nitric oxide synthase
IRS1	Insulin receptor substrate 1
LBP	LPS-binding protein
LFD	Low fat diet
LPL	Lipoprotein lipase
LPS	Lipopolysaccharide
MCP1	Macrophage chemoattractant protein 1
MD-2	Myeloid differentiation protein 2
moDC	Monocyte-derived dendritic cell
MyD88	Myeloid differentiation primary response gene 88
NAFLD	Non-alcoholic fatty liver disease
NASH	Non-alcoholic steatohepatitis
NK	Natural killer
NLR	NOD-like receptor
NLRP	NOD-like receptor pyrin-domain containing
NOD	Non-obese diabetic

PAMP	Pathogen-associated molecular patterns
PCA	Principal component analysis
PCoA	Principal coordinate analysis
pDC	Plasmacytoid dendritic cells
PKC	Protein kinase C
PPAR	Peroxisome proliferator-activated receptor
PRR	Pattern recognition receptor
PUFA	Poly-unsaturated fatty acids
ROS	Reactive oxygen species
SCFA	Short chain fatty acid
SNP	Single nucleotide polymorphism
SREBP-1c	Sterol regulatory element-binding protein 1
STAT	Signal transducer and activator of transcription
TGFβ	Transforming growth factor β
TLR	Toll-like receptor
TNFα	Tumor necrosis factor α
TRIF	TIR-domain-containing adapter-inducing interferon-β

Introduction

Morbidity and mortality associated with changes in lifestyle are increasing worldwide. Multiple factors, including labor type and intensity, stress, exercise, substance abuse, are thought to be involved in the establishment of lifestyle-related imbalances. Along with the increasing industrialization, urbanization and economic growth, diet has become a major factor involved in the progression of lifestyle diseases. In 1990 and 2010, dietary composition was the most significant risk factor associated with death and disability-adjusted life years, and poor diet was the cause of 678,000 premature deaths in the US in 2010 (Murray et al., 2013). Importantly, the rise in diet-associated deaths is not limited to industrialized countries, but has proven to be an increasing concern in low and middle income countries as well (Popkin et al., 2012).

Diet, obesity and the metabolic syndrome

From a health perspective, diet-related disease has traditionally been associated with under- and malnutrition. However, the lifestyle transformation associated with the massive urbanization and economic growth in the western hemisphere throughout the 20th century has led to a remarkable increase in the incidence of obesity and obesity-associated illnesses, most notably the metabolic syndrome. Over the past few decades, obesity has gone from being a largely North American phenomenon to a global health concern of pandemic proportions. Obesity, defined as Body Mass Index (BMI) above 30, has increased from an initial prevalence in the US of 13.4 % in 1960-1962 to 37.7 % in 2013-2014 (Flegal et al., 2016). Similarly, the metabolic syndrome was at a prevalence of 34.7 % in the US in 2011-2012, and had increased independently of ethnicity and sex since 2003-2004.

While a large part of the increase in the incidence of the metabolic syndrome can be attributed to the rise in obesity, not all cases can be explained simply in terms of visceral adiposity, as metabolically benign obesity has been reported (Stefan et al., 2008). Importantly, metabolic dysfunction has been observed among normal weight individuals (St-Onge et al., 2004), and metabolically healthy and unhealthy obese individuals have different adipose tissue, muscle and liver transcriptomes (Kogelman et al., 2016), thus further complicating the pathophysiology of this syndrome.

Although the diagnostic criteria for the definition of the metabolic syndrome are rather inconsistent throughout the literature, common features usually include high triglyceride levels, low high-density lipoprotein (HDL) levels, elevated arterial blood pressure, high fasting plasma glucose, and usually a measure of obesity (such as BMI or waist circumference). The presence of one or more of these factors increases the risk of cardiovascular diseases and type 2 diabetes. Additionally, several other factors are expected to be equally important for the development of metabolic dysfunction, such as chronic inflammation, atherosclerotic vascular diseases and non-alcoholic fatty liver disease (NAFLD)

(Kassi et al., 2011; Popkin, 2006). As these definitions tend to be rather rigid, they do not take into account the differences in genetic variation and lifestyle between populations.

Factors contributing to obesity and development of the metabolic syndrome

Several factors are thought to contribute to the global rise in the prevalence of disorders related to the metabolic syndrome. This includes *in utero* programming, genetic background, physical activity and diet composition. However, the rise in obesity is mainly thought to be caused by two factors – a sedentary lifestyle and altered dietary composition resulting in excess caloric intake. Certain new trends such as the addition of caloric sweeteners, increased vegetable oil and animal-source food intake, and reduced vegetable intake are all involved in the massive increase in obesity prevalence (Kassi et al., 2011; Popkin, 2006).

The metabolic syndrome, glucose regulation and diabetes

The metabolic syndrome constitutes a cluster of metabolic abnormalities with obesity, hyperglycemia, hyperlipidemia and hypertension being fundamental for the diagnosis and pathogenesis of this disease. The initial term “Insulin resistance syndrome” (or “Syndrome X”) emphasizes the importance of glycemic control for the maintenance of metabolic health. Since insulin resistant individuals are at increased risk of developing any of the diagnostic criteria for the metabolic syndrome, insulin resistance is a major driver of diabetes symptoms (Guo, 2014; Moller and Kaufman, 2005). Insulin is the primary regulator of glucose levels, and insulin has numerous effects on metabolism. Primarily, insulin stimulates glucose uptake in skeletal muscle, adipose tissues and liver, while inhibiting hepatic gluconeogenesis. Secondly, insulin induces lipogenesis, glycogen and protein synthesis, while inhibiting fatty acid oxidation, and glycogen and protein breakdown (Saltiel and Kahn, 2001).

Obesity is not harmful *per se* (Kloting et al., 2010), but rather represents a biological means to overcome periods of limited nutrient availability (Soeters and Soeters, 2012). However, central obesity predisposes to conditions such as insulin resistance, i.e. the inability of the secreted insulin to stimulate glucose uptake as expected, which may progress to type 2 diabetes (Kahn et al., 2006), and result in typical diabetes-related complications, including neuropathy, nephropathy, eye damage, and cardiovascular complications (Forbes and Cooper, 2013).

While an initial pre-diabetic state, marked by a compensatory increase in pancreatic islet release of insulin, has been observed, impaired glucose uptake results in hyperglycemia and glucose intolerance. If persistent, this may progress to β-cell dysfunction, a hallmark of type 2 diabetes, which manifests itself as reduced insulin release from β-cells, possibly due to loss of β-cell mass (Kahn, 2001). Furthermore, elevated glucose levels promote β-cell failure and lowers insulin sensitivity, thus creating a vicious cycle of events culminating in overt glucose dysregulation.

The global disease burden of diabetes is massive and ever expanding. In 2010, the global prevalence of diabetes was at 6.4 %, affecting 285 million, and is expected to have increased by over 50 % in 2030 with the greatest rise expected in developing countries (Shaw et al., 2010).

Thus, maintaining normoglycemic levels is instrumental for metabolic health. Although the etiology of insulin resistance is complex and multifactorial, three major aspects are believed to affect insulin sensitivity; dietary excess leading to chronic tissue inflammation, dyslipidemia, and a dysregulated intestinal microbiota (Johnson and Olefsky, 2013).

Dyslipidemia in metabolic disease

The insulin resistant state is linked with an increased flux of free fatty acids associated with dyslipidemia, marked by high levels of serum triglycerides, low levels of high density lipoprotein and high levels of small, dense lipoprotein particles. Numerous studies in rodents and humans on the metabolic impact of HFD-induced obesity have been performed. Several aspects are involved in shaping the circulating and tissue lipid profile, such as the dietary fatty acid composition (Ferramosca and Zara, 2014), insulin sensitivity of the host, mitochondrial function (Serviddio et al., 2008), channeling of fatty acids from adipose tissues, and even the gut microbiota composition (Caesar et al., 2016; Velagapudi et al., 2010).

A fundamental aspect of obesity and lipid deposition is the observation that lipid storage outside of the adipose tissues imposes several metabolic complications. This concept, termed *the adipose tissue expandability hypothesis* (Virtue and Vidal-Puig, 2010), argues that adipose tissue depots are instrumental in the regulation of whole-body metabolic health, since the inability of adipose tissues to expand (due to impaired hypertrophy and/or hyperplasia), results in ectopic lipid deposition and several subsequent complications, such as impaired insulin signaling in afflicted organs (Lee et al., 1994; Virtue and Vidal-Puig, 2010). Indeed, a recent large study of the genetic basis for insulin resistance in a human cohort, revealed that insulin resistance is associated with limited peripheral adipose tissue storage capacity mainly due to single nucleotide polymorphisms (SNPs) in five genes expressed in adipocytes (Lotta et al., 2016).

Several aspects of the dyslipidemic state contribute to metabolic disease and the related inflammatory imbalances owing to the dual potential of many lipid species functioning as metabolic substrates as well as signaling molecules. In this respect the development of NAFLD, and its strong association with insulin resistance, is of particular importance, partly due to the fact that the liver receives host, diet and microbial metabolites via the portal vein from gut and mesenteric adipose tissues, and partly due to the key role of the liver in the regulation of glucose and lipid homeostasis (Kirpich et al., 2015).

Role of individual fatty acids

The lipotoxic potential, and, more specifically, the role of fatty acids in the shaping of the immune and metabolic host response in various organs, is, however, not entirely understood. Historically, the changes in dietary patterns from a hunter-gatherer culture to a post-industrialization type diet are manifested in a dramatic increase in the omega-6 to omega-3 ratio (Simopoulos, 2002). In the twentieth century, the even more dramatic rise in n-6 poly-unsaturated fatty acid (PUFA) consumption is mainly due to increased focus on saturated fats and the idea that a switch to n-6 PUFAs would reduce the prevalence of cardiovascular disease.

Despite the fact that all aspects of the contribution of dietary fatty acids to host metabolism and inflammation are not entirely understood, different dietary lipids exert various metabolic and immunemodulatory functions.

Firstly, this includes the direct action of dietary lipids on host cells and tissues, and, secondly, the action of the derivatives of dietary fatty acids (such as eicosanoids) on the modulation of inflammation (Hubler and Kennedy, 2016). This is illustrated by the putative pro-inflammatory potential of saturated fatty acids via their engagement of Toll-like receptor (TLR) signaling mechanisms although highly debated, and their role as precursors for DAG and ceramides. Also, the putative anti- and pro-inflammatory effects of omega-3 and omega-6 PUFAs, respectively, and their derivatives, such as arachidonic acid (AA) formation from omega-6 and docosahexaenoic acid (DHA) and eicosapentaenoic acid (EPA) from omega-3 PUFAs, should be considered. This includes the induction of IL-1β, IL-6 and TNFα production by n-6 PUFA arachidonic acid via cyclooxygenase activation in adipose tissue macrophages, consequently contributing to adipose tissue inflammation (Kim et al., 2013). Conversely, n-3 PUFA intake has been associated with cytokines changes in adipose tissues such as higher IL-10, and lower MCP-1 and IL-6 (Martinez-Fernandez et al., 2015). Similarly, an n-3 rich diet favours M2 polarization of adipose tissue macrophages (Oh et al., 2010), and the n-3 PUFAs EPA and DHA serve as substrates for the synthesis of proresolving lipid mediators (named resolvins, protectins and maresins) (Serhan, 2014). In addition, the putative role of specific PUFAs on cellular metabolic homeostasis, such as n-3 PUFA-related effects on adipogenesis, lipogenesis, insulin signalling and adipokine expression, constitutes important aspects of dietary PUFA intake (Martinez-Fernandez et al., 2015). Yet, the role of dietary n-3 PUFAs in body weight regulation is disputed, as contradictory results in this regard have been reported (Kim et al., 2013). Furthermore, n-6 and n-3 PUFAs are thought to serve as substrates for endocannabinoids, with the former contributing negatively and the latter positively to the optimization of endocannabinoid tone, involved in appetite control, inflammation, lipid synthesis, adiponectin regulation, and, potentially, intestinal integrity (Cani et al., 2016; Kim et al., 2013).

Important for the development of insulin resistance, certain fatty acid compounds act not only as intermediates in lipogenesis, but also function as intracellular signaling molecules. This includes diacylglycerol (DAG) and ceramides (Jornayvaz and Shulman, 2012; Samuel and Shulman, 2012).

DAG, besides from being a substrate for triglyceride synthesis, is a potent activator of the novel Protein kinase C (PKC) family, thus impairing insulin receptor signaling and, consequently, glucose uptake, while stimulating hepatic gluconeogenesis (Perry et al., 2014). Still, the impaired insulin receptor signaling does not limit hepatic lipogenesis, since signaling via the hepatic, lipogenic master regulator Sterol regulatory element-binding protein 1 (SREBP-1c) remains functional, thus inducing the transcription of genes required for fatty acid synthesis, such as Acetyl CoA-carboxylase (ACC) and Fatty acid synthase (FAS) (Brown and Goldstein, 2008). Interestingly, lipid droplet-associated DAG is not associated with insulin resistance, thus the compartmentalization of DAG (and other fatty acids) is of importance in the development of liver insulin resistance (Perry et al., 2014). Nonetheless, lipid mediators such as DAG and ceramide could be causative agents in the progression from uncomplicated NAFLD to the more severe inflammatory liver disease, non-alcoholic steatohepatitis (NASH) (Tilg and Moschen, 2010).

Taken together, this emphasizes the role of lipid mediators in glucose and lipid metabolism, yet other factors are linked with lipid imbalances, namely pancreatic, hepatic and adipose tissue endoplasmic reticulum stress, liver and adipose inflammation, and inflammatory mediators from the gut and adipose tissues (Hotamisligil, 2010).

The immune system and its modulation of host metabolism

Metabolic regulation and the immune system were largely considered independent entities for a long time, but increasing amounts of data show that these two systems are inextricably linked and that inflammatory and metabolic regulation hinge on complex immune and non-immune crosstalk. This is manifested in the adipose tissues and the liver, where complex inflammatory responses modulate metabolic function.

Adipose tissue inflammation

The various adipose tissue depots were largely considered passive storage sites until the establishment of a sub-clinical pro-inflammatory response marked by TNFα overexpression in the adipose tissue of obese mice (Hotamisligil et al., 1993). Its subsequent effects on insulin signaling (Hotamisligil et al., 1996) was essential for the now well-established idea that the immune and metabolic axes are strongly linked.

The occurrence of insulin resistance is mainly attributed to a T_h1/T_h17-directed pro-inflammatory phenotype defined by M1 macrophages, mast cells, neutrophils and T_h1 and CD8+ T cells and B cells (Fig. 1). Similarly, maintenance of the insulin sensitive state relies, at least in part, on a type 2 or regulatory phenotype, illustrated by the presence of eosinophils, type 2 innate lymphoid cells, iNKT cells, and T_{reg} and T_h2 cells in the lean state (Odegaard and Chawla, 2013b). Hence, the inflammatory tone of metabolic organs, such as adipose tissues, the liver, pancreas or skeletal muscle, is equally important to the metabolic outcome.

Macrophages

Initially, inflammation-induced metabolic dysfunction following excess nutrient intake was described as an immunological hyper-response owing to adipose tissue macrophages (Weisberg et al., 2003; Xu et al., 2003). The detrimental effects of adipose tissue macrophages were exemplified by the increase in M1-polarized macrophages overexpressing inducible nitric oxide synthase (iNOS), TNFα and IL-6 (Lumeng et al., 2007a), thereby inhibiting insulin receptor substrate 1 (IRS-1) phosphorylation and thus insulin signalling (Odegaard and Chawla, 2013b), while also resulting in a subsequent macrophage chemoattractant protein 1 (MCP1)-dependent chemo-attraction of $Ly6C^{hi}$ $CCR2^{hi}$ monocytes (Kamei et al., 2006; Takahashi et al., 2003; Weisberg et al., 2006).

Similar to observations from brain, spleen, skin and pancreas, macrophages of adipose tissues derive from two different embryonic lineages. Adipose tissues are dominated by the presence of yolk sac-derived mononuclear phagocytes with a considerable self-renewal potential (Italiani and Boraschi, 2014). In response to chemotactic factors, mainly MCP1 (Gordon and Taylor, 2005), monocytes of various maturation and/or differentiation states (exemplified by differences in Ly6C expression and half-life) are able to infiltrate and undergo tissue-specific differentiation, thus contributing to the pool of bone marrow-derived mononuclear phagocytes (Sunderkötter et al., 2004). Tissue-resident, yolk sac-derived macrophages (generally characterized by higher expression levels of F4/80), are

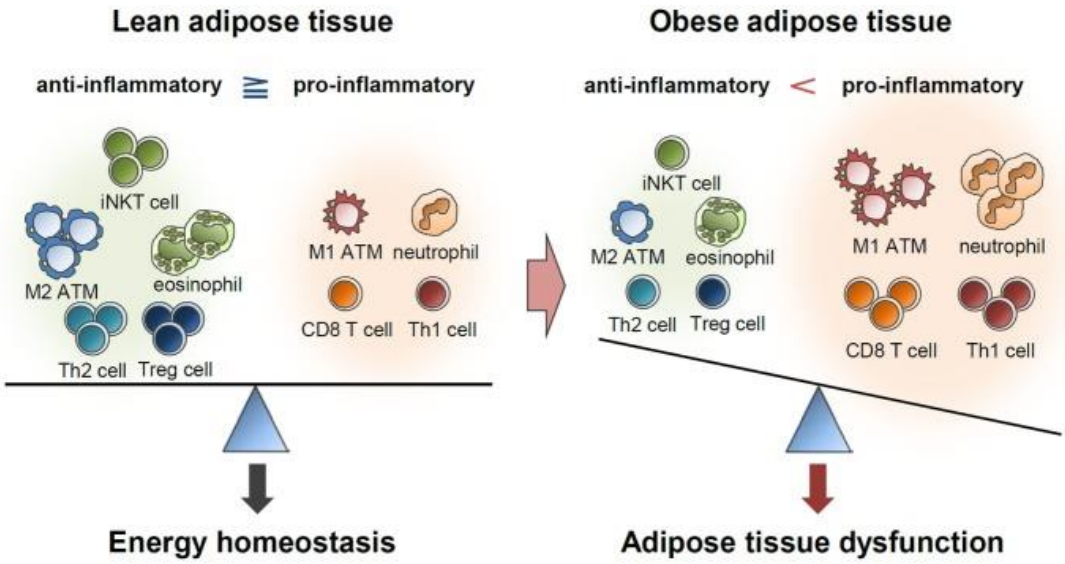

Fig. 1
Adipose tissue immune cell infiltration (Choe et al., 2016)

considered a homeostatic subset able to initiate inflammation, and in addition adipose tissue macrophages contribute to metabolism, adipogenesis and thermogenesis. While the mononuclear phagocytes deriving from infiltrating monocytes are of a more potent inflammatory type responding to cues of tissue inflammation, they may adopt both M1 and M2-like phenotypes in the tissues, likely depending on inflammatory and anti-apoptotic signals (eg. CX3CL1) (Italiani and Boraschi, 2014).

Macrophages in the visceral adipose tissues are abundant even in the lean, insulin sensitive state (10 %) but may account for up to 60 % of total adipose tissue cells (Chawla et al., 2011). The skewing of macrophages towards a pro-inflammatory M1-like phenotype is associated with increased reorganization of macrophages around so-called crown-like structures formed by necrotic adipocytes, rather than a more even distribution in the lean state (Ferrante, 2013). Lipid-engulfing macrophages switch their metabolic regulation (but not necessarily their inflammatory potential (Xu et al., 2013)),increase their expression of genes encoding proteins involved in lipid and cholesterol metabolism (Lumeng et al., 2007b), expand in size and increase their expression of the integrin CD11c, a common marker to identify M1-like macrophages in adipose tissue (Lumeng et al., 2007a). Similarly, M2-like macrophages, making up an anti-inflammatory macrophage subset of little uniformity, also increase in concentration of expanding adipose tissue. These macrophages of an M2-like state are characterized by increased expression of Arg-1, transforming growth factor β (TGFβ) and IL-10 in addition to proteins favoring angiogenesis, adipose tissue remodeling and resolution of inflammation (Shaul et al., 2010). However, macrophages are highly heterogeneous and display some degree of plasticity (Xue et al., 2014).

Notably, in regards to the polarization of macrophages, a metabolic dichotomy exists between macrophage subsets. Classically activated macrophages, typically M1-skewed macrophages, engage in aerobic glycolysis, whereas the alternatively activated macrophages, often adopting a more M2-like phenotype, rely on oxidative metabolism (Ganeshan and Chawla, 2014). The increased aerobic glycolysis permits the increased production of the microbicidal reactive oxygen species (ROS) such as nitric oxide (NO), whereas expression of proteins involved in fatty acid oxidation is observed among alternatively activated macrophages (Castoldi et al., 2015). While it seems that adipocytes actively promote the M2-phenotype via PPARδ activation by Th2 type cytokines (Kang et al., 2008), the exact mechanisms responsible for the positive impact of alternatively activated macrophages on metabolism is still not entirely defined, but iron-storage capacity of some subsets, increased lipolysis and browning of adipose tissue via production of catecholamines have been proposed, in addition to the inherent benefits of not being skewed towards a pro-inflammatory macrophage phenotype (Brestoff and Artis, 2015).

Whereas the importance of adipose tissue macrophages is evident for the inflammatory response to diet-induced obesity, several other immune cells mediate the pro-inflammatory signaling that converges to affect metabolic regulation.

Neutrophils

Only three days after high fat diet intake, neutrophils accumulate in visceral adipose tissues (Elgazar-Carmon et al., 2008; Talukdar et al., 2012), thus resembling the acute phase immune response to trauma. Although the cues leading to this rapid neutrophilic accumulation in adipose tissues have still not been identified, the effect of neutrophil accumulation in adipose tissue and liver is evident. Neutrophils secrete large amounts of the protease elastase, and treatment of hepatocytes with

elastase increases cellular insulin resistance, while deletion of the elastase gene from neutrophils improves glucose tolerance and insulin resistance and inhibits neutrophil and macrophage accumulation in adipose tissues (Talukdar et al., 2012). Also, deletion of myeloperoxidase of neutrophils inhibits HFD-induced insulin resistance and macrophage infiltration in epididymal adipose tissue (Wang et al., 2014a), thus further implicating neutrophils in the sequence of events leading to HFD-associated adipose tissue inflammation.

Mast cells

Mast cells, potent hyper-secretory granulocytes mainly characterized in relation to their roles in allergic and auto-immune diseases (Wernersson and Pejler, 2014), are also reported to be present in visceral adipose tissue and negatively impact glucose homeostasis and body weight. Adipose tissue from obese mice and humans contain a higher concentration of mast cells compared to lean counterparts and higher levels of mast cell-derived IFNγ, IL-6, chemokines and cysteine proteases, while mast cell deficiency reduces obesity adipose tissue mass (Liu et al., 2009). Mast cells are abundant in subcutaneous adipose tissue, but only increase in visceral adipose depots in response to HFD (Altintas et al., 2011). In addition, mast cell deficiency results in the higher expression of preadipocyte marker genes (Ishijima et al., 2013), while maturation of mast cells in adipose depots induces mast cell protease 5 expression, which likely acts to stimulate collagen deposition and thus reduce preadipocyte differentiation (Hirai et al., 2014).

Eosinophils

While neutrophils and mast cells are recruited to expanding adipose tissue, eosinophils are adipose tissue-harboring cells in the lean state. Unlike neutrophils and mast cells, eosinophils are protective of insulin signaling, an effect mainly due to their potent secretion of IL-4. In the lean state, eosinophils have been shown to contribute with 90 % of all IL-4 in the perigonadal adipose tissue, and, interestingly, high eosinophil concentration in adipose tissue is associated with lower adiposity and glucose regulation. Furthermore, the same study found eosinophil numbers to sustain the presence of Arg-1^+ alternatively activated macrophages (Wu et al., 2011a). The alternative activation state of macrophages is likely involved in the beneficial effects on glucose metabolism, which is maintained by signal transducer and activator of transcription 6 (STAT6) induction by IL-4 or IL-13 (Brestoff and Artis, 2015; Odegaard and Chawla, 2013a). The exact mechanisms that are involved in the lowering of eosinophil concentrations with increased adiposity are yet to be identified, however their dependency on IL-5 suggests that this may be a causative agent in their disappearance (Brestoff and Artis, 2015).

Dendritic cells

In addition to macrophages, another type of innate antigen presenting cell, the dendritic cell (DC), is implicated in the obesity-associated immune response. Dendritic cells show high diversity, but are broadly divided into plasmacytoid dendritic cells (pDCs) involved in antiviral immunity, and the highly heterogeneous group of conventional dendritic cells (cDCs), and monocyte-derived dendritic cells

(moDCs), the latter much resembling cDCs after differentiation in the tissues towards a DC phenotype. The cDCs are mainly characterized by surface markers such as CD8α, CD11b and CD103, where CD8α+ DCs are restricted to lymphoid organs (Mildner and Jung, 2014; Satpathy et al., 2012).

Although distinction between macrophages and dendritic cells is difficult due to overlapping surface molecule expression (Hashimoto et al., 2011), depletion of CD11c+ cells, thus mainly DCs and macrophages, results in a remarkable improvement in glucose homeostasis, inflammation and body weight (Patsouris et al., 2008). Several observations indicate that DCs are part of balancing the immune response in adipose tissue. One study found that CD11c+ F4/80^{lo} cells induce a switch from an initial IFNγ expressing T_h1 to an IL-17 expressing T_h17 response after HFD feeding (Bertola et al., 2012), while another found that DCs are necessary for the accumulation of the heterogeneous triple positive CD11b$^+$ CD11c$^+$ F4/80$^+$ population, likely mainly M1 type macrophages (Stefanovic-Racic et al., 2012). In support of adipose tissue DCs inducing a T_h17 response in the setting of obesity and/or HFD intake, another study found that adipose tissue DCs express higher levels of IL-6, TGFβ and IL-23 and induce higher IL-17 in CD4+ T cells than the LFD (Chen et al., 2014).

T cells

The adipose tissue inflammation induced by diet-induced obesity is not just limited to innate immunity, but is also manifested in a local adaptive response, likely mediated by antigen presenting cells such as DCs presenting obesity-associated antigens to T cells.

In support of this, CD4+ and CD8+ T cells accumulate in epididymal and inguinal adipose tissue after HFD feeding of mice and F4/80+ macrophages present antigen to CD4+ T cells in an MHC II dependent manner *in vitro* and *in vivo*, and CD4+ adipose T cells are able to proliferate following antigenic stimulation (Morris et al., 2013). HFD fed mice increase the total concentration of subcutaneous and visceral CD4+ T cells, which express high amounts of IFNγ, and CD4+ lymphocyte replenishment to RAG1 deficient mice ameliorated the glucose homeostasis of HFD fed mice (Winer et al., 2009). Moreover, the deletion of *stat-6* increased fasting glucose and insulin levels and body weight, indicative of a protective role of T_h2 cells .In addition, following HFD feeding CD8+ T cells accumulate (after 6 weeks) prior to macrophages (after 8 weeks), while the concentration of CD4+ T cells decrease from 10 weeks and onwards, altogether suggesting that CD8+ T cells are involved in the accumulation of macrophages in adipose tissue, while a CD4+ T cell-dependent adaptive response is beneficial for metabolic regulation (Nishimura et al., 2009).

Importantly, the timing of immune cell infiltration seems very context dependent. One study found T cells to accumulate more abundantly than the LFD control after 4 weeks of HFD – two weeks later than macrophages (Winer et al., 2011). In contrast, another study found that CD8+ T cells were not present at a higher concentration than the LFD control until after 22 weeks of HFD, even though CD11c+ macrophages were more abundant after 8 weeks (Strissel et al., 2010).

Regulatory T (T_{reg}) cells also play a significant role in controlling adipose tissue inflammation. T_{reg} cells represent a remarkably high fraction of CD4+ T cells in abdominal adipose tissue at 40-50 % in the lean state. However, leptin deficient *ob*/*ob* mice have reduced abundance of FoxP3+ T_{reg} cells and, similarly, HFD fed mice have a lower fraction of FoxP3+ CD4+ T cells than normal chow fed mice in abdominal adipose tissue (Feuerer et al., 2009). The exact role of adipose tissue T_{reg} cells still needs to be elucidated, but it seems that adipose tissue T_{reg} cells are dependent on IL-33 signaling (Kolodin et al., 2015), thus implicating them in the IL-33-dependent ILC2-eosinophil-macrophage signaling axis (Brestoff and Artis, 2015).

B cells

In addition to T cells, immune signalling also involves B cells of adipose tissues, which have been reported to accumulate after 2 weeks of HFD. Although this aspect of metabolic immunity is less well-characterized, it seems that B cells contribute negatively to the overall metabolic homeostasis, since B cell depletion attenuates glucose dysregulation, while B cell transfer induces insulin resistance and glucose intolerance. These B cells produce IgG that skews macrophages toward TNFα production *in vitro* (Winer et al., 2011). Moreover, B cell depletion induces higher T_{reg} cell concentration, and hence B cells seem to negatively affect T cells (DeFuria et al., 2013).

Innate-type lymphocytes

In addition to immune cell types which have been more conventionally assigned to either the innate or adaptive arm of immunity, several data exists on cells that are more loosely defined in this respect. This includes various subsets of the lymphocytes γδ T, natural killer T (NKT) and NK cells.

NKT cells are typically classified as either invariant NKT (iNKT) or type 2 NKT and both generally recognize glycolipid antigens presented by CD1d. However, a wealth of contradicting results exists on the role of NKT cells in adipose tissue inflammation in diet-induced obesity (Mathis, 2013). Transfer of both iNKT and type 2 cells induces weight loss and glucose normalization (Hams et al., 2013), iNKT cells have been shown to induce inflammation and glucose dysregulation (Ohmura et al., 2010), and, in contrast, the type 2 NKT subset was found to contribute to insulin resistance (Satoh et al., 2012), and in another study IL-4 was increased following only four days of HFD feeding, which was attributed to NKT cells, since CD1d knock-out abolished the effect (Ji et al., 2012). Also, iNKT cells have been shown to display a mixed phenotype following activation by α-galcer, increasing IL-4, IL-13 and IFNγ, an effect that was increased following coculture with adipocytes, suggestive of adipocyte presentation of lipid antigens to iNKT cells (Schipper et al., 2012). The most compelling finding was that iNKT cells are reduced during the progression of obesity, express IL-4, IL-10 and IFNγ upon α-galcer stimulation and that restoration of iNKT levels rescues the glucose metabolism (Lynch et al., 2012).

Similar to NKT cells, γδ T cells constitute an innate-like lymphocyte with a role in lipid sensing via CD1d-presented antigens (although in a slightly different manner than iNKT and type 2 NKT cells)

(Zajonc and Girardi, 2014). In this respect, various adipose tissue depots show different characteristics. Epididymal adipose tissues of mice are rich in “ancestral” lymphocytes, with NKT cells, γδ T cells and NK cells making up 18.5 %, 15 % and 38.6 %, respectively, of total lymphocytes. In sharp contrast, inguinal adipose tissue has a total of less than 30 % of these cell types, while adaptive lymphocytes (αβ T cells and B cells) account for more than 70 % of total lymphocytes (Caspar-Bauguil et al., 2005). Yet, the role of γδ T cells in visceral adipose tissue homeostasis is not completely understood. γδ T cells increase in epididymal adipose tissue after five weeks on a HFD relative to a normal diet and depletion of γδ T cells results in less M1-mediated epididymal adipose tissue inflammation. Of note, the concentration of γδ T cells staining positive for IFNγ, IL-17 or IL-6 diminish after five weeks on HFD, and deletion of one of the γδ T cell receptor variants, Vγ4/6, but not depletion of all γδ T cells, results in an M2-skewed macrophage profile when compared to the wild type after HFD feeding. In line with this, γδ T cell depletion does not result in insulinemia when fed a HFD, while deletion of Vγ4/6 does, thus the activators of a γδ T cell response and the biological implication of γδ T cell receptor diversity needs to be elucidated (Mehta et al., 2015).

Furthermore, γδ T cells contribute with most of the IL-17A expression in epididymal and inguinal adipose tissue, and IL-17A has been shown to reduce adipogenesis and glucose uptake by adipocytes *in vitro*. Remarkably, IL-17 deletion results in aggravated adiposity and total body mass, although depletion of γδ T cells did not confer this phenotype, suggesting that γδ T cells contribute with more than just T_h17 skewing or that other cell types than γδ T cells compensate for the loss of γδ T cell-derived IL-17 (Zuniga et al., 2010).

Finally, a relatively newly identified immune cell subset, innate lymphoid cell (ILC), was shown to affect adipose tissue metabolism and inflammation. ILCs can broadly be divided into ILC1, ILC2 and ILC3, much adhering to the T_h1, T_h2, T_h17 paradigm, based on their cytokine profile (Brestoff and Artis, 2015). Interestingly, ILC2s provide new insight into the mechanisms guarding adipose tissue homeostasis. ILC2s have been shown to sustain eosinophils and alternatively activated macrophages, since lack of ILC2s results in lower concentration of eosinophils and macrophages, and, on the other hand, exogenously administered IL-33 was shown to increase the presence of IL-5+ and IL-13+ ILCs in visceral adipose tissue, with a concomitant loss of splenic and bone marrow eosinophils, suggesting IL-33 dependent tissue redistribution (Molofsky et al., 2013).

Liver inflammation and host metabolism

While adipose tissue obesity-associated inflammation has been thoroughly studied since the initial findings by Hotamisligil et al. (Hotamisligil et al., 1993), the liver seems contrastingly underappreciated, also in the light of its huge metabolic importance, large influx of blood-borne and gut-derived substances and strategic localization.

The liver immune response reflects the fact that the liver is exposed to multiple gut-derived molecules, thus innate signaling mediated by pattern recognition receptors such as TLRs or NLRs is

widely present in immune and non-immune cells, but still seems in a relatively tolerogenic state (Bieghs and Trautwein, 2013). The liver harbors abundant bone marrow derived macrophages named Kupffer cells (Klein et al., 2007) in addition to infiltrating macrophages. Kupffer cells are involved in lipid metabolism, toxin and microbe removal, erythrocyte clearance, and iron recycling (Italiani and Boraschi, 2014). In a manner much analogous to that of the adipose tissues, macrophages accumulate in the liver of mice upon HFD intake via MCP1-mediated recruitment of $CCR2^{+}$ myeloid cells (Obstfeld et al., 2010). However, compared with the adipose tissue, inflammation is delayed, as markers of myeloid cells and cytokines such as IL-6, TNFα, IL-1β, IFNγ, IL-10 and TGFβ only higher after 16 weeks of high fat and cholesterol intake (compared to prior to the feeding start) (and this effect was even more pronounced after 26 weeks) (Stanton et al., 2011).

The negative impact of liver macrophages was shown by chemical depletion of all liver macrophages, which reversed HFD-induced systemic insulin resistance (Lanthier et al., 2010; Neyrinck et al., 2009). However, liver macrophages also exert insulin sensitizing effects, as seen from the fact that liver-specific ablation of macrophages in diet-induced obese mice results in a lowering of IL-6 and IL-10, and hepatic steatosis and insulin resistance (Clementi et al., 2009). In support of liver macrophages also showing M2-like characteristics, are findings that PPARδ deficiency causes hepatic dysfunction and insulin resistance, and that IL-4 activates PPARδ signaling resulting in Arg-1 expression (Odegaard et al., 2008), while $Ly6C^{hi}$ monocyte infiltration is necessary for a TGFβ-induced initiation of fibrosis (Karlmark et al., 2009). Thus, much seems to depend on the inflammatory polarization of liver macrophages. In this respect stimulation via CX3CR1 has been shown to function as a survival signal and induce a pro-resolution phenotype of invading monocytes (Karlmark et al., 2010).

Although the mechanisms responsible for increasing liver macrophage concentration are still not entirely elucidated, liver DCs have been shown to increase following HFD intake of mice, and these DCs actively recruit macrophages and T cells to the liver following transfer of DCs to the blood, while *Flt3l*$^{-/-}$ reduces monocyte and macrophage infiltration in the liver (Stefanovic-Racic et al., 2012).

NKT cells in the liver

Another putative role of liver myeloid cells is in obesity-associated reduction of liver NKT cells. Obesity has been shown to induce an accumulation of $CD11b^{+}$ $Ly6C^{hi}$ $Ly6G^{-}$ myeloid cells in mice, which display an increased expression of CD115, MHCII and CD1d. These cells induce inflammation and apoptosis of NKT cells in a TLR7-dependent manner when transferred to lean recipients (Deng et al., 2009). In line with this, the *ob*/*ob* genotype (Guebre-Xabier et al., 2000) and HFD feeding of mice induces a loss of NKT cells (Li et al., 2005; Mantell et al., 2011), and hepatosteatotic patients show an inverse relationship between steatosis grade and NKT concentration (Kremer et al., 2010).

In the liver, just as in the adipose tissues, NKT cells of mice are usually grouped into either of the two canonical subsets, iNKT (being $Vα14Jα18^{+}$) or type 2 NKT (showing greater αβ T cell receptor diversity) cells. The mode of activation, e.g. lipid antigen and/or cytokine secretion by antigen-

presenting cells, defines the cytokine response of iNKT cells, as they often respond to activation by IFNγ expression, while the prototypical model-activator, α-galcer, induces a mixed phenotype of IL-4, IL-17 and IFNγ (Brigl and Brenner, 2010). However, liver iNKT cells seem more pro-inflammatory than those of the adipose tissue (Lynch et al., 2012), possibly reflecting tissue differences in NKT-stimulatory antigenic substances.

In accordance with the observation that both liver macrophages and NKT cells are able to induce T_h1 and T_h2 responses, a choline-deficient diet, which induces hepatosteatosis and NKT cell depletion, show higher *Il12* mRNA levels than the choline-supplemented diet. IL-12 deficiency led to lower transcript levels of Th1 cytokines, *Tnfa* and *Ifng*, and Th2 cytokines, *Il4* and *Il10*, and, importantly, protected against diet-induced NKT cell depletion. This was mediated by liver macrophages, as chemical depletion of liver macrophages lowered IL-12 and IFNγ, with no effect on IL-4 and IL-10 (Kremer et al., 2010). In a different model, sulfatide stimulation of type 2 NKT cells induced IL-12 expression by pDCs which recruited anergic iNKT cells from the circulation, thus NKT responses (via antigen presenting cells) are highly dependent on the mode of stimulation (Halder et al., 2007). In addition, sulfatide-mediated type 2 NKT cell stimulation can also modulate neutrophil and B cell activation (Bandyopadhyay et al., 2016). Finally, making NKT cell inflammatory responses even more complex, an IL-17 expressing $NK1.1^-$ NKT cell subset exists in liver, spleen and thymus (Coquet et al., 2008).

Taken together, NKT cells play a significant role in the modulation of liver inflammation, but more insight into the mechanisms, e.g. the antigens mediating an NKT-dependent response, is warranted.

Despite the central role of the liver in governing an modulating lipid and glucose metabolism, the temporal changes in the abundance and phenotype of immune cells in the liver are still poorly understood.

The microbiota and host metabolism

While host immune and metabolic regulation is massively interdependent, both of these systems have also adapted to the environment. The human body harbors trillions of foreign organisms, mainly bacteria, but also yeast, viruses and archaea, on the skin and in mucosal body cavities. These microbes are estimated to contribute more than ten times as many cells as in the human body, the majority residing in the extremely dynamic environment that constitutes the mammalian gut, engaged in a mutually beneficial relationship with the host (Burcelin et al., 2012). The human gut microbiota, mainly composed of the phyla Firmicutes and Bacteroidetes, is greatly influenced by diet and thus short-term and long-term dietary shifts induce changes in microbiota composition (David et al., 2014; Wu et al., 2011b).

The rather novel idea that host health is dependent on and to a large degree shaped by the abundance and composition of the gut microbiota is well-documented. Obesity is associated with a

distinct microbiota composition (Ley et al., 2005), and seminal studies of germ-free mice have shown that such germ-free mice possess an intrinsic resistance to weight gain upon high-fat diet feeding (Backhed et al., 2007). Recolonization with conventional microbiota is by itself obesogenic, owing partly to increased energy harvest and partly to the bacterial suppression of Angiopoietin-like protein 4 (ANGPTL4) expression in the intestine, an inhibitor of lipoprotein lipase (LPL) in adipose tissue, thus inducing adipose tissue lipogenesis (Backhed et al., 2004). In further support of the gut microbiota being a host metabolic regulator is the finding that transfer of gut microbiota from obese donor mice promotes adiposity of the lean recipient mice to a much greater extent than when transferred from lean donor mice (Turnbaugh et al., 2006).

Intestinal dysbiosis and insulin resistance

A large part of studies of intestinal composition is done in models of excess nutrient intake, and are thus confounded by the ensuing adiposity, and therefore it is still unknown to what extent intestinal dysbiosis is a driver of insulin resistance independently of adiposity (Vrieze et al., 2010). Still, low microbial diversity is associated with obesity (Turnbaugh et al., 2009), and low bacterial gene richness is associated with greater adiposity, insulin resistance, dyslipidemia and a pro-inflammatory phenotype when compared to individuals with high bacterial gene richness (Cotillard et al., 2013; Le Chatelier et al., 2013), altogether suggesting that bacterial dysbiosis is an essential factor in the development of insulin resistance and the metabolic syndrome.

With the advent of various high-throughput sequencing techniques, a plethora of studies characterizing the gut microbiota composition under various circumstances have been published. Numerous bacteria at genus and species level have been suggested to be involved in metabolic disease – often based on correlations rather than causality. Perhaps the most compelling being *Akkermansia muciniphila*, which has been reported to correlate in an inverse manner with obesity in humans, while the addition of *Akkermansia muciniphila* results in lower adipose tissue inflammation and higher intestinal integrity (Everard et al., 2013). However, efforts to clarify the causality between the presence or absence of specific phylogenetic groups and host metabolism is still in its infancy.

Gut bacterial factors and host response

The gut bacterial community represents an ecological niche with bi-directional signaling not just between microbial species but also between bacteria and host cells (Thaiss et al., 2016). The microbial factors often depend on or even derive from food components, thus dietary composition greatly defines not only the gut microbiota composition but also its microbial phenotype. Several of these metabolites serve as regulators of host metabolic processes and among others include short chain fatty acids (SCFAs), branched chain fatty acids (BCFAs), and bile acids (Sonnenburg and Backhed, 2016). The importance of many of these metabolites is highlighted by their multiple actions on host physiology, affecting metabolism and immune function in intestinal but also extra-intestinal tissues (Ang and Ding, 2016; Taoka et al., 2016).

Short-chain fatty acids

SCFAs are produced from bacterial fermentation in the gut of dietary fiber, and mainly comprise the fatty acids acetate, propionate and butyrate, which make up 90-95 % of SCFAs in the human colon (Koh et al., 2016; Rios-Covian et al., 2016). Besides from representing an energetically favorable source of energy for many gut bacterial species, SCFAs are potent signaling molecules in intestinal and extra-intestinal tissues (Figure 2). Their varied functions include modulation of metabolic and immunological homeostasis, and of the nervous system, mainly through the activation of the G-protein coupled receptors 41 (GPR41), -43 (GPR43), and -109a (GPR109a).

The metabolic and inflammatory potential of SCFAs is highlighted by studies of GPR41 and GPR43 knock-outs, although conflicting phenotypes have been observed (Ang and Ding, 2016). Deletion of GPR43 has been reported to aggravate obesity and worsen glucose and lipid metabolism (Kimura et al., 2013), and to inhibit insulin secretion from β cells (McNelis et al., 2015; Priyadarshini et al., 2015), but also in one instance to improve glucose control and body fat mass (Bjursell et al., 2011). Similarly, deletion of GPR41 has been observed to limit adiposity (Samuel et al., 2008), but in another study was found to increase adiposity (Bellahcene et al., 2013). Still, the beneficial effects of supplementation with dietary fiber or SCFAs on insulin sensitivity are well-described (De Vadder et al., 2014; Gao et al., 2009; Sahuri-Arisoylu et al., 2016; Yamashita et al., 2007), an effect likely attributed to the down-regulation of PPARγ in liver and adipose tissue (den Besten et al., 2015), or to the induction of a beige adipose phenotype (Lu et al., 2016). Yet, increased levels of intestinal SCFAs suggest an increased energy harvest from the diet (Turnbaugh et al., 2006), in line with the increased colonic levels of SCFAs in obese individuals (Rahat-Rozenbloom et al., 2014), thus complicating the issue of the anti- and pro-obesogenic properties of SCFAs.

Additionally, SCFAs contribute to intestinal homeostasis; butyrate functions as fuel for colonocytes (Donohoe et al., 2011), increases mucin production (Jung et al., 2015) and tight junction integrity in colonic cells *in vitro* (Peng et al., 2009) and *in vivo* (Kelly et al., 2015), and acetate production from *Bifidobacteria* improve epithelial integrity (Fukuda et al., 2011). SCFAs regulate gut immunity to commensals by activating the inflammasome (Macia et al., 2015) and shaping the tolerogenic/inflammatory potential of lamina propria-resident macrophages, dendritic cells and T cells (Koh et al., 2016). Most butyrate is absorbed in the intestine, but propionate and acetate (and unabsorbed butyrate) is transported via the portal vein, where butyrate and propionate is involved in hepatic gluconeogenesis. While the effect on lipid metabolism is still unclear, acetate is engaged in the biosynthesis of cholesterol and long chain fatty acids (den Besten et al., 2013), but also limits hepatic steatosis and induces adipose tissue lipolysis (Sahuri-Arisoylu et al., 2016) and leptin secretion (Zaibi et al., 2010).

However, more research in the source of the dietary fibers, mechanisms of SCFA signaling in the gut, gut-associated lymphoid tissues, and metabolic organs such as liver and adipose tissues, biosynthesis of SCFAs and dependency of specific bacterial species and the interplay with other gut-derived

ligands on immune activation are warranted to increase the understanding of SCFA-dependent modulation of host physiology.

The SCFA subtype termed BCFAs make up a minority of total SCFAs (5 %) and are exclusively derived from fermentation of the ingested branched-chain amino acids leucine, isoleucine and valine (Neis et al., 2015). While the branched-chain amino acids are involved in reducing insulin sensitivity (Newgard et al., 2009), the biological implication of their fatty acid fermentation products, BCFAs such as iso-butyrate and iso-valerate, is largely unknown (Rios-Covian et al., 2016).

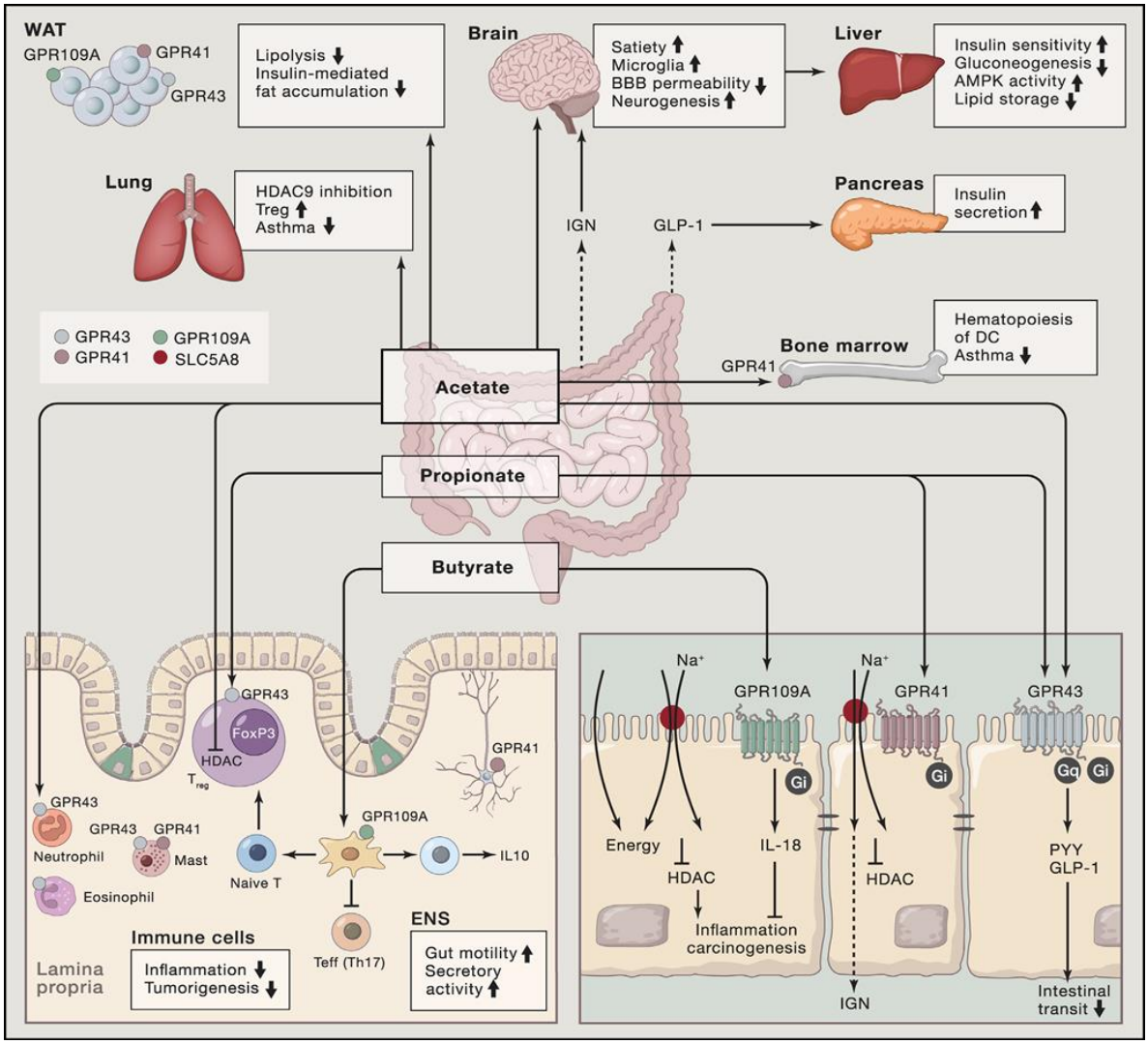

Fig. 2
The multiple effects of gut-derived short-chain fatty acids (Koh et al., 2016)

Bile acids

Bile acids are produced from cholesterol in the liver and primarily serve to facilitate the absorption of lipids and fat-soluble vitamins in the intestine. Furthermore, bile acids help maintain mucosal homeostasis via their anti-microbial action, and bile acids themselves regulate bile acid and cholesterol levels mainly via downregulation of the Farnesoid X receptor (FXR)-regulated hepatic

cholesterol 7α-hydroxylase (CYP7a1). Additionally, bile acids function as signaling molecules playing a part in the regulation of host homeostasis. For example, FXR-activation by bile acids of FXR target genes is a central switch primarily involved in lipid (e.g. cholesterol homeostasis (Caesar et al., 2016)) and glucose metabolism in the liver (Taoka et al., 2016), but also in the regulation of intestinal innate immunity (Vavassori et al., 2009).

Deconjugation of bile acids to form secondary bile acids is highly dependent on the microbiota composition (Swann et al., 2011), and is instrumental for the enterohepatic cycle, thus facilitating bile acid re-uptake in the liver via the portal vein. Bile acids exert multiple functions in relation to glucose and lipid metabolism; they regulate the hepatic triglyceride pool via FXR-dependent inhibition of sterol regulatory element binding protein-1 (SREBP-1c), thus inhibiting lipogenesis (Watanabe et al., 2004), and bile acids stimulate the secretion of the incretin glucagon-like peptide-1 (GLP-1) through binding to the G protein-coupled receptor TGR5 on enteroendocrine L cells, thereby ameliorating insulin sensitivity, attenuating weight gain and increasing energy expenditure in models of HFD-induced diet-induced obesity (Thomas et al., 2009).

A more comprehensive understanding of the effects of not just the bile acid pool size but the composition of the bile acid subtypes, as various bile acids have opposing roles for activation of FXR and other bile acid receptors (Ridlon et al., 2014), will be instrumental in furthering our understanding of the gut-liver axis in metabolic disease.

Bacteria, their metabolites and nutrient sensing

A wealth of other gut bacterial metabolites and cell wall components exists that are known to have metabolic and immune modulatory effects on the host. This microbe-to- gut signaling and *vice versa* heavily depends on innate signaling receptors, termed pattern recognition receptors (PRRs) on

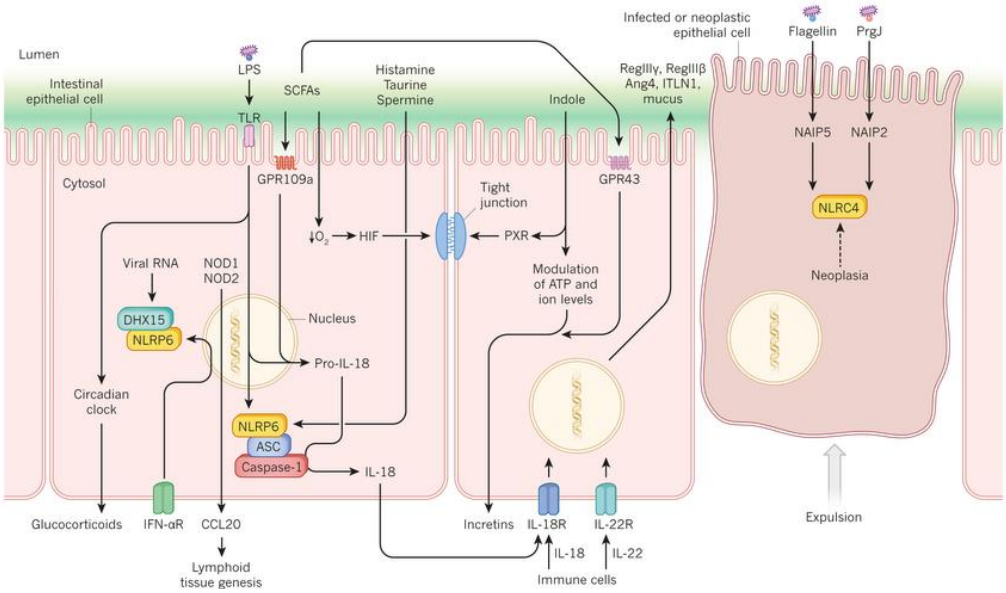

Fig. 3
Microbial signaling at the host-microbiota interface (Thaiss et al., 2016)

immune as well as non-immune cells recognizing danger- or pathogen-associated molecular patterns (DAMPs or PAMPs, respectively).

These PRRs group into various families, such as Toll-like receptors (TLRs), C-type lectins and NOD-like receptors (NLRs). Sampling via these on immune and epithelial cells of intact microorganisms and microbial-derived factors from the intestinal lumen elicits immune modulation including secretion of antimicrobial peptides, IgA and antigenic presentation and induction of an adaptive immune response (Thaiss et al., 2016).

Most thoroughly described is the pathogen-associated molecular pattern of Gram-negative bacteria lipopolysaccharide (LPS). LPS is a potent inducer of endotoxemia and subclinical inflammation via sequential interactions with LPS-binding protein (LBP), CD14, Myeloid differentiation protein 2 (MD-2) and, finally, Toll-like receptor 4 (TLR4) (although its acylation and phosphorylation status greatly defines its inflammatory potency in humans, but not in mice) (Park and Lee, 2013; Park et al., 2009; Teghanemt et al., 2005), and thus induce a pro-inflammatory cascade via NF-κB (Akira and Takeda, 2004). In an LPS infusion study, TLR4 activation increased TNFα, IL-6 and MCP1 with concomitant post-translational modification of the insulin receptor substrate 1 (IRS-1), thus resulting in hepatic insulin resistance and glucose intolerance of mice, and deletion of the co-receptor for LPS, CD14, or TLR4 itself protects against HFD-induced obesity (Cani et al., 2007; Davis et al., 2008). Although indicative of a role of TLR4 signaling in glucose metabolism, an *Escherischia coli* monocolonization study did not find LPS (either penta- or hexa-acylated forms) to aggravate glucose dysregulation, thus suggestive of other bacterial components playing a substantial role (Caesar et al., 2012).

The hypothesis that gut signaling affects whole-body metabolism is supported by the observation that deletion of the TLR adaptor molecule MyD88 in the intestinal epithelium induces resensitization to insulin, resistance to the development of adiposity and obesity, lower energy expenditure and increased intestinal T_{reg} cell numbers when fed a HFD, with no effect when fed a normal diet. This beneficial effect was maintained after fecal transplantation to HFD-fed mice, thus implicating the microbiota in this blunted microbe-intestine signaling (Everard et al., 2014).

The host also controls the gut microbiota via PRR sensing. This is evident from knock-out studies of various PRRs, such as NOD2, NOD-like receptor pyrin-domain containing (NLRP)6 and TLR5, as these mice develop intestinal dysbiosis (Fig. 3) (Thaiss et al., 2016). This loss of control over the microbiota may precipitate as metabolic dysfunction. For example, deletion of the flagellin receptor TLR5 resulted in metabolic syndrome characteristics, which was mainly due to the induction of hyperphagia, although insulin resistance was still present even under caloric restriction conditions (Vijay-Kumar et al., 2010). Furthermore, the immune response elicited by gut microbial signaling also affects host metabolism, since IL-22 receptor deficient mice are prone to obesity and IL-22 administration reverses *ob*/*ob* or HFD-induced metabolic dysfunction (Wang et al., 2014b). Interestingly, sensing of microbially derived ligands is not necessarily restricted to epithelial surfaces,

as also PRRs are expressed in the adipose tissue, skeletal muscle, liver, and by various immune cells (Thaiss et al., 2016).

Gut-derived signals influence the metabolic state

Inflammasome activation in the gut has not only effects on immune regulation but also affects host metabolism and energy expenditure. Obese individuals have been shown to have increased IL-18 (Esposito et al., 2002; Hung et al., 2005), but, interestingly, the NLRP1 inflammasome, which cleaves and activates pro-IL-18, reduces adiposity, steatosis and normalizes glucose regulation in mice (Murphy et al., 2016). This effect is observed following high fat or high protein challenge, but, strikingly, not after a fiber-rich high fat diet challenge, hence in agreement with the notion that gut-microbe crosstalk depends on diet and/or metabolic conditions. On the other hand, deletion of NLRP3 improves glucose regulation and lowers IL-1β levels in adipose tissue. Interestingly, this effect was dependent on ceramide induced NLRP3 activation in macrophages (Vandanmagsar et al., 2011). Further implicating NLRP3 in adipose tissue immune-metabolic regulation, is the finding that IL-1β and IL-18 increase in adipose tissue following HFD feeding of mice, but that only IL-1β (via caspase-1) function to inhibit adipogenesis (Stienstra et al., 2011). In line with this, in a HFD study *Caspase1*$^{-/-}$ mice are more obese than wild type mice, while, in the liver, Caspase1 deficiency limits liver steatosis and inflammation (Dixon et al., 2013). Interestingly, in a HFD-context, LPS activates the NLRP3 inflammasome in the liver (Ganz et al., 2011), an effect potentiated by palmitic acid (Csak et al., 2011), thus presenting as a potential causative agent of diet-induced liver inflammation. In summary, this highlights the importance of intestinal and peripheral sensing of diet- and gut-derived substances on metabolic and immunological homeostasis.

Intestinal permeability

The establishment of intestinal, bacterial factors as key in the development of insulin resistance and other symptoms related to the metabolic syndrome emphasizes the importance of intestinal transport for metabolic health. In this respect, the absorption of lipid messengers, such as LPS, via chylomicron-based transport from the gut is of particular importance in HFD-induced obesity, since this transport route is inherently increased (Ghoshal et al., 2009). In addition, chylomicron-independent, paracellular transport across the epithelium represents another means of transportation. This leaky gut phenotype is massively shaped by the microbiota, or the lack hereof.

The mucus layer formed in the small and large intestine provides a physical and biochemical barrier practically devoid of commensal bacteria, but, still, commensal bacteria are essential for the development of a proper intestinal integrity, as these bacteria promote mucus secretion from the epithelium to avoid pathogenic bacteria from reaching the intestinal mucosa (Bergstrom et al., 2010; Johansson et al., 2008). Interestingly, bacterial factors alone can induce the maturation of the mucus layer, as evidenced in germ-free mice, where the administration of the TLR ligands peptidoglycan or LPS stimulate mucus production (Petersson et al., 2011).

High fat diet and leaky gut syndrome

Emphasizing the role of high-fat diet intake for intestinal permeability is the observation that intestinal integrity is reduced after four weeks of feeding a corn oil and lard-based high-fat diet (Cani et al., 2008), although the dietary fat profile matters, since a saturated fat-based HFD is associated with greater transepithelial resistance in the colon than n-3 and n-6 based diets after eight weeks of feeding (despite mice on saturated fat and ω-6 based HFD develop similar weight and fat mass gain profiles) (Lam et al., 2015).

In support of intestinal permeability playing a role in metabolic inflammation is the finding that HFD induced intestinal permeability precedes obesity (Ding et al., 2010). Also, live bacteria and their metabolites are present in the systemic circulation and extra-intestinal tissues. After only one week of HFD feeding, translocation across the intestinal barrier to the systemic circulation and mesenteric adipose tissue is observed, a process dependent on the bacterial sensors CD14 and NOD1, but not NOD2. Conversely, the intracellular TLR signaling molecule myeloid differentiation primary response gene 88 (MyD88) seemed protective of this translocation, as MyD88 knock-out dramatically increased bacterial translocation, in addition to insulin resistance and body weight (Amar et al., 2011).

Similarly, the liver, a richly vascularized organ receiving most of its blood supply from the intestine via the portal vein, is a tissue site that is chronically exposed to gut-derived factors and even live bacterial remnants. In a study of NAFLD patients, intestinal permeability is significantly higher among NAFLD diagnosed patients, while small intestinal bacterial overgrowth and intestinal permeability correlate with liver steatosis among NAFLD patients (Miele et al., 2009). Also, activation of liver pattern recognition receptor TLR4 by LPS is important for the development of diet-induced steatohepatitis and hepatic inflammation (Meli et al., 2014; Rivera et al., 2007; Spruss et al., 2009). Additionally, in a study of the role of NLRP3 and NLRP6 inflammasomes in NAFLD, inflammasome deficient mice have an altered gut microbiota, aggravated hepatic steatosis and glucose regulation, and increased weight gain, while deletion of the intracellular signalling molecules downstream of TLR, MyD88 and TIR-domain-containing adapter-inducing interferon-β (TRIF), abolishes the NASH phenotype, which is TLR4 and TLR9 dependent (Henao-Mejia et al., 2012). This altogether indicates that the sensing of bacterial components in the gut and the liver is involved in metabolic liver disease.

Thus, although it is still not clear which intestinally-derived substances that drive the pro-inflammatory phenotype resulting in insulin resistance *in vivo*, this collectively indicates that intestinal permeability and gut-derived factors play a pivotal role in the development of metabolic tissue inflammation.

Diet-derived substances and inflammation

Most dietary components are degraded in the upper bowel. However, some dietary components harbor an intrinsic resistance to degradation. This includes the protein gliadin, a prolamin protein which together with glutenin forms the gluten complex of grains such as wheat, barley and rye. Intake of certain grains may result in pathologies such as wheat allergy and celiac disease. Celiac disease is caused by gliadin, almost exclusively in patients with the HLA-DQ2 and HLA-DQ8 haplotype, thereby displaying an adaptive immune response in the intestine via the presentation of gliadin peptides to T cells, the consequent production of autoantibodies, and a pro-inflammatory cytokine release (Bardella et al., 2016; Sapone et al., 2012).

In addition, gliadin has been reported to disturb the intestinal barrier also in non-celiac disease patients, individuals therefore characterized as suffering from non-celiac gluten sensitivity. Various randomized, double-blind studies of inflammatory bowel syndrome patients without celiac disease identified about 5-15 % to respond negatively to gluten (Bardella et al., 2016).
Gliadin induces intestinal inflammation and permeability via several potential mechanisms. Intake of pre-digested gliadin recruits neutrophils to the lamina propria and reorganization of the zonula occludens protein, markers of tight junction function (Lammers et al., 2008) and causes substantial tight junction alterations *in vitro* (Sander et al., 2005). This is likely mediated by binding of gliadin to the CXCR3 receptor, expressed on intestinal epithelial cells and immune cells (Lammers et al., 2015). In addition, gliadin peptides promote human dendritic cell migration *in vitro* (Chladkova et al., 2011).

The host metabolic consequences of gluten intake has also been described, initially in non-obese diabetic (NOD) mice, prone to the development of type 1 diabetes, which show a delay or complete abolishment of diabetes when fed a gluten free diet (Funda et al., 1999). Also, mice without any genetic predisposition are sensitive to gluten, as mice fed a HFD with 4.5 % gluten increase adiposity, inflammatory markers and insulin resistance after 8 weeks of feeding compared to HFD fed mice (Soares et al., 2013). HFD and gluten fed mice have been reported to decrease their thermogenesis in brown adipose tissue, which may be involved in the gluten-induced build-up of adiposity, although HFD and gluten intake was not associated with increased inflammation (Freire et al., 2016). Finally, in another study, gluten and a HFD did not augment intestinal inflammation, but did worsen glucose intolerance and decrease β-cell mass (Haupt-Jorgensen et al., 2016). In conclusion, gluten is associated with several intestinal, metabolic and inflammatory complications, but the actual mechanisms by which gluten exerts its potentially detrimental functions are still not entirely understood.

Concluding remarks

Diet is considered one of the most important factors defining human metabolic health. Diet affects several aspects of host homeostasis, but its effects on metabolic and immune regulation and intestinal microbiota composition have been shown to be of particular importance for the metabolic shifts associated with metabolic dysfunction. Importantly, host metabolism, the immune response and gut bacterial composition cannot be regarded as independent entities. Rather they function in an inter-dependent manner, thus greatly affecting each other and altogether defining the host metabolic outcome.

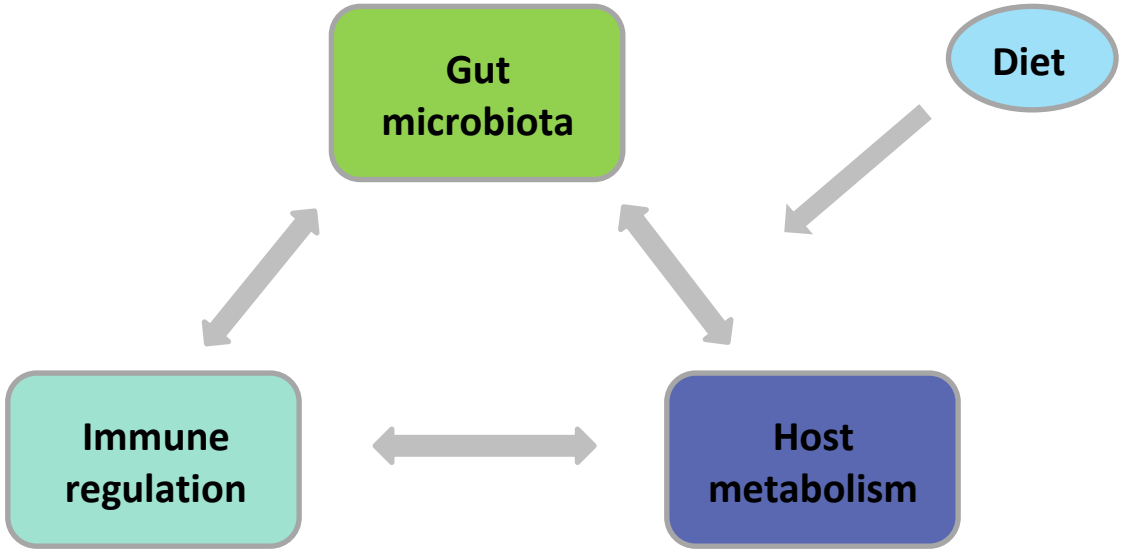

Objectives

The studies presented in this thesis commonly aimed at describing the manifestation of diet-dependent disease through extensive analysis of host metabolic parameters. With the increasing appreciation of the association between host metabolic regulation and the fine-tuning of the immune response, we have included a detailed analysis of the immunological aspects of these diet-induced pathologies. We are hopeful that the application of multivariate analyses will facilitate a multilevel characterization of the interplay between different host and bacterial factors, which are intricately linked in metabolic disease.

Project I: Gliadin study

Introduction and objectives

The metabolic syndrome constitutes a cluster of several metabolic imbalances that altogether challenges global public health. While multiple factors are involved in the pathogenesis of metabolic dysfunction, dietary composition is one of the most important factors in the shaping of metabolic function. Controversially, dietary intake of gluten has been associated with detrimental effects on metabolic function. Intake of gluten, and more specifically one of its constituents, gliadin, has been proposed to exert several metabolic imbalances, even among non-coeliac disease subjects (Sapone et al., 2012). These effects include glucose dysregulation, and intestinal inflammation and dysbiosis.

In addition to a considerable amount of dietary gluten, Western diets are typically rich in fats. Whereas the long-term detrimental effects of high-fat diet intake on metabolism and inflammation have been well established, the combined effect of a high-fat and gliadin-rich diet on host metabolic and inflammatory status has not been properly addressed.

Thus, this study aimed at describing the metabolic and inflammatory effects of long-term intake of the detrimental gluten component, gliadin, in combination with a high-fat diet of male C57BL/6NTac mice.

Experimental setup

Male C57BL/6NTac mice (n=20) housed two-by-two were fed either a HFD or a HFD with 4% gliadin (substituted for casein) for 22 weeks. Metabolic performance was monitored closely by oral glucose tolerance tests and measurements of HbA1c levels in blood during the feeding period, while the faecal microbiota composition was characterized at regular intervals.

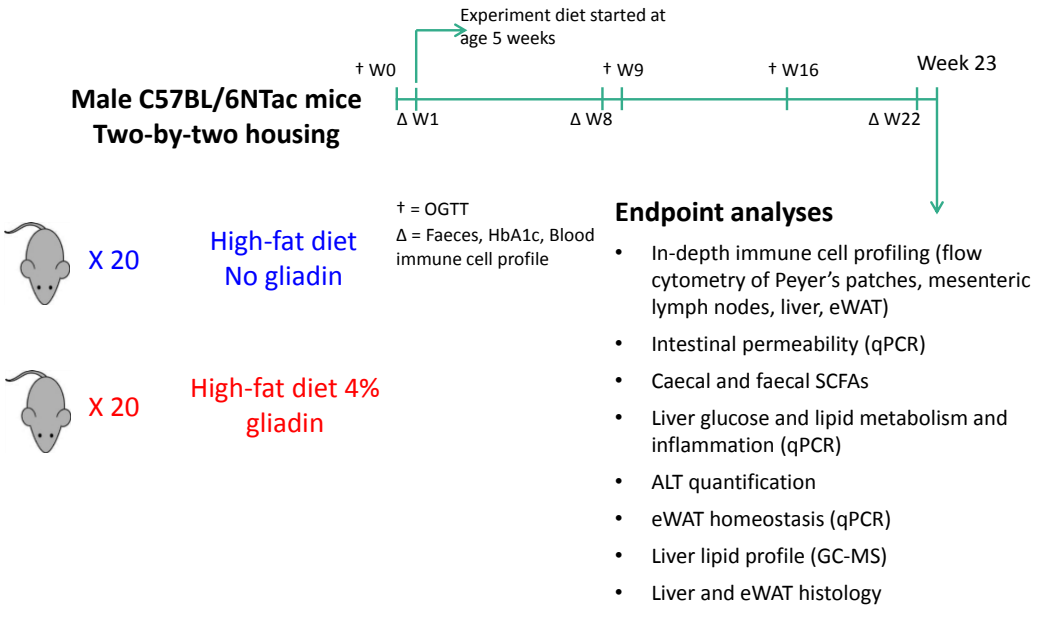

At the endpoint, after a 22 week feeding period, epididymal adipose tissue, liver tissue, and ileal and colonic tissues were harvested from all mice (n=20 for each group). In addition, one mouse from each cage (n=10 for each group) was reserved for an in-depth characterization of their immune cell composition by flow cytometry, which therefore included tissue harvest of liver, epididymal adipose tissue, Peyer's patches and mesenteric lymph nodes. We intended to use the other mouse in each cage (n=10 for each group) for a characterization of intestinal permeability, so prior to tissue harvest they were fasted and subsequently subjected to an oral gavage with a FITC-dextran compound. Additionally, ileal, caecal and colonic luminal samples and urine samples were collected in order to characterize the intestinal microbiota and the urine metabolome, respectively, of all mice.

Specific aims

This study aimed to identify

- the long-term metabolic effects of dietary gliadin intake in combination with a high fat diet
- the effect of gliadin on gut microbiota composition and intestinal health
- immune cell composition and inflammatory status of gliadin-fed mice
- mechanistic links between a gliadin-rich diet, intestinal microbiota and host metabolism and inflammation

Key findings

The most significant findings from this study are

- Addition of gliadin to a HFD induces marked changes in the gut microbiota composition and activity
- A gliadin-rich HFD disturbs metabolic function by increasing blood HbA1c levels and HOMA-IR
- A gliadin-rich HFD does not increase adiposity or body weight, but affects epididymal adipose tissue and liver homeostasis by limiting adipocyte expansion and increasing liver steatosis
- We could not identify an effect of a gliadin-rich HFD on intestinal, lymphoid immune cells
- But, a gliadin-rich HFD reshapes the inflammatory potential of epididymal adipose tissue immune cells and increases adipose tissue *Il33* expression
- The urine metabolome of gliadin and HFD fed mice is significantly different from that of HFD fed mice

Publication status

In preparation for resubmission to Scientific Reports

Manuscript I

Effects of Gliadin consumption on the Intestinal Microbiota and Metabolic Homeostasis in Mice Fed a High-fat Diet

Li Zhang[1,3,a], Daniel Andersen[2,a], Henrik Munch Roager[1], Martin Iain Bahl[1], Camilla Hartmann Friis Hansen[3], Niels Banhos Danneskiold-Samsøe[2,4], Karsten Kristiansen[4], Ilinca Daria Radulescu[2], Christian Sina[5], Henrik Lauritz Frandsen[1], Axel Kornerup Hansen[3,*], Susanne Brix[2,*], Lars I. Hellgren[2,*], Tine Rask Licht[1,*]

[1]National Food Institute, Technical University of Denmark, 2860 Søborg, Denmark
[2]Department of Systems Biology, Technical University of Denmark, 2800 Kgs. Lyngby, Denmark
[3]Department of Veterinary Disease Biology, University of Copenhagen, 1871 Frederiksberg C, Denmark
[4]Department of Biology, University of Copenhagen, 2100 København Ø, Denmark
[5]Department of Internal Medicine I, University Hospital of Schleswig-Holstein, Lübeck, Germany

[a]These authors contributed equally to this work
*Corresponding authors: Tine Rask Licht, trli@food.dtu.dk; Lars I. Hellgren, lih@bio.dtu.dk; Susanne Brix, sbp@bio.dtu.dk; Axel Kornerup Hansen, akh@sund.ku.dk

Short Title: Gliadin Affects Microbiota and Metabolism

ABSTRACT

Dietary gluten causes severe disorders like celiac disease in gluten-intolerant humans. However, currently understanding of its impact in tolerant individuals is limited. Our objective was to test whether gliadin, one of the detrimental parts of gluten, would impact the metabolic effects of an obesogenic diet. Mice were fed either a defined high-fat diet (HFD) containing 4% gliadin (n = 20), or a gliadin-free, isocaloric HFD (n = 20) for 23 weeks. Combined analysis of several parameters including insulin resistance, histology of liver and adipose tissue, intestinal microbiota in three gut compartments, gut barrier function, gene expression, urinary metabolites and immune profiles in intestinal, lymphoid, liver and adipose tissues was performed. Mice fed the gliadin-containing HFD displayed higher glycated hemoglobin and higher insulin resistance as evaluated by the homeostasis model assessment, more hepatic lipid accumulation and smaller adipocytes than mice fed the gliadin-free HFD. This was accompanied by alterations in the composition and activity of the gut microbiota, gut barrier function, urine metabolome, and immune phenotypes within liver and adipose tissue. Our results reveal that gliadin disturbs the intestinal environment and affects metabolic homeostasis in obese mice, suggesting a detrimental effect of gluten intake in gluten-tolerant subjects consuming a high-fat diet.

INTRODUCTION

Gluten is the main structural protein complex in cereal seed endosperm, and is as such a natural component of flour-based bread, cakes, and pasta included in many Western diets. However, besides the recognized symptoms related to diagnosed gluten intolerance such as wheat allergy and celiac disease [1], gluten may also hold disease-driving potentials in so-called gluten-tolerant individuals. This is especially evident in gluten elimination studies undertaken in subjects suffering from Irritable Bowel Syndrome, which report reduced bowel symptoms after short term intake of gluten-free diets [2,3], but gluten-free diets may also have a beneficial effect on human type 1 diabetes [4]. The latter is supported by the observation that gluten increases incidences of type 1 diabetes in animal models [5,6].

The metabolic effects of gluten in combination with a high-fat diet (HFD) is hitherto addressed in four animal studies. Two of these report marked detrimental effects of gluten intake on obesity and insulin resistance within eight weeks [7,8], while two long-term studies show either no effects on these parameters or a fluctuating effect on glucose tolerance. [9,10]. The causal mechanisms behind the effects of gluten in the context of a HFD however remain elusive, and explorative studies that map the interaction between the many involved host responses are thus highly needed to decipher the impact of gliadin in gluten-tolerant hosts.

Gluten is a heterogeneous compound based on prolamin and glutelin, and the prolamin fraction of wheat, gliadin, which contains peptides rich in glutamine and proline, is reported to play a key role in gluten intolerance [1]. The gliadin-derived proline-rich peptides are particularly resistant to proteolysis by digestive enzymes [11], which means that gliadin peptides, including the gut-permeating peptides designated 111–130 and 151–170, the cytotoxic peptide 31–43, and the immune-modulating 33-mer peptide 57–89 [12], remain partly undigested and biologically active in the gastrointestinal tract. Activities of these peptides are not limited to induction of autoimmunity, but may also affect gluten-tolerant individuals [13,14].

The gut microbiota interacts with host metabolism and immune system [15,16], and thus also influences parameters related to metabolic syndrome [17]. Several bacteria isolated from the human gut are able to metabolize gluten [18,19]. Specifically, some strains of *Bifidobacterium* and *Lactobacillus* have been shown to hydrolyze gliadin peptides into inactive peptides, thereby counteracting gliadin-mediated effects on permeability [20], inflammation [21], and cell agglutination [22]. A change in gut microbiota composition and activity induced by gliadin consumption may therefore influence several factors of importance for host physiology. Nevertheless, only very few studies have addressed the effects of gluten/gliadin intake on intestinal microbes in gluten-tolerant mice [5,9]or humans [23,24], and effects of specific intervention with gliadin awaits comprehensive investigation.

Here, we aimed to comprehensively investigate the long-term effects of gliadin intake on host and microbiota in HFD-fed mice serving as a model of gluten-tolerant, obese humans. We fed mice a synthetic diet with 60% of the energy originating from fat, and containing either 4% gliadin or no gliadin, for 23 weeks (S1 Table). We measured the effects on systemic host physiology, including glucose homeostasis, lipid metabolism and inflammation. Furthermore, we addressed whether and how these alterations were promoted by changes in specific host features including microbiota composition and activity, barrier function and immune responses within the gut, as well as the urinary metabolic signature and immune responses in liver and adipose tissue.

Our results demonstrate that gliadin affects both the intestinal microbiota and the ileal barrier function, and that consumption of this wheat component affects metabolic homeostasis as well as extra-intestinal immune responses in animals fed HFD. Importantly, explorative approaches and network analyses raise novel hypotheses about the underlying mechanisms behind effects of gliadin intake on metabolic health.

RESULTS

Gliadin Intake Affected Glucose and Lipid Metabolic Homeostasis

After 23 weeks of HFD-based dietary intervention, Gliadin+ mice displayed significantly higher levels of glycated hemoglobin (HbA1c) than Gliadin- mice (Fig 1A), suggesting a higher average blood glucose level in the Gliadin+ mice during the intervention period. Likewise, insulin resistance as determined by the Homeostasis Model Assessment of Insulin Resistance (HOMA-IR) was higher in the Gliadin+ group (Fig 1B). Additionally, we observed marked differences in lipid storage. Gliadin+ mice exhibited more abundant lipid droplets in the liver (Fig 1C and 1D), but smaller adipocyte size in the epididymal white adipose tissue (eWAT), also reflected in the adipocyte size distribution that revealed higher frequencies of small adipocytes of Gliadin+ mice in the range of 2,000 – 4,000 μm^2 (Fig 1E, 1F, 1G). Moreover, the adipocyte size and hepatic total lipid droplet area were strongly negatively correlated (Fig 1H), suggesting a link between lipid storage capacity in the eWAT and lipid accumulation in the liver.

In spite of these differences, the Gliadin- and Gliadin+ mice had similar levels of many of the assessed metabolic parameters. Mice in both groups reacted similarly to a glucose challenge in oral glucose tolerance tests (OGTT), and showed impaired glucose clearance with increasing age and body weight (S1B Fig). No differences were observed between the two groups with respect to fasting insulin levels (S1C Fig), fasting glucose levels (S1D Fig), or hepatic gene expression of enzymes involved in gluconeogenesis, glucose 6-phosphatase (*G6pase*) and phosphoenolpyruvate carboxykinase (*Pepck*, S1Q Fig). Additionally, there was no gliadin-induced difference in ileal expression of *Pepck* (S1O Fig), although Gliadin+ mice showed a lower ileal expression of *G6pase* (S1O Fig). Furthermore, no effect on total liver weight was observed (S1E Fig). Evaluation for non-alcoholic steatohepatitis parameters

confirmed the higher steatosis grade of Gliadin+ mice, while all mice displayed the same degree of lobular inflammation and hepatocellular ballooning after 23 weeks of HFD (S1F-1H Fig). The dysregulated lipid phenotype of Gliadin + mice did not manifest in the triglyceride profile (S2 Table) or in the expression levels of a series of lipid metabolism related genes in the liver (S1Q Fig), nor in the levels of alanine aminotransferase in plasma (S1I Fig), a marker of liver damage. Likewise, the weight of the eWAT and expression levels of genes directly related to lipo- and adipogenic properties were unaffected (S1J and S1P Fig). Finally, body weight development did not differ between Gliadin- and Gliadin+ mice during 23 weeks of HFD (S1L Fig), and no differences in feed consumption or feed conversion ratio assessed by feed consumption per body weight gain were observed (S1M and S1N Fig).

Taken together, these results suggested that gliadin intake in itself only moderately affected glucose and lipid metabolism. This should however be interpreted in the context that gliadin was able to add even to the severe detrimental effect on metabolic dysregulation caused by HFD consumption for 23 weeks.

Gliadin Intake Altered Gut Microbial Composition and Activity

To elucidate whether changes in the gut microbiome were accompanying the observed effects of gliadin on glucose and lipid metabolism, we sequenced the V3 region of the 16S rRNA genes in community DNA extracted from fecal samples at Weeks 0, 9, 16, and 23, and from terminal ileal, cecal, and colonic samples. As anticipated, gut microbiotas of both Gliadin- and Gliadin+ mice were strongly affected by HFD. Principal coordinate analysis (PCoA) clearly separated the Week 0 fecal microbiota from that obtained at Weeks 9, 16 and 23 (Fig 2A), and alpha diversity was significantly reduced by the shift from normal chow diet at Week 0 to HFD in the following weeks (S2B Fig).

PCoA analysis of unweighted UniFrac distance matrices furthermore showed a clear separation of the Gliadin- and Gliadin+ groups by their fecal microbiotas at Week 9, 16 and 23, as well as by ileal, cecal and colonic microbiotas at Week 23 (p values < 0.001, ADONIS test, Fig 2B-2E). The difference between the two groups was most significant in the ileal segments when assessed by weighted UniFrac distances (S2C Fig). Interestingly, the ileal microbiota of Gliadin+ mice exhibited a significantly larger divergence than that of Gliadin- mice (within-group UniFrac distances: unweighted, 0.60 ± 0.07 versus 0.52 ± 0.09, weighted, 0.17 ± 0.08 versus 0.08 ± 0.08, $p < 0.001$), which is also manifested by the more scattered distribution of the Gliadin+ samples in the PCoA plots (Figs 2C and S2C). This indicates individually divergent responses of the ileal microbiota to gliadin. No significant differences of α-diversity within fecal, ileal, cecal or colonic samples were observed when comparing the Gliadin- and Gliadin+ groups (S2B Fig).

Gliadin intake altered the relative abundances of a total of 44 Operational Taxonomic Units (OTUs), of which the ones with more than ten-fold differences in relative abundance included OTUs

identified as *Lactobacillus* that were less abundant in fecal samples of Gliadin+ mice at Week 9, as well as ileal OTUs identified as Coriobacteriaceae, *Enterorhabdus*, *Clostridium XI*, *Dorea*, and a colonic OTU identified as *Akkermansia* that were all more abundant in Gliadin + mice (Fig 2F and 2G). Findings at the genus/family level were generally consistent with the findings based on OTUs (S2F and S2G Fig).

The observed effects of gliadin on microbial composition led us to examine whether also the gut microbial activity was affected. Total cecal short chain fatty acid (SCFA) concentrations tended to be higher in Gliadin+ mice than in Gliadin- mice ($p = 0.05$), which was mainly explained by higher levels of acetic acid (Fig 2H). In feces, butyric acid was also higher in Gliadin+ mice than in Gliadin- mice (S2A Fig). In relation to possible microbiome-induced effects on bile acid metabolism, we observed that the hepatic bile acyl-CoA synthetase gene (*Bacs*) was expressed at a significantly lower level in Gliadin+ mice (Fig 2I), suggesting gliadin-induced changes in bile acid metabolism within the liver. Similarly, another gene regulated by the farnesoid X receptor, the cholesterol 7 alpha-hydroxylase gene (*Cyp7a1),* was expressed at a slightly (but not significantly) lower levels in Gliadin+ mice ($p = 0.08$, Fig 2I).

Gliadin Intake Caused Lower Expression of Gut Barrier Function Related Genes in Ileum

To analyze whether intake of gliadin affected the gut barrier function, we measured expression of genes in ileal and colonic tissues encoding five tight junction proteins including ZO-1 (*Tjp1*), occludin (*Ocln*), and claudin2-4 (*Cldn2*, *Cldn3*, *Cldn4*), as well as the adherens junction protein cadherin-1 (*Cdh1*) and two mucins (*Muc2*, *Muc3*). Gliadin+ mice showed lower ileal expression of *Tjp1*, *Ocln*, *Cdh1*, *Muc3*, and tended ($p = 0.06$) towards lower expression of *Muc2* (Fig 3), suggesting a disturbed barrier function. These effects were local to the ileum, as colonic expression of the same genes was similar between the two groups of mice (S3 Fig), suggesting that gliadin mainly disturbs the ileal environment.

Gliadin Intake Changed the Metabolic Signature of Urine

Since intake of gliadin changed host physiology (Fig 1), intestinal microbiota composition and activity (Fig 2), along with gut barrier function (Fig 3), we examined whether these changes were reflected in urine metabolite profiles. Exploratory metabolic profiling by Ultra Performance Liquid Chromatography Mass Spectrometry (UPLC-MS) of urine samples at Week 23 confirmed that intake of gliadin consistently modified the urinary metabolite signature. Principal component analysis (PCA) of metabolite profiles derived from both positive and negative ionization modes clearly separated Gliadin+ and Gliadin- mice (p values < 0.001, Hotelling's T^2 test, Fig 4A).

In total we found 43 urinary metabolites to differ significantly in abundance between the two groups (Fig 4B, S3 Table). Of these, the large majority (37 metabolites) were found in higher levels in Gliadin+ mice, suggesting a higher intestinal permeability of Gliadin+ mice (Fig 4B). Several of the metabolites were tentatively identified as intermediates and breakdown-products of amino acid

metabolism, protein degradation, and tocopherol β-oxidation end products. Five dipeptides containing the amino acids proline or hydroxyproline were observed, most likely originating from gliadin itself. Furthermore, five oxidized tocopherol metabolites, carboxyethyl-hydroxychromans, were more abundant in Gliadin+ mice than in Gliadin- mice. Additionally, six metabolites associated with tyrosine and tryptophan metabolism including dopamine-glucuronide were identified among the metabolites more abundant in Gliadin+ mice than in Gliadin- mice, underpinning the observed gliadin-induced changes in the composition and/or activity of the gut microbiota, as these metabolites may be derived from intestinal bacteria.

Gliadin Did Not Affect Systemic Inflammatory Markers but Altered Immune Cell Composition in Liver and Inflammatory Phenotype of Visceral Adipose Tissue

Given the observed disturbance of gut barrier function and alterations in host and microbial metabolism, we speculated that gliadin might affect HFD-induced systemic inflammation. However, no gliadin-induced differences were found among the measured circulating cytokines (IL-1β, IL-6, IFNγ, TNFα and IL-10) at termination (S4A Fig). Additionally, while the percentage of blood neutrophils was higher in Gliadin+ mice after 9 weeks (S4B Fig), gliadin did not impact the percentage of blood monocytes and neutrophils after 23 weeks (S4B and S4C Fig). Still, since multiple previous studies of metabolic dysregulation have emphasized the importance of specific immune cell subsets as a key etiological factor [25,26], we examined whether immune responses within metabolic- and gut-related tissues were altered by gliadin intake. We performed a deep phenotyping of all major immune cell subsets within intestinal lymphoid tissues including Peyer's patches and mesenteric lymph nodes, and within liver and eWAT (S4D-4G, S5, S6 Fig). Gliadin induced no statistically significant differences in the total number of leukocytes in any of the tissues (Fig 5A). Notably, gliadin intake was not reflected in local differences in immune cell composition within intestinal Peyer's patches and mesenteric lymph nodes (S4D and S4E Fig), or in the phenotypes of these gut-associated immune cells (S4 Table).

Within the liver, we found that numbers of the major liver immune cell subsets were changed by gliadin as revealed in a PCA showing that Gliadin+ mice displayed a generally different immune profile mainly driven by higher numbers of innate-like cell types such as various myeloid dendritic cell subsets, NK, NKT, and γδ T cells ($p < 0.05$, Hotelling's T^2 test, Fig 5B). Characterization of the inflammatory phenotype of the liver immune cell subsets through intracellular cytokine staining did not show any differences in immune cell activities between the two groups (S4 Table).

Within eWAT, the numbers of several of the immune cell subsets tended to be influenced by gliadin (S4G Fig), but no general changes in the immune cell profiles were identified based on PCA analysis. However, a functional characterization of the activity of eWAT immune cell subsets revealed a gliadin-induced change in cellular levels of the anti-inflammatory IL-4 within several different immune cell subsets (Fig 5C). IL-4 production was not different among eosinophils, generally

considered as the primary immune cell type responsible for IL-4 secretion in adipose tissue [27], but rather, IL-4 levels were higher in mast cells, the innate-like γδ T cells and NKT cells, as well as in antigen-specific αβ T cells within Gliadin+ mice (Figs 5C and S6B). Additionally, we found that the overall levels of IL-4, IL-17A, and IFN-γ in both αβ T cells as well as in innate-like T cells and NK cells were higher in Gliadin+ mice (Fig 5D), altogether showing that the overall activity of both adaptive and innate T cells, as well as NK cells in eWAT was altered by gliadin consumption. Moreover, higher gene expression levels of the IL-1 family cytokine IL-33, involved in adipose tissue homeostasis, were observed in Gliadin+ mice (Fig 5E). Collectively, the data showed that gliadin intake modulated the inflammatory milieu in both eWAT and liver.

Combining Alterations in Microbiome and Host Metabolic Features

Network analysis of significant Spearman correlations ($p < 0.05$) between the four gliadin-affected metabolic endpoints (i.e. hepatic lipid droplets, adipocyte size, HbA1c and HOMA-IR) and either microbiome-derived features (bacterial groups, diversity, SCFA), urinary metabolome, or other host parameters, respectively, revealed the most significantly interacting parameters with regard to the observed phenotypes (Fig 6A). To narrow down correlations included in the network, which were not subjected to correction for multiple testing, only parameters correlating with at least two of the four metabolic endpoints were considered.

Fasting insulin, OGTT, eWAT weight, liver weight and triglyceride profile, did not (as described above) differ significantly between Gliadin- and Gliadin+ mice, but were correlated with three or all of the four differing metabolic endpoints, which supports the observed moderate effect of gliadin on metabolic dysregulation. Ileal gene expression of the rate-limiting gluconeogenesis gene *pepck* was negatively correlated with HbA1c, HOMA-IR and hepatic lipid droplets, which is in line with previous reports about the beneficial effects of intestinal gluconeogenesis on glucose and energy homeostasis [28]. Expression of *Il33* in eWAT also stood out in the network, negatively correlated with adipocyte size and positively correlated with HbA1c and HOMA-IR.

Additionally, two groups of urinary metabolites altered by gliadin intake were of notice in the network. These two groups of gliadin-affected metabolites were associated with both the gut microbiota and the host metabolic parameters, and thus potentially contributed to the gliadin disturbed host-microbiota homeostasis. The first group comprises γ-glutamyl-γ-aminobutyraldehyde, and unknown metabolites of tryptophan and tyramine, which were all correlated to three of the gliadin-affected host parameters (Fig 6A). These three metabolites are involved in the microbial metabolism of γ-aminobuturic acid (GABA), tryptophan and tyrosine [29]. GABA is a neurotransmitter, while tyrosine and tryptophan can be converted into the mood-determining molecules, dopamine and serotonin [29], suggesting that gliadin intake may affect cognitive functions. The second group of urinary metabolites includes acetylhomoserine and 2-[3-carboxy-3-(methylammonio)propyl]-histidine. Hepatic lipid droplet area was negatively correlated to the former but positively to the latter. These two metabolites are both involved in the microbial metabolism of S-adenosyl

methionine [30], which is depleted during chronic liver disease and is widely adopted as a therapy for the disease and intra-hepatic cholestasis [31,32].

In addition to the associations related to metabolic endpoints differently affected in the two feeding groups, a large number of correlations were identified between the abundance of specific bacterial OTUs/phylotypes with different abundances in the two feeding groups, and given host parameters (S7 Fig).

In our further exploration of correlated parameters, we focused on specific hypothesis-based correlations (Fig 6B-6H). In general, the Gliadin+ group displayed more variation within the ileal microbiota as well as in eWAT immune responses (Figs S2C, 5C and 5D). We therefore hypothesized that the observed variations in gliadin-induced differences in immune responses in eWAT were caused by individual response patterns within the microbiota of the mice. This hypothesis was supported by correlations between the principal coordinate 2 (PC2) of the ileal microbiota profiles and principal component 1 (PC1) of eWAT IL-4 expressing cell types (Fig 6B) and eWAT T-cell cytokine profiles (Fig 6C), respectively. Strong correlations were also identified between urinary dopamine-glucuronide and immune response profiles in eWAT (Fig 6D and 6E). This is in line with previous reports about interaction of dopamine with receptors in adipose tissues [33,34]. Finally, Gliadin+ mice displayed higher urinary levels of aldosine, which is an amino acid derived from aldol crosslinking of elastin and collagen. Urinary aldosine positively correlated with gene expression of *Col6a3* in eWAT, but not with *Col3a1* in the liver (Fig 6F and 6G), suggesting that the higher aldosine levels were eWAT-derived. Increased collagen deposition in the adipose tissue would limit the capacity of adipocytes to expand [35]. However, no significant correlation between aldosine and adipocyte size was detected (Fig 6H).

DISCUSSION

The impact of gluten in gluten-tolerant subjects is only scarcely elucidated although it may play an important role for development of life-style related diseases in populations with a high consumption of products based on refined wheat together with a high fat intake. Although a few studies have previously investigated the combination of a HFD and gluten intake has in mice [7,8,10], conflicting results are reported, and the underlying mechanisms are not understood. We aimed to conduct a comprehensive explorative study that would take our current understanding of the interaction between gluten consumption and host metabolism a big step forward. We thus tested the effects of the specific wheat gluten component, gliadin, in a HFD mouse model, and found that a number of physiological parameters including long-term blood glucose levels (HbA1c), HOMA-IR, as well as total area of hepatic lipid droplets and eWAT adipocyte size, were affected by gliadin intake (Fig 1). The use of completely defined diets allowed us to focus explicitly on the effect of a specific dietary

component, and we find it notable that the relatively small change (exchanging casein for 4% gliadin) resulted in a considerable impact on the host response in the HFD mouse model.

To elucidate the mechanisms behind the observed macroscopic effects, we investigated the impact of gliadin on gut microbiota, gut barrier function, urinary metabolome and immune responses in liver and adipose tissue (Fig 7). Gliadin peptides are not fully degraded by host digestive enzymes [11], and thus interact with both the host epithelium and the microbes present in the intestine. Accordingly, we observed a significant impact on the composition of bacteria in the ileal and cecal environments, as well as on microbial activity, as reflected in a higher production of acetic acid and higher total SCFA levels (Fig 2). As several previous reviews suggest that the gut microbiome affects intestinal integrity [36,37], we speculate that not only the gliadin peptides themselves [13,14], but also the gliadin-induced alterations in the ileal microbiota led to aberrations in the gut barrier function as measured by reduced expression of tight junction, adherens junction and mucin protein encoding genes (Fig 3). Reduced intestinal barrier function in the gliadin-fed animals was additionally reflected in the observation that out of 43 specific urinary metabolites observed to be differentially abundant in gliadin-fed vs gliadin-free mice, 37 were found to be most abundant in the gliadin-fed mice (Fig 4), suggesting a generally increased leakiness of the gut mucosa. The mode of influx of bacterial factors or dietary components from the gut lumen to the systemic circulation is thought to rely on passage through epithelial tight junctions or via chylomicron-facilitated transport from the gut [38], two phenomena likely to be permitted by dietary intake of gliadin and HFD, respectively. In line with this, a recent study shows that dietary gluten can reach extra-intestinal organs including adipose tissues in HFD-fed mice [8].

We suggest that the increased intestinal permeability caused by gliadin in the HFD mouse model led to translocation of substances that affected the immune response in liver and adipose tissue as seen by a different immune cell profile with higher numbers of innate-like cell types in the liver (Figs 5B and S4F), and a higher expression of the anti-inflammatory IL-4 by specific immune cells present in eWAT of gliadin-fed animals (Figs 5C and S6B). The IL-4-expressing immune cells were mainly of an innate-like T cell phenotype involving γδ T cells and NKT cells, but also included the memory-promoting αβ T cells (Fig 5C). The gliadin-fed mice also showed higher *Il33* expression in the eWAT (Fig 5E), which is in line with the idea that IL-33 favors an anti-inflammatory response [39]. However, adipose tissue T cells displayed an increased pro-inflammatory phenotype with higher levels of IFN-γ and IL-17A (Figs 5D, S6A and S6C). This suggests the presence of several different types of antigens in eWAT. T cells react against different antigenic products (glycolipids, phospho- and peptide antigens), and some of the antigens could be constituted by peptides originating from gliadin breakdown, bacterial lipopolysaccharide, intact bacteria, or perhaps lipid products derived from rearrangement of the lipid pool within the adipose tissue. In line with this, translocation of intestinal bacteria to systemic circulation, mesenteric adipose tissue and mesenteric lymph nodes is known to increase with a high fat diet [40], and a recent study of lard and fish oil based diets indicates that dietary lipid composition affects toll-like receptor-based activation within eWAT [41]. The heterogeneous

inflammatory response in eWAT illustrates that multiple negative as well as counter-regulatory positive effects might be induced by gliadin. Similarly, pro- as well as anti-inflammatory characteristics have previously been shown in local adipose tissue depots in Crohn's Disease [42].

The observed altered immune responses in eWAT may be related to the reduced size of adipocytes in the gliadin-fed animals. This is supported by the negative correlation between *Il33* expression and adipocyte cell size (Fig 6A), which is in line with previous reports showing that IL-33 administration leads to reduced adipocyte size [43], while IL-33 deficiency increases adipocyte size [39]. In a situation of energy surplus, limited adipose tissue expandability can be regarded as an adverse event, because an increased proportion of adipocytes with reduced capacity for lipid storage will lead to enhanced ectopic lipid deposition [44], as reflected in more hepatic lipid accumulation in the gliadin-fed mice (Fig 1C and 1D), and the strong negative correlation between adipocyte size and hepatic total lipid droplet area (Fig 1H). Additionally, relative eWAT weight was negatively correlated to hepatic total lipid droplet area but positively to adipocyte size, further substantiating that adipose tissue dysregulation was causing hepatic steatosis. In humans, a larger proportion of small adipocytes is found in insulin resistant than in insulin sensitive obese subjects [45]. Thus, the gliadin-disturbed adipocyte potential for lipid accumulation may contribute to systemic metabolic dysregulation, manifested as a gliadin-induced increase of HbA1c and HOMA-IR.

Analysis of the specific effects of bacterial group abundances within the intestinal microbial community (Fig 2F and 2G) revealed that nine weeks of gliadin intake caused a more than ten-fold lower abundance of *Lactobacillus*, which is generally considered to be a beneficial member of the gut bacterial community. Furthermore, gliadin intake caused more than ten-fold higher abundances of *Clostridium* XI, *Dorea* and Coriobacteriaceae than seen in mice on a gliadin-free diet after 23 weeks. Strains belonging to *Clostridium* XI, including also the opportunistic pathogen *C. difficile*, are associated with compromised health [46]. *Dorea* spp. are found to be overrepresented in irritable bowel syndrome patients [47,48], and patients with non-alcoholic fatty liver disease [49].

Coriobacteriaceae spp. have repeatedly been shown to be involved in host lipid metabolism [50,51], and many bacteria within this group are considered as opportunistic pathogens [50]. Given these previously reported adverse functions of particularly *Clostridium* XI, *Dorea* and Coriobacteriaceae, which were all increased by the gliadin intake, we regard the observed changes to be dysbiotic, and speculate that they might be involved in some of the detrimental metabolic responses identified after gliadin intake. In this regard it is also notable that *Akkermansia* was increased ten-fold in colonic samples from gliadin-fed animals (Fig 2G). This genus has been linked to beneficial effects on metabolic health and inflammatory processes, and is suggested to be a biomarker for a healthy intestine [52–54].

Akkermansia muciniphila is specifically known for its ability to use mucins secreted from the epithelium as a sole carbon source [55]. As we observed lower expression of mucin genes in the ileum of gliadin-fed animals (Fig 3) and a generally disturbed ileal environment, we speculate that a

disturbed ileal mucosal turnover in these mice may have led to increased accessibility of mucins in colonic lumen, increasing the relative abundance of *Akkermansia* in this compartment (Fig 2G). In addition, several microbial metabolites involved in neuronal signaling and S-adenosyl methionine metabolism were altered by gliadin intake and associated with metabolic phenotypes (Fig 6A), and therefore may represent the mechanistic explanation for gliadin-disturbed host-microbiota homeostasis.

The gliadin content in feed adopted in this study was comparable to that in regular wheat flour, while the fat content was extremely high compared to that in an average human meal. Although our observations were done in mice and thus not necessarily translatable to humans, our findings suggest that the adverse effects of an obesogenic diet also in a human setting may be aggravated by consumption of gliadin-containing foods.

EXPERIMENTAL PROCEDURES

Animals

All animal experiments were approved by the Danish Animal Experiments Inspectorate and carried out in accordance with existing Danish guidelines for experimental animal welfare. Forty male C57BL/6NTac mice (Taconic, Lille Skensved, Denmark) aged four weeks at arrival were housed two by two and fed ad libitum with a standard rodent diet Altromin 1324 (Altromin, Lage, Germany) from Week 0. Experimental diets were fed starting from Week 1. For selected analyses, only one mouse from each cage was used. Details of the experiments are provided in the supplemental procedures.

Biochemical Measurements

Blood HbA1c, blood glucose, insulin, alanine aminotransferase and cytokines in plasma, as well as intestinal SCFAs were measured as described in the supplemental material. Hepatic triglycerides were assessed by gas chromatography mass spectrometry as previously described [56].

Urine Metabolome Profiling

Urine samples were analyzed by UPLC-MS as described in the supplemental procedures.

16S rRNA Gene Sequencing and Analysis

Sequencing of the V3 region of bacterial 16S rRNA genes was performed with the Ion Torrent PGM system as previously described [57]. The average sequencing depth was 55,147 reads. Taxonomy was assigned with the Ribosomal Database Project Classifier v2.10.1 [58], and OTUs were generated with UPARSE v8.0.1623 [59], sorting 8,869,069 quality-filtered sequences into 2,932 OTUs at 97% sequence homology. Bioinformatical processing was performed with Qiime v1.8.0 [60]. Further details are given in the supplemental procedures. The microbial DNA sequences encoding bacterial 16S rRNA V3

regions reported in this paper have been deposited in the Sequence Read Archive (SRA) under the accession number SRP063048.

Gene Expression Analysis by Real Time RT-PCR

Expression of gut barrier function related genes was determined by SYBR green based real time PCR (S5 Table), and the remaining analyses were based on Taqman primers and probes (S6 Table). Further details are given in the supplemental procedures.

Flow Cytometry

Anaesthetized mice were subject to intracardial perfusion with PBS followed by tissue harvest and preparation of single cell suspensions, which were analyzed as described in the supplemental procedures.

Histology

Liver and adipose tissues were stained with Hematoxylin and Eosin stain, and subjected to histological analysis as described in supplemental procedures.

Statistical Analysis

Student's t test, Mann-Whitney test or other statistics were used as described in figure legends. P or q values below 0.05 were considered significant. Further details of statistical analysis are provided in the supplmental procedures.

AUTHOR CONTRIBUTIONS

L.Z., M.I.B., C.H.F.H., A.K.H., S.B., L.I.H. and T.R.L. conceived and designed the study. L.Z., D.A., H.M.R., N.B.D.S., I.D.R., C.S. and H.L.F. performed the experiments. L.Z., D.A., K.K., H.M.R., S.B., and T.R.L. wrote the paper. All authors participated in analysis and interpretation of the data, and commented on the manuscript.

ACKNOWLEDGMENTS

This work was funded by the Danish Council for Independent Research (Mobility Grant no. 09-067572) and by the "Gut, Grain & Greens (3G) Center", supported by the Innovation Fund Denmark (Grant no. 11-116163/ 0603-00487B). The authors thank Helene Farlov, Mette Nelander, Jannie Felskov Agersten, Lisbeth Buus Rosholm, Bodil Madsen and Kate Vina Vibefeldt for excellent technical assistance. Ellen Gerd Christensen is thanked for help with primer design and Marie Kragh for help with antibody design. Additionally, Linfei Zhou is acknowledged for help with data analysis.

ADDITIONAL INFORMATION

The authors have no competing financial interests to declare.

REFERENCES

1. Sapone, A. *et al.* Spectrum of gluten-related disorders: consensus on new nomenclature and classification. *BMC Med.* **10,** 13 (2012).
2. Biesiekierski, J. R. *et al.* Gluten causes gastrointestinal symptoms in subjects without celiac disease: a double-blind randomized placebo-controlled trial. *Am. J. Gastroenterol.* **106,** 508–14; quiz 515 (2011).
3. Vazquez-Roque, M. I. *et al.* A controlled trial of gluten-free diet in patients with irritable bowel syndrome-diarrhea: effects on bowel frequency and intestinal function. *Gastroenterology* **144,** 903–911.e3 (2013).
4. Pastore, M.-R. *et al.* Six months of gluten-free diet do not influence autoantibody titers, but improve insulin secretion in subjects at high risk for type 1 diabetes. *J. Clin. Endocrinol. Metab.* **88,** 162–5 (2003).
5. Hansen, C. H. F. *et al.* A maternal gluten-free diet reduces inflammation and diabetes incidence in the offspring of NOD mice. *Diabetes* **63,** 2821–32 (2014).
6. Funda, D. P., Kaas, A., Bock, T., Tlaskalova-Hogenova, H. & Buschard, K. Gluten-free diet prevents diabetes in NOD mice. *Diabetes Metab Res.Rev.* **15,** 323–327 (1999).
7. Soares, F. L. P. *et al.* Gluten-free diet reduces adiposity, inflammation and insulin resistance associated with the induction of PPAR-alpha and PPAR-gamma expression. *J. Nutr. Biochem.* **24,** 1105–11 (2013).
8. Freire, R. H. *et al.* Wheat gluten intake increases weight gain and adiposity associated with reduced thermogenesis and energy expenditure in an animal model of obesity. *Int. J. Obes. (Lond).* (2015). doi:10.1038/ijo.2015.204
9. Rune, I. *et al.* Modulating the Gut Microbiota Improves Glucose Tolerance, Lipoprotein Profile and Atherosclerotic Plaque Development in ApoE-Deficient Mice. *PLoS One* **11,** e0146439 (2016).
10. Haupt-Jorgensen, M., Buschard, K., Hansen, A. K., Josefsen, K. & Antvorskov, J. C. Gluten-free diet increases beta-cell volume and improves glucose tolerance in an animal model of type 2 diabetes. *Diabetes. Metab. Res. Rev.* (2016). doi:10.1002/dmrr.2802
11. Shan, L. *et al.* Identification and Analysis of Multivalent Proteolytically Resistant Peptides from Gluten: Implications for Celiac Sprue. *J. Proteome Res.* **4,** 1732–1741 (2005).
12. Fasano, A. Zonulin and its regulation of intestinal barrier function: the biological door to inflammation, autoimmunity, and cancer. *Physiol. Rev.* **91,** 151–75 (2011).
13. Lammers, K. M. *et al.* Gliadin induces an increase in intestinal permeability and zonulin release by binding to the chemokine receptor CXCR3. *Gastroenterology* **135,** 194–204.e3 (2008).
14. Sander, G. R., Cummins, A. G., Henshall, T. & Powell, B. C. Rapid disruption of intestinal barrier function by gliadin involves altered expression of apical junctional proteins. *FEBS Lett.* **579,** 4851–5 (2005).
15. Hooper, L. V, Littman, D. R. & Macpherson, A. J. Interactions between the microbiota and the immune system. *Science* **336,** 1268–73 (2012).
16. Tremaroli, V. & Bäckhed, F. Functional interactions between the gut microbiota and host metabolism. *Nature* **489,** 242–9 (2012).
17. Qin, J. *et al.* A metagenome-wide association study of gut microbiota in type 2 diabetes.

Nature **490,** 55–60 (2012).

18. Caminero, A. *et al.* Diversity of the cultivable human gut microbiome involved in gluten metabolism: isolation of microorganisms with potential interest for coeliac disease. *FEMS Microbiol. Ecol.* **88,** 309–19 (2014).

19. Caminero, A. *et al.* Duodenal Bacteria From Patients With Celiac Disease and Healthy Subjects Distinctly Affect Gluten Breakdown and Immunogenicity. *Gastroenterology* **151,** 670–83 (2016).

20. Lindfors, K. *et al.* Live probiotic Bifidobacterium lactis bacteria inhibit the toxic effects induced by wheat gliadin in epithelial cell culture. *Clin. Exp. Immunol.* **152,** 552–8 (2008).

21. Laparra, J. M. & Sanz, Y. Bifidobacteria inhibit the inflammatory response induced by gliadins in intestinal epithelial cells via modifications of toxic peptide generation during digestion. *J. Cell. Biochem.* **109,** 801–7 (2010).

22. Di Cagno, R. *et al.* Proteolysis by sourdough lactic acid bacteria: effects on wheat flour protein fractions and gliadin peptides involved in human cereal intolerance. *Appl. Environ. Microbiol.* **68,** 623–33 (2002).

23. De Palma, G., Nadal, I., Collado, M. C. & Sanz, Y. Effects of a gluten-free diet on gut microbiota and immune function in healthy adult human subjects. *Br. J. Nutr.* **102,** 1154–60 (2009).

24. Caminero, A. *et al.* A gluten metabolism study in healthy individuals shows the presence of faecal glutenasic activity. *Eur. J. Nutr.* **51,** 293–9 (2012).

25. Brestoff, J. R. & Artis, D. Immune regulation of metabolic homeostasis in health and disease. *Cell* **161,** 146–60 (2015).

26. Bieghs, V. & Trautwein, C. The innate immune response during liver inflammation and metabolic disease. *Trends Immunol.* **34,** 446–52 (2013).

27. Wu, D. *et al.* Eosinophils Sustain Adipose Alternatively Activated Macrophages Associated with Glucose Homeostasis. *Science (80-.).* **332,** 243–247 (2011).

28. Mithieux, G. A novel function of intestinal gluconeogenesis: central signaling in glucose and energy homeostasis. *Nutrition* **25,** 881–4 (2009).

29. Norris, V., Molina, F. & Gewirtz, A. T. Hypothesis: bacteria control host appetites. *J. Bacteriol.* **195,** 411–6 (2013).

30. Ferla, M. P. & Patrick, W. M. Bacterial methionine biosynthesis. *Microbiology* **160,** 1571–84 (2014).

31. Anstee, Q. M. & Day, C. P. S-adenosylmethionine (SAMe) therapy in liver disease: a review of current evidence and clinical utility. *J. Hepatol.* **57,** 1097–109 (2012).

32. Mato, J. M. & Lu, S. C. Role of S-adenosyl-L-methionine in liver health and injury. *Hepatology* **45,** 1306–12 (2007).

33. Borcherding, D. C. *et al.* Dopamine receptors in human adipocytes: expression and functions. *PLoS One* **6,** e25537 (2011).

34. Levite, M. *et al.* Dopamine interacts directly with its D3 and D2 receptors on normal human T cells, and activates beta1 integrin function. *Eur. J. Immunol.* **31,** 3504–12 (2001).

35. Wernstedt Asterholm, I. *et al.* Adipocyte inflammation is essential for healthy adipose tissue expansion and remodeling. *Cell Metab.* **20,** 103–18 (2014).

36. Sanz, Y., Olivares, M., Moya-Pérez, Á. & Agostoni, C. Understanding the role of gut

microbiome in metabolic disease risk. *Pediatr. Res.* **77,** 236–44 (2015).

37. Huang, X.-Z., Zhu, L.-B., Li, Z.-R. & Lin, J. Bacterial colonization and intestinal mucosal barrier development. *World J. Clin. Pediatr.* **2,** 46–53 (2013).

38. Ghoshal, S., Witta, J., Zhong, J., de Villiers, W. & Eckhardt, E. Chylomicrons promote intestinal absorption of lipopolysaccharides. *J. Lipid Res.* **50,** 90–7 (2009).

39. Brestoff, J. R. *et al.* Group 2 innate lymphoid cells promote beiging of white adipose tissue and limit obesity. *Nature* **519,** 242–6 (2015).

40. Amar, J. *et al.* Intestinal mucosal adherence and translocation of commensal bacteria at the early onset of type 2 diabetes: molecular mechanisms and probiotic treatment. *EMBO Mol. Med.* **3,** 559–72 (2011).

41. Caesar, R., Tremaroli, V., Kovatcheva-Datchary, P., Cani, P. D. & Bäckhed, F. Crosstalk between Gut Microbiota and Dietary Lipids Aggravates WAT Inflammation through TLR Signaling. *Cell Metab.* **22,** 658–668 (2015).

42. Jung, S. H. *et al.* The role of adipose tissue-associated macrophages and T lymphocytes in the pathogenesis of inflammatory bowel disease. *Cytokine* **61,** 459–68 (2013).

43. Miller, A. M. *et al.* Interleukin-33 induces protective effects in adipose tissue inflammation during obesity in mice. *Circ. Res.* **107,** 650–8 (2010).

44. Virtue, S. & Vidal-Puig, A. Adipose tissue expandability, lipotoxicity and the Metabolic Syndrome — An allostatic perspective. *Biochim. Biophys. Acta - Mol. Cell Biol. Lipids* **1801,** 338–349 (2010).

45. McLaughlin, T. *et al.* Enhanced proportion of small adipose cells in insulin-resistant vs insulin-sensitive obese individuals implicates impaired adipogenesis. *Diabetologia* **50,** 1707–15 (2007).

46. Rajilić-Stojanović, M. & de Vos, W. M. The first 1000 cultured species of the human gastrointestinal microbiota. *FEMS Microbiol. Rev.* **38,** 996–1047 (2014).

47. Rajilić-Stojanović, M. *et al.* Global and deep molecular analysis of microbiota signatures in fecal samples from patients with irritable bowel syndrome. *Gastroenterology* **141,** 1792–801 (2011).

48. Saulnier, D. M. *et al.* Gastrointestinal microbiome signatures of pediatric patients with irritable bowel syndrome. *Gastroenterology* **141,** 1782–91 (2011).

49. Raman, M. *et al.* Fecal Microbiome and Volatile Organic Compound Metabolome in Obese Humans With Nonalcoholic Fatty Liver Disease. *Clin. Gastroenterol. Hepatol.* **11,** 868–875.e3 (2013).

50. Clavel, T. *et al.* Intestinal microbiota in metabolic diseases: from bacterial community structure and functions to species of pathophysiological relevance. *Gut Microbes* **5,** 544–51 (2014).

51. Martínez, I. *et al.* Diet-induced alterations of host cholesterol metabolism are likely to affect the gut microbiota composition in hamsters. *Appl. Environ. Microbiol.* **79,** 516–24 (2013).

52. Belzer, C. & de Vos, W. M. Microbes inside--from diversity to function: the case of Akkermansia. *ISME J.* **6,** 1449–58 (2012).

53. Everard, A. *et al.* Cross-talk between Akkermansia muciniphila and intestinal epithelium controls diet-induced obesity. *Proc. Natl. Acad. Sci. U. S. A.* **110,** 9066–71 (2013).

54. Hansen, C. H. F. *et al.* Early life treatment with vancomycin propagates Akkermansia muciniphila and reduces diabetes incidence in the NOD mouse. *Diabetologia* **55,** 2285–94 (2012).

55. Derrien, M. *et al.* Mucin-bacterial interactions in the human oral cavity and digestive tract. *Gut Microbes* **1,** 254–268 (2010).

56. Pedersen, M. H., Lauritzen, L. & Hellgren, L. I. Fish oil combined with SCFA synergistically prevent tissue accumulation of NEFA during weight loss in obese mice. *Br. J. Nutr.* **106,** 1449–56 (2011).

57. Tulstrup, M. V.-L. *et al.* Antibiotic Treatment Affects Intestinal Permeability and Gut Microbial Composition in Wistar Rats Dependent on Antibiotic Class. *PLoS One* **10,** e0144854 (2015).

58. Wang, Q., Garrity, G. M., Tiedje, J. M. & Cole, J. R. Naive Bayesian classifier for rapid assignment of rRNA sequences into the new bacterial taxonomy. *Appl. Environ. Microbiol.* **73,** 5261–7 (2007).

59. Edgar, R. C. UPARSE: highly accurate OTU sequences from microbial amplicon reads. *Nat. Methods* **10,** 996–8 (2013).

60. Caporaso, J. G. *et al.* QIIME allows analysis of high-throughput community sequencing data. *Nat. Methods* **7,** 335–6 (2010).

61. Benjamini, Y. & Hochberg, Y. Controlling the False Discovery Rate - a Practical and Powerful Approach to Multiple Testing. *J. R. Stat. Soc. Ser. B-Methodological* **57,** 289–300 (1995).

FIGURE LEGENDS

Fig 1. Gliadin affected glucose homeostasis, liver lipid accumulation and adipocyte size in eWAT.
Mice were fed 60% HFD with gliadin (Gliadin+, n = 20) or without (Gliadin-, n = 19) for 23 weeks and subjected to measurements of metabolic features at termination. Panel A shows HbA1c levels in blood, B HOMA-IR, C percentage of lipid droplet area of the liver (each data point represents the average of six squares of 40,000 μm^2), D hematoxylin- and eosin-stained hepatic sections, E the median adipocyte size of four different adipose tissue sections, F the relative frequency of the mean adipocyte size of four different adipose tissue sections, G hematoxylin- and eosin-stained eWAT sections, and H Spearman correlation between adipocyte size in eWAT and total lipid droplet area in the liver. In panels A-C and E, horizontal lines represent the means, while asterisks represent statistically significant differences between the two feeding groups (*p < 0.05, **p < 0.01, unpaired t test or Mann-Whitney test). In panel F, asterisks represent false discovery rate (FDR) corrected p values [61] from multiple t tests (*q<0.05, ***q<0.001). In panel H, the p value and r coefficient of Spearman correlation are listed, and the linear regression line is shown. In panels C-H, n = 9-10 mice per group. See also S1 Fig and S2 Table.

Fig 2. Gliadin intake altered intestinal microbial composition and activity.
Microbiota analysis was performed on fecal samples collected from 10-11 cages per group at Week 0, 9, 16 and 23 and on terminal ileal, cecal and colonic luminal samples (n = 18-20 mice per group) by sequencing the V3 region of bacterial 16S rRNA genes followed by PCoA on unweighted UniFrac distances (A-E). Panel A shows that the HFD feeding, initiated after Week 0, affected the first coordinate (PC1) of the microbiota composition, while B shows the longitudinal effect of Gliadin feeding. Panels C-E show that Gliadin feeding affected the ileal, cecal and colonic microbiota in samples obtained at termination. In panel A, asterisks represent significant differences between the two groups (*p < 0.05, **p < 0.01, unpaired t test or Mann-Whitney test), while in panels B-E, p values are listed for differential clustering (ADONIS test) and R^2 values represent the percentages of variation explained by gliadin intake. NCD designates Normal Chow Diet, HFD designates High-Fat Diet. Heatmaps (F-G) show the relative abundances of OTUs differing between the Gliadin- and Gliadin+ mice in fecal and intestinal samples. Taxonomy is reported at the lowest identifiable level. OTUs that are more abundant in the Gliadin+ group are indicated in red and those less abundant in blue. Statistical comparison of the two groups was done by 10,000 times of permutation ; p values represent fraction of times that permuted differences assessed by Welch's t test were greater than or equal to real differences, and were adjusted by FDR correction [61] (*q < 0.05, **q < 0.01). Boxes surrounding asterisks indicate > ten-fold differences in OTU abundances between the two groups. For fecal samples, only OTUs that have at least one q < 0.02 are shown. Short chain fatty acid concentrations in cecum (H) and hepatic mRNA levels of bile acid related genes (I) were measured at termination (n = 9-10 non-fasted mice per group). The mean of each group is shown by a horizontal line. Asterisks represent statistically significant differences (*p < 0.05, unpaired t test or Mann-Whitney test). See also S2 Fig.

Fig 3. Gliadin intake decreased ileal expression of barrier function related genes.
Ileal tissue mRNA levels of barrier function related genes in Gliadin- (n = 19) and Gliadin+ (n = 20) mice at termination. The mean of each group is shown by a horizontal line. Asterisks represent statistically significant differences between the two groups (*p < 0.05, **p < 0.01, ***p < 0.001, unpaired t test or Mann-Whitney test). See also S3 Fig.

Fig 4. Gliadin affected the metabolic signature of urine.
UPLC-MS-based global profiling of metabolites in urine from non-fasted Gliadin- (n = 15) and Gliadin+ (n = 13) mice at termination. PCA was performed on urine metabolome in positive (ESI+) and negative ionization (ESI-) mode respectively (A). Data were log-transformed and mean-centered. P values originate from Hotelling's T^2 test with 100,000 permutations. The heatmap (B) shows the normalized relative abundances of urinary metabolites differing between Gliadin- and Gliadin+ mice (q < 0.05, unpaired t test with Welch's correction followed by FDR correction). Blue colors indicate relative abundances below and red indicate relative abundances above the mean of all samples. Data were log-transformed and the most abundant ion representing each metabolite was included. See also S3 Table.

Fig 5. Gliadin altered the composition of immune cells in liver and inflammatory phenotype in eWAT.
Composition of immune cells measured by flow cytometry of samples from Gliadin- and Gliadin+ non-fasted mice (n = 6-10 per group) at termination. Panel A shows total CD45+ leukocyte numbers in Peyer's patches (PP), mesenteric lymph nodes (MLN), liver and eWAT. Horizontal lines represent means. Panel B shows a PCA of the major immune cell subsets in liver, C of the median fluorescence intensity of IL-4 in IL-4 expressing immune cells in eWAT, and D of the median fluorescence intensity of intracellular IFN-γ, IL-4 and IL-17A production in T and NK cells in eWAT. Panel E shows *Il33* mRNA levels in eWAT. In panels A and E, the mean of each group is shown by a horizontal line, while asterisks represent statistically significant differences (*p < 0.05, unpaired t test or Mann-Whitney test). In panels B-D, data were center log ratio-transformed and mean-centered, and p values originate from Hotelling's T^2 test with 100,000 permutations. See also S4-S6 Fig and S4 Table.

Fig 6. Combining Alterations in Microbiome and Host Metabolic Features.
Panel A shows an interaction network built from Spearman correlations (p < 0.05) between four metabolic endpoints (hepatic lipid droplets, adipocyte size, HbA1c and HOMA-IR) and other parameters, including discriminating bacterial groups (q < 0.05) and microbial α diversity, discriminating urinary metabolites (q < 0.05), cecal SCFAs and other host parameters. Each node represents a parameter and the size of the node reflects the number of correlating nodes. Nodes associated with 3-4 key metabolic endpoints are shown by names instead of numbers. Lines represent correlations, and are colored red for positive and blue for negative correlations, while their thickness represents the strength of the correlation. Nodes are positioned using an organic layout in Cytoscape, and only nodes that connect to more than 2 other nodes are shown. 1, ileal *Clostridium*

XI; 2, ileal *Enterorhabdus*; 3, cecal microbiota Shannon index; 4, ileal *Tjp1*; 5, ileal *Ocln*; 6, ileal *Cdh1*; 7, hepatic *Bacs*; 8, eWAT *Dgat1*; 9, circulating IL-1β; 10, circulating IFN-γ; 11*, acetylhomoserine; 12*, 2-[3-carboxy-3-(methylammonio)propyl]-histidine; 13, sugar alcohol (6-carbon); 14, unidentified glucoside; 15, N-acetyl-leucyl-isoleucine; 16, prolyl-proline; 17, trihydroxydecanoic acid/analog; 18, U148.1332; 19, U222.0441; 20, U301.212; 21, U344.2276; 22, U359.2176. Specific correlations (B-H) based on biological hypotheses generated by observations of Gliadin+ and Gliadin- samples. The individual hypotheses are described in the section 'Combining Alterations in Microbiome and Host Metabolic Features'. P values and r coefficients of Spearman correlations are listed, and linear regression lines are shown. See also S7 Fig.

Fig 7. Schematic representation of the hypothesized effects of gliadin intake in a HFD-fed host.
Ingested gliadin is not fully degraded by host digestive enzymes, leaving biologically active peptides in the gut. Gliadin peptides may directly affect gut barrier integrity, but can also alter the gut microbial composition and activities, thereby disturbing particularly the ileal gut barrier function. HFD together with increased gut permeability facilitate the influx of substances including microbial metabolites from the gut lumen to systemic circulation, affecting the metabolism and immune responses in extra-intestinal organs, including altered lipid metabolism and immune cell composition in the liver as well as altered inflammatory phenotype in the eWAT. The expandability of adipocytes in the eWAT is disturbed, resulting in reduced capacity for lipid storage and lipid spill-over to other organs, which subsequently causes increased hepatic lipid accumulation and increased systemic insulin resistance. Alterations in metabolism all over the body are reflected in the urine metabolite profile. Parameters higher in Gliadin+ mice are indicated in red, while parameters lower in Gliadin+ mice are indicated in green.

FIGURES

Fig. 1

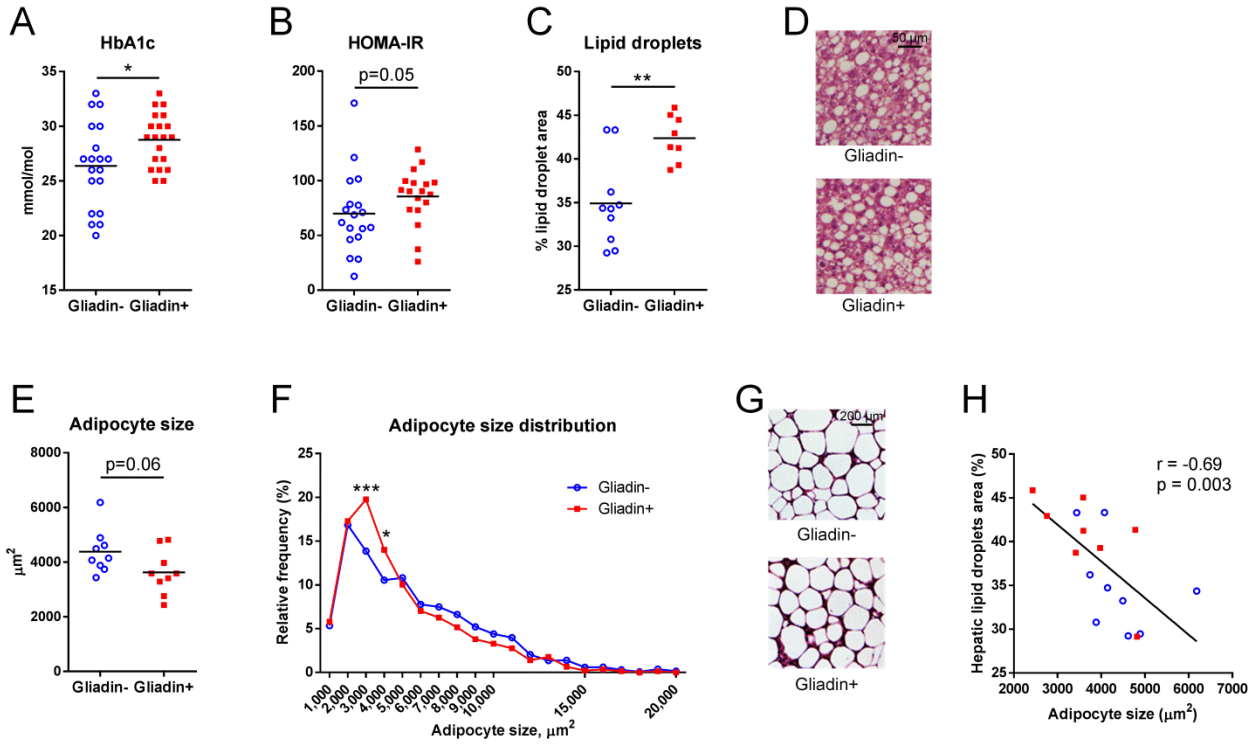

Fig. 2

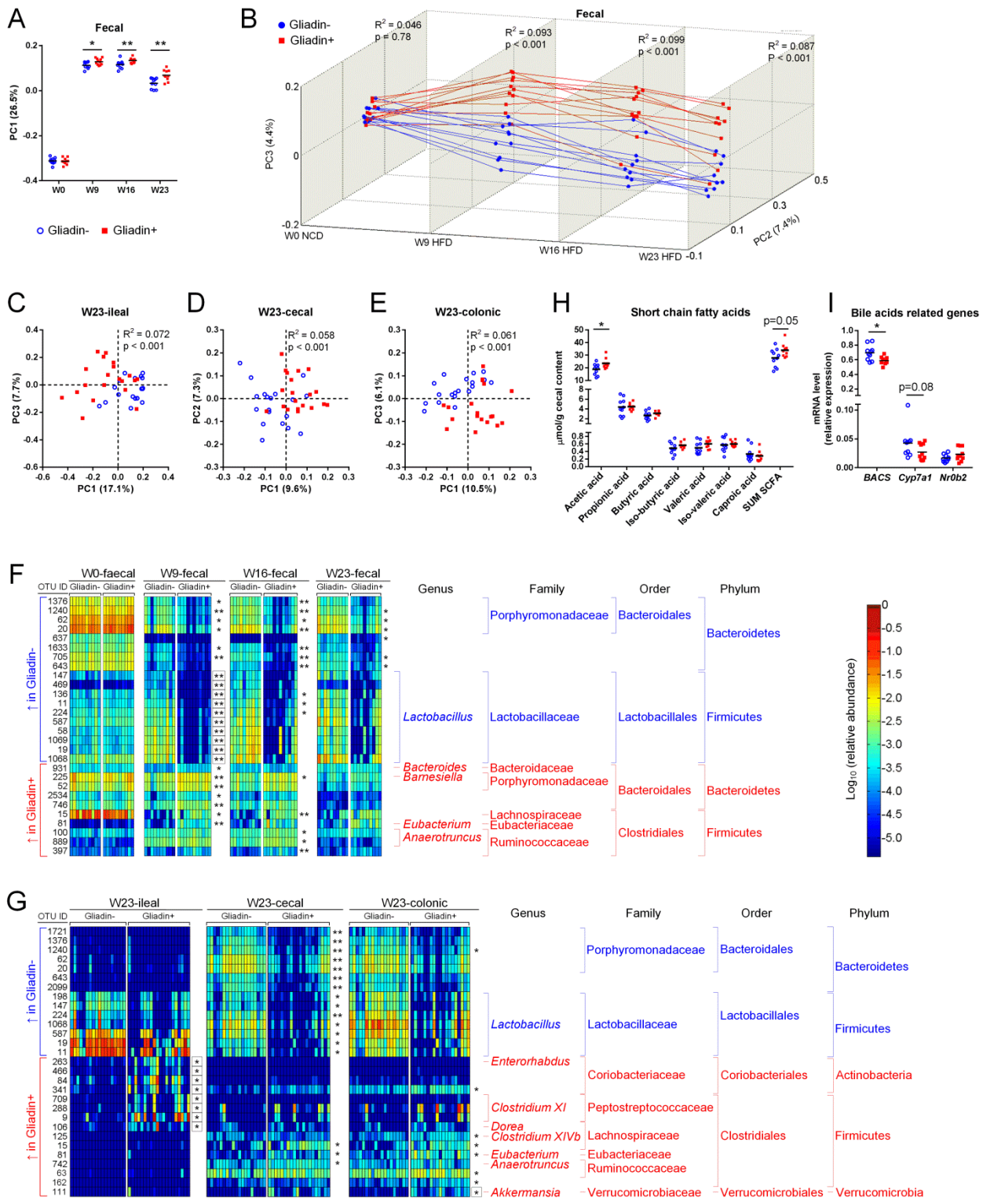
A
Fecal
PC1 (26.5%)
W0
W9
W16
W23
Gliadin-
Gliadin+
B
Fecal
Gliadin-
Gliadin+
R² = 0.046
p = 0.78
R² = 0.093
p < 0.001
R² = 0.099
p < 0.001
R² = 0.087
P < 0.001
PC3 (4.4%)
W0 NCD
W9 HFD
W16 HFD
W23 HFD
PC2 (7.4%)
C
W23-ileal
R² = 0.072
p < 0.001
PC3 (7.7%)
PC1 (17.1%)
D
W23-cecal
R² = 0.058
p < 0.001
PC2 (7.3%)
PC1 (9.6%)
E
W23-colonic
R² = 0.061
p < 0.001
PC3 (6.1%)
PC1 (10.5%)
H
Short chain fatty acids
p=0.05
µmol/g cecal content
Acetic acid
Propionic acid
Butyric acid
Iso-butyric acid
Valeric acid
Iso-valeric acid
Caproic acid
SUM SCFA
I
Bile acids related genes
p=0.08
mRNA level (relative expression)
BACS
Cyp7a1
Nr0b2
F
W0-faecal
W9-fecal
W16-fecal
W23-fecal
OTU ID
Gliadin-
Gliadin+
↑ in Gliadin-
↑ in Gliadin+
Genus
Family
Order
Phylum
Porphyromonadaceae
Bacteroidales
Bacteroidetes
Lactobacillus
Lactobacillaceae
Lactobacillales
Firmicutes
Bacteroides
Barnesiella
Bacteroidaceae
Porphyromonadaceae
Bacteroidales
Bacteroidetes
Eubacterium
Anaerotruncus
Lachnospiraceae
Eubacteriaceae
Ruminococcaceae
Clostridiales
Firmicutes
Log10 (relative abundance)
G
W23-ileal
W23-cecal
W23-colonic
Enterorhabdus
Coriobacteriaceae
Coriobacteriales
Actinobacteria
Clostridium XI
Peptostreptococcaceae
Dorea
Clostridium XIVb
Lachnospiraceae
Clostridiales
Firmicutes
Akkermansia
Verrucomicrobiaceae
Verrucomicrobiales
Verrucomicrobia

Fig. 3

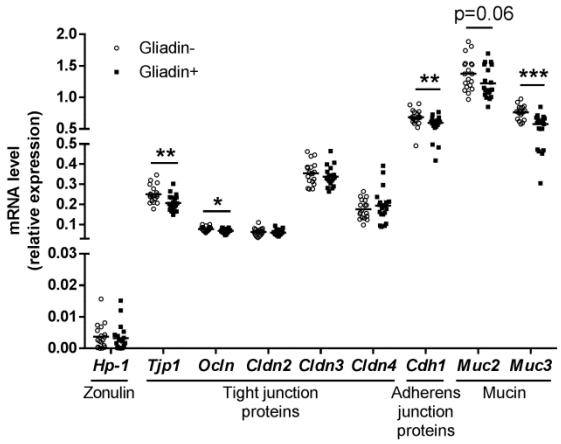
p=0.06
Gliadin-
Gliadin+
mRNA level
(relative expression)
2.0
1.5
1.0
0.5
0.4
0.3
0.2
0.1
0.03
0.02
0.01
0.00
**
*
**
***
Hp-1
Tjp1
Ocln
Cldn2
Cldn3
Cldn4
Cdh1
Muc2
Muc3
Zonulin
Tight junction proteins
Adherens junction proteins
Mucin

Fig. 4

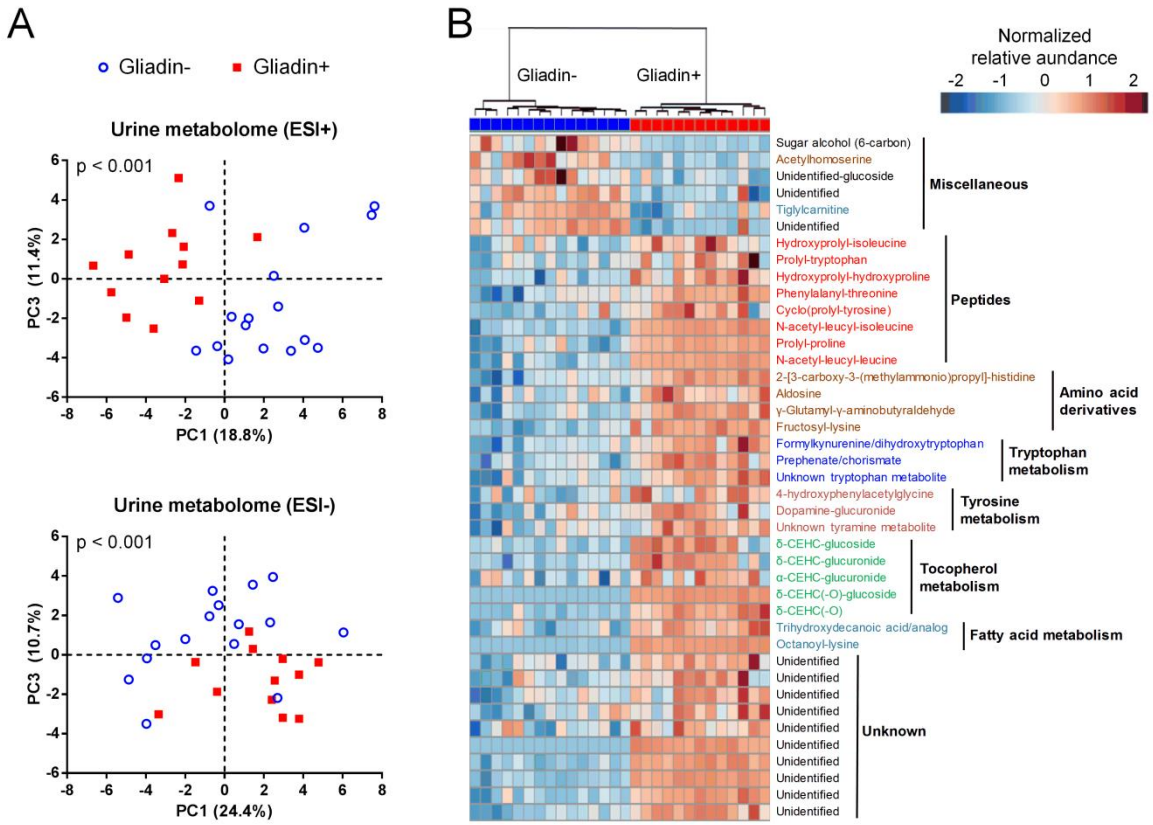
A
Gliadin-
Gliadin+
Urine metabolome (ESI+)
p < 0.001
PC3 (11.4%)
PC1 (18.8%)
Urine metabolome (ESI-)
p < 0.001
PC3 (10.7%)
PC1 (24.4%)
B
Gliadin-
Gliadin+
Normalized
relative aundance
-2
-1
0
1
2
Sugar alcohol (6-carbon)
Acetylhomoserine
Unidentified-glucoside
Unidentified
Tiglylcarnitine
Unidentified
Miscellaneous
Hydroxyprolyl-isoleucine
Prolyl-tryptophan
Hydroxyprolyl-hydroxyproline
Phenylalanyl-threonine
Cyclo(prolyl-tyrosine)
N-acetyl-leucyl-isoleucine
Prolyl-proline
N-acetyl-leucyl-leucine
Peptides
2-[3-carboxy-3-(methylammonio)propyl]-histidine
Aldosine
γ-Glutamyl-γ-aminobutyraldehyde
Fructosyl-lysine
Amino acid derivatives
Formylkynurenine/dihydroxytryptophan
Prephenate/chorismate
Unknown tryptophan metabolite
Tryptophan metabolism
4-hydroxyphenylacetylglycine
Dopamine-glucuronide
Unknown tyramine metabolite
Tyrosine metabolism
δ-CEHC-glucoside
δ-CEHC-glucuronide
α-CEHC-glucuronide
δ-CEHC(-O)-glucoside
δ-CEHC(-O)
Tocopherol metabolism
Trihydroxydecanoic acid/analog
Octanoyl-lysine
Fatty acid metabolism
Unidentified
Unidentified
Unidentified
Unidentified
Unidentified
Unidentified
Unidentified
Unidentified
Unidentified
Unidentified
Unknown

Fig. 5

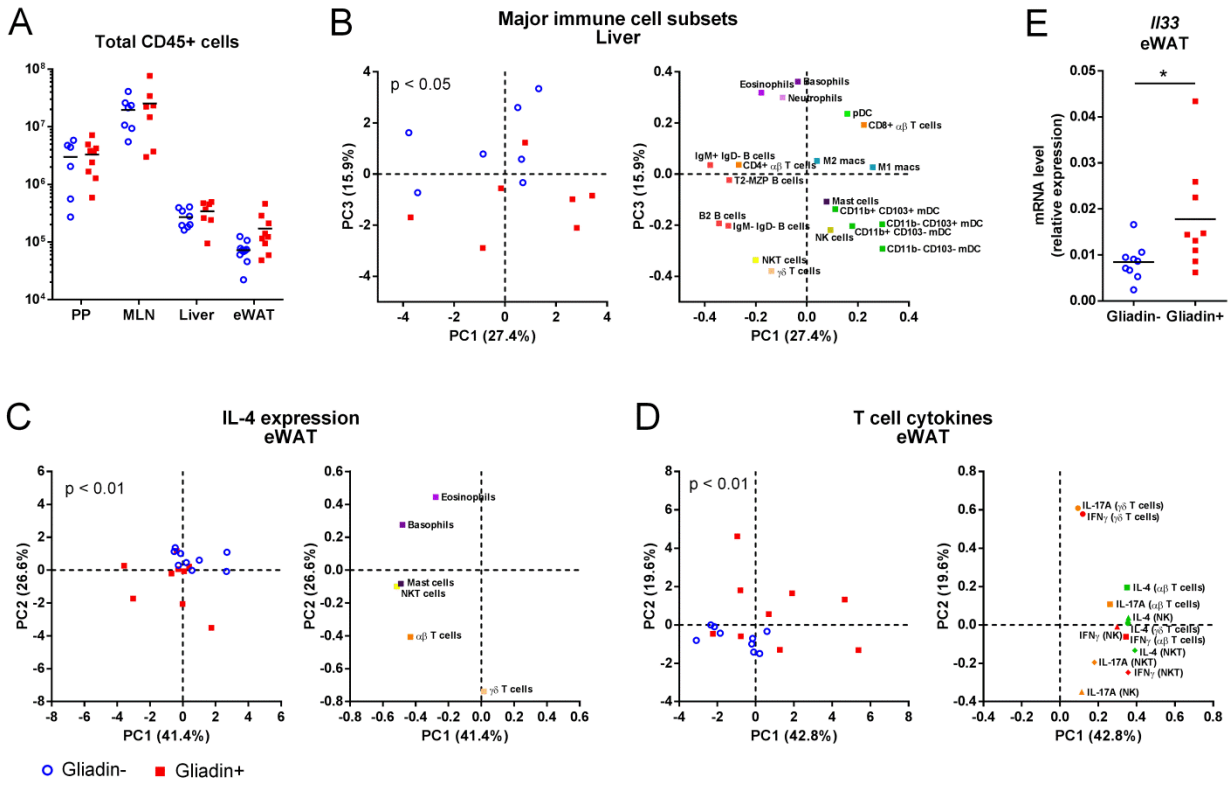
A
Total CD45+ cells
PP
MLN
Liver
eWAT
B
Major immune cell subsets
Liver
p < 0.05
PC1 (27.4%)
PC3 (15.9%)
Eosinophils
Basophils
Neutrophils
pDC
CD8+ αβ T cells
IgM+ IgD- B cells
CD4+ αβ T cells
M2 macs
M1 macs
T2-MZP B cells
Mast cells
CD11b+ CD103+ mDC
B2 B cells
IgM- IgD- B cells
CD11b- CD103+ mDC
CD11b+ CD103- mDC
NK cells
CD11b- CD103- mDC
NKT cells
γδ T cells
E
Il33
eWAT
mRNA level
(relative expression)
Gliadin-
Gliadin+
C
IL-4 expression
eWAT
p < 0.01
PC1 (41.4%)
PC2 (26.6%)
Eosinophils
Basophils
Mast cells
NKT cells
αβ T cells
γδ T cells
Gliadin-
Gliadin+
D
T cell cytokines
eWAT
p < 0.01
PC1 (42.8%)
PC2 (19.6%)
IL-17A (γδ T cells)
IFNγ (γδ T cells)
IL-4 (αβ T cells)
IL-17A (αβ T cells)
IL-4 (NK)
IL-4 (γδ T cells)
IFNγ (NK)
IFNγ (αβ T cells)
IL-4 (NKT)
IL-17A (NKT)
IFNγ (NKT)
IL-17A (NK)

Fig. 6

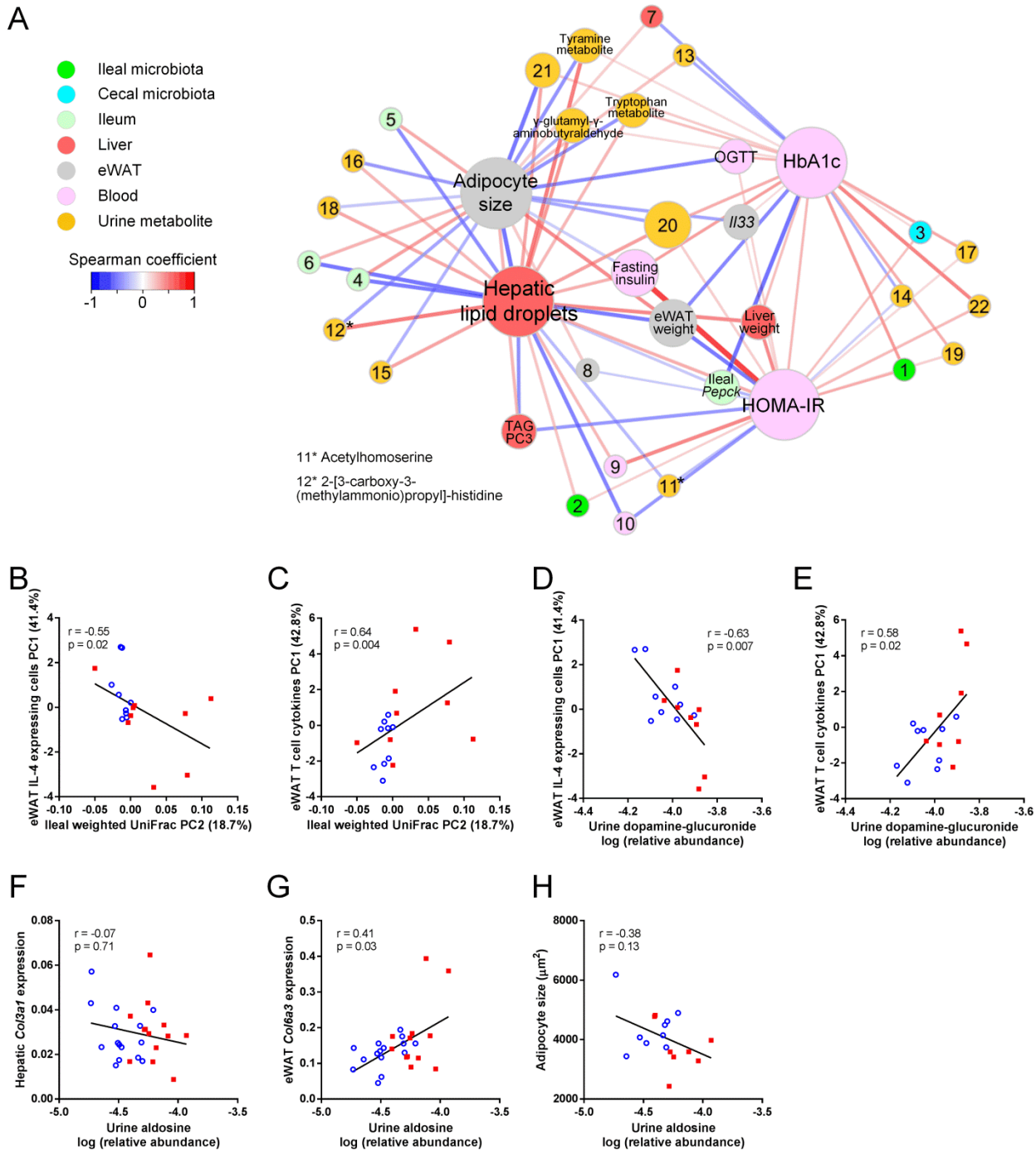
A
Ileal microbiota
Cecal microbiota
Ileum
Liver
eWAT
Blood
Urine metabolite
Spearman coefficient
-1
0
1
Tyramine metabolite
Tryptophan metabolite
γ-glutamyl-γ-aminobutyraldehyde
Adipocyte size
OGTT
HbA1c
Il33
Fasting insulin
Hepatic lipid droplets
eWAT weight
Liver weight
Ileal Pepck
HOMA-IR
TAG PC3
11* Acetylhomoserine
12* 2-[3-carboxy-3-(methylammonio)propyl]-histidine
B
eWAT IL-4 expressing cells PC1 (41.4%)
r = -0.55
p = 0.02
Ileal weighted UniFrac PC2 (18.7%)
C
eWAT T cell cytokines PC1 (42.8%)
r = 0.64
p = 0.004
Ileal weighted UniFrac PC2 (18.7%)
D
eWAT IL-4 expressing cells PC1 (41.4%)
r = -0.63
p = 0.007
Urine dopamine-glucuronide log (relative abundance)
E
eWAT T cell cytokines PC1 (42.8%)
r = 0.58
p = 0.02
Urine dopamine-glucuronide log (relative abundance)
F
Hepatic Col3a1 expression
r = -0.07
p = 0.71
Urine aldosine log (relative abundance)
G
eWAT Col6a3 expression
r = 0.41
p = 0.03
Urine aldosine log (relative abundance)
H
Adipocyte size (µm²)
r = -0.38
p = 0.13
Urine aldosine log (relative abundance)

Fig. 7

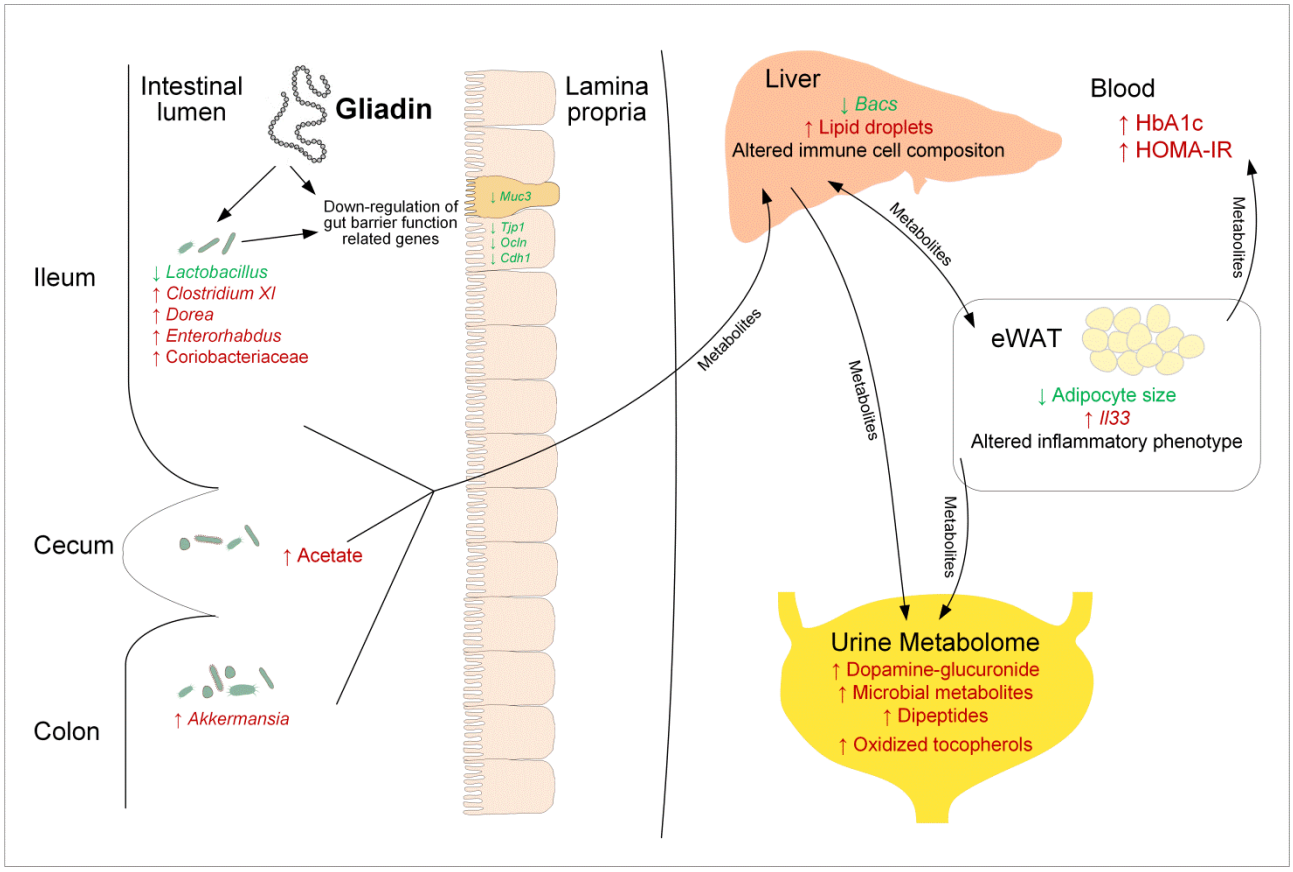
Intestinal lumen
Gliadin
Lamina propria
Down-regulation of gut barrier function related genes
↓ Muc3
↓ Tjp1
↓ Ocln
↓ Cdh1
Ileum
↓ Lactobacillus
↑ Clostridium XI
↑ Dorea
↑ Enterorhabdus
↑ Coriobacteriaceae
Cecum
↑ Acetate
Colon
↑ Akkermansia
Liver
↓ Bacs
↑ Lipid droplets
Altered immune cell compositon
Blood
↑ HbA1c
↑ HOMA-IR
eWAT
↓ Adipocyte size
↑ Il33
Altered inflammatory phenotype
Urine Metabolome
↑ Dopamine-glucuronide
↑ Microbial metabolites
↑ Dipeptides
↑ Oxidized tocopherols
Metabolites
Metabolites
Metabolites
Metabolites
Metabolites

SUPPLEMENTARY TABLES AND FIGURES CONTENT:

S1 Fig.

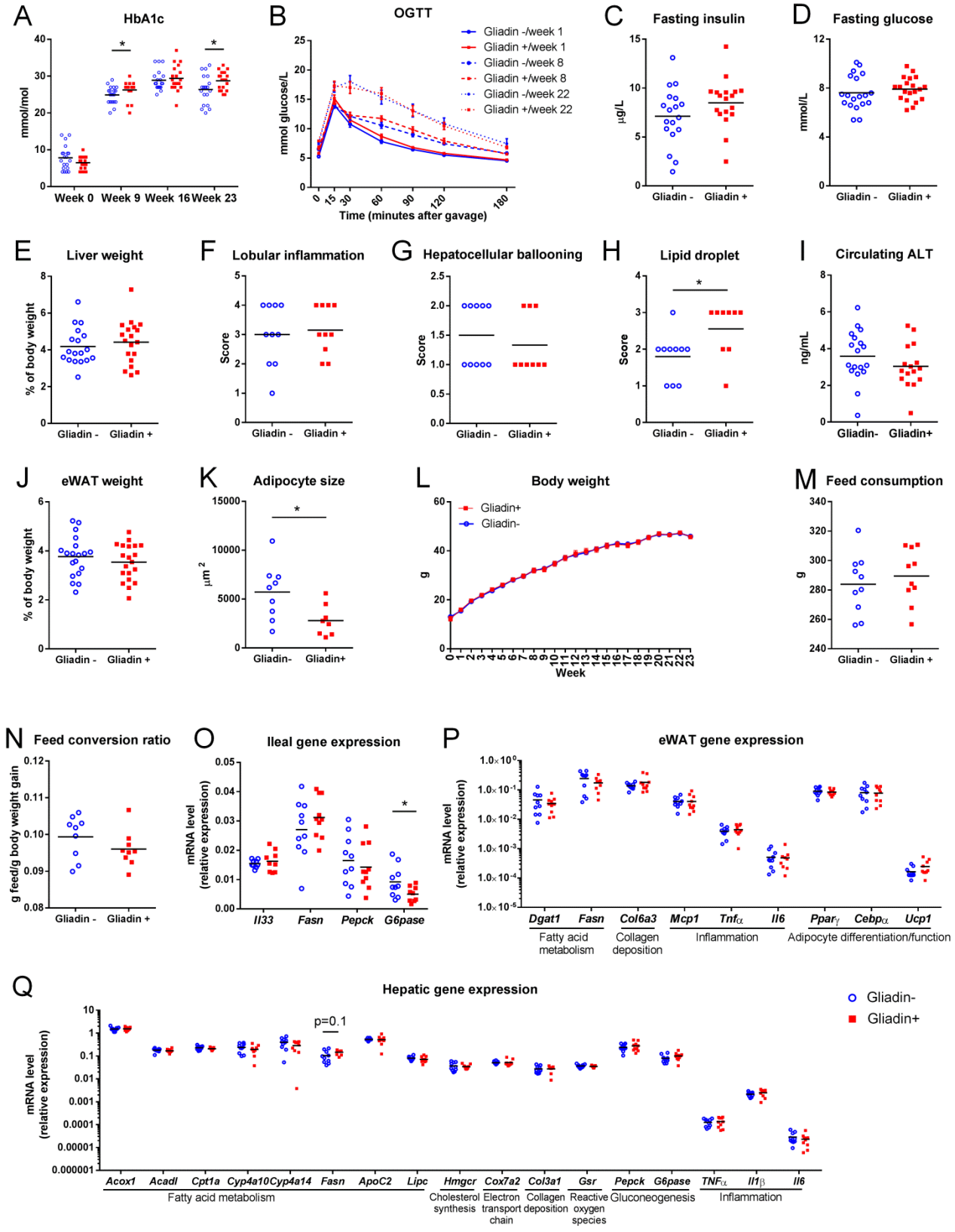
A
HbA1c
mmol/mol
Week 0
Week 9
Week 16
Week 23
B
OGTT
mmol glucose/L
Time (minutes after gavage)
Gliadin -/week 1
Gliadin +/week 1
Gliadin -/week 8
Gliadin +/week 8
Gliadin -/week 22
Gliadin +/week 22
C
Fasting insulin
µg/L
D
Fasting glucose
mmol/L
E
Liver weight
% of body weight
F
Lobular inflammation
Score
G
Hepatocellular ballooning
Score
H
Lipid droplet
Score
I
Circulating ALT
ng/mL
J
eWAT weight
% of body weight
K
Adipocyte size
µm 2
L
Body weight
Gliadin+
Gliadin-
g
Week
M
Feed consumption
g
N
Feed conversion ratio
g feed/g body weight gain
O
Ileal gene expression
mRNA level (relative expression)
Il33
Fasn
Pepck
G6pase
P
eWAT gene expression
mRNA level (relative expression)
Dgat1
Fasn
Col6a3
Mcp1
Tnfα
Il6
Pparγ
Cebpα
Ucp1
Fatty acid metabolism
Collagen deposition
Inflammation
Adipocyte differentiation/function
Q
Hepatic gene expression
mRNA level (relative expression)
p=0.1
Acox1
Acadl
Cpt1a
Cyp4a10
Cyp4a14
Fasn
ApoC2
Lipc
Hmgcr
Cox7a2
Col3a1
Gsr
Pepck
G6pase
TNFα
Il1β
Il6
Fatty acid metabolism
Cholesterol synthesis
Electron transport chain
Collagen deposition
Reactive oxygen species
Gluconeogenesis
Inflammation
Gliadin-
Gliadin+

S1 Fig. Additional host metabolic features and gene expression analyses.
Panel A shows HbA1c levels in blood at Week 0, 9, 16 and 23, and Panel B shows OGTT at Week 1, 8 and 22. Panel C shows plasma levels of fasting insulin and D fasting glucose at Week 22. Panel E shows relative liver weight at Week 23, F-H show non-alcoholic steatohepatitis parameters including hepatic lobular inflammation, hepatocellular ballooning and lipid droplet size as evaluated by three independent pathologists, and I show plasma levels of alanine transaminase (ALT). Panel J shows relative eWAT weight at termination, and K shows eWAT adipocyte size measured using ImageJ software. Panel L shows body weight development during the 23 weeks of dietary intervention. Panels M-N show Cage-wise (n = 10-11 cages per group) measurements of total feed consumption per mouse and feed conversion ratio assessed by feed consumption per body weight gain. Panels O-Q show mRNA levels of multiple genes in ileum, eWAT and liver. In panels A-E, I, J and L, n = 16-20 mice per group, while in panels F-H, K and O-Q, n = 9-10 non-fasted mice per group. In panels A, C-K and M-Q, the mean of each group is shown by a horizontal line. In panels B and L, data are shown as mean ± SEM. Asterisks represent significant differences between the two groups (*$p < 0.05$, unpaired t test or Mann-Whitney test).

S2 Fig.

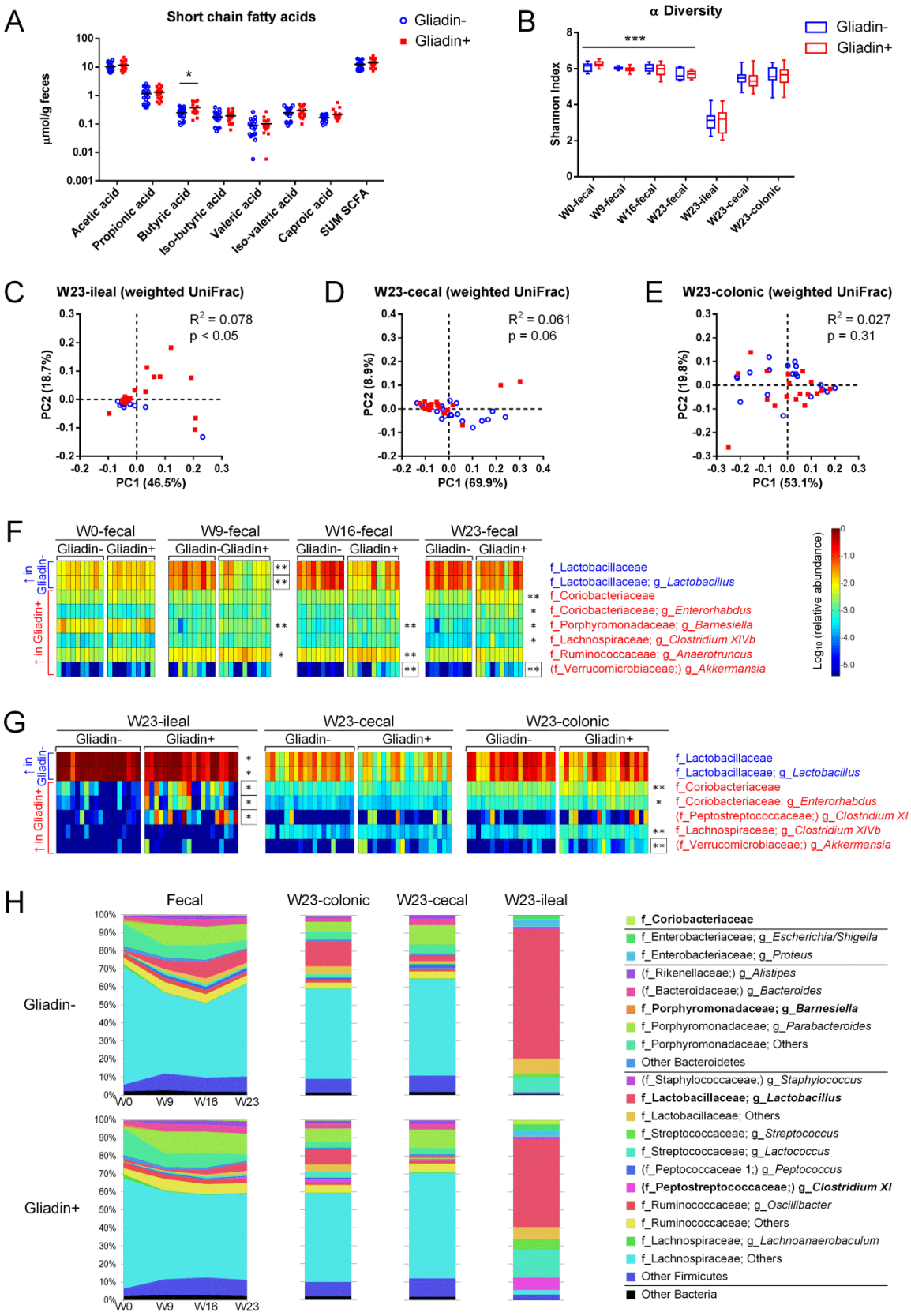
A
Short chain fatty acids
Gliadin-
Gliadin+
µmol/g feces
Acetic acid
Propionic acid
Butyric acid
Iso-butyric acid
Valeric acid
Iso-valeric acid
Caproic acid
SUM SCFA
B
α Diversity
Shannon Index
W0-fecal
W9-fecal
W16-fecal
W23-fecal
W23-ileal
W23-cecal
W23-colonic
C
W23-ileal (weighted UniFrac)
R² = 0.078
p < 0.05
PC2 (18.7%)
PC1 (46.5%)
D
W23-cecal (weighted UniFrac)
R² = 0.061
p = 0.06
PC2 (8.9%)
PC1 (69.9%)
E
W23-colonic (weighted UniFrac)
R² = 0.027
p = 0.31
PC2 (19.8%)
PC1 (53.1%)
F
W0-fecal
W9-fecal
W16-fecal
W23-fecal
↑ in Gliadin-
↑ in Gliadin+
f_Lactobacillaceae
f_Lactobacillaceae; g_Lactobacillus
f_Coriobacteriaceae
f_Coriobacteriaceae; g_Enterorhabdus
f_Porphyromonadaceae; g_Barnesiella
f_Lachnospiraceae; g_Clostridium XlVb
f_Ruminococcaceae; g_Anaerotruncus
(f_Verrucomicrobiaceae;) g_Akkermansia
Log10 (relative abundance)
G
W23-ileal
W23-cecal
W23-colonic
f_Lactobacillaceae
f_Lactobacillaceae; g_Lactobacillus
f_Coriobacteriaceae
f_Coriobacteriaceae; g_Enterorhabdus
(f_Peptostreptococcaceae;) g_Clostridium XI
f_Lachnospiraceae; g_Clostridium XlVb
(f_Verrucomicrobiaceae;) g_Akkermansia
H
Fecal
W23-colonic
W23-cecal
W23-ileal
Gliadin-
Gliadin+
W0
W9
W16
W23
f_Coriobacteriaceae
f_Enterobacteriaceae; g_Escherichia/Shigella
f_Enterobacteriaceae; g_Proteus
(f_Rikenellaceae;) g_Alistipes
(f_Bacteroidaceae;) g_Bacteroides
f_Porphyromonadaceae; g_Barnesiella
f_Porphyromonadaceae; g_Parabacteroides
f_Porphyromonadaceae; Others
Other Bacteroidetes
(f_Staphylococcaceae;) g_Staphylococcus
f_Lactobacillaceae; g_Lactobacillus
f_Lactobacillaceae; Others
f_Streptococcaceae; g_Streptococcus
f_Streptococcaceae; g_Lactococcus
(f_Peptococcaceae 1;) g_Peptococcus
(f_Peptostreptococcaceae;) g_Clostridium XI
f_Ruminococcaceae; g_Oscillibacter
f_Ruminococcaceae; Others
f_Lachnospiraceae; g_Lachnoanaerobaculum
f_Lachnospiraceae; Others
Other Firmicutes
Other Bacteria

S2 Fig. Gliadin intake alters intestinal microbial composition and activity.
Panel A shows short chain fatty acid concentrations in feces of mice at termination (n = 19-20 mice per group). The mean of each group is shown by a horizontal line. Asterisks represent significant differences between the two groups (*p < 0.05, unpaired t test or Mann-Whitney test). Panel B shows microbial alpha diversity in feces (n = 10-11 cages per group) at Week 0, 9, 16 and 23, and in terminal samples from ileum, cecum and colon (n = 18-20 mice per group). Whiskers of the box plot represent the min and max values of each data set. Asterisks represent significant differences between fecal samples at Week 0, 9, 16 and 23 (***p < 0.001, two-way ANOVA).
Panels C-E show microbial beta diversity assessed by PCoA on weighted UniFrac distances between terminal samples from ileum, cecum and colon, respectively (n = 18-20 mice per group). P values are listed for differential clustering (ADONIS test), and R^2 values represent the percentage of variation explained by gliadin intake.
Panels F-G are heatmaps showing the relative abundances of bacterial groups differing between the Gliadin- and Gliadin+ mice. Bacteria that are more abundant in the Gliadin+ group are indicated in red and those less abundant in blue. Statistical comparison between the two groups was done by 10,000 times of permutation; p values represent fraction of times that permuted differences assessed by Welch's t test were greater than or equal to real differences, and were adjusted by FDR correction (*q < 0.05, **q < 0.01). Boxes surrounding asterisks indicate > ten-fold differences in abundances of bacterial groups between the two groups.
Panel H shows relative abundances of predominant bacterial groups. Groups that are differentially abundant between the Gliadin- and Gliadin+ mice are indicated in bold. In panels F-H, analyses were based on the phylotype data table. Taxonomies are reported at the lowest identifiable level, indicated by the letter preceding the underscore: f, family and g, genus. If one genus represents more than 90% of the family it belongs to, only the genus is shown, and the corresponding family is indicated with brackets.

S3 Fig.

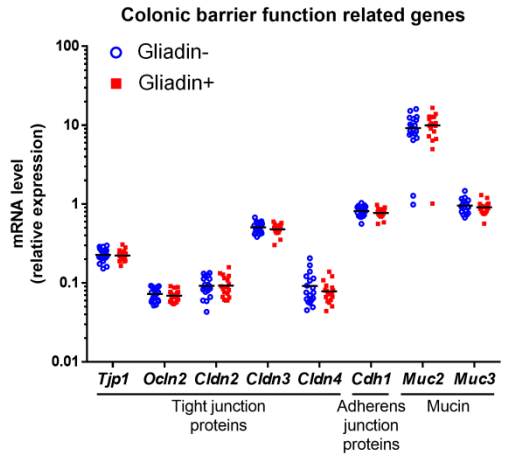

S3 Fig. Gliadin intake did not affect colonic expression of barrier function related genes.
The mean of each group (n = 19-20) is shown by a horizontal line. Asterisks indicate significant differences between the two groups (*$p < 0.05$, unpaired t test).

S4 Fig.

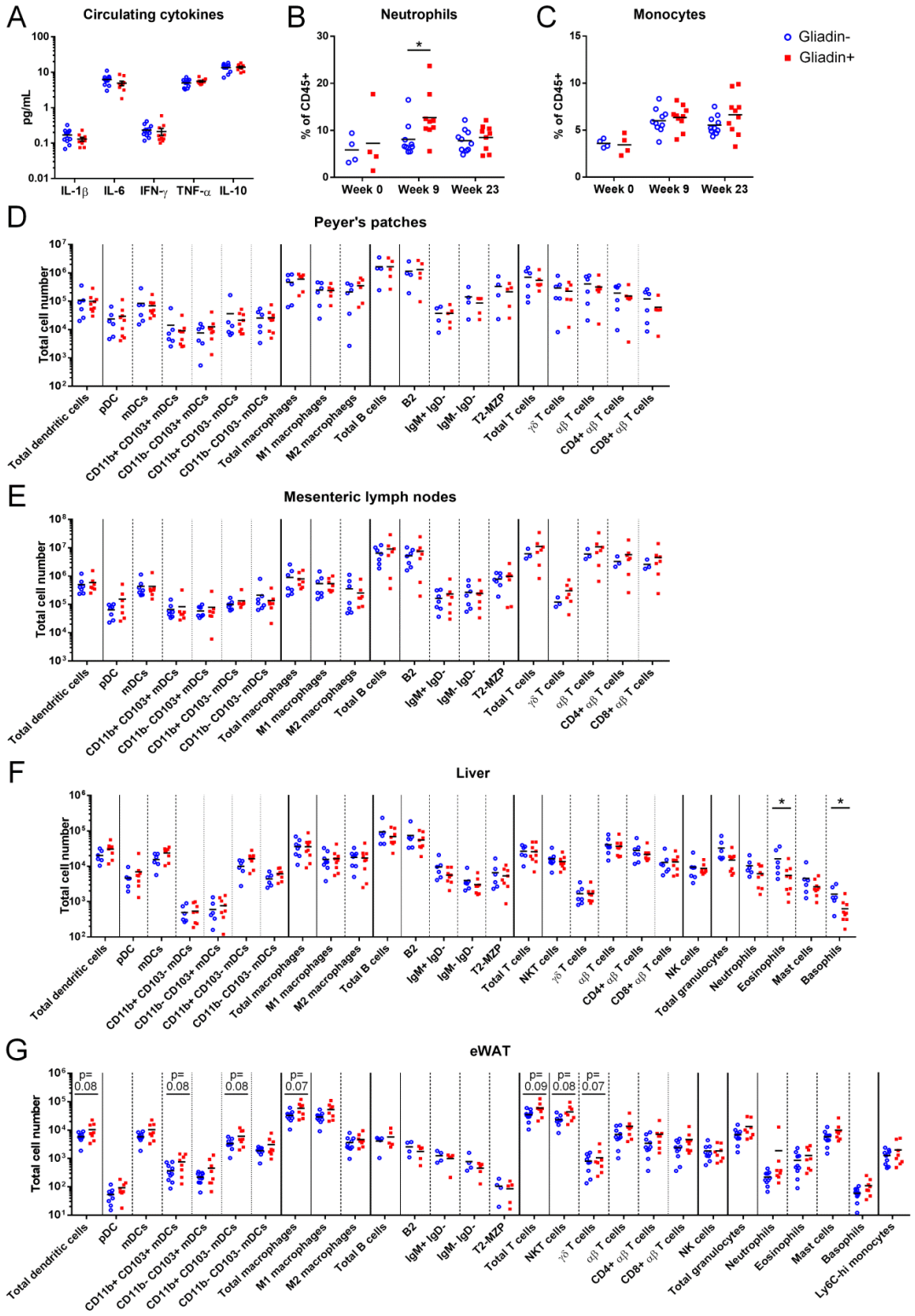

Panel A shows pro-inflammatory and anti-inflammatory cytokines in plasma measured by ELISA at Week 23 (n = 10 non-fasted mice). Panels B and C show frequencies of neutrophils and monocytes in peripheral blood (n = 4 pooled samples per group at Week 0, and n = 10 mice per group at Week 9 and 23). Panels D-G show total numbers of major immune cell subsets in Peyer's patches, mesenteric lymph nodes, liver and eWAT at Week 23 (n = 7-10 non-fasted mice per group). Asterisks represent significant differences between the two groups (*p < 0.05, unpaired t test or Mann-Whitney test).

S5 Fig.

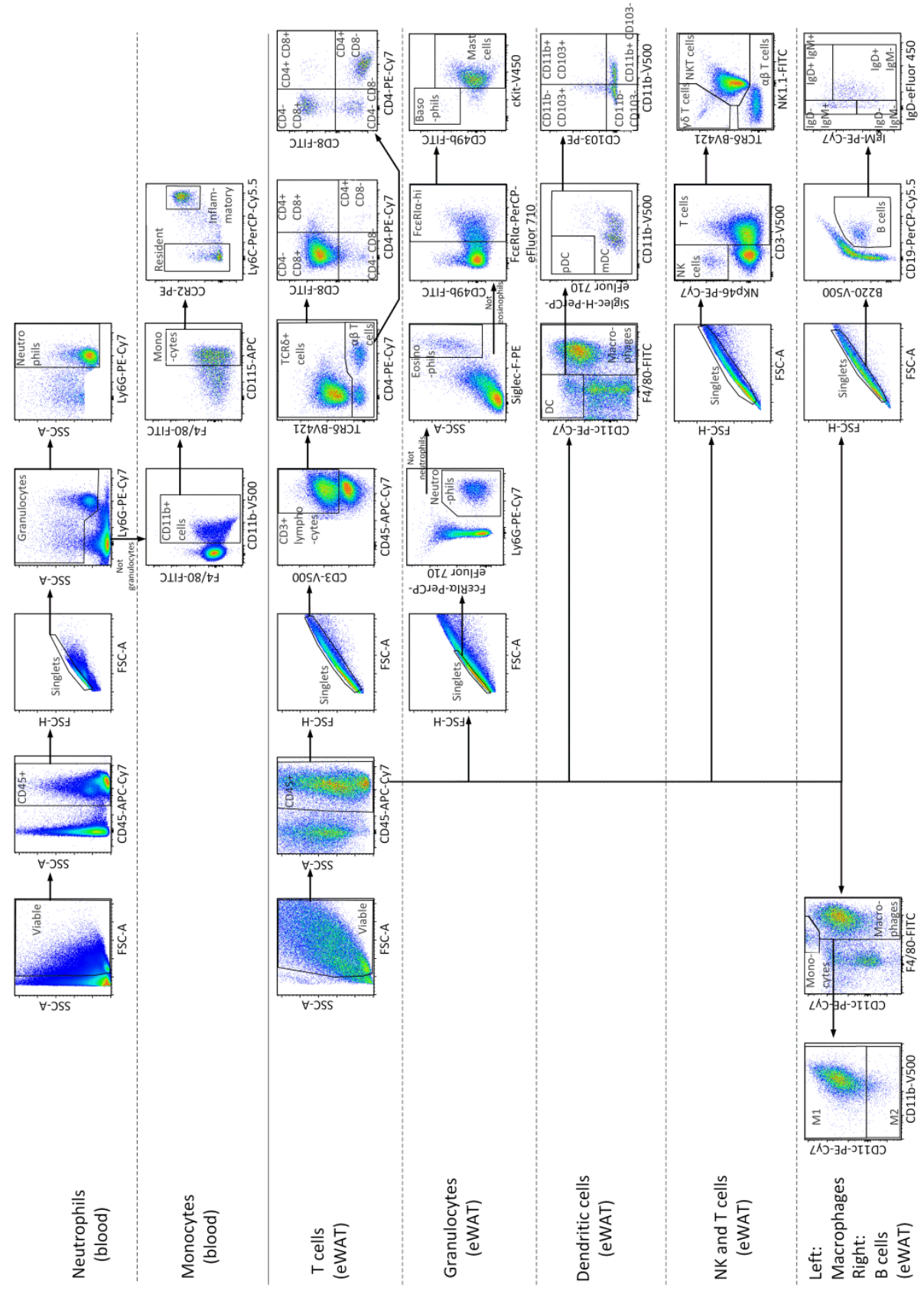
Neutrophils (blood)
Monocytes (blood)
T cells (eWAT)
Granulocytes (eWAT)
Dendritic cells (eWAT)
NK and T cells (eWAT)
Left: Macrophages Right: B cells (eWAT)
Viable
FSC-A
SSC-A
CD45+
CD45-APC-Cy7
Singlets
FSC-H
Granulocytes
Ly6G-PE-Cy7
Not granulocytes
Neutro phils
CD11b+ cells
F4/80-FITC
CD11b-V500
Mono -cytes
CD115-APC
Resident
Inflam- matory
CCR2-PE
Ly6C-PerCP-Cy5.5
CD3+ lympho -cytes
CD3-V500
αβ T cells
TCRδ-BV421
CD4-PE-Cy7
CD4+ CD8+
CD4+ CD8-
CD4- CD8+
CD4- CD8-
CD8-FITC
Not neutrophils
Eosino -phils
Siglec-F-PE
FcεRIα-hi
FcεRIα-PerCP-eFluor 710
Baso -phils
Mast cells
cKit-V450
CD49b-FITC
Not eosinophils
DC
pDC
mDC
Siglec-H-PerCP-eFluor 710
CD11c-PE-Cy7
CD11b+ CD103+
CD11b- CD103+
CD11b+ CD103-
CD103-PE
F4/80-FITC
Macro- phages
NK cells
T cells
NKp46-PE-Cy7
CD3-V500
NKT cells
γδ T cells
αβ T cells
TCRδ-BV421
NK1.1-FITC
B cells
CD19-PerCP-Cy5.5
B220-V500
IgD+ IgM+
IgD+ IgM-
IgD- IgM+
IgD- IgM-
IgM-PE-Cy7
IgD-eFluor 450
Mono- cytes
Macro- phages
M1
M2

S5 Fig. Representative flow cytometry gating strategy.
Subsets of macrophages, dendritic cells, B cells, T cells, NK/NKT cells, and granulocytes in eWAT as well as neutrophils and monocytes in blood are shown.

S6 Fig.

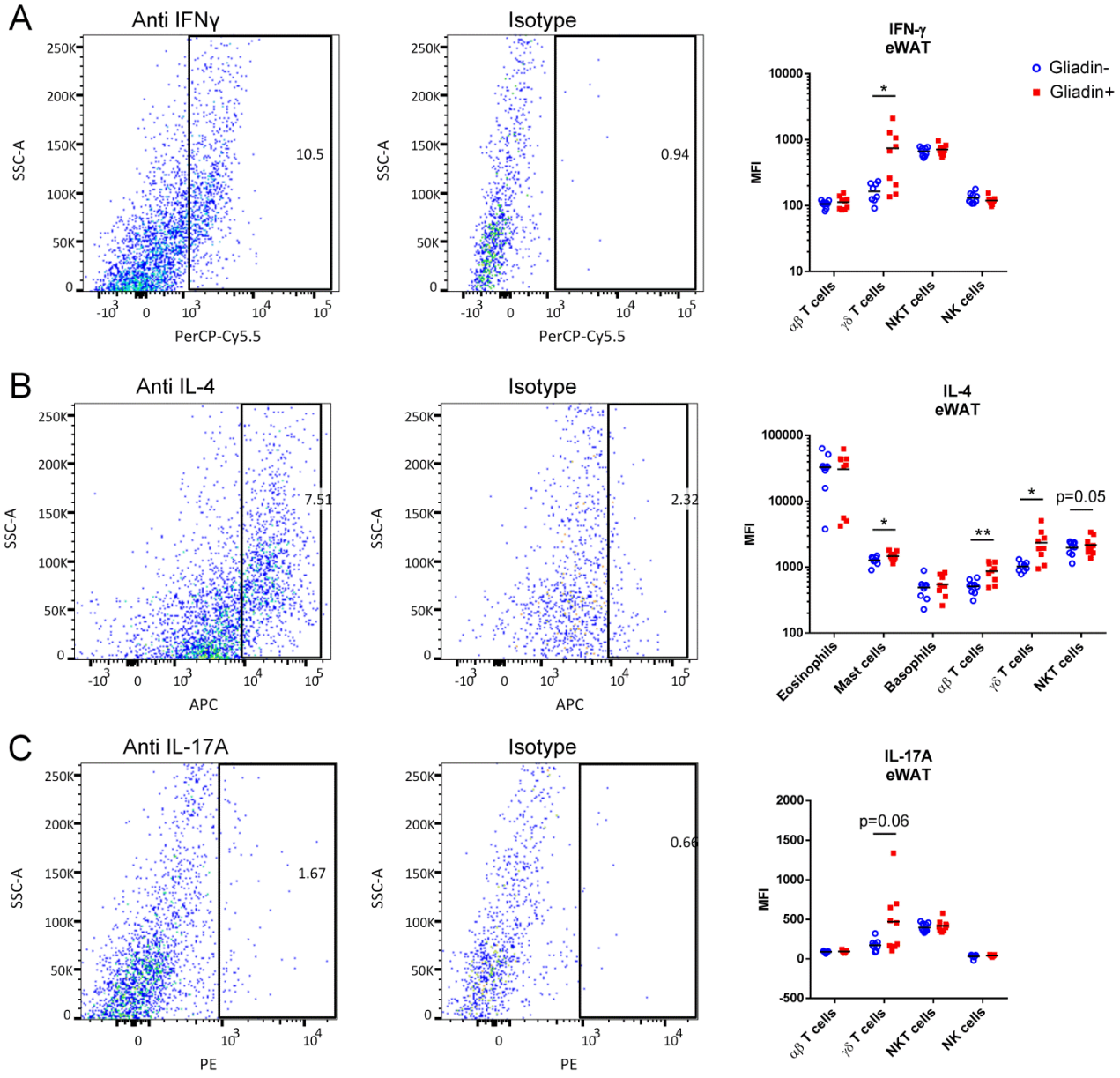

S6 Fig. Representative intracellular cytokine staining of all CD3+ lymphocytes in eWAT. IFN-γ, IL-4, IL-17A or appropriate isotype controls are shown.

S7 Fig.

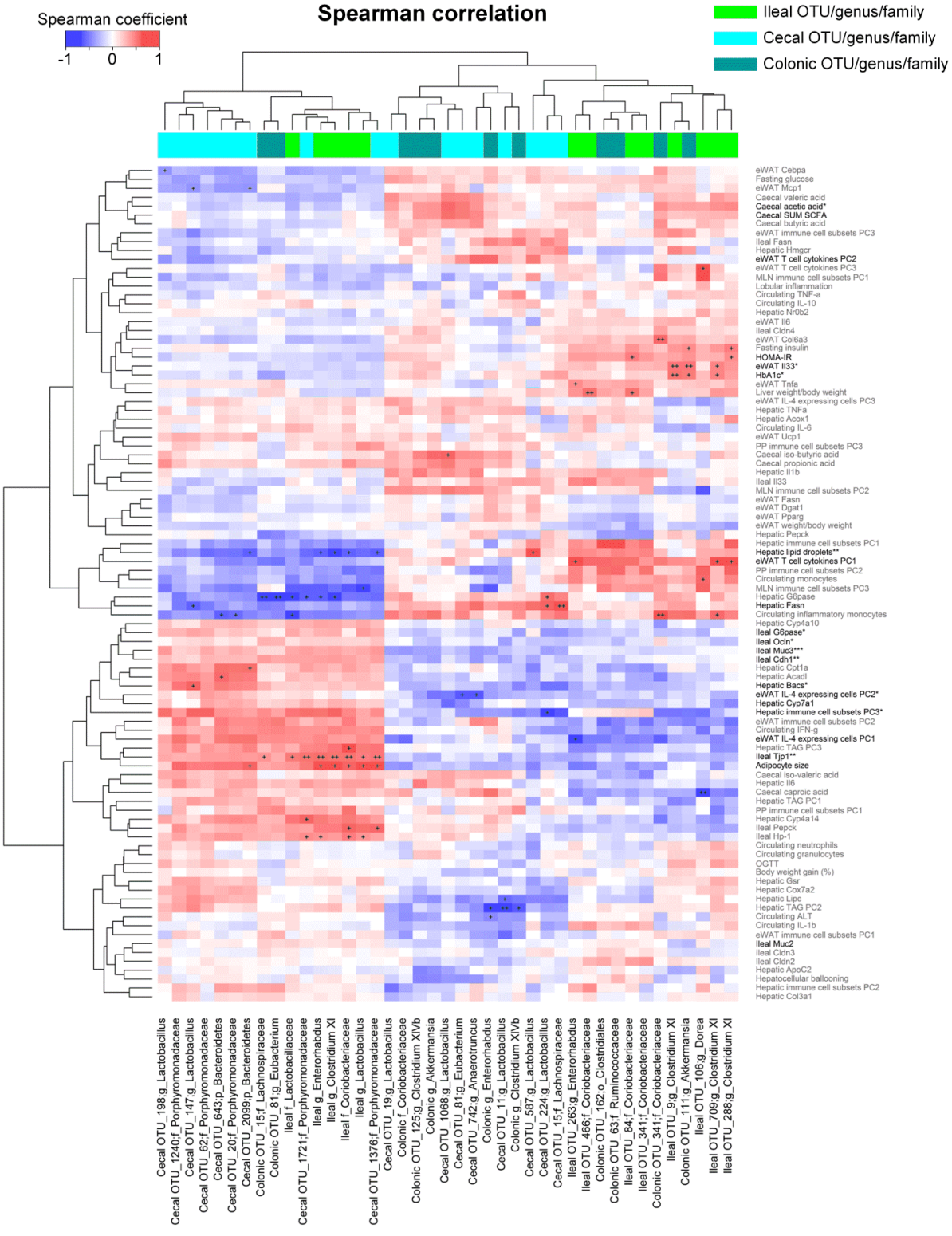

S7 Fig. Correlation heatmap.

Spearman correlations between host parameters/cecal SCFAs and OTUs/bacterial groups (genus/family level) that are differently abundant ($q < 0.05$) in Gliadin- and Gliadin+ mice. The letter preceding the underscore indicates the taxonomic level: f, family and g, genus. Plus signs represent correlation p values ($+p < 0.01$, $++p < 0.001$). For row-names, parameters not differing between the two groups are indicated in gray; parameters with $p < 0.1$ are indicated in black; asterisks indicate

significant differences between the two groups (*p < 0.05, **p < 0.01, unpaired t test or Mann-Whitney test). Clustering was performed using Euclidean distances of Spearman coefficients.

S1 Table. Composition of the Gliadin- and Gliadin+ diets.

		Gliadin-		Gliadin+	
		gm%	kcal%	gm%	kcal%
Protein		26.23	20.01	26.23	20.01
	Gliadin, Sigma G3375	0	0	4.01	3.06
	Casein	25.84	19.72	21.84	16.66
	L-Cystine	0.39	0.30	0.39	0.30
Carbohydrate		31.50	19.10	31.50	19.10
	Maltodextrin 10	16.15	12.32	16.15	12.32
	Sucrose	8.89	6.78	8.89	6.78
	Cellulose, BW200	6.46	0	6.46	0
Fat		34.89	59.90	34.89	59.90
	Soybean Oil	3.23	5.55	3.23	5.55
	Lard	31.66	54.35	31.66	54.35
Other		7.37	0.99	7.37	0.99
	Mineral Mix, S10026	1.29	0	1.29	0
	DiCalcium Phosphate	1.68	0	1.68	0
	Calcium Carbonate	0.71	0	0.71	0
	Potassium Citrate, 1 H_2O	2.13	0	2.13	0
	Vitamin Mix, V10001	1.29	0.99	1.29	0.99
	Choline Bitartrate	0.26	0	0.26	0
	FD&C Red Dye #40	0	0	0	0
	FD&C Blue Dye #1	0.01	0	0.01	0
Total		100		100	
kcal/gm		5.2		5.2	
Amino acid		(gm%)[a]		(gm%)[b]	
	Aspartate	0.91		0.78	
	Asparagine	1.04		0.98	
	Threonine	0.65		0.56	
	Serine	2.08		1.96	
	Glutamate	3.12		2.71	
	Glutamine	1.95		3.06	
	Proline	2.21		2.44	
	Glycine	1.17		1.09	
	Alanine	1.17		1.07	
	Valine	1.43		1.41	
	Methionine	0.65		0.59	
	Isoleucine	1.43		1.40	
	Leucine	2.21		2.21	
	Tyrosine	1.30		1.24	
	Phenylalanine	1.04		1.02	
	Lysine	1.82		1.55	
	Histidine	0.65		0.65	
	Tryptophan	0.26		0.28	
	Arginine	0.78		0.75	
	Cysteine	0.39		0.47	
	total	26.23		26.23	

[a]Calculation based on α-s1 casein; [b]Calculation based on α-gliadin

S2 Table. Hepatic triglyceride profile.

	Gliadin-		Gliadin+		p value
	Concentration (mg/g)	Standard deviation	Concentration (mg/g)	Standard deviation	
Myristic acid (C14:0)	1.70	0.55	1.88	0.56	0.51
Pentadecyclic acid (C15:0)	1.02	0.56	1.10	0.64	0.80
Palmitic acid (C16:0)	88.10	25.25	94.03	27.83	0.65
Palmitoleic acid (C16:1)	6.63	2.48	7.85	2.80	0.36
Margaric acid (C17:0)	0.76	0.21	0.81	0.18	0.58
Stearic acid (C18:0)	5.22	1.41	6.08	1.40	0.22
Oleic acid (C18:1 n-9 cis)	114.29	31.93	133.37	41.88	0.31
Vaccenic acid (C18:1 n-7)	6.53	2.54	7.77	3.28	0.40
Linoleic acid (C18:2 n-6 cis)	93.97	30.89	90.89	29.39	0.84
γ-linoleic acid (C18:3 n-6)	3.18	1.42	2.96	1.15	0.73
Arachidic acid (C20:0)	0.63	0.27	0.72	0.27	0.52
α-linolenic acid (C18:3 n-3)	3.37	1.39	3.14	1.20	0.72
Gondoic acid (C20:1 n-9)	1.99	0.56	2.41	0.74	0.22
Dihomo-γ-linolenic acid (C20:3 n-6)	4.00	1.53	4.88	2.07	0.34
Arachidonic acid (C20:4 n-6)	10.83	4.99	11.31	5.07	0.85
Erucic acid (C22:1 n-9)	0.12	0.10	0.14	0.10	0.75
Eicosatetraenoic acid (C20:4 n-3)	0.38	0.17	0.45	0.21	0.51
Eicosapentaenoic acid (C20:5 n-3)	1.42	0.71	1.46	0.72	0.91
Adrenic acid (C22:4 n-6)	2.89	1.37	3.09	1.54	0.78
Docosapentaenoic acid (C22:5 n-6)	1.44	0.79	1.53	1.13	0.84
Docosapentaenoic acid (C22:5 n-3)	3.43	1.67	3.61	1.81	0.83
Docosahexaenoic acid (C22:6 n-3)	12.29	5.99	14.00	7.79	0.62
Total triglycerides	378.65	116.84	410.53	135.51	0.61

S3 Table. List of urinary metabolites discriminating between Gliadin- and Gliadin+ mice.

Metabolite	Type	Adduct	Retention time (min)	Experimental m/z	Experimental unconjugated[e] m/z	Authentic standard m/z	Database /theoretical m/z	Mass error (mDa)	Gliadin+ versus Gliadin- (Non-fasted)		
									Mean ratio	P value below	Q value below
Amino acid metabolites											
Fructosyl-lysine[b]	Maillard reaction product	$[M+H]^+$	0.6	309.1656			309.1656	0.0	2.2	0.001	0.001
		$[M+K]^+$	0.6	347.1217			347.1215	0.2	2.1	0.001	0.001
Dopamine glucuronide[a]	Dopamine metabolite	$[M+H]^+$	1.1	330.1181	154.0865	154.0865 Dopamine[a] $[M+H]^+$	330.1183	0.2	1.3	0.001	0.05
L-Formylkynurenine/ dihydroxytryptophan[b]	Tryptophan metabolite	$[M+H]^+$	1.4	237.0868			237.0870	0.2	1.8	0.001	0.05
2-[3-Carboxy-3-(methylammonio)propyl]-L-histidine[b]	Histidine metabolite	$[M+H]^+$	1.5	271.1399			271.1401	0.2	2.0	0.001	0.001
γ-Glutamyl-γ-aminobutyraldehyde	Microbial metabolite	$[M-H]^-$	2.7	215.1037			215.1026	1.1	3.2	0.001	0.001
Aldosine[b]	Amino acid derivate	$[M+H]^+$	3.1	255.1338			255.1339	0.1	1.8	0.001	0.01
Unknown tyramine metabolite[c] ($C_{11}H_{20}N_2O_4$)	Tyrosine metabolite	$[M+H]^+$	3.3	243.1335			243.1339	0.4	1.6	0.001	0.05
4-Hydroxyphenylacetylglycine[b]	Tyrosine metabolite	$[M+H]^+$	3.9	210.0759			210.0761	0.2	1.3	0.001	0.05
Prephenate/Chorismate[b]	Tyrosine/phenyl-alanine metabolite	$[M+H]^+$	4.0	227.0547			227.0550	0.3	1.9	0.001	0.001
Unknown tryptophan-metabolite[c] ($C_{13}H_{14}N_2O_4$)	Tryptophan-derived metabolite	$[M-H]^-$	4.2	261.0881			261.0870	1.1	1.7	0.001	0.001
		$[M+H]^+$	4.2	263.1026			263.1026	0.0	1.8	0.001	0.01
		$[M+Na]^+$	4.2	285.0844			285.0846	0.2	1.8	0.001	0.01
Fatty acid related metabolites											

Octanoyl-lysine[b]	Acyl carrier protein component	$[M+H]^+$	4.5	273.2172		273.2173	0.1	169	0.001	0.001
Trihydroxydecanoic acid or analog[c]	Fatty acid	$[M-H]^-$	4.8	219.1237		219.1227	1.0	2.1	0.001	0.001
Tiglylcarnitine[b]	Acyl carnitine	$[M-H_2O-H]^-$	6.3	224.1289		224.1281	0.8	0.7	0.001	0.05
Protein digestion products										
Hydroxyprolyl-isoleucine[b]	Dipeptide	$[M+H]^+$	0.9	245.1495		245.1496	0.1	1.3	0.001	0.05
Phenylalanyl-threonine[b]	Dipeptide	$[M+H]^+$	1.9	267.1338		267.1339	0.1	2.2	0.001	0.001
Hydroxyprolyl-hydroxyproline[b]	Dipeptide	$[M-H_2O-H]^-$	3.1	225.0873		225.0875	0.2	1.5	0.001	0.001
		$[M-H_2O+H]^+$	3.1	227.1030		227.1032	0.2	1.6	0.001	0.001
		$[M-H_2O+H]^+$ isotope	3.1	228.1057		228.1062	0.5	1.5	0.001	0.001
Prolyl-proline[b]	Dipeptide	$[M+H]^+$	3.3	213.1229		213.1234	0.5	7.1	0.001	0.001
N-acetyl-leucyl-leucine[b]	Acetyl-dipeptide	$[M+H]^+$	3.6	287.1967		287.1965	0.0	10.7	0.001	0.001
Prolyl-tryptophan[b]	Dipeptide	$[M+H]^+$	4.4	302.1497		302.1499	0.2	1.3	0.01	0.05
Cyclo(prolyl-tyrosine)[b]	Cyclic-dipeptide	$[M+H-H_2O]^+$	4.6	243.1135		243.1134	0.1	1.4	0.001	0.05
N-acetyl-leucyl-isoleucine[b]	Acetyl-dipeptide	$[M-H]^-$	5.2	285.1819		285.1809	1.0	75	0.001	0.001
		$[M+H]^+$	5.2	287.1964		287.1965	0.0	21.8	0.001	0.001
		$[M+Na]^+$	5.2	309.1785		309.1785	0.0	20.0	0.001	0.001
Tocopherol metabolites										
δ-CEHC (-O)[b]	Oxidized tocopherol	$[M+NH_4]^+$	5.0	252.1593		252.1594	0.1	4.0	0.001	0.001
δ-CEHC-glucoside (-O)[b]	Oxidized tocopherol	$[M+NH_4]^+$	4.4	414.2121	252.1596 $[M+NH_4]^+$	414.2122	0.1	108	0.001	0.001
δ-CEHC-glucoside[b]	Oxidized tocopherol	$[M+NH_4]^+$	5.1	430.2071	251.1275 $[M+H]^+$	430.2072	0.1	2.5	0.001	0.01
δ-CEHC-glucuronide[b]	Oxidized tocopherol	$[M+NH_4]^+$	5.1	444.1863	251.1280 $[M+H]^+$	444.1864	0.1	2.7	0.001	0.01
α-CEHC-glucuronide[b]	Oxidized tocopherol	$[M-H]^-$	5.5	453.1770	277.1451 $[M-H]^-$	453.1755	0.5	1.4	0.001	0.05
	Oxidized tocopherol	$[M+NH_4]^+$	5.5	472.2176	279.1591 $[M+H]^+$	472.2177	0.1	1.4	0.01	0.05
Other										

metabolites										
Sugar alcohol (6-carbon)[c]	Sugar derivative	$[M-H]^-$	0.6	181.0718		181.0707	1.1	0.4	0.002	0.10
		$[M+H]^+$	0.6	183.0864		183.0863	0.1	0.3	0.001	0.01
Acetylhomoserine[b]	-	$[M-H]^-$	1.1	160.0616		160.0604	1.2	0.9	0.01	0.13
		$[M+H]^+$	1.1	162.0761		162.0761	0.0	0.7	0.001	0.01
Unidentified metabolites[d]						-				
Unidentified	-	$[M+NH_4]^+$	0.7	148.1332		-		2.9	0.001	0.001
Unidentified-Glucoside	-	$[M+H]^+$	0.7	441.1003	279.0477 $[M+H]^+$	-		0.4	0.001	0.05
Unidentified	-	$[M+H]^+$	0.8	184.0756		-		1.5	0.001	0.01
Unidentified (Not Tyramine-sulfate)	-	$[M-H]^-$	1.0	216.0344		-		259	0.001	0.001
Unidentified	-	$[M-H]^-$	1.1	222.0441		-		3.0	0.001	0.001
		$[M+H]^+$	1.1	224.0587		-		3.0	0.001	0.001
Unidentified	-	$[M+H]^+$	1.2	259.1651		-		0.4	0.001	0.001
Unidentified	-	$[M+H]^+$	4.1	277.1181		-		1.4	0.001	0.01
Unidentified	-	$[M+H]^+$	4.1	344.2276		-		1.4	0.01	0.05
Unidentified	-	$[M+H]^+$	4.4	301.2120		-		3.2	0.001	0.001
Unidentified	-	$[M+H]^+$	4.4	302.1497		-		1.4	0.01	0.05
Unidentified	-	$[M+H]^+$	4.6	359.2176		-		14.8	0.001	0.001
Unidentified	-	$[M+H]^+$	4.7	327.2024		-		38.0	0.001	0.001
Unidentified	-	$[M-H]^-$	5.3	189.1131		-		1.6	0.001	0.05
Unidentified	-	$[M+H]^+$	5.7	270.1699		-		0.8	0.001	0.01
Unidentified	-	$[M-H]^-$	5.8	286.1658		-		1.5	0.001	0.05
		$[M+H]^+$	5.8	288.1802		-		1.7	0.001	0.001
		$[M+Na]^+$	5.8	310.1624		-		2.0	0.001	0.01

[a]Identified using commercial standard. [b]Tentatively identified using MS/MS and METLIN and HMDB databases. [c]Putatively characterized compound class. [d]Unidentified and unclassified metabolite. [e]Unconjugated mass obtained measured by MS/MS experiment or glucuronidase treatment. CEHC, carboxyethyl-hydroxychroman.

S4 Table. Intracellular cytokines in immune cell subsets of Peyer's patches, mesenteric lymph nodes, liver and eWAT.

Cytokine	Population	Peyer's patches			Mesenteric lymph nodes			Liver			eWAT		
		Gliadin-	Gliadin+	P value	Gliadin-	Gliadin+	P value	Gliadin-	Gliadin+	P value	Gliadin-	Gliadin+	P value
IL-12p35	All DCs	1217.6 ± 260.4	1290.3 ± 221.5	0.58	1764.9 ± 299.9	1543.4 ± 221.0	0.17	1844.8 ± 644.7	2227.0 ± 1205.1	0.48	903 ± 111.5	1003 ± 155.4	0.18
	mDC	1304.6 ± 212.9	1366.3 ± 236.7	0.62	1745.4 ± 311.3	1580.9 ± 249.9	0.33	1956.3 ± 644.7	2265.9 ± 1254.5	0.58	900.4 ± 107.7	1003.5 ± 156.7	0.16
	pDC	979.1 ± 190.5	1001.7 ± 247.1	0.85	1651.7 ± 265.7	1318.7 ± 283.2	0.06	1243.9 ± 676.5	1467 ± 1166.2	0.68	904.5 ± 649.3	838.6 ± 531.0	0.83
	CD11b+ CD103+ mDC	1626.1 ± 248.7	1713.9 ± 533.7	0.69	2354.4 ± 504.4	2146.5 ± 365.2	0.43	2748 ± 1266.1	3655.1 ± 2387.1	0.40	1305.6 ± 285.3	1438.5 ± 205.5	0.30
	CD11b- CD103+ mDC	1232.7 ± 239.0	1171.9 ± 279.7	0.67	1695.9 ± 187.2	1458.1 ± 201.1	0.06	2018.8 ± 742.7	2460.9 ± 1205.9	0.43	994.9 ± 230.2	1010.9 ± 308.0	0.91
	CD11b+ CD103- mDC	1561.6 ± 309.6	1770.7 ± 425.7	0.31	1849.7 ± 458.8	1634.3 ± 309.4	0.36	1941.8 ± 613.6	2254.2 ± 1266.8	0.58	886.1 ± 115.4	976.6 ± 167.7	0.25
	CD11b- CD103- mDC	953.7 ± 160.6	1054.2 ± 188.0	0.30	1430.6 ± 189.0	1262.4 ± 171.6	0.13	1846.6 ± 655.2	2135.9 ± 1220.2	0.60	847.7 ± 77.1	953.1 ± 136.4	0.10
	Macrophages	1007 ± 139.6	961 ± 105.2	0.52	1310 ± 198.7	1119.1 ± 191.8	0.12	2049.7 ± 1076.1	2315.3 ± 1520.0	0.72	1039.2 ± 191.5	1289.3 ± 255.9	0.05
	M1 macrophages	965.9 ± 204.8	944.8 ± 113.3	0.83	1323 ± 237.1	1150.6 ± 189.9	0.19	2136.9 ± 1109.2	2381.3 ± 1582.6	0.75	1066.6 ± 196.2	1320.1 ± 264.8	0.05
	M2 macrophages	1054.7 ± 102.5	999.1 ± 148.5	0.42	1299.7 ± 214.7	1099.9 ± 189.8	0.11	1857.4 ± 1013.4	2185.8 ± 1403.0	0.63	893 ± 158.9	1114 ± 230.2	0.05
TNFa	Macrophages	2361.7 ± 633.2	1741.5 ± 694.8	0.17	9141.5 ± 2150.2	13955.8 ± 6050.8	0.11	2345.9 ± 1314.1	2177.6 ± 1341.6	0.79	1488.9 ± 283.5	1746.6 ± 655.5	0.33
	M1 macrophages	4494.3 ± 1408.8	3514.8 ± 1218.1	0.27	11104.5 ± 2398.9	15064.2 ± 7043.5	0.23	3026.7 ± 812.3	4199.5 ± 2828.3	0.26	1534.5 ± 283.7	1786.4 ± 665.7	0.34
	M2	1015	1023	0.9	6442	9327	0.1	1629	1128	0.1	1271	1572	0.2

	macrophages	.7 ± 176.4	.3 ± 445.6	7	.6 ± 2583.6	.3 ± 4270.7	9	.7 ± 968.6	.8 ± 426.1	8	± 675.8	.4 ± 221.2	6
	Ly6C-hi monocytes	-	-	-	-	-	-	-	-	-	3204.5 ± 1238.5	2828.9 ± 580.5	0.45
IL-4	Neutrophils	NA	NA	NA	NA	NA	NA	11056 ± 3776.8	8832.2 ± 3870.5	0.27	6359.7 ± 1910.8	6815.1 ± 211.4	0.65
	Eosinophils	NA	NA	NA	NA	NA	NA	30507 ± 7340.7	29696.4 ± 12740.4	0.88	34862.7 ± 16606.9	30854.9 ± 19853.6	0.66
	Mast cells	NA	NA	NA	NA	NA	NA	5265.9 ± 3142.8	3471.3 ± 1821.3	0.21	1286.1 ± 167.0	1469.5 ± 208.4	<0.05
	Basophils	NA	NA	NA	NA	NA	NA	1615.5 ± 484.7	1300.6 ± 472.9	0.21	485.8 ± 166.3	548.8 ± 178.4	0.46
	T cells	NA	NA	NA	NA	NA	NA	1616.7 ± 256.2	1880.6 ± 1109.9	0.50	1654.6 ± 374.3	1853.7 ± 666.6	0.50
	αβ T cells	NA	NA	NA	NA	NA	NA	1309.4 ± 250.3	1549.5 ± 977.5	0.50	510.1 ± 112.0	868 ± 262.8	<0.01
	γδ T cells	NA	NA	NA	NA	NA	NA	1673.4 ± 346.4	2159.6 ± 1479.1	0.36	1120.8 ± 314.8	2352.6 ± 1217.9	<0.05
	NKT cells	NA	NA	NA	NA	NA	NA	3736 ± 836.4	4357 ± 2380.4	0.48	1980.1 ± 418.1	2176 ± 653.9	0.49
	NK cells	NA	NA	NA	NA	NA	NA	1109.9 ± 214.7	1272.6 ± 733.1	0.54	662.4 ± 347.3	1103.2 ± 483.1	0.05
IFN-γ	T cells	667.0 ± 674.1	506.4 ± 501.3		216 ± 41.0	238.6 ± 67.5		187.7 ± 30.0	174.7 ± 38.8	0.45	531.7 ± 87.4	542.9 ± 140.4	0.85
	αβ T cells	252.3 ± 51.1	305.4 ± 160.7	0.46	222.8 ± 48.0	234.1 ± 53.3	0.76	81 ± 10.0	93 ± 26.8	0.24	105.7 ± 11.9	113 ± 23.7	0.45
	γδ T cells	817.7 ± 981.5	469.2 ± 525.1	0.43	207.8 ± 79.9	821.4 ± 935.3	0.16	146.6 ± 29.4	180.4 ± 44.3	0.08	261.7 ± 277.8	740.8 ± 624.0	<0.05
	NKT cells	NA	NA	NA	NA	NA	NA	841.	780.	0.4	664.	710.	0.4

								6 ± 172.9	8 ± 169.2	8	1 ± 91.7	3 ± 122.9	1
	NK cells	NA	NA	NA	NA	NA	NA	73.9 ± 10.3	84.3 ± 21.7	0.22	119.2 ± 15.6	130.9 ± 23.0	0.25
IL-17A	T cells	NA	NA	NA	NA	NA	NA	62.9 ± 10.5	53.3 ± 4.5	<0.05	310.7 ± 44.7	309.4 ± 49.4	0.96
	αβ T cells	NA	NA	NA	NA	NA	NA	31.7 ± 3.9	30.6 ± 6.0	0.65	87.8 ± 8.9	93.4 ± 15.3	0.39
	γδ T cells	NA	NA	NA	NA	NA	NA	52.8 ± 6.0	66.3 ± 17.7	0.05	173.8 ± 66.1	470.9 ± 371.4	0.06
	NKT cells	NA	NA	NA	NA	NA	NA	238.6 ± 36.4	208.3 ± 36.0	0.10	397.3 ± 52.2	417.9 ± 68.2	0.51
	NK cells	NA	NA	NA	NA	NA	NA	24.4 ± 6.5	30.3 ± 14.6	0.30	40.9 ± 10.4	30.5 ± 19.4	0.21

Data are shown as mean of the median fluorescence intensity ± standard deviation. mDC, myeloid dendritic cells, and pDC, plasmacytoid dendritic cells.

S5 Table. Primers used in SYBR green based real time PCR.

Gene	Primer	Reference
Pgk1	Forward CTCCGCTTTCATGTAGAGGAAG Reverse GACATCTCCTAGTTTGGACAGTG	1
Gapdh	Forward CGACTTCAACAGCAACTCCCACTCTTCC Reverse TGGGTGGTCCAGGGTTTCTTACTCCTT	2
Actb	Forward GTCCACCTTCCAGCAGATGT Reverse GAAAGGGTGTAAAACGCAGC	3
Cldn2	Forward GTGGCTGTAGTGGGTGGAGT Reverse CCAAAGAAAACAGGGCTGAG	4
Cldn3	Forward CCACTACCAGCAGTCGATGA Reverse CAGCCTGTCTGTCCTCTTCC	5
Cldn4	Forward TCGCGCTTGGTAGCTGGTGC Reverse GATCCCCAGCCAGCCCAGGA	6
Muc2	Forward GTGTGGGACCTGACAATGTG Reverse ACAACGAGGTAGGTGCCATC	7
Muc3	Forward CGTGGTCAACTGCGAGAATGG Reverse CGGCTCTATCTCTACGCTCTCC	8
Ocln	Forward ACTGGGTCAGGGAATATCCA Reverse TCAGCAGCAGCCATGTACTC	9
Tjp1	Forward TGGGAACAGCACACAGTGAC Reverse GCTGGCCCTCCTTTTAACAC	10
Cdh1	Forward GTATCGGATTTGGAGGGACA Reverse CAGGACCAGGAGAAGAGTGC	11

S6 Table. Primers and probes used in Taqman based real time PCR.

Gene	Primer	Probe
Acadl	Forward AATATCTGAGTGGAGGCTGAAG Reverse GCATCAACATCGCAGAGAAAC	/56-FAM/TACTTGGGA/ZEN/AGAGCAAGCGTACTCC/3IABkFQ/
Acox1	Forward TCATTCAAGTACGACACCATACC Reverse ACACTGTTATGATGCTGCAGA	/56-FAM/TCCCCGACT/ZEN/GAACCTGGTCATAGA/3IABkFQ/
Apoc2	Forward AGGAGAGTAAGGAGCTGGTC Reverse GAAGACATACCCGATCAGCAT	/56-FAM/CCATGAGCA/ZEN/CTTACGCAGGCATTT/3IABkFQ/
B2m	Forward GGGTGGAACTGTGTTACGTAG Reverse TGGTCTTTCTGGTGCTTGTC	/56-FAM/CCGGAGAAT/ZEN/GGGAAGCCGAACATAC/3IABkFQ/
Ccl2	Forward AACTACAGCTTCTTTGGGACA Reverse CATCCACGTGTTGGCTCA	/56-FAM/ACTCACCTG/ZEN/CTGCTACTCATTCACC/3IABkFQ/
Cebpa	Forward TCATTGTCACTGGTCAACTCC Reverse ACAAGAACAGCAACGAGTACC	/56-FAM/CGCAAGAGC/ZEN/CGAGATAAAGCCAAAC/3IABkFQ/
Col3a1	Forward TCTCTAGACTCATAGGACTGACC Reverse TTCTTCTCACCCTTCTTCATCC	/56-FAM/CATCTACGT/ZEN/TGGACTGCTGTGCCA/3IABkFQ/
Col6a3	Forward CATGTCTCCATCTGCTCCATC Reverse ACGCTGAAGTTGTACCAGAAC	/56-FAM/TGAATGACT/ZEN/ACCTTCACAGTATCAGGCGA/3IABkFQ/
Cox7a2	Forward GCATCCCATTATCCTCCTGAA Reverse AGCCAAGATGTTGCGGAAT	/56-FAM/CGTGAAGTG/ZEN/GTGCTGATGGTCCT/3IABkFQ/
Cpt1a	Forward AGTGTCCATCCTCTGAGTAGC Reverse CAGCAAGATAGGCATAAACGC	/56-FAM/ATGACATAC/ZEN/TCCCACAGATGGCCC/3IABkFQ/
Cyp4a10	Forward TCCATTCAACAAGAGCAAACC Reverse TTCTGGGGAAGCAAGGC	/56-FAM/TTAGCCTTT/ZEN/GGATCTGATCGCCCC/3IABkFQ/
Cyp4a14	Forward CCACCTTCAGCTCGTTCATAG Reverse CCAGATTCTTCTCACCATAGCC	/56-FAM/TCCCAATGC/ZEN/AGTTCCTTGATCCTCC/3IABkFQ/
Cyp7a1	Forward GTGAAGTCCTCCTTAGCTGTC Reverse GCCATTTACTTGGATCAAGAGC	/56-FAM/CCGCAGAGC/ZEN/CTCCTTGATGATGC/3IABkFQ/
Dgat1	Forward CACCAGGATGCCATACTTGA Reverse TCTTTGTTCAGCTCAGACAGTG	/56-FAM/AGCATCACC/ZEN/ACACACCAATTCAGGA/3IABkFQ/
Fasn	Forward ACTCCTGTAGGTTCTCTGACTC Reverse GCTCCTCGCTTGTCGTC	/56-FAM/TGGCTCTTC/ZEN/TCTGTCTGGGCTCT/3IABkFQ/
G6pase	Forward GGAGGCTGGCATTGTAGATG Reverse TCTACCTTGCTGCTCACTTTC	/56-FAM/TGGAGTCTT/ZEN/GTCAGGCATTGCTGT/3IABkFQ/
Gapdh	Forward AATGGTGAAGGTCGGTGTG Reverse GTGGAGTCATACTGGAACATGTAG	/56-FAM/TGCAAATGG/ZEN/CAGCCCTGGTG/3IABkFQ/
Gsr	Forward AGCATCTCATCACAGCCAATC Reverse TCTACTCGACTGCCTTTACCC	/56-FAM/TGCCAACCA/ZEN/CCTTTTCCTCTTTGTTG/3IABkFQ/
Hmgcr	Forward ACTGACATGCAGCCGAAG Reverse CACATTCACTCTTGACGCTCT	/56-FAM/CATGGTGCC/ZEN/AACTCCAATCACAAGG/3IABkFQ/
Il1b	Forward CTCTTGTTGATGTGCTGCTG Reverse GACCTGTTCTTTGAAGTTGACG	/56-FAM/TTCCAAACC/ZEN/TTTGACCTGGGCTGT/3IABkFQ/
Il33	Forward TCATGTTCACCATCAGCTTCT Reverse GTGCTACTACGCTACTATGAGTC	/56-FAM/ACCGTCGCC/ZEN/TGATTGACTTGCA/3IABkFQ/
Il6	Forward TCCTTAGCCACTCCTTCTGT Reverse AGCCAGAGTCCTTCAGAGA	/56-FAM/CCTACCCCA/ZEN/ATTTCCAATGCTCTCCT/3IABkFQ/
Lipc	Forward CCACTAACCCCACATTCACA Reverse AGCCGCTTATCATGATCATCC	/56-FAM/AGCAAGCCA/ZEN/TCCACCGACCA/3IABkFQ/
Nr0b2	Forward TCCAAGACTTCACACAGTGC Reverse CAAGGAGTATGCGTACCTGAAG	/56-FAM/ATCCTCTTC/ZEN/AACCCAGATGTGCCAG/3IABkFQ/
Pepck	Forward GCGAGTCTGTCAGTTCAATACC Reverse GGATGTCGGAAGAGGACTTTG	/56-FAM/CATACATGG/ZEN/TGCGGCCTTTCATGC/3IABkFQ/
Pparg	Forward TGCAGGTTCTACTTTGATCGC Reverse CTGCTCCACACTATGAAGACAT	/56-FAM/AGCTGACCC/ZEN/AATGGTTGCTGATTACA/3IABkFQ/
Bacs	Forward ACTCTCTCCACACATCTCCTC Reverse ACGGTCATTCAGTACATTGGT	/56-FAM/CGGTCATTT/ZEN/GGTTTCTGCGGTGT/3IABkFQ/
Tnfa	Forward TCTTTGAGATCCATGCCGTTG Reverse AGACCCTCACACTCAGATCA	/56-FAM/CCACGTCGT/ZEN/AGCAAACCACCAAGT/3IABkFQ/
Ucp1	Forward CACACCTCCAGTCATTAAGCC Reverse CAAATCAGCTTTGCCTCACTC	/56-FAM/AAACACCTG/ZEN/CCTCTCTCGGAAACAA/3IABkFQ/

SUPPLEMENTAL PROCEDURES

General materials

All aqueous solutions were prepared using ultrapure water obtained from the Milli-Q system (Merck Millipore, Bedford, MA, USA).

Animal experiments

Forty male C57BL/6NTac mice (Taconic, Lille Skensved, Denmark) aged four weeks at arrival were housed two by two and fed ad libitum a standard rodent diet Altromin 1324 (Altromin, Lage, Germany) at Week 0. From Week 1, one group of mice (n = 20) were fed a synthetic D12492 high-fat diet (Gliadin-) containing 60% of the energy from fat (54.4% of lard and 5.6% of soybean oil), while the other group of mice (n = 20) were fed a modified high-fat diet containing 4% gliadin (Gliadin+), replacing a corresponding amount of casein (Research Diets, New Brunswick, NJ, USA, S1 Table), for 23 weeks. All mice were caged two by two at 20-24 °C, humidity 55% ± 10% with a strict 12 h light cycle. Body weight was recorded weekly and food intake per cage was recorded twice a week. One mouse died during cheek blood sampling at Week 9.

Sampling

The mice were transferred to clean cages the day before feces sampling. From each cage, around 50-100 fecal pellets from the two mice were collected for microbiota analysis. In the meantime, the two mice were kept in two clean cages until defecation, and fecal pellets were collected immediately after defecation for short chain fatty acids (SCFAs) analysis.

Urine samples were collected at the terminal week (Week 23). Blood was sampled from the cheek into EDTA-coated micro tubes for flow cytometry analysis at Week 0, 9 and 23. At Week 22, fasting blood from the cheek was sampled into EDTA-coated tubes and centrifuged (2000 g, 5 min) to obtain plasma for insulin analysis before the oral glucose tolerance test (OGTT). All samples were kept on ice until transfer to -80 °C.

At the terminal week, one mouse from each cage was fasted for 6 hours after onset of the light cycle, while the other one was not fasted. (Fasting was carried out to allow measurements of intestinal permeability, which failed and are therefore not included). All mice were anesthetized with a Hypnorm/Dormicum mixture (0.315 mg/mL Fentanyl, 10 mg/mL Fluanisone and 5 mg/mL Midazolam) injected subcutaneously as a 1:1:2 water solution (0.006 mL/g body weight). Blood was sampled from the periorbital plexus into EDTA-coated tubes and centrifuged (2000 g, 5 min) to obtain plasma. The mice were then euthanized by cervical dislocation and dissected. Liver and epididymal white adipose tissue (eWAT) were weighed. Samples from ileum, colon and liver were placed in the RNA*later* RNA stabilization reagent (QIAGEN, Hilden, Germany) overnight; liver samples were flash-frozen in liquid nitrogen for triglyceride analysis and eWAT samples were flash-frozen for RNA extraction and additional samples of liver and eWAT were placed in 4% paraformaldehyde for

histological analyses. Luminal contents from ileum, cecum and colon were flash-frozen. All samples except the paraformaldehyde fixed tissues were stored at -80 °C until further analyses.

Biochemical Measurements in blood and plasma

HbA1c was measured in tail vein blood using a DCA Vantage Analyzer (Siemens, Erlangen, Germany). OGTT was performed by oral administration of 75 mg glucose in 0.15 mL solution after 6 hours of fasting. Glucose in the tail vein blood was measured before glucose dosage and at 15, 30, 60, 90, 120 and 180 minutes after dosage using a FreeStyle Lite glucometer (Abbott Diabetes Care Inc., Berkshire, UK).

Plasma insulin was measured using a Mouse Insulin ELISA Kit (Mercodia, Uppsala, Sweden). HOMA-IR was calculated as insulin [mU/L]*glucose [mmol/L])/22.5. Plasma alanine aminotransferase was measured with an ELISA kit (MyBioSource, San Diego, CA, USA). Plasma cytokines, IL-1β, IL-6, IFN-γ, TNF-α and IL-10, were measured using a custom V-PLEX Mouse Biomarkers ELISA Kit (Meso Scale Discovery, Rockville, MD, USA).

SCFA analysis

SCFAs were analyzed in cecal samples and feces by Gas Chromatography Mass Spectrometry essentially as previously described [12,13].

Frozen cecum content and fecal pellets were thawed on ice. Cecum contents (5-25 mg) were homogenized in 250 µl methanol, 250 µL Milli-Q water and 10 µL internal standard (100 mM 2-ethylbutyric acid in 12% formic acid, Sigma-Aldrich, St.Louis, MO, USA) using a micro-homogenizer. Similarly, one or two fecal pellets per sample were homogenized in 1.5 mL water and 100 µl internal standard using a bead-beater, and incubated for 10 min at room-temperature with slow shaking. Acidity of samples was adjusted to pH = 2-3 using 3M HCl. The samples were then centrifuged at 10,000 g for 10 min, and supernatants were filtered through 0.45 µm Phenex-NY syringe filters (Phenomenex, Værløse, Denmark). External calibration was performed using standard solution mixtures of acetic acid, propionic acid, butyric acid, iso-butyric acid, valeric acid, iso-valeric acid, caproic acid and 2-ethylbutyric acid (Sigma-Aldrich) in the concentrations 10, 20, 50, 100, 250, 500 and 1,000 mM with extra acetic acid, propionic acid and butyric acid in the concentrations 2000 and 5000 mM.

Aliquots (3 µL) of each sample were injected into a HP 6890 GC system (Agilent Technologies, Santa Clara, CA, USA) with a CP-FFA WCOT fused silica capillary column (25 m x 0.53 mm i.d. coated with 1 µm film thickness, Chrompack, EA Middelburg, The Netherlands). The carrier gas was helium at a flow rate of 20 mL/min. The initial oven temperature of 60 °C was maintained for 0.25 min, raised to 180 °C at 8 °C/min and held for 3 min, then increased to 215 °C at 20 °C/min, and finally held at 215 °C for 5 min. The temperature of the front inlet detector and the injector was 250 °C. The flow rates of hydrogen, air and helium as makeup gas were 40, 450, and 45 mL/min, respectively. The run time

for each analysis was 22 min. Data handling was performed using the OpenLAB Chromatography Data System ChemStation Edition software (Rev.A.10.02). The concentration of SCFA in the samples was calculated against the individual external standards, and adjusted according to the loss of internal standard.

Urine metabolome profiling with Ultra Performance Liquid Chromatography Mass Spectrometry (UPLC-MS)

Frozen urine samples were thawed on ice and centrifuged at 10,000 g for 10 min at 4 °C to remove particles. Subsequently, samples were diluted 1:100 with Milli-Q water, mixed by vortexing, and pipetted into LC vials. Pooled quality control (QC) samples were prepared by mixing aliquots of all urine samples, thereby ensuring the QC sample represented the whole sample set. The samples were kept on ice during preparation.

The column was conditioned by running a couple of blank samples (water) followed by five injections of the QC sample before urine samples were injected. The QC sample was analysed once for every ten urine samples throughout the LC-MS analysis to provide data from which the reproducibility could be assessed. For each sample, 2 µL of diluted urine (1:100 in water) was analysed in both negative and positive mode by a UPLC-QTOF-MS system consisting of Dionex Ultimate 3000 RS liquid chromatograph (Thermo Scientific, Sunnyvale, CA, USA) coupled to a Bruker maXis time of flight mass spectrometer equipped with an electrospray interphase (Bruker Daltonics, Bremen, Germany). The analytes were separated on a Poroshell 120 SB-C18 column with a dimension of 2.1 x 100 mm and 2.7 µm particle size (Agilent Technologies, CA, USA) based on the settings according to Want et al. [14]. Shortly, the column was held at 40 °C and the sampler at 4 °C. The UPLC mobile phases consisted of 0.1% formic acid in water (solution A) and 0.1% of formic acid in acetonitrile (solution B). While containing a constant flow rate of 0.4 mL/min, the analytes were eluted using the following gradient. Solvent programming was isocratic 1% B for 1 min followed by a linear gradient up to 15% at 3 min, then a linear gradient up to 50% B at 6 min, and finally a linear gradient up to 95% B at 9 min. The final gradient composition, 95% B, was held constant until 10 min, followed by a return of the solvent composition to initial conditions at 10.1 min and equilibration until 13 min. Mass spectrometry data were collected in full scan mode at 2 Hz with a scan range of 50-1000 mass/charge (m/z).

The following electrospray interphase settings were used: nebulizer pressure 2 bar, drying gas 10 L/min, 200 °C, capillary voltage 4500 V. For MS/MS analyses, a ramp collision energy ranging from 10 to 30 eV was applied on a scheduled precursor list. To improve the measurement accuracy, external and internal calibrations were done using sodium formate clusters (Sigma-Aldrich) and in addition a lock-mass calibration was applied (hexakis(1H,1H,2H-perfluoroetoxy)phosphazene, Apollo Scientific, Manchester, UK).

The raw LC-MS data were converted to mzXML files using Bruker Compass DataAnalysis 4.2 software (Bruker Daltonics) and were then pre-processed through noise filtering, peak detection, and

alignment using the open-source R package XCMS (v1.38.0) [15]. Noise filtering settings included that features should be detected in minimum 50 % of samples within a group. Data tables were generated comprising m/z, retention time, and intensity (peak area) for each variable in every sample. For each sample, the urinary features were normalized to the total intensity of the given sample. Subsequently, the data were filtered using the pooled QC samples: features with coefficient of variation above 30% in the QC samples were excluded, and features with a retention time above 8 min were also excluded. The resultant data was imported into the LatentiX 2.12 software (Latent5; http://www.latentix.com) for further multivariate analysis. Unsupervised principal component analysis (PCA) was performed on mean-centered data to visualize general clustering trends. Discriminating features were evaluated by an unpaired t test with Welch's correction followed by the Benjamini-Hochberg false discovery rate (FDR) correction [16] with a significance level of 0.05 (q value). Metabolite candidates were identified by searching the accurate masses of parent ions and fragments (from MS/MS), against the METLIN [17] and HMDB databases [18]. The metabolites were identified according to the four different levels described by the Metabolomics Standard Initiative [19]. To confirm the identity of dopamine-glucuronide, a urine sample was diluted in 0.1 M sodium phosphate buffer (pH = 7.4) and incubated with β-glucuronidase from *E. coli* K12 (Roche Diagnostics GmbH) at 37 °C for 1-2 hours. Subsequently, the urine sample was injected onto the UPLC-MS for analysis, which allowed the deglucuronidated dopamine *m/z* feature to be compared with the authentic standard of dopamine, which was obtained from Sigma-Aldrich (Schnelldorf, Germany). A heat-map showing the log-transformed relative abundance of the discriminating metabolites was generated by the Heatmap function of MetaboAnalyst [20] using Euclidean distance measure and the ward clustering algorithm.

16s rRNA gene sequencing

Bacterial DNA was extracted from feces and luminal contents using the PowerLyzer PowerSoil DNA Isolation Kit (Mo Bio Laboratories, Carlsbad, CA, USA). Around 10-20 fecal pellets (100 mg) per sample were used to make sure that both mice in the cage were represented. DNA concentrations were measured using the Nanodrop Spectrophotometer ND-1000 (Thermo Scientific, Wilmington, DE, USA). Variable Region 3 (V3) of the 16S rRNA gene was amplified using a universal forward primer with a unique 10-12 bp barcode (IonXpress barcode, Ion Torrent) for each bacterial community (PBU 5'-A-adapter-TCAG-barcode-GAT-CCTACGGGAGGCAGCAG-3') and a universal reverse primer (PBR 5'-trP1-adapter-ATTACCGCGGCTGCTGG-3'). The PCR reactions were conducted with 5 ng template DNA, 10 mmol/L dNTP, 1 µmol/L forward/reverse primer, 4 µL HF-buffer and 0.2 µL Phusion High-Fidelity DNA polymerase (Thermo Scientific, Vilnius, Lithuania) in a total reaction volume of 20 µL. PCR conditions were 30 s at 98 °C, 24 cycles of 15 s at 98 °C, 30 s at 72 °C, followed by 5 min at 72 °C. For a few samples that did not yield sufficient PCR products, an initial PCR was performed with universal primers without barcodes or adaptors (30 cycles) followed by a second round of PCR (15 cycles) with barcoded primers using a 10-fold dilution of the first PCR product as template. PCR products were separated on a 1.5% agarose gel at 3.5 V/cm for 90 minutes, and bands of the expected size (approximately 260 bp) were excised from the gel. DNA was purified from the

excised gel using the MinElute Gel Extraction Kit (Qiagen, Germany) according to the instructions of the manufacturer. DNA concentrations were determined using the Qubit 2.0 fluorometer (Invitrogen, Carlsbad, CA, USA) with the dsDNA HS assay (Invitrogen, Eugene, OR, USA), and equal amounts of PCR products from each community were pooled to construct a library. Sequencing was performed using the Ion PGM Template OT2 200 Kit and the Ion PGM Sequencing 200 Kit v2 with the 318-chip (Ion Torrent).

Sequencing data analysis

Sequences were de-multiplexed, trimmed to eliminate primers, and filtered with a length range of 125-180 bp using the CLC Genomic Workbench v7.0.3 (Qiagen, Aarhus, Denmark). Each sequence was classified to the lowest possible taxonomic rank (assignment confidence ≥ 50%) using the Ribosomal Database Project (RDP) Classifier v2.10.1 [21], and collapsed at genus, family, phylum and domain levels. The depths (range, median) of the resulting phylotype data table were: 35,156-95,090, 59,500 for fecal samples, 35,672-93,032, 73,251 for ileal samples, 23,216-57,266, 42,276 for cecal samples and 25,066-52,617, 42,754 for colonic samples.

Operational taxonomic units (OTUs) were generated using UPARSE v8.0.1623 [22]. All sequences were subjected to quality filtering with a cut-off of maxee of 3.5 (discard reads with > 3.5 total expected errors for all bases in the read). Unique sequences except singletons were clustered at 97% sequence homology. Chimeras were first filtered by the UPARSE-OTU algorithm and then by the UCHIME algorithm [23] using the RDP classifier training database v9 and the default threshold. Taxonomies of OTU representative sequences were also assigned using the RDP classifier. The depths (range, median) of the resulting OTU data table were: 28,606-74,454, 47230 for fecal samples, 30,421-89,534, 67,731 for ileal samples, 14,542-41,654, 29,559 for cecal samples and 15,495-37,974, 29,731 for colonic samples.

Microbiota α diversity (Shannon index) and β diversity were analyzed using Qiime 1.8.0 [24]. OTU representative sequences were pooled with a 16S rRNA gene sequence assigned as *Methanosarcina* within the Archaea, and aligned to the Greengenes core set (Greengenes 13_5 PyNAST aligned 85% OTU representative sequences) [25] using PyNAST [26]. A phylogenetic tree was created using FastTree [27]. Using Dendroscope v3.3.2, the tree was re-rooted with the Archaea outgroup, and then the outgroup was pruned from the tree, thereby generating a phylogenetic tree for downstream analyses. The Principle coordinate analyses (PCoA) was performed on UniFrac distances [28] between microbial communities, and the OTU tables were rarefied to the lowest number of reads in each PCoA model. The ADONIS test was performed to assess the differential clustering of microbial communities using the *vegan* R package v2.3-0 [29], and feeding status (fasted/non-fasted) was included as a variable when the ileal, cecal and colonic samples were analysed.

To discover features, i.e. OTUs and bacterial groups at genus/family/phylum levels (based on the phylotype data table), that were differentially abundant in the Gliadin- and Gliadin+ mice, features

that were less abundant than 0.02% of average numbers of total bacteria in both groups and features that presented in less than 50% of samples in both groups were filtered out. The matrices of relative abundances were permutated 10,000 times, and p values represent fraction of times that permuted differences assessed by Welch's t test were greater than or equal to real differences, followed by the FDR correction.

Gene expression analysis using real time RT-PCR

Total RNA from liver, ileal and colonic tissues was extracted using the RNeasy Plus Mini Kit (Qiagen, Germany) according to the product protocol, while for adipose tissue, total RNA was harvested by trizol and chloroform based purification followed by kit extraction. For gut barrier function related genes, RNA concentration and purity were determined using the Nanodrop Spectrophotometer ND-1000, and cDNA was synthesized from 1.4 µg RNA in 20 µL reactions using the SuperScript VILO cDNA Synthesis Kit (Invitrogen, Carlsbad, CA, USA), and diluted 20-fold for further use. Quantitative real time RT-PCR was performed with a SYBR Green I Master (Roche Diagnostics GmbH, Mannheim, Germany) and a LightCycler 480 system (Roche Diagnostics GmbH) using the described primer sets (S5 Table), and the PCR reactions were run under the following conditions: 95 °C for 5 min; 40 cycles of 95 °C for 10 sec, 55 °C for 10 sec, and 72 °C for 30 sec; melting curve generation with preparation with 95 °C for 5 sec, 65 °C for 1min and increasing the temperature to 98 °C with a rate of 0.11 °C/sec with continuous fluorescence detection. The amplification efficiency of each primer was assessed by a standard curve. The amount of each mRNA was normalized to the geometric mean of expression levels of phosphoglycerate kinase 1 gene (*Pgk1*), actin beta gene (*Actb*) and glyceraldehyde 3-phosphate dehydrogenase gene (*Gapdh*). For the remaining analyses, RNA concentrations were measured using a Qbit 2.0 fluorometer, and cDNA was synthesized by a High Capacity cDNA Reverse Transcription Kit (Applied Biosystems) from 2 µg RNA. Real time PCR of the cDNA was performed with a TaqMan Fast Universal PCR Master Mix (Applied Biosystems, Foster city, CA, USA) and a 7900HT Fast Real-time PCR system (Applied Biosystems) using primers and probes (S6 Table) purchased from Integrated DNA Technologies (Leuven, Belgium). The PCR reactions were run under the following conditions: 95 °C for 20 sec; 40 cycles of 95 °C for 1 sec and 60 °C for 20 sec. Normalization was done with the beta-2 microglobulin gene (*B2m*) and *Gapdh*.

Flow cytometry

Blood samples were lysed in a red blood cell lysis buffer (ACK buffer, 154.95 mM ammonium chloride, 9.99 mM sodium hydrogen carbonate, 0.0995 mM Disodium EDTA, in PBS) for 5 minutes at room temperature. Dissected and cleaned adipose tissue was homogenized by 40 minutes incubation at 37 °C with collagenase II (Sigma-Aldrich C6885), while liver tissue was cleaned and manually grinded with a piston. Homogenized liver and adipose tissues were filtered using a BD Falcon cell strainer (70 µm filter, BD Bioscience, Bedford, MA, USA) and washed in PBS with 1% FCS and 2 µM monensin (Sigma-Aldrich). Dissected lymphoid tissues (MLN and PP) were washed in PBS (without Ca^{2+} and Mg^{2+}) with 1% FCS, 2 µM monensin (Sigma-Aldrich) and 3 mM EDTA and filtered in

a 70 µm filter. All single cell suspensions were counted on a Nucleocounter NC-100 (ChemoMetec, Denmark) and plated.

All cell suspensions were Fc-blocked (CD16/CD32, BD Biosciences) and surface stained in PBS with 1% fetal calf serum and 2 µM monensin and subsequently fixed and permeabilized for 20 min at 4 °C (Cytofix/Cytoperm, BD Biosciences) followed by intracellular staining. Samples were washed and re-suspended in PBS with 1% fetal calf serum and 0.1% sodium azide, and Count Bright beads were added (Invitrogen Molecular Probes) according to manufacturer's instructions. Samples were run on a BD FACSCanto II (BD Biosciences) flow cytometer. Data were analysed using Flowjo software (V10.0.7, Treestar). Gating strategies are shown in S5 Fig and S6 Fig.

Antibodies for surface and intracellular staining included CD45-APC-Cy7 (BD, 30-F11), CD8-FITC (BD, 53-6.7), CD3 (BD, 500A2), NK1.1-FITC (BD, PK136), B220-V500 (BD, RA3-6B2), Siglec-F-PE (BD, E50-2440), cKit-V450 (BD, 2B8), CD11c-PE-Cy7 (BD, HL3), Arg1-Alexa Fluor 647 (BD, 19/Arginase-1), CD103-PE (BD, M290), Ly6G-PE-Cy7 (BD, 1A8), TCRδ-BV421 (BD, GL3), CD11b-V500 (BD, M1/70), IFN-γ-PerCP-Cy5.5 (BD, XMG1.2), FoxP3-Alexa Fluor 647 (BD, MF23), TNFα-PE (BD, MP6-XT22), CD4-PE-Cy7 (eBioscience, GK1.5), CD1d-PE (eBioscience, 1B1), CD19-PerCP-Cy5.5 (eBioscience, 1D3), IgD-eFluor 450 (eBioscience, 11-26c), F4/80-FITC (eBioscience, BM8), Ly6C-PerCP-Cy5.5 (eBioscience, HK1.4), IgM-PE-Cy7 (eBioscicence, II/41), IL-4-APC (eBioscience, 11B11), IL-17A-PE (eBioscience, 17B7), IL-12p35-eFluor 660 (eBioscience, 4D10p35), Siglec-H-PerCP-eFluor 710 (eBioscience, 440c), NKp46-PE-Cy7 (29A1.4), CD49b-FITC (eBioscience, HMa2), FcεRIα-PerCPeFluor 710 (eBioscience, MAR-1), IL-10-APC (eBioscience, JES5-16E3), CD5-FITC (eBioscience, 53-7.3), CD115-APC (eBioscience, AFS98), IL-4-PE (eBioscience, 11B11), CX3CR1-Pacific Blue (eBioscience, polyclonal) and CCR2-PE (R&D, 475301).

Histology

Liver and adipose tissues were fixed for 24 h in 4% paraformaldehyde (Sarstedt, 51.1703.009) and then kept in PBS for 21 days until dehydration in ethanol followed by paraffin embedding. Tissues were sectioned and stained with hematoxylin and eosin stain (Sigma Aldrich, St. Louis, MO, USA). Liver steatosis was initially analyzed by automated quantification of lipid droplets (ImageJ, v1.49). This was followed by a second evaluation by an independent lab using a non-alcoholic steatohepatitis grading score of steatosis, inflammation and hepatocellular ballooning. For the adipose tissue, adipocytes were measured manually in four independent tissue sections per tissue sample, and an average of 150 cells were quantified per section. In order to confirm our observations, adipocyte sizes were also measured blindly by an independent lab using ImageJ.

Statistical analysis

Unless specified, Student's t test (if normally distributed) or Mann-Whitney test (if non-continuous data or not normally distributed) were performed using GraphPad Prism 6.02, and maximally one outlier from each group detected by Grubbs' test

(http://www.graphpad.com/quickcalcs/Grubbs1.cfm, alpha = 0.05) was excluded before these tests. Spearman's rank correlation, multiple t tests and two-way ANOVA were also performed using GraphPad. Network based on Spearman correlations was built with Cytoscape v3.2.1.

SUPPLEMENTAL REFERENCES

1. MS, B. *et al.* CD73 is critical for the resolution of murine colonic inflammation. *J Biomed Biotechnol* 260983 (2012).
2. Liu, G. *et al.* miR-147, a microRNA that is induced upon Toll-like receptor stimulation, regulates murine macrophage inflammatory responses. *Proc. Natl. Acad. Sci. U. S. A.* **106,** 15819–24 (2009).
3. Bergström, A. *et al.* Nature of bacterial colonization influences transcription of mucin genes in mice during the first week of life. *BMC Res. Notes* **5,** 402 (2012).
4. Acharya, P. *et al.* Distribution of the tight junction proteins ZO-1, occludin, and claudin-4, -8, and -12 in bladder epithelium. *Am. J. Physiol. Renal Physiol.* **287,** F305-18 (2004).
5. Corridoni, D. *et al.* Probiotic bacteria regulate intestinal epithelial permeability in experimental ileitis by a TNF-dependent mechanism. *PLoS One* **7,** e42067 (2012).
6. Reynolds, J. M. *et al.* Cutting edge: regulation of intestinal inflammation and barrier function by IL-17C. *J. Immunol.* **189,** 4226–30 (2012).
7. Becker, S. *et al.* Bacteria regulate intestinal epithelial cell differentiation factors both in vitro and in vivo. *PLoS One* **8,** e55620 (2013).
8. Hoebler, C., Gaudier, E., De Coppet, P., Rival, M. & Cherbut, C. MUC genes are differently expressed during onset and maintenance of inflammation in dextran sodium sulfate-treated mice. *Dig. Dis. Sci.* **51,** 381–9 (2006).
9. Hwang, I. *et al.* Alteration of tight junction gene expression by calcium- and vitamin D-deficient diet in the duodenum of calbindin-null mice. *Int. J. Mol. Sci.* **14,** 22997–3010 (2013).
10. Bull-Otterson, L. *et al.* Metagenomic analyses of alcohol induced pathogenic alterations in the intestinal microbiome and the effect of Lactobacillus rhamnosus GG treatment. *PLoS One* **8,** e53028 (2013).
11. Kristensen, M. B. *et al.* Neonatal microbial colonization in mice promotes prolonged dominance of CD11b(+)Gr-1(+) cells and accelerated establishment of the CD4(+) T cell population in the spleen. *Immunity, Inflamm. Dis.* **3,** 309–20 (2015).
12. Zhao, G., Nyman, M. & Jönsson, J. A. Rapid determination of short-chain fatty acids in colonic contents and faeces of humans and rats by acidified water-extraction and direct-injection gas chromatography. *Biomed. Chromatogr.* **20,** 674–82 (2006).
13. Nejrup, R. G. *et al.* Lipid hydrolysis products affect the composition of infant gut microbial communities in vitro. *Br. J. Nutr.* **114,** 63–74 (2015).
14. Want, E. J. *et al.* Global metabolic profiling procedures for urine using UPLC-MS. *Nat. Protoc.* **5,** 1005–1018 (2010).

15. Smith, C. A., Want, E. J., O'Maille, G., Abagyan, R. & Siuzdak, G. XCMS: Processing Mass Spectrometry Data for Metabolite Profiling Using Nonlinear Peak Alignment, Matching, and Identification. *Anal. Chem.* **78,** 779–787 (2006).

16. Benjamini, Y. & Hochberg, Y. Controlling the False Discovery Rate - a Practical and Powerful Approach to Multiple Testing. *J. R. Stat. Soc. Ser. B-Methodological* **57,** 289–300 (1995).

17. Smith, C. A. *et al.* METLIN: a metabolite mass spectral database. *Ther. Drug Monit.* **27,** 747–51 (2005).

18. Wishart, D. S. *et al.* HMDB 3.0--The Human Metabolome Database in 2013. *Nucleic Acids Res.* **41,** D801-7 (2013).

19. Sumner, L. W. *et al.* Proposed minimum reporting standards for chemical analysis Chemical Analysis Working Group (CAWG) Metabolomics Standards Initiative (MSI). *Metabolomics* **3,** 211–221 (2007).

20. Xia, J. & Wishart, D. S. Web-based inference of biological patterns, functions and pathways from metabolomic data using MetaboAnalyst. *Nat. Protoc.* **6,** 743–60 (2011).

21. Wang, Q., Garrity, G. M., Tiedje, J. M. & Cole, J. R. Naive Bayesian classifier for rapid assignment of rRNA sequences into the new bacterial taxonomy. *Appl. Environ. Microbiol.* **73,** 5261–7 (2007).

22. Edgar, R. C. UPARSE: highly accurate OTU sequences from microbial amplicon reads. *Nat. Methods* **10,** 996–8 (2013).

23. Edgar, R. C., Haas, B. J., Clemente, J. C., Quince, C. & Knight, R. UCHIME improves sensitivity and speed of chimera detection. *Bioinformatics* **27,** 2194–200 (2011).

24. Caporaso, J. G. *et al.* QIIME allows analysis of high-throughput community sequencing data. *Nat. Methods* **7,** 335–6 (2010).

25. McDonald, D. *et al.* An improved Greengenes taxonomy with explicit ranks for ecological and evolutionary analyses of bacteria and archaea. *ISME J.* **6,** 610–8 (2012).

26. Caporaso, J. G. *et al.* PyNAST: a flexible tool for aligning sequences to a template alignment. *Bioinformatics* **26,** 266–7 (2010).

27. Price, M. N., Dehal, P. S. & Arkin, A. P. FastTree: computing large minimum evolution trees with profiles instead of a distance matrix. *Mol. Biol. Evol.* **26,** 1641–50 (2009).

28. Lozupone, C. & Knight, R. UniFrac: a new phylogenetic method for comparing microbial communities. *Appl. Environ. Microbiol.* **71,** 8228–35 (2005).

29. Oksanen, J. *et al.* vegan: Community Ecology Package. (2015).

Project II: Safflower study

Introduction and objectives

Dietary composition and increased energy intake is a main driver of the global obesity epidemic often resulting in glucose intolerance and insulin resistance. Combined with a more sedentary lifestyle, the evolutionary changes in dietary habits illustrated by increased intake of n-6 polyunsaturated fatty acids (PUFAs) in combination with energy-dense, high-glycemic carbohydrates, such as sucrose, has proven obesogenic. Whereas the typical diet-induced obesity model is based on saturated fats, less is known about the effects of an n-6 PUFA rich diet. Safflower oil is rich in the n-6 PUFA linoleic acid (C18:2 n-6), which may be metabolized via arachidonic acid (C20:4 n-6) to pro-inflammatory eicosanoids by the host, thus proving a potential health challenge. However, the effect of long-term intake of an n-6 PUFA rich diet on obesity, glucose regulation, adipose tissue and liver immune cell infiltration and gut microbiota composition has not been thoroughly described.

Experimental setup

Single-caged, male C57BL/6 mice were either fed a linoleic acid-rich high-fat/high-sucrose (HF/HS) diet based on safflower oil or a low-fat/low-sucrose (LF/LS) diet for 40 weeks. To monitor the inflammatory and metabolic phenotype during the entire dietary challenge, mice were sacrificed at regular intervals at 0, 2, 5, 10 and 40 weeks, n=4 per time point. Since glucose and insulin tolerance tests pose a significant stress factor to the mice, specific mice (n=5) were dedicated to the glucose assays during the time course. The limited sample size necessitated a repetition of the setup, thus resulting in a doubling of the total sample size.

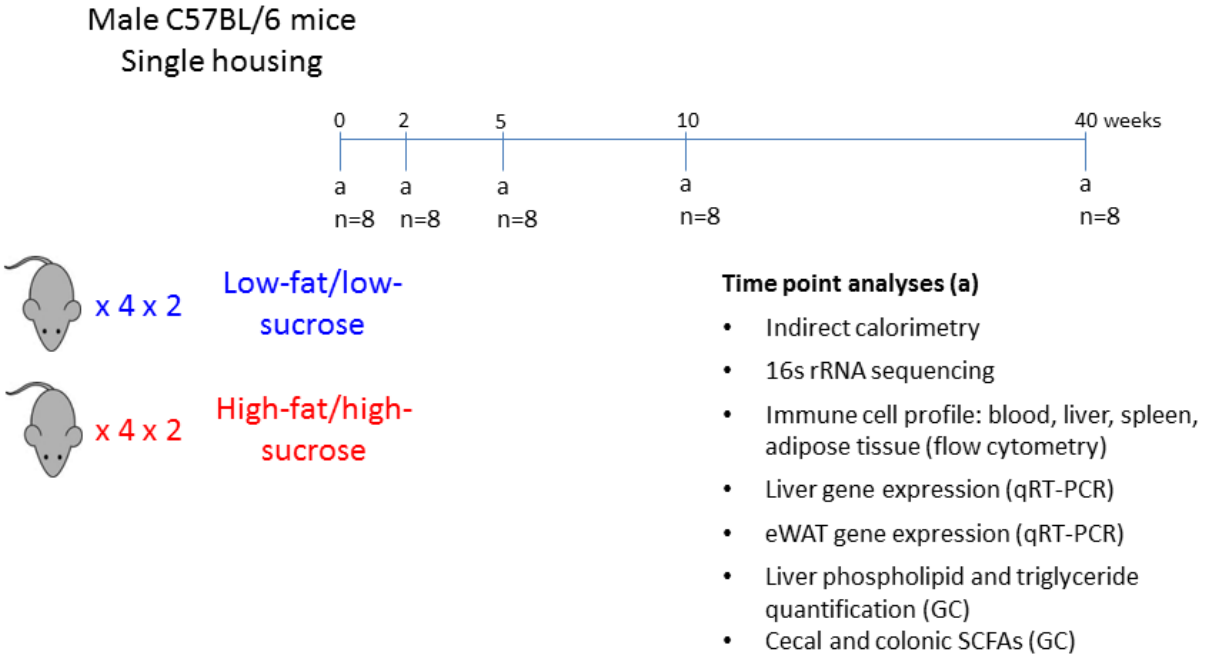

Specific aims

This study aimed to identify

- the long-term metabolic and inflammatory effects of intake of an HF/HS diet compared to a LF/LS diet
- the timing and sequential order of phenotypic changes induced by an HF/HS diet
- the interplay between diet, host metabolism, tissue immune cell infiltration and the gut microbiota

Key findings

The most significant findings from this study are

- Long-term intake of a safflower-based HF/HS diet only leads to moderate weight gain
- Glucose intolerance develops in HF/HS fed mice at week 5 at the same time as the increase in liver phospholipids containing linoleic and arachidonic acid
- No difference in hepatic steatosis between diets or in liver inflammation, rather, HF/HS fed mice show a reduction in the number of immune cells (primarily granulocyte and lymphocyte subsets)
- Insulin resistance develops much after glucose intolerance as it presents only at week 40
- Higher fat mass of HF/HS fed mice from week 10
- Higher M1/M2 ratio of adipose tissue macrophages at week 40, and higher TNFα expression of M1 macrophages compared to LF/LS at week 40
- No change in other adipose tissue immune cells or inflammatory markers
- Increase in Blautia among HF/HS mice after two weeks, coinciding with a reduction in the relative abundance of Barnesiella

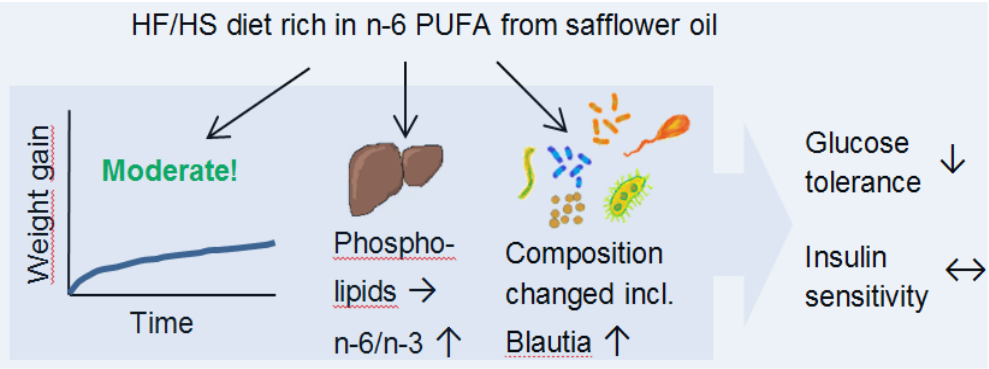

Publication status

Accepted in Molecular Nutrition & Food Research, December, 2016

Manuscript II

A safflower oil-based high fat/high-sucrose diet modulates the gut microbiota and liver phospholipid profiles associated with early glucose intolerance in the absence of tissue inflammation

Niels Banhos Danneskiold-Samsøe[1,*†], Daniel Andersen[2,*], Ilinca Daria Radulescu[3], Ann Normann-Hansen[1], Asker Brejnrod[1], Marie Kragh[2], Tobias Madsen[2], Christian Nielsen[2], Knud Josefsen[3], Xavier Fretté[4], Even Fjære[5], Lise Madsen[1,5], Lars I Hellgren[2], Susanne Brix[2†] and Karsten Kristiansen[1,6†]

[1]Laboratory of Genomics and Molecular Biomedicine, Department of Biology, University of Copenhagen, Universitetsparken 13, DK-2100 Copenhagen, Denmark

[2]Department of Biotechnology and Biomedicine, Technical University of Denmark, Søltofts Plads, DK-2800 Kgs. Lyngby, Denmark

[3]The Bartholin Institute, Rigshospitalet Dept. 3733, Copenhagen Biocenter, Ole Maaløes Vej 5, DK-2200 Copenhagen, Denmark

[4]Department of Chemical Engineering, Biotechnology and Environmental Technology, University of Southern Denmark, Campusvej 55, 5230 Odense M, Denmark

[5]National Institute of Nutrition and Seafood Research, Postboks 2029, Nordnes, 5817 Bergen, Norway

[6]BGI-Shenzhen, 518083 Shenzhen, China

[*]Equal contribution

[†]To whom correspondence should be addressed; Dr. Niels Banhos Danneskiold-Samsøe (nds@bio.ku.dk, phone: +45 35 33 03 49), Dr. Susanne Brix (sbp@bio.dtu.dk, phone: +45 45 25 27 84, fax: +45 45 88 63 07), Dr. Karsten Kristiansen (kk@bio.ku.dk, phone: +45 35 32 44 43).

Abbreviations: **Acaca**, acetyl-CoA carboxylase; **Adipoq**, adiponectin; **Cpt1a**, carnitine palmitoyltransferase 1A; **eWAT**, epididymal white adipose tissue; **Fasn**, fatty acid synthase; **G6pc**, glucose 6-phosphatase; **GTT**, glucose tolerance test; **HF/HS**, high-fat/high-sucrose; **HOMA-IR**, homeostatic model assessment; **ITT**, insulin tolerance test; **LF/LS**, low-fat/low-sucrose; **MFI**, median fluorescence intensity; **NK**, natural killer cell; **NKT**, natural killer T cells; ***n*-3**, omega-3, ***n*-6**, omega-6; **OTU**, Operational Taxonomic Units; **Ppara**, peroxisome proliferator-activated receptor alpha; **Pck**, phosphoenolpuryvate carboxykinase; **PCoA**, principal coordinates analysis; **Pparg,** proliferator-activated receptor gamma; **RER**, respiratory exchange ratio; **Srebf1**, sterol regulatory element-binding protein 1; **TG**, Triglyceride; **TNFα/Tnfa**, tumor necrosis factor-α.

Keywords: glucose intolerance, hepatic lipid metabolism, inflammation, leucocytes, safflower oil

ABSTRACT

Scope: *n*-6 PUFA-rich diets are generally considered obesogenic in rodents. Here we examined how long-term intake of a high fat/high sucrose (HF/HS) diet based on safflower oil affected metabolism, inflammation and gut microbiota composition.

Methods and results: We fed male C57BL/6J mice a HF/HS diet based on safflower oil - rich in *n*-6 PUFAs - or low-fat/low-sucrose (LF/LS) diet for 40 weeks. Compared to the LF/LS diet, intake of the safflower-based HF/HS diet only led to moderate weight gain, while glucose intolerance developed at week 5 prior to signs of inflammation, but concurrent with increased levels of linoleic acid and arachidonic acid in hepatic phospholipids. Intake of the HF/HS diet resulted in early changes in the gut microbiota, including an increased abundance of *Blautia*, while late changes coincided with altered inflammatory profiles and increased fasting plasma insulin. Analysis of immune cells in visceral fat and liver revealed no differences between diets before week 40, where the number of immune cells decreased in the liver of HF/HS-fed mice.

Conclusion: We suggest that a diet-dependent increase in the *n*-6 to *n*-3 PUFA ratio in hepatic phospholipids together with gut microbiota changes contributed to early development of glucose intolerance without signs of inflammation.

1 Introduction

During several decades, vegetable oils were regarded as healthier than saturated fats, and intake of *n*-6 PUFA increased following recommendations by health authorities, and because of the increased use of vegetable oil for animal feed [1]. However, the health-beneficial effects of increased intake of vegetable oils, especially oils rich in linoleic acid, has later been challenged as epidemiological studies and animal studies indicated that high intake of *n*-6 PUFAs was associated with increased adiposity [2-5]. Furthermore, several animal studies showed that the obesogenic effect of *n*-6, and also of *n*-3 PUFAs, was modulated by the type of carbohydrate and the balance between carbohydrates and protein in the diet [6-10]. In animal studies, most obesogenic diets are based on high levels of saturated fat (especially from lard). Consequently, little is known as to how prolonged high intake of *n*-6 PUFAs effects metabolism, glucose tolerance, insulin sensitivity and systemic low-grade inflammation.

In general, high-fat/high-glycemic carbohydrate rich diets are associated with low-grade systemic inflammation, which decreases insulin sensitivity [11-13]. By contrast, local inflammation is necessary for healthy expansion of white adipose tissue, evident in mice lacking key inflammatory mediators or pro-inflammatory cell types. Such mice display increased ectopic fat deposition in the liver associated with glucose intolerance [14, 15]. High levels of certain dietary components may initialize high-fat diet associated inflammation, either directly [16, 17] or indirectly via formation of immune-regulatory lipid mediators [18]. Additionally, diet-induced changes of the gut microbiota can activate inflammatory pathways resulting in insulin resistance and dysregulated glucose homeostasis [19, 20]. Recent studies have emphasized the importance of diets in regulation of the gut microbiota composition [21, 22], which in turn modulate host lipid metabolism including liver lipid profiles [23], and host glucose metabolism [24, 25]. Of note, high-fat diets as well as specific dietary fat sources independently shape the microbiota [22, 26], and this may in turn regulate metabolism via changes in production of SCFAs, branched chain amino acids, and secondary bile acids [25, 27, 28]. Thus, information on how specific dietary lipids affect the microbiota and how the microbiota in turn affect host metabolism is important in order to understand the development of the metabolic consequences of energy-dense diets.

Here we investigated the effects of prolonged intake of an *n*-6 PUFA rich high-fat/high-sucrose (HF/HS) diet on glucose homeostasis, insulin sensitivity, inflammation and gut microbiota in male C57BL/6J mice. We observed that the mice became glucose-intolerant prior to significant changes in body fat mass and without a measurable, significant decrease in systemic insulin sensitivity. Glucose intolerance was associated with changes in the gut microbiota and hepatic lipid profiles without concomitant inflammatory changes in visceral fat, liver and spleen.

2 Materials and methods

2.1 Animals.

Individually housed C57BL/6J BomTac male mice (8 weeks of age) (Taconic, Ejby, Denmark) with free access to water were fed a low fat/low sucrose (LF/LS) diet (Ssniff, Germany, S8672-E050) *ad libitum* at room temperature (21-24°C) with a 12-hour light and dark cycle. After two weeks of acclimatization, half were (n=4 per study, replicated once) shifted to a safflower oil based high fat/high sucrose (HF/HS) diet (Ssniff, Germany, S8672-E056). Food intake was recorded twice a week and body weight once a week. Body composition was measured by MRI scan (echoMRI, USA). Animal experiments were approved by the Danish National Animal Experiments Inspectorate (Reg. no. 2014-15-2934-01027).

2.2 Indirect calorimetry.

After 4 weeks on diets and a 3 day acclimatization period, activity, O_2 and CO_2 gas exchange measurements were determined for a 72-hour period as previously described [29].

2.3 Insulin and glucose tolerance test.

Separate groups (n=5, experiment repeated once) of mice were used for insulin (ITT) and glucose (GTT) tolerance tests. For ITT, 0.75 mU human insulin (Actrapid, Novo Nordisk, Denmark)/g lean body mass was injected i.p. after a two-hour fast. For GTT, mice were injected i.p. with 3 mg glucose/g lean body mass after a 6-hour fast. For plasma insulin, blood was collected from the tail vein into EDTA tubes. Blood glucose was measured using a glucometer (Contour, Bayer).

2.4 Termination and tissue harvest.

Before dissection, mice were anesthetized with hypnorm/midazolam, and venous blood collected followed by systemic perfusion with PBS. For RNA, liver samples were placed in Ambion RNAlater (Invitrogen) overnight at 4°C while epididymal white adipose tissue (eWAT) samples were flash-frozen. Liver- and eWAT samples were placed in 4% paraformaldehyde for histological analyses. Luminal contents from cecum and colon were flash-frozen. All samples except fixed tissues were stored at -80 °C.

2.5 Flow cytometry.

Liver and spleen tissue was mechanically dissociated and filtered through a 70 µm tissue strainer, washed using PBS with 1% FCS and 2 µM monensin (Sigma-Aldrich) (monensin buffer) and centrifuged at 300*g* at 4°C for 10 min. Spleen cells were incubated in lysis buffer (154 mM NH_4Cl, 10 mM $NaHCO_3$, 0.1 mM EDTA-Na_2 in PBS) for 5 min on ice. Cells were washed and resuspended in monensin buffer. Dispersed adipose tissue was incubated in a shaker-incubator at 37°C for 40 minutes in monensin buffer with 1 mg/mL collagenase II (Sigma-Aldrich). Cells were centrifuged at 300*g* at 4°C for 10 min and the stromal vascular fraction was resuspended in monensin buffer.

Cell suspensions were Fc receptor-blocked (anti-CD16/CD32 antibody, BD Biosciences), surface-stained in monensin buffer, and fixed and permeabilized using Cytofix/Cytoperm (BD Biosciences) for 20 min at 4°C followed by intracellular staining. Antibodies are listed in Suppl. Table 1 and gating strategy in Suppl. Fig. 1. Samples were washed and resuspended in PBS with 1% fetal calf serum and 0.1% NaN_3, and Count Bright beads (Life technologies) were added according to manufacturer's instructions. Samples were analyzed on a BD FACSCanto II (BD Biosciences) flow cytometer and data analyzed using Flowjo software (V10.0.7, Treestar).

2.6 Reverse transcription and qPCR.

RNA was extracted using Trizol (Ambion) using a modified product protocol with centrifugation for 20 minutes for RNA precipitation and washings. RNA yield was determined using a Nanodrop 2000 Spectrophotometer, and 1 µg liver and 100 ng eWAT RNA was used for cDNA synthesis using RevertAid Reverse Transcriptase (Thermo Scientific, USA), according to product protocol. RT-PCRs were performed using the SensiFAST SYBR Lo-ROX kit (Bioline, USA) on an Mx3000P system (Agilent Technologies, USA). See Suppl. Table 2 for primers. The thermal profile used was: 95°C, 5 min; 40 cycles of: 95°C, 15 sec, 55-63°C, 20 sec, 72°C, 15 sec. Expression was subsequently normalized to mRNA encoding TATA-binding protein (Tbp).

2.7 Extraction and quantification of liver lipids.

Samples were weighed and chloroform:methanol (2:1) containing 100 µg/mL butylated hydroxytoluene and internal standards (pentadecanoic acid, di C15:0 phophatidylcholine and tri C17:0 trialcylglycerol) was added. Samples were homogenized and 20% volume of 0.73% NaCl was added followed by centrifugation (4000 rpm, 5 min, 5°C). The lower phase was retrieved and stored at -20°C. Lipid extracts were fractionated on an aminopropyl-cartridge (Phenomenex Strata NH2, 500 mg) as previously described [30].

2.8 Histological examinations.

Paraffin embedded sections of eWAT were stained with haematoxylin and eosin (H&E). The mean diameter of 200 intact cells was measured on 3-4 sections from each mouse, using the ImageJ software. Adipocyte numbers were estimated as previously described [31].

2.9 Bacterial 16S rDNA amplicon sequencing and bioinformatics.

Bacterial DNA from cecal and fecal samples was extracted and libraries were prepared, sequenced and bioinformatically processed as previously described [32] with the exception of using the Greengenes database (4feb2011) and QIIME v1.8.0. Data was filtered by removal of Operational Taxonomic Units (OTUs) present in fewer than 3 samples or a relative abundance across all samples ≤0.005%. Samples containing ≤10,000 or ≥60,000 sequences were excluded (3 colon and 3 cecum samples). The ANOSIM function and LefSe [33] was used to calculate differences in bacterial composition and abundance.

2.10 Statistics.

Unless specified, two-way ANOVA (on normally distributed data) was used in GraphPad Prism 6.07. P values lower than 0.05 were considered significant with correction for multiple comparisons by false discovery rate. Differences between experimental replications were tested using Wilcoxon Rank Sum test as were differences in groups in case n<6 for all time points. Data are presented as mean±SEM, *P≤0.05, **P≤0.01, ***P≤0.001. Outliers were detected using the Grubbs' test in R v3.1.3.

3 Results

3.1 C57BL/6J mice fed a safflower oil-based n-6 PUFA-rich high fat/high sucrose diet develop early glucose intolerance in absence of insulin resistance.

Mice were fed a safflower-based HF/HS diet or a LF/LS diet for 40 weeks (Suppl. Table 3). Compared to the LF/LS-fed mice, mice on the HF/HS diet had no significant weight gain until week 28 (Fig. 1A), or increase in body fat mass until week 40 (Fig. 1B). Weight gain was associated with increased accumulated energy intake from week 10 and onwards (Fig. 1C and Suppl. Fig. 2A), whereas overall higher feed efficiency only tended to be increased (p=0.08) (Fig. 2D) in HF/HS-fed mice compared to the LF/LS-fed mice. Despite lower voluntary activity by HF/HS-fed mice (Fig. 1E and Suppl. Fig. 2B), differences in energy expenditure could not explain differences in weight gain (Fig. 1F and Suppl. Fig. 2C-E). Since respiratory exchange ratio (RER) was significantly lower in HF/HS-fed mice (Suppl. Fig. 2F-G) differences in the metabolism of dietary nutrients may have contributed to the observed difference in weight gain.

The late weight gain facilitated the investigation of metabolic and inflammatory effects of a HF/HS diet without major changes in fat mass. We observed that HF/HS-fed mice exhibited increased fasting plasma insulin by week 40 concomitant with changes in fat mass (Fig. 1G). Although homeostatic model assessment (HOMA-IR) at week 40 pointed to significantly reduced insulin sensitivity (Fig. 1H), no significant difference was found as determined by insulin tolerance tests (ITTs) in HF/HS-fed compared to LF/LS-fed mice (Fig 1I and J). However, fasting plasma glucose was significantly higher in the HF/HS-fed mice from week 5 (Fig. 1K), and glucose tolerance was significantly impaired already from week 5 and onwards (Fig. 1L and M).

3.2 Intake of a safflower oil-based n-6 PUFA-rich high fat/high sucrose diet results in adipocyte hypertrophy but not in hyperplasia.

Since impaired adipose tissue expansion is associated with glucose intolerance [14], we examined visceral adipose tissue expandability. Notably, the overall mass of eWAT increased from week 10 (Fig. 2A) and was associated with increased mean adipocyte size at week 10 and 40 (Fig. 2B-C). However, surprisingly we observed no increase in the number of adipocytes even after 40 weeks in HF/HS-fed mice (Fig. 2D). Expression of peroxisome proliferator-activated receptor gamma 2 (*Pparg2*), adiponectin (*Adipoq*) (Suppl. Fig. 3A-B), sterol regulatory element-binding protein 1 (*Srebf1*) and

carnitine palmitoyltransferase 1A (*Cpt1a*) (Suppl. Fig. 3C-D) mRNAs revealed no overall alterations in adipocyte function in eWAT. Thus, the lack of adipocyte hyperplasia in response to n-6 PUFA-rich safflower oil-based HF/HS diets might contribute to the development of persistent glucose intolerance.

3.3 Glucose intolerance associated with intake of a safflower-based n-6 PUFA-rich high-fat/high sucrose diet is not dependent on inflammation in eWAT.

To investigate if inflammation might contribute to the observed metabolic changes, we performed a detailed profiling of the immune cell composition in eWAT. Unexpectedly, we observed no differences in abundances of major immune cell subsets between LF/LS and HF/HS-fed mice at any time (Fig. 3A). As expected, macrophages made up a large fraction of immune cells in eWAT (Fig. 3A). Surprisingly, natural killer T cells also constituted a large proportion (20-40 %) of immune cells in eWAT until week 40 where their abundance declined causing a diet-independent reduction in immune cell numbers (Fig. 3A). Although we observed no differences in the total number of macrophages in eWAT between diets, the M1/M2 macrophage ratio was higher in HF/HS-fed mice at week 40 (Fig. 3B). This coincided with increased tumor necrosis factor-α (TNFα) levels at week 40 within M1 macrophages in HF/HS-fed mice (Fig. 3C). Of note, TNFα levels in M1 macrophages also differed between diets at week 2 due to low expression in LF/LS-fed mice (Fig. 3C). No differences in TNFα were found in M2 macrophages (Suppl. Fig. 4). RT-PCR of TNFα mRNA expression revealed no differences between diets (Fig. 3D). Thus, despite impaired glucose tolerance from week 5, eWAT showed no sign of inflammation before week 40 coinciding with the appearance of commencing insulin resistance (Fig. 1H).

3.4 Intake of a safflower-based n-6 PUFA-rich high-fat/high sucrose diet leads to early changes in hepatic phospholipid profiles without immune cell infiltration and hepatic steatosis.

Hepatic lipid accumulation and inflammation may lead to sustained hepatic glucose output. We observed an increase in total liver mass at week 10, and increased triglyceride (TG) levels over time from week 2 and onwards in HF/HS-fed compared to LF/LS-fed mice (Fig. 4A-B). However, we observed no visible formation of lipid droplets, and liver morphology remained normal without signs of hepatic steatosis (Fig. 4C). Conversely, hepatic phospholipid profiles rapidly distinguished the two diets, and the differences remained throughout the study (Fig. 4D-E) with changes in the *n*-6/*n*-3 ratio as early as week 2 (Fig. 4D) caused by increased abundance of linoleic acid (C18:2n-6) and arachidonic acid (C20:4n-6), while the fraction of docosahexaenoic acid (C22:6n-3), a precursor for inflammation-resolving resolvins, decreased in the HF/HS group (Fig. 4E). Eicosapentaenoic acid (C20:5n-3) was almost undetectable in both groups (data not shown). Despite changes in hepatic lipid profiles, expression of genes involved in regulation of lipid metabolism including sterol regulatory element-binding transcription factor 1 (*Srebf1*) (Suppl. Fig 5A), *Cpt1a* (Suppl. Fig. 5B), acetyl-CoA carboxylase (*Acaca*) (Suppl. Fig. 5C), fatty acid synthase (*Fasn*) (Suppl. Fig. 5D), *Pparg1* (Suppl. Fig 5E) and peroxisome proliferator-activated receptor alpha (*Ppara*) (Suppl. Fig. 5F) was unchanged by intake of the HF/HS diet (Suppl. Fig. 5A-F). Together this indicated that changes in fatty

acid profile of hepatic phospholipids, but not transcriptional regulation of hepatic lipid metabolism, might contribute to glucose intolerance. Expression of mRNAs encoding enzymes involved in hepatic gluconeogenesis including glucose 6-phosphatase (G6pc) and phosphoenolpuryvate carboxykinase (Pck) were unchanged in HF/HS-fed compared to LF/LS-fed mice (Fig. 4F-G), indicating that increased expression of these key genes transcriptional regulation of hepatic gluconeogenesis did not contribute to glucose intolerance. Since *n*-6 PUFAs are important precursors of pro-inflammatory lipid mediators, we next investigated changes in liver immune function. However, no differences between diets were found until week 40, where a lower number of innate and adaptive immune cells were found in the liver of HF/HS-fed compared to LF/LS-fed mice (Fig. 4H). Specifically, the number of neutrophils, eosinophils and basophils, B cells, CD4+ and CD8+ αβ T cells was lower in the HF/HS-fed mice (Fig. 4H), and we did not detect an increased expression of *Tnfa* (Suppl. Fig. 5G). Collectively, this indicates that liver inflammation did not contribute to early glucose intolerance in HF/HS-fed mice. Finally, characterization of immune cell profiles in the spleen did not reveal differences in the systemic inflammatory environment between diets (Suppl. Fig. 5H).

3.5 Intake of safflower oil rich high-fat/high sucrose diet leads to rapid changes in gut bacterial composition.

We performed 16S rDNA amplicon sequencing of bacterial DNA and measured short chain fatty acids in the cecum and colon of HF/HS and LF/LS-fed mice. Principal Coordinates Analysis (PCoA) using Bray-Curtis distances of microbial communities revealed separation according to diets at week 5 concomitant with reduced glucose tolerance (Fig. 5A, $p<0.05$ for difference between diets for both cecum and colon) and pronounced separation at week 40 ($p<0.05$ and $p<0.01$ for cecum and colon, respectively). Of note, similarities between bacterial communities were higher in LF/LS-fed mice from week 5 to 40 compared to HF/HS fed mice (ADONIS test for variance, $p<0.001$, $p<0.05$, $p<0.01$ for colon and $p<0.01$, $p<0.05$, $p<0.01$ for cecum at week 5, 10, and 40 respectively) (Fig. 5A). PCoA using weighted UNIFRAC yielded similar results (Suppl. Fig. 6). Alpha diversity in HF/HS-fed mice was higher in the cecum at all weeks compared to LF/LS-fed mice (Fig. 5B). In the colon, significant differences in alpha diversity was found only at week 2 and 40 (Fig. 5C). We observed a tendency towards lower abundance of Bacteroidetes in HF/HS-fed compared to LF/LS-fed mice in both the cecum and the colon, though only significantly different at week 5 and 40 for the cecum and at week 5 for the colon (Fig. 5D). A minor increase in the abundance of Deferribacteres in the cecum and a decrease in Proteobacteria in the cecum and colon was also observed by week 40 in HF/HS-fed mice (Fig. 5D). In addition, a minor decrease in the abundance of Actinobacteria was found in the HF/HS-fed mice in the cecum from week 10 and onwards (included in group termed “Other” in Fig. 5D). At the genus level, relatively small temporal differences were found between diets. We noted that colonic and cecal abundances of *Alistipes* tended to decrease over time in the LF/LS-fed mice (Fig. 5E and Suppl. Fig. 7A). Interestingly, the abundance of *Blautia* increased already after 2 weeks of HF/HS feeding and remained elevated throughout the study, covering on average 0.9% of the cecal microbiota in HF/HS-fed versus 0.3% in LF/LS-fed mice (Fig. 5F). In the colon the same tendency was observed for *Blautia* although they displayed lower abundance (Suppl. Fig. 7B). Conversely, the relative abundance

of *Barnesiella* was significantly higher in LF/LS-fed compared to HF/HS-fed mice from week 5 and onwards (Fig. 5G and Suppl. Fig. 7C for cecum and colon respectively). Notably, the *Barnesiella* genus dominated in LF/LS-fed mice constituting 49.0% and 52.8% of the microbiota in the cecum and colon, respectively. Late increases in abundance of *Lachnospiracea incertae sedis* for both the cecum and colon, and *Mucispirillum* for the cecum were found at week 40 (Fig. H-I and Suppl. Fig. D-E). In addition, significant differences in abundances, but without a consistent tendency, between HF/HS-fed and LF/LS-fed mice at different time points were found for a number of genera. These included *Bilophila*, *Olsenella*, *Clostridium* XIVa, *Parasutterella* and *Pseudoflavonifactor* in the cecum as well as *Allobaculum* and *Parasutterella* in the colon (Suppl. Fig. 7F-L).

Since the microbiota produces SCFAs modulating host metabolism, we determined SCFA levels in the cecum and the colon (Suppl. Fig. 8B-G). Except for a higher concentration of acetic acid in the cecum of HF/HS-fed mice at week 40 (Suppl. Fig. 8D) no differences were found between the diets indicating that differences in SCFAs in the gut did not contribute to glucose intolerance.

4 Discussion

Reports on glucose intolerance in the absence of insulin resistance are sparse, although this phenotype has previously been observed in mice fed a HF/HS diet with a high protein:carbohydrate ratio [29], and in mice with impaired inflammatory responses preventing high-fat diet-induced adipose tissue expansion [14]. Here we found that C57BL/6J mice fed a safflower oil-based *n*-6 PUFA rich HF/HS diet exhibited early onset of glucose intolerance prior to increased fat mass and before development of insulin resistance. Development of glucose intolerance was accompanied by rapid and sustained changes in the cecal and colonic bacterial composition. The increased abundance of *Blautia* after only 2 weeks of HF/HS feeding is intriguing. The study design did not allow for correlations between microbiota and metabolic parameters. Nevertheless, the results suggest a relation between *Blautia* abundance and glucose intolerance. However, an increase in the abundance of butyrate-producing *Blautia* has previously been associated with treatments that improve glucose homeostasis [34, 35], questioning whether the early increase in *Blautia* might be implicated in glucose intolerance. The same conclusion holds for the *Lachnospiracea incertea sedis* genus that was increased in HF/HS-fed mice at later time points. In contrast, *Mucispirillum* has been associated with high-fat diets and glucose intolerance [36], but since we only observed late changes in this genus it seems unlikely to be the cause of early induction of glucose intolerance. In this context, it is noteworthy that no differences were found in cecal or colonic SCFA content between the diets before week 40.

The early onset of glucose intolerance was not accompanied by accumulation of immune cells in adipose tissue or liver, nor in hepatic steatosis, but coincided with changes in hepatic phospholipids including dominance of the *n*-6 PUFAs, linoleic acid and arachidonic acid, at the expense of the *n*-3

PUFAs. These *n-6* PUFAs may serve as precursors for both pro- and anti-inflammatory mediators [5]. However, we first observed an increase in the M1/M2 macrophage ratio and inflammatory markers at week 40, concomitant with increased HOMA-IR. We found that the relative abundance of *Barnesiella* was lower and the relative abundance of *Alistipes* higher in HF/HS-fed compared to LF/LS-fed mice at week 40. The extent to which these differences contributed to inflammation, the increase in HOMA-IR, and impairment of glucose tolerance remains to be established, but a high abundance of *Barnesiella* has been associated with negative metabolic effects (33) and increased levels of branched chain amino acids (35), which have been correlated with insulin resistance and diabetes (14). In our experiment, the low *Barnesiella* abundance in HF/HS could be speculated to have a counterregulatory effect. In the case of *Alistipes*, the situation is also unclear as this genus was reported to increase in response to weight loss [37], and further, the abundance of *Alistipes* was higher in undernourished compared to normally nourished mice [38].

The safflower oil-based diet was chosen due to high linoleic acid content suspected to promote obesity [5]. Surprisingly the intake of the safflower oil-based HF/HS diet resulted in lower weight gain and accumulation of adipose tissue than observed in previous studies in rodents on high-fat diet using safflower oil [39-41], and similar diets based on corn oil or soybean oil with lower linoleic acid content [6-8]. Thus the delayed and reduced weight gain and adiposity development was unexpected, but then allowed for analysis of a case of reduced glucose tolerance in the absence of adipose mass gain, inflammation and insulin resistance. The disparate results may relate to differences in baseline microbiota composition resulting in different responses to high-fat feeding [25, 42], but effects of minor components such as carotenoids and polyphenols in the safflower oil cannot be excluded. Future studies comparing gut microbiota of mice from other vendors on the same diet or using different dietary oils could contribute to understanding the interplay between dietary fat and particular bacterial taxa contributing to the host phenotype. The gut microbiota may increase energy efficiency by producing SCFA, as observed in obesity (39). In this study, energy efficiency in HF/HS-fed mice was higher only during the first 5 weeks without increased concentration of SCFAs in cecum and feces. Whether this could be a contributing factor to the low energy efficiency in the safflower oil-based *n*-6 PUFA rich HF/HS diet remains to be established.

We identified insulin resistance at week 40 coinciding with body fat mass gain and inflammatory changes in the liver, suggesting that one or both of these changes were necessary for initiation of insulin resistance. Detailed analyses of immune cell subsets within eWAT, liver and spleen substantiated that no inflammation was evident in the examined organs before week 40. A general depletion of hepatic immune cells at week 40 in HF/HS-fed mice is consistent with previous results showing depletion of natural killer T cells and CD4+ T cells in inflamed liver [43]. However, to our knowledge, hepatic depletion of neutrophils, eosinophils, basophils, B cells and CD8+ αβ T cells in HF/HS-fed mice has not been described previously.

In conclusion, our study report on an unusual condition where intake of a diet based on high levels of safflower oil and sucrose, normally considered to be highly obesogenic, resulted in moderate and delayed weight gain and adiposity without changes in immune cell abundance and HOMA-IR before week 40. Yet, HF/HS-fed mice exhibited impaired glucose tolerance already after week 5. We found marked changes in the composition of the gut microbiota preceding the development of glucose intolerance and concomitant with late initiation of inflammation at week 40, but the relation between these changes and the metabolic phenotypes remains unclear. In contrast we found a strong association between early changes in hepatic phospholipids with dietary *n*-6 PUFAs that serve as precursors for pro-inflammatory lipid mediators suggesting that such changes may explain the early onset of glucose intolerance, even though we did not observe changes in liver metabolism.

All authors of this manuscript have directly participated in the execution and/or analysis of the study. Conceived and designed the experiments: N.D.S., D.A. L.M., L.I.H., K.K., S.B. Performed the experiments: N.D.S., D.A., I.D.R., A.N.H., T.M., C.N., E.F., X.F. Analyzed the data: All authors. Wrote the paper: N.D.S., D.A., S.B, K.K. All authors approved the manuscript.

The authors would like to thank Lisbeth Buus Rosholm, Mohammed-Samir Belmaâti, Martin Asser Hansen, Tao Ma, Jannie Agersten, Anne Christine Heerup-Larsson, Una Ursula Lund, Mikkel Trøst Nielsen for help during dissections, initial bioinformatics, and technical assistance for lipid analysis. This work was supported by a grant from the Øllingesøe Foundation, the Novo Nordisk Foundation, and the Carlsberg Foundation.

The authors have no conflict of interest to disclose.

5 References

[1] Blasbalg, T. L., Hibbeln, J. R., Ramsden, C. E., Majchrzak, S. F., Rawlings, R. R., Changes in consumption of omega-3 and omega-6 fatty acids in the United States during the 20th century. *Am J Clin Nutr* 2011, *93*, 950-962.

[2] Ailhaud, G., Massiera, F., Weill, P., Legrand, P.*, et al.*, Temporal changes in dietary fats: role of n-6 polyunsaturated fatty acids in excessive adipose tissue development and relationship to obesity. *Prog Lipid Res* 2006, *45*, 203-236.

[3] Massiera, F., Saint-Marc, P., Seydoux, J., Murata, T.*, et al.*, Arachidonic acid and prostacyclin signaling promote adipose tissue development: a human health concern? *Journal of Lipid Research* 2003, *44*, 271-279.

[4] Madsen, L., Petersen, R. K., Kristiansen, K., Regulation of adipocyte differentiation and function by polyunsaturated fatty acids. *Biochim Biophys Acta* 2005, *1740*, 266-286.

[5] Alvheim, A. R., Malde, M. K., Osei-Hyiaman, D., Lin, Y. H.*, et al.*, Dietary linoleic acid elevates endogenous 2-AG and anandamide and induces obesity. *Obesity (Silver Spring)* 2012, *20*, 1984-1994.

[6] Madsen, L., Pedersen, L. M., Liaset, B., Ma, T.*, et al.*, cAMP-dependent signaling regulates the adipogenic effect of n-6 polyunsaturated fatty acids. *J Biol Chem* 2008, *283*, 7196-7205.

[7] Ma, T., Liaset, B., Hao, Q., Petersen, R. K.*, et al.*, Sucrose counteracts the anti-inflammatory effect of fish oil in adipose tissue and increases obesity development in mice. *PLoS One* 2011, *6*, e21647.

[8] Hao, Q., Lillefosse, H. H., Fjaere, E., Myrmel, L. S.*, et al.*, High-glycemic index carbohydrates abrogate the antiobesity effect of fish oil in mice. *Am J Physiol Endocrinol Metab* 2012, *302*, E1097-1112.

[9] Madsen, L., Liaset, B., Kristiansen, K., Macronutrients and obesity: views, news and reviews. *Future Lipidol* 2008, *3*, 43-74.

[10] Madsen, L., Kristiansen, K., The importance of dietary modulation of cAMP and insulin signaling in adipose tissue and the development of obesity. *Ann Ny Acad Sci* 2010, *1190*, 1-14.

[11] Osborn, O., Olefsky, J. M., The cellular and signaling networks linking the immune system and metabolism in disease. *Nat Med* 2012, *18*, 363-374.

[12] Brestoff, J. R., Artis, D., Immune regulation of metabolic homeostasis in health and disease. *Cell* 2015, *161*, 146-160.

[13] Johnson, A. R., Milner, J. J., Makowski, L., The inflammation highway: metabolism accelerates inflammatory traffic in obesity. *Immunol Rev* 2012, *249*, 218-238.

[14] Wernstedt Asterholm, I., Tao, C., Morley, T. S., Wang, Q. A.*, et al.*, Adipocyte inflammation is essential for healthy adipose tissue expansion and remodeling. *Cell Metab* 2014, *20*, 103-118.

[15] Lee, Y. S., Li, P., Huh, J. Y., Hwang, I. J.*, et al.*, Inflammation is necessary for long-term but not short-term high-fat diet-induced insulin resistance. *Diabetes* 2011, *60*, 2474-2483.

[16] Lee, J. Y., Zhao, L., Youn, H. S., Weatherill, A. R.*, et al.*, Saturated fatty acid activates but polyunsaturated fatty acid inhibits Toll-like receptor 2 dimerized with Toll-like receptor 6 or 1. *J Biol Chem* 2004, *279*, 16971-16979.

[17] Dasu, M. R., Jialal, I., Free fatty acids in the presence of high glucose amplify monocyte inflammation via Toll-like receptors. *Am J Physiol Endocrinol Metab* 2011, *300*, E145-154.

[18] Iyer, A., Fairlie, D. P., Prins, J. B., Hammock, B. D., Brown, L., Inflammatory lipid mediators in adipocyte function and obesity. *Nat Rev Endocrinol* 2010, *6*, 71-82.

[19] Tremaroli, V., Backhed, F., Functional interactions between the gut microbiota and host metabolism. *Nature* 2012, *489*, 242-249.

[20] Brestoff, J. R., Artis, D., Commensal bacteria at the interface of host metabolism and the immune system. *Nat Immunol* 2013, *14*, 676-684.

[21] Wu, G. D., Chen, J., Hoffmann, C., Bittinger, K.*, et al.*, Linking long-term dietary patterns with gut microbial enterotypes. *Science* 2011, *334*, 105-108.

[22] David, L. A., Maurice, C. F., Carmody, R. N., Gootenberg, D. B.*, et al.*, Diet rapidly and reproducibly alters the human gut microbiome. *Nature* 2014, *505*, 559-563.

[23] Velagapudi, V. R., Hezaveh, R., Reigstad, C. S., Gopalacharyulu, P.*, et al.*, The gut microbiota modulates host energy and lipid metabolism in mice. *J Lipid Res* 2010, *51*, 1101-1112.

[24] Karlsson, F. H., Tremaroli, V., Nookaew, I., Bergstrom, G.*, et al.*, Gut metagenome in European women with normal, impaired and diabetic glucose control. *Nature* 2013, *498*, 99-103.

[25] Khan, M. T., Nieuwdorp, M., Backhed, F., Microbial modulation of insulin sensitivity. *Cell Metab* 2014, *20*, 753-760.

[26] Huang, E. Y., Leone, V. A., Devkota, S., Wang, Y.*, et al.*, Composition of dietary fat source shapes gut microbiota architecture and alters host inflammatory mediators in mouse adipose tissue. *JPEN J Parenter Enteral Nutr* 2013, *37*, 746-754.

[27] Qin, J., Li, Y., Cai, Z., Li, S.*, et al.*, A metagenome-wide association study of gut microbiota in type 2 diabetes. *Nature* 2012, *490*, 55-60.

[28] Sayin, S. I., Wahlstrom, A., Felin, J., Jantti, S.*, et al.*, Gut microbiota regulates bile acid metabolism by reducing the levels of tauro-beta-muricholic acid, a naturally occurring FXR antagonist. *Cell Metab* 2013, *17*, 225-235.

[29] Fjaere, E., Aune, U. L., Roen, K., Keenan, A. H.*, et al.*, Indomethacin treatment prevents high fat diet-induced obesity and insulin resistance but not glucose intolerance in C57BL/6J mice. *J Biol Chem* 2014, *289*, 16032-16045.

[30] Ingvorsen, C., Thysen, A. H., Fernandez-Twinn, D., Nordby, P.*, et al.*, Effects of pregnancy on obesity-induced inflammation in a mouse model of fetal programming. *Int J Obes (Lond)* 2014, *38*, 1282-1289.

[31] Sackmann-Sala, L., Berryman, D. E., Munn, R. D., Lubbers, E. R., Kopchick, J. J., Heterogeneity among white adipose tissue depots in male C57BL/6J mice. *Obesity* 2012, *20*, 101-111.

[32] Holm, J. B., Sorobetea, D., Kiilerich, P., Ramayo-Caldas, Y.*, et al.*, Chronic Trichuris muris Infection Decreases Diversity of the Intestinal Microbiota and Concomitantly Increases the Abundance of Lactobacilli. *PLoS One* 2015, *10*, e0125495.

[33] Segata, N., Izard, J., Waldron, L., Gevers, D.*, et al.*, Metagenomic biomarker discovery and explanation. *Genome Biol* 2011, *12*, R60.

[34] Zhang, X., Zhao, Y., Xu, J., Xue, Z.*, et al.*, Modulation of gut microbiota by berberine and metformin during the treatment of high-fat diet-induced obesity in rats. *Sci Rep* 2015, *5*, 14405.

[35] Zhang, X., Zhao, Y., Zhang, M., Pang, X.*, et al.*, Structural changes of gut microbiota during berberine-mediated prevention of obesity and insulin resistance in high-fat diet-fed rats. *PLoS One* 2012, *7*, e42529.

[36] Serino, M., Luche, E., Gres, S., Baylac, A.*, et al.*, Metabolic adaptation to a high-fat diet is associated with a change in the gut microbiota. *Gut* 2012, *61*, 543-553.

[37] Louis, S., Tappu, R. M., Damms-Machado, A., Huson, D. H., Bischoff, S. C., Characterization of the Gut Microbial Community of Obese Patients Following a Weight-Loss Intervention Using Whole Metagenome Shotgun Sequencing. *PLoS One* 2016, *11*, e0149564.

[38] Preidis, G. A., Ajami, N. J., Wong, M. C., Bessard, B. C*., et al.*, Composition and function of the undernourished neonatal mouse intestinal microbiome. *J Nutr Biochem* 2015, *26*, 1050-1057.

[39] Zhang, Z., Li, Q., Liu, F., Sun, Y., Zhang, J., Prevention of diet-induced obesity by safflower oil: insights at the levels of PPARalpha, orexin, and ghrelin gene expression of adipocytes in mice. *Acta biochimica et biophysica Sinica* 2010, *42*, 202-208.

[40] Poudyal, H., Kumar, S. A., Iyer, A., Waanders, J*., et al.*, Responses to oleic, linoleic and alpha-linolenic acids in high-carbohydrate, high-fat diet-induced metabolic syndrome in rats. *The Journal of nutritional biochemistry* 2013, *24*, 1381-1392.

[41] de Wit, N., Derrien, M., Bosch-Vermeulen, H., Oosterink, E*., et al.*, Saturated fat stimulates obesity and hepatic steatosis and affects gut microbiota composition by an enhanced overflow of dietary fat to the distal intestine. *Am J Physiol-Gastr L* 2012, *303*, G589-G599.

[42] Xiao, L., Feng, Q., Liang, S., Sonne, S. B*., et al.*, A catalog of the mouse gut metagenome. *Nat Biotechnol* 2015, *33*, 1103-1108.

[43] Li, Z., Soloski, M. J., Diehl, A. M., Dietary factors alter hepatic innate immune system in mice with nonalcoholic fatty liver disease. *Hepatology* 2005, *42*, 880-885.

FIGURE LEGENDS

Figure 1. Metabolic characteristics of C57BL/6J mice fed a safflower oil-based HF/HS or a LF/LS diet. (A) Body weight gain. (B) Percent fat mass. (C) Accumulated energy intake. (D) Energy efficiency (weight gain relative to energy intake in kcal). For metabolic chambers, mice were on HS/HS diet for 4 weeks prior to adaptation, average metabolic values were calculated from three consecutive days, n=5. (E) Average daily activity, (F) Average daily oxygen consumption. (G) Fasting (6h) plasma insulin levels. (H) HOMA-IR calculated from fasting plasma (6h) levels of insulin and glucose. (I) ITT at 5, 10, 40 weeks on diet and, (J) area under the curve from ITT. (K) GTT at 5, 10, 40 weeks on diet and, (L) area under the curve from GTT. In A-D, E-F: n=6-8 from two experiments, in G-L, n=7-11 from two experiments. Wilcoxon Rank Sum test used to test for differences in accumulated energy intake. White circles or squares = LF/LS-fed mice, black circles or squares = HF/HS-fed mice.

Figure 2. Characterization of epididymal white adipose tissue. (A) eWAT pad weight. (B) Representative hematoxylin and eosin stains of eWAT at week 10 and 40. (C) Mean adipocyte diameter at week 10 and 40. (D) Estimated number of adipocytes in HF/HS fed and LF/LS fed mice. For all data, n=6-8 from two experiments. White squares = LF/LS-fed mice, black squares = HF/HS-fed mice.

Figure 3. Immunological characterization of epididymal white adipose tissue (A) Number of different immune cells per gram eWAT. (B) Ratio between M1 and M2 macrophages in eWAT. (C) Median fluorescence intensity of TNFα in M1 macrophages in eWAT. (D) *Tnfa* expression in eWAT. For all data, n=6-8 from two experiments. White squares = LF/LS-fed mice, black squares = HF/HS-fed mice.

Figure 4. Hepatic morphology, lipids, gene expression and infiltrating immune cells. (A) Liver weight. (B) Liver triglyceride concentration. (C) Representative images of liver Hematoxylin and Eosin (H&E)-stained paraffin-embedded sections at week 10 and 40. (D) Ratio between liver n-6/n-3 fatty acids. (E) Percentages of selected phospholipids of total phospholipids. (F) Expression of liver *Pck*. (G) Expression of liver *G6pc*. (H) Percentages of leukocyte populations of total immune cells in the liver. In D and E, n=5-8, otherwise n=6-8 from two experiments. Wilcoxon Rank Sum test used to test for differences in liver triglyceride concentration. White squares = LF/LS-fed mice, black squares = HF/HS-fed mice.

Figure 5. Cecum and colon microbiota composition. (A) PCoA of operational-taxonomic units (OTUs) from 16S rDNA amplicon sequencing of cecal and colonic bacteria. (B) α-diversity in the cecum, and (C) colon. (D) Phylum abundance in the cecum and the colon. (E-I) Changes in relative abundances of genera in the colon (E) and cecum (F-I) with at least one significant difference between diets, a mean abundance above one percent for a diet at any week, and with a consistently lower or higher mean abundance between the diets across weeks. For all data, n=6-8 from two experiments. White circles and squares = LF/LS-fed mice, grey circles and black squares = HF/HS-fed mice.

FIGURES

Fig. 1

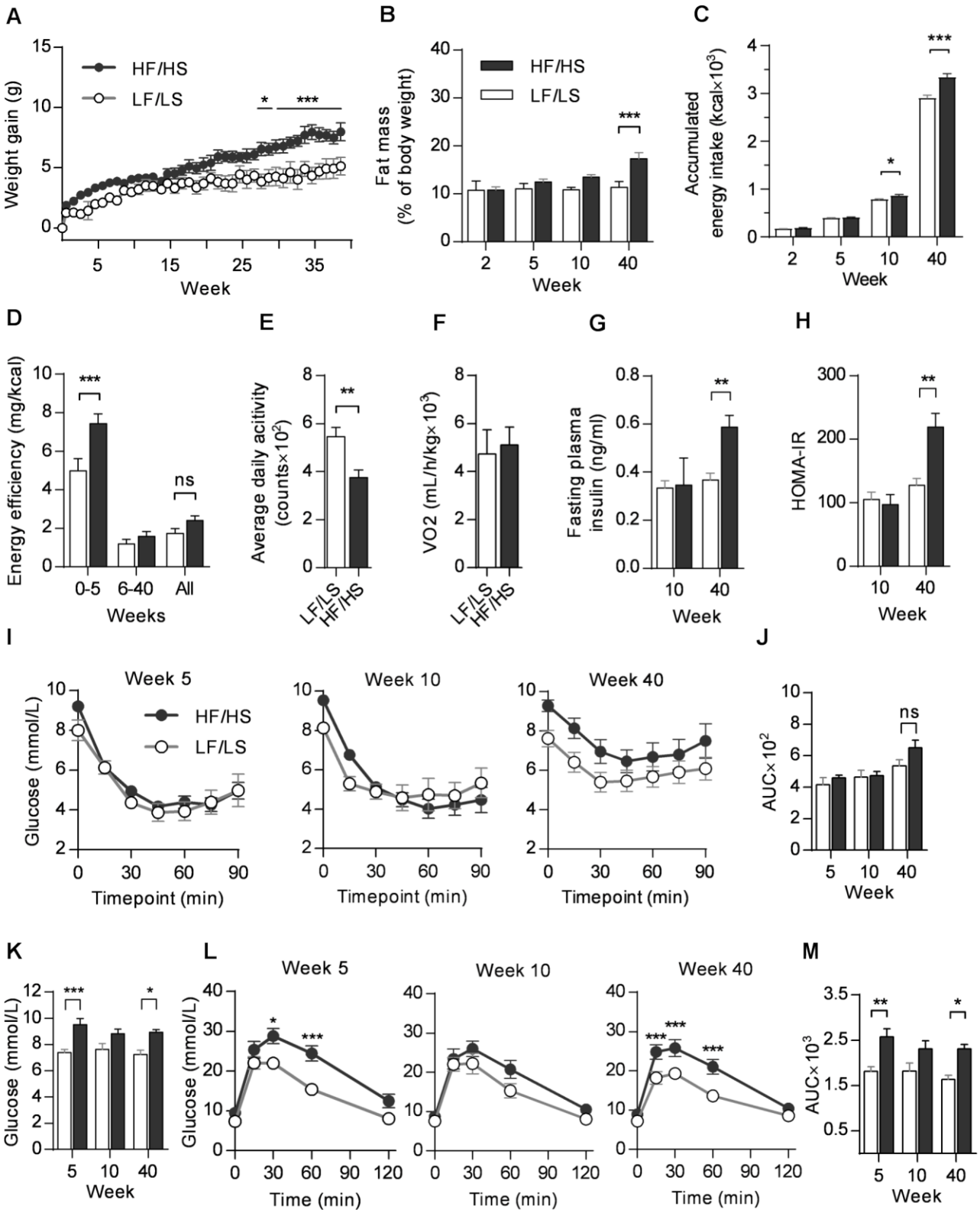

Fig. 2

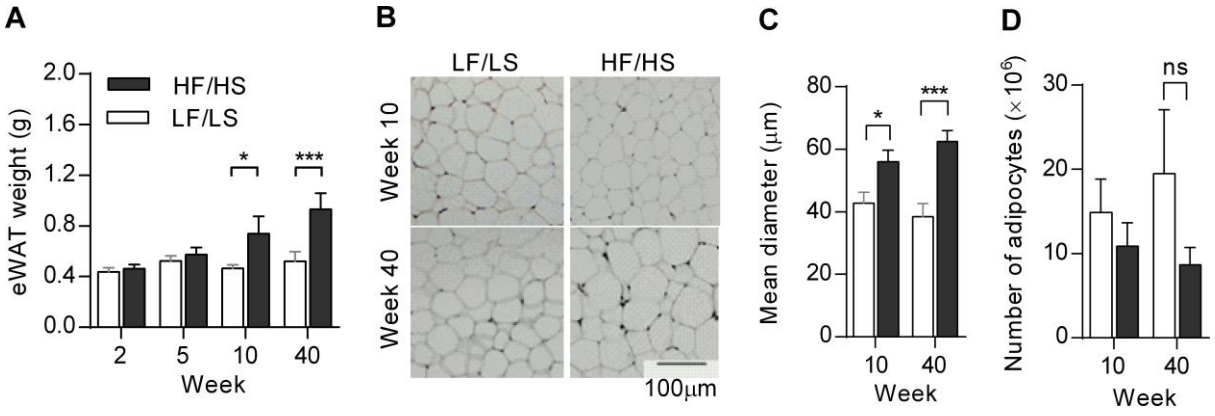
A
eWAT weight (g)
HF/HS
LF/LS
Week
B
LF/LS
HF/HS
Week 10
Week 40
100µm
C
Mean diameter (µm)
Week
D
Number of adipocytes (×10^6)
ns
Week

Fig. 3

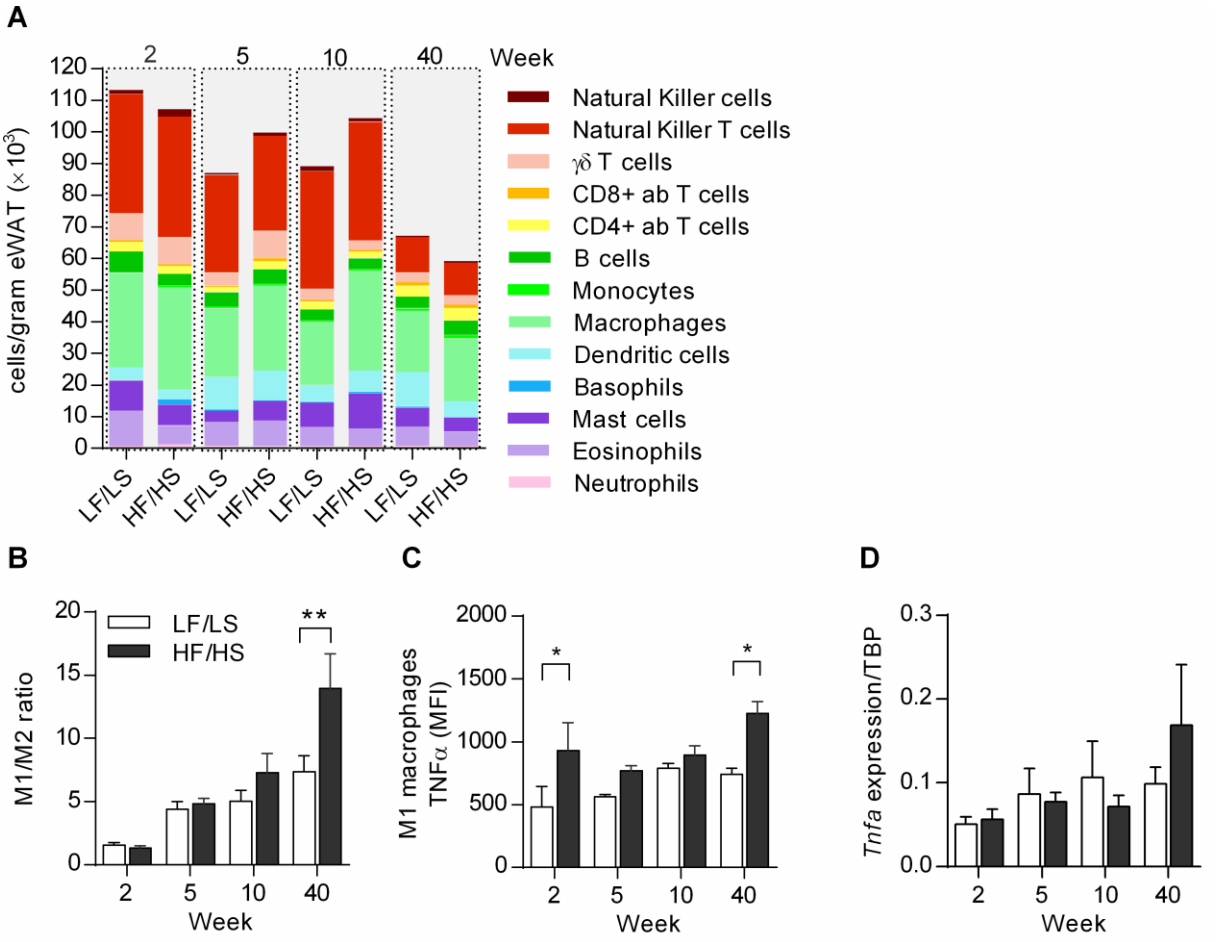
A
cells/gram eWAT (×10^3)
Week
Natural Killer cells
Natural Killer T cells
γδ T cells
CD8+ ab T cells
CD4+ ab T cells
B cells
Monocytes
Macrophages
Dendritic cells
Basophils
Mast cells
Eosinophils
Neutrophils
LF/LS
HF/HS
B
M1/M2 ratio
C
M1 macrophages TNFα (MFI)
D
Tnfa expression/TBP
Week

Fig. 4

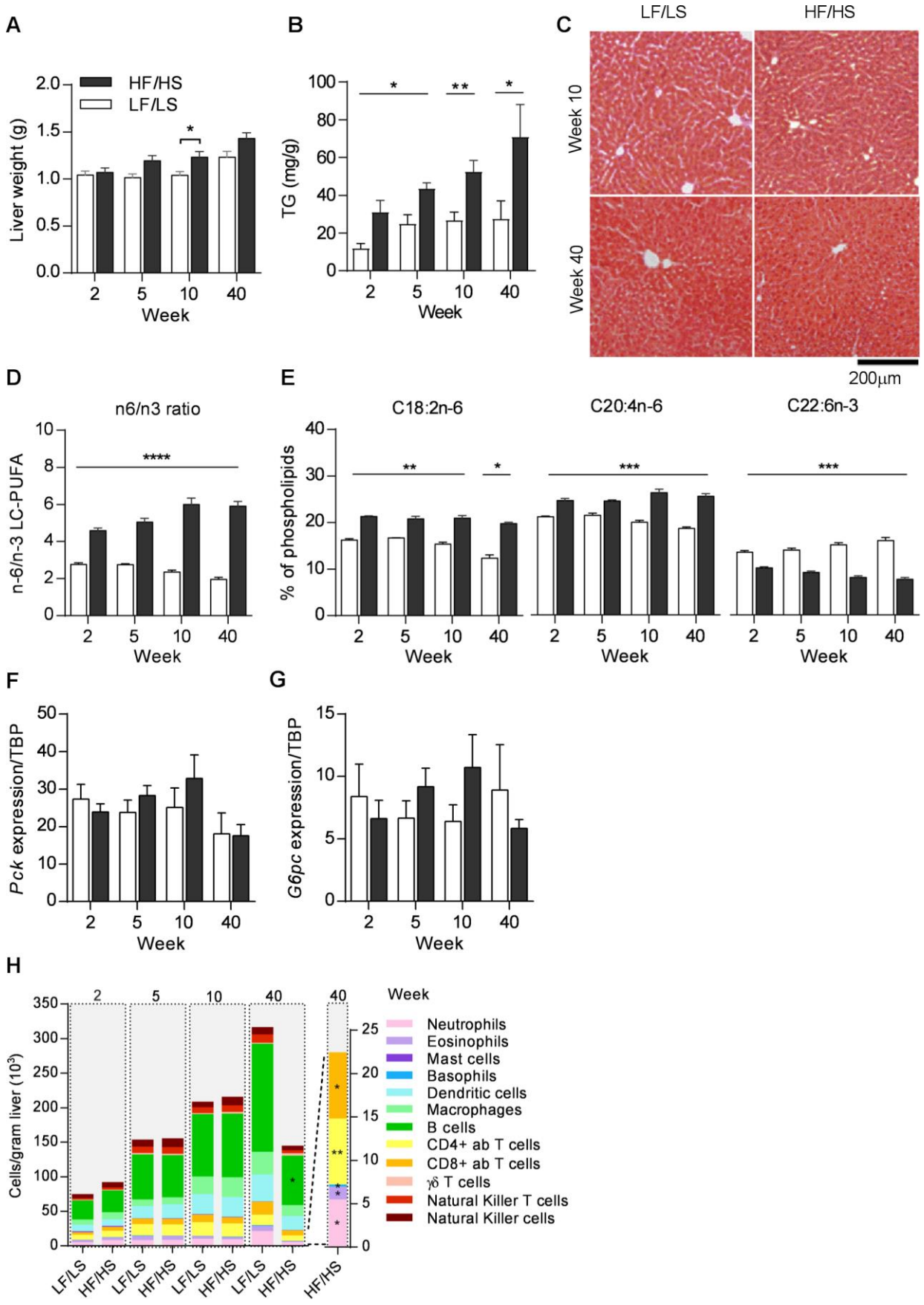
A
B
C
LF/LS
HF/HS
Liver weight (g)
HF/HS
LF/LS
Week
TG (mg/g)
Week 10
Week 40
200μm
D
E
n6/n3 ratio
n-6/n-3 LC-PUFA
C18:2n-6
C20:4n-6
C22:6n-3
% of phospholipids
F
G
Pck expression/TBP
G6pc expression/TBP
H
Cells/gram liver (10³)
Week
Neutrophils
Eosinophils
Mast cells
Basophils
Dendritic cells
Macrophages
B cells
CD4+ ab T cells
CD8+ ab T cells
γδ T cells
Natural Killer T cells
Natural Killer cells

Fig. 5

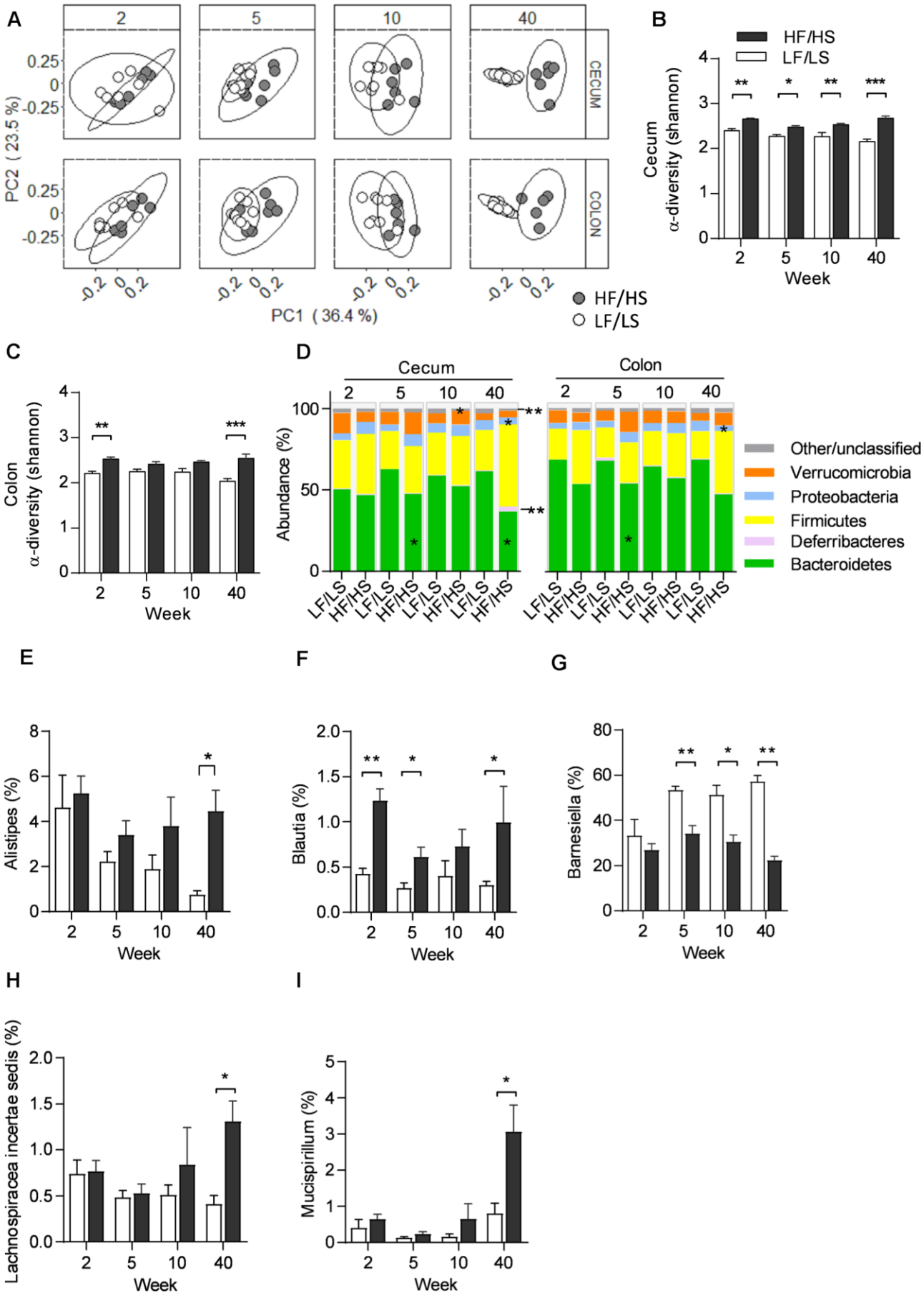
A
2
5
10
40
CECUM
COLON
PC2 (23.5 %)
PC1 (36.4 %)
HF/HS
LF/LS
B
Cecum α-diversity (shannon)
Week
C
Colon α-diversity (shannon)
Week
D
Cecum
Colon
Abundance (%)
LF/LS
HF/HS
Other/unclassified
Verrucomicrobia
Proteobacteria
Firmicutes
Deferribacteres
Bacteroidetes
E
Alistipes (%)
Week
F
Blautia (%)
Week
G
Barnesiella (%)
Week
H
Lachnospiracea incertae sedis (%)
Week
I
Mucispirillum (%)
Week

SUPPLEMENTARY TABLES AND FIGURES

- **Supplementary Table 1-3.**
- **Supplementary Figures 1-8.**

Supplementary table 1. Antibodies

Panel	Antibodies/conjugates/clones							
Dendritic cell	CD11b V500 (M1/70)*	CX3CR1-Pacific Blue (polyclonal)†	CD45 APC-Cy7 (30-F11)*	*IL-12p35 APC* (4D10p35)†	CD11c PE-Cy7 (HL3)*	Siglec-H PerCP-eFluor-710 (440c)†	CD103 PE (M290)*	F4/80 FITC (BM8)†
Macrophage	CD11b V500 (M1/70)*	*CD206 BV421 (C068C2)*‡	CD45 APC-Cy7 (30-F11)*	*Arg1 AF647* (19/Arginase-1)*	CD11c PE-Cy7 (HL3)*	Ly6C PerCP-Cy5.5 (HK1.4)†	*TNFa PE* (MP6-XT22)*	F4/80 FITC (BM8)†
Monocyte	CD11b V500 (M1/70)*	CX3CR1 Pacific Blue (polyclonal)†	CD45 APC-Cy7 (30-F11)*	CD115 APC (AFS98)†	Ly6G PE-Cy7 (1A8)†	Ly6C PerCP-Cy5.5 (HK1.4)†	CCR2 PE (polyclonal)§	F4/80 FITC (BM8)†
Granulocyte	Empty	cKit V450 (2B8)*	CD45 APC-Cy7 (30-F11)*	*IL-4 APC* (11B11)†	Ly6G PE-Cy7 (1A8)†	FcERIa PerCP-eFluor-710 (MAR-1)†	Siglec-F PE (E50-2440)*	CD49b FITC (HMa)†
B cell	B220 V500 (RA3-6B2)*	IgD eFluor 450 (11-26c)†	CD45 APC-Cy7 (30-F11)*	*IL-10 APC* (JES5-16E3)†	IgM PE-Cy7 (II/41)†	CD19 PerCP-Cy5.5 (1D3)†	CD1d PE (1B1)†	CD5 FITC (53-7.3)†
T cell	CD3 V500 (500A2)*	TCRgd BV421 (GL3)†	CD45 APC-Cy7 (30-F11)*	*FoxP3 AF647* (FJK-16s)*	CD4 PE-Cy7 (GK1.5)†	*IFNg PerCP-Cy5.5* (XMG1.2)*	*IL-4 PE* (11B11)†	CD8 FITC (53-6.7)*
NK/NKT	CD3 V500 (500A2)*	TCRgd BV421 (GL3)†	CD45 APC-Cy7 (30-F11)*	*IL-4 APC* (11B11)†	NKp46 PE-Cy7 (29A1.4)†	*IFNg PerCP-Cy5.5* (XMG1.2)*	*IL-17A PE* (17B7)†	NK1.1 FITC (PK136)*

Rows refer to panels, Columns to antibodies in panel. Clone marked by parenthesis. *BD Biosciences, †eBioscience, ‡Biolegend, §R&D Systems.

Supplementary table 2. Primers used.

Gene	**Forward primer, 5'-**	**Reverse primer, 5'-**
G6pc	ACCGGACCAGGAAGTCCC	GCAATGCCTGACAAGACTCC
Pepck	GTGCCTGTGGGAAGACTAAC	CCTTAAGTTGCCTTGGGCAT
Cpt1a	TACTGCTGTATCGTCGCACG	GACGAATAGGTTTGAGTTCCTCAC
Acaca	TGCTGCCCCATCCCCGGG	TCGAACTCTCACTGACACG
Ppara	AGAGAGGACAGATGGGGCTC	CGTTTGTGGCTGGTCAAGTT
Srebp1	GGAGCCATGGATTGCACATT	GCTTCCAGAGAGGAGGCCAG
Tnf	CCCTCACACTCAGATCATCTTCT	GCTACGACGTGGGCTACAG
Fasn	ATTGGTGGTGTGGACATGGTC	CCCAGCCTTCCATCTCCTG
Actb	ATGGGTCAGAAGGACTCCTACG	AGTGGTACGACCAGAGGCATAC
Pparg1	GTGTGACAGACAAGATTTGAAAG	GCTTGATGTCAAAGGAATGCG
Pparg2	ACAGCAAATCTCTGTTTTATGC	TGCTGGAGAAATCAACTGTGG
Gapdh	CAAATTCAACGGCACAGTCAA	GTCTCGCTCCTGGAAGATGG
Tbp	ACCCTTCACCAATGACTCCTATG	ATGATGACTGCAGCAAATCGC
Adipoq	GATGGCAGAGATGGCACTCC	CTTGCCAGTGCTGCCGTCAT
Scd	ACACCTGCCTCTTCGGGATT	TGATGCCCAGAGCGCTG

Supplementary table 3. Macronutrient composition and fatty acid profile of diets.

Diet	**HF/HS**	**LF/LS**
Ingredients	%w	%w
Casein	20	20
Corn starch	-	52
Sucrose	43.7	9.7
Cellulose power	5	5
L-Cystine	0.3	0.3
DL-Methionine	0.2	0.2
Vitamin premix	1	1
Mineral & trace element premix	3.5	3.5
Choline chloride	0.3	0.3
Vitamin K3	<0.1	<0.1
Vitamin B12	<0.1	<0.1
Butylated hydroxytoluene	<0.1	<0.1
Dye (Blue / Green)	<0.1	<0.1
Na Carboxymethylcellulose	0.1	0.1
Soybean oil	2.5	7
Safflower oil	22.5	-
Macronutrients	%E	%E
Carbohydrate	42.8	67.6
Fat	42.1	14.3
Protein	13.3	16.0
Fiber	1.8	2.1
Fatty acids	%	%
C14:0	0.2	0.3
C16:0	7.3	12.0
C16:1	0.1	0.1
C18:0	2.7	3.3
C18:1n9	15.3	23.6
C18-1n7	0.5	1.7
C18:2n6	72.9	53.3
C18:3n6	0.4	0.3
C18:3n3	0.7	5.4
SAT	10.2	15.6
MUFA	15.9	25.4
PUFA	73.9	59.0
n-6/n-3 ratio	105	9.9

Legend. Ingredients (per cent of weight) in diet, energy (per cent of total energy) derived from macronutrients, per cent of total lipids. SAT: Saturated fatty acid.

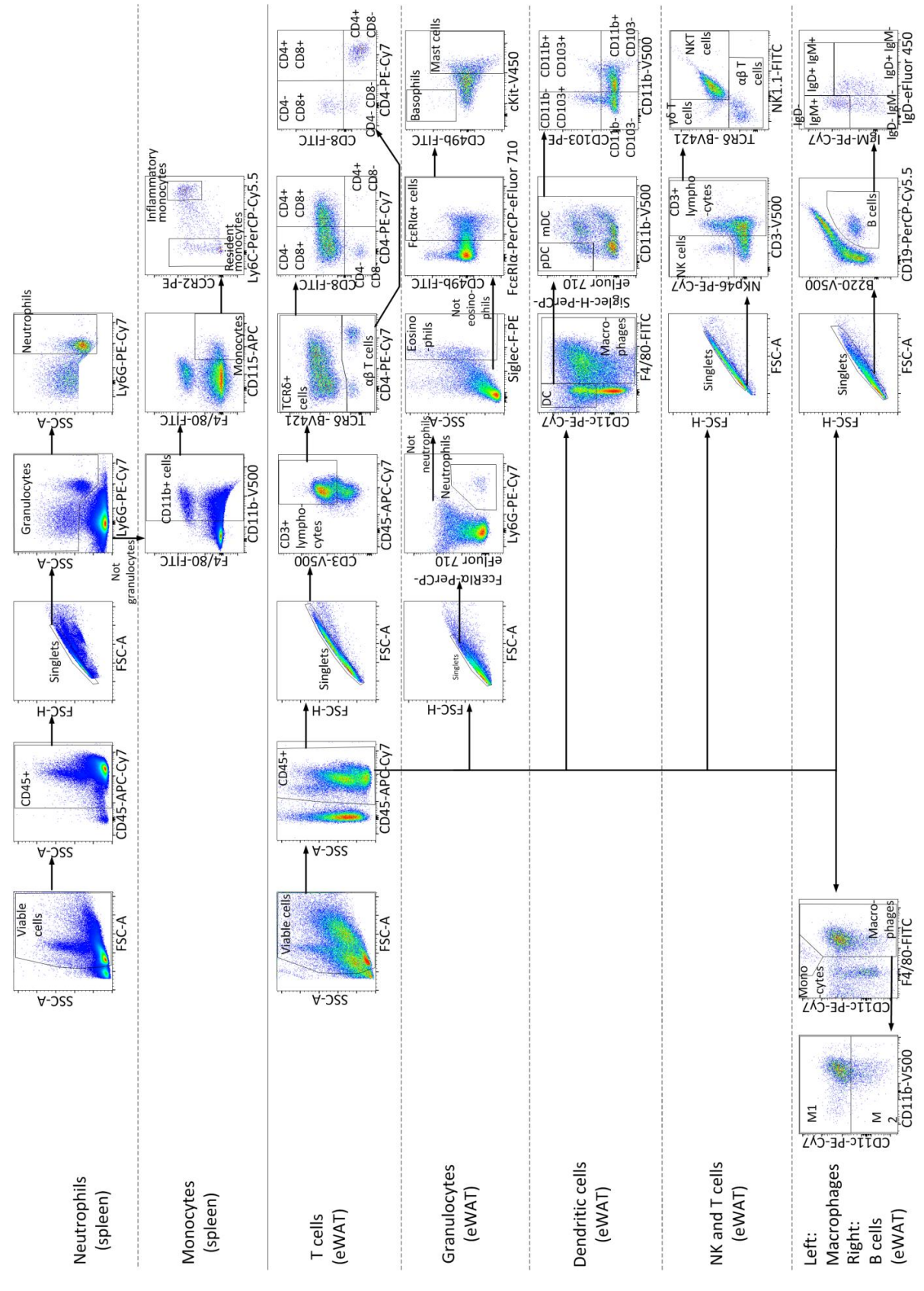

Supplementary figure 1. Gating strategies for flow cytometry panels.

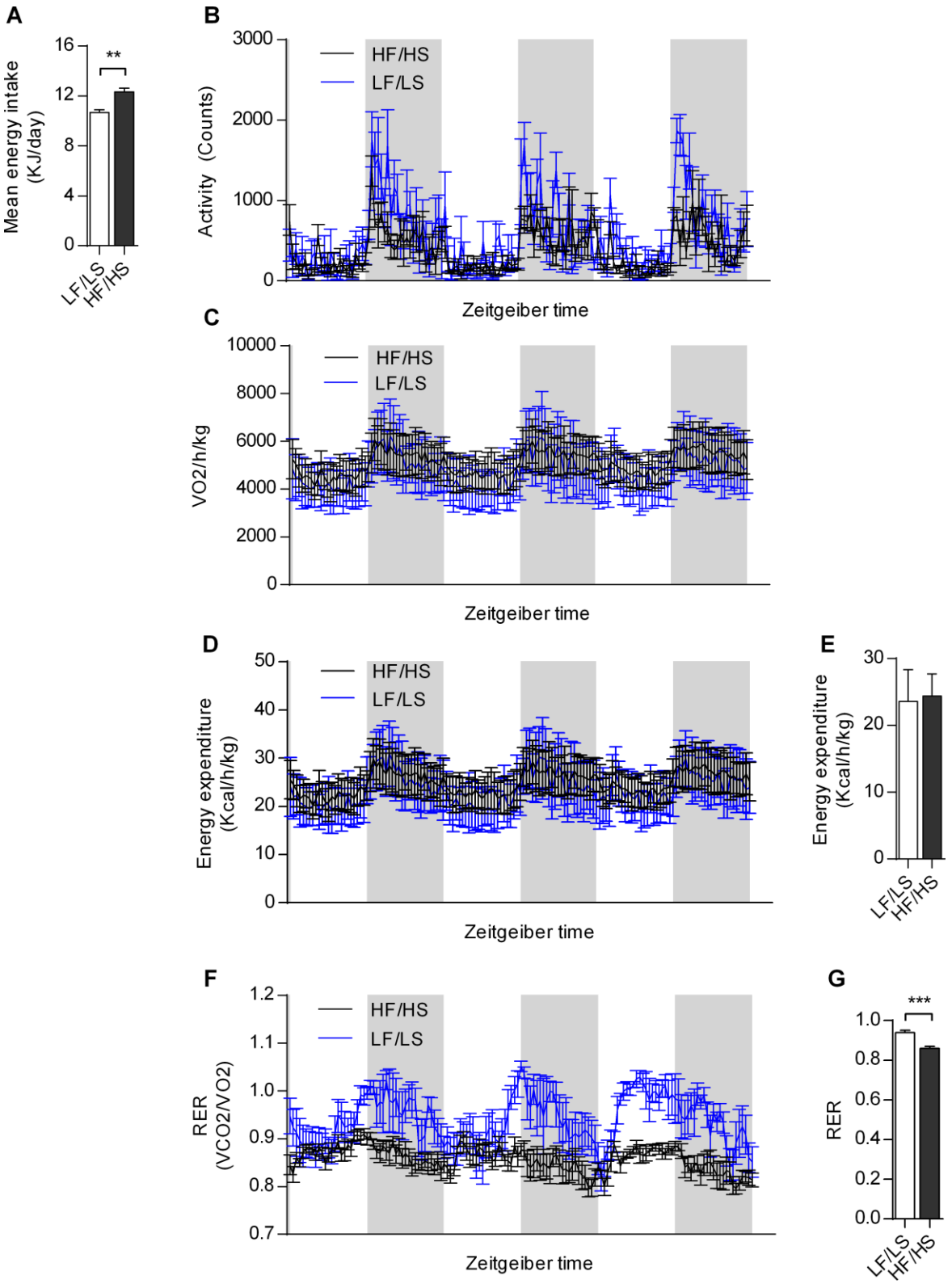

Supplementary figure 2. Legend on next page.

Supplementary figure 2. Metabolic characteristics of C57BL/6J mice fed a safflower oil-based n-6 PUFA rich HF/HS- versus a LF/LS diet **(A)** Mean energy intake over 40 weeks, n=6-7, experiment repeated once. For metabolic chambers, after 4 weeks on diet, a separate single-house group of mice were adapted for 3 days prior to measurements at room temperature with ad-libitum access to food and water, Non-shaded area, lights on. Shaded area, lights off, n=5. **(B)** Beam breaks over 3 days. **(C)** Oxygen consumption (VO_2/h/kg). **(D)** Energy expenditure **(EE)** (kcal/h/kg), and **(E)** average EE. **(F)** Respiratory exchange ratio (RER) and **(G)** average RER. Black lines and squares = HF/HS-fed mice, blue lines and white squares = LF/LS-fed mice.

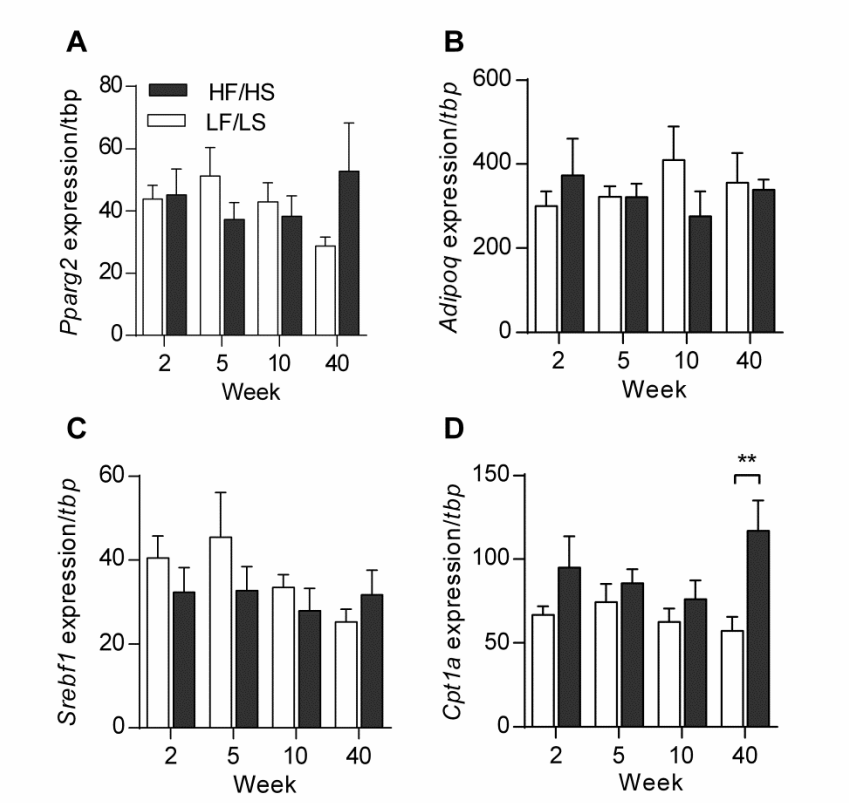

Supplementary figure 3. Expression of genes involved in adipocyte function and lipid metabolism in eWAT. (A) *Pparg2*, **(B).** *Adipoq*, **(C)** *Srebf1*, **(D)** *Cpt1a***.** For all data, n=6-8 from two experiments. Black squares = HF/HS-fed mice, white squares = LF/LS-fed mice.

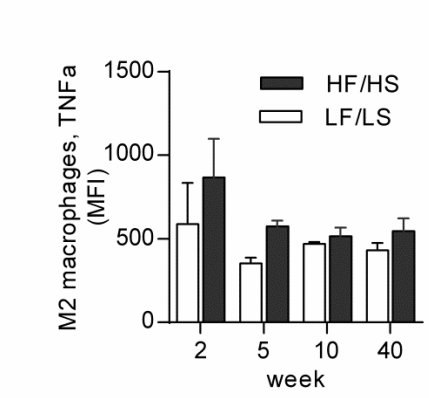

Supplementary figure 4. TNFα expression in M2 macrophages. Mean fluorescence intensity of TNFα in M2 macrophages, n=6-8, from two experiments. Black squares = HF/HS-fed mice, white squares = LF/LS-fed mice.

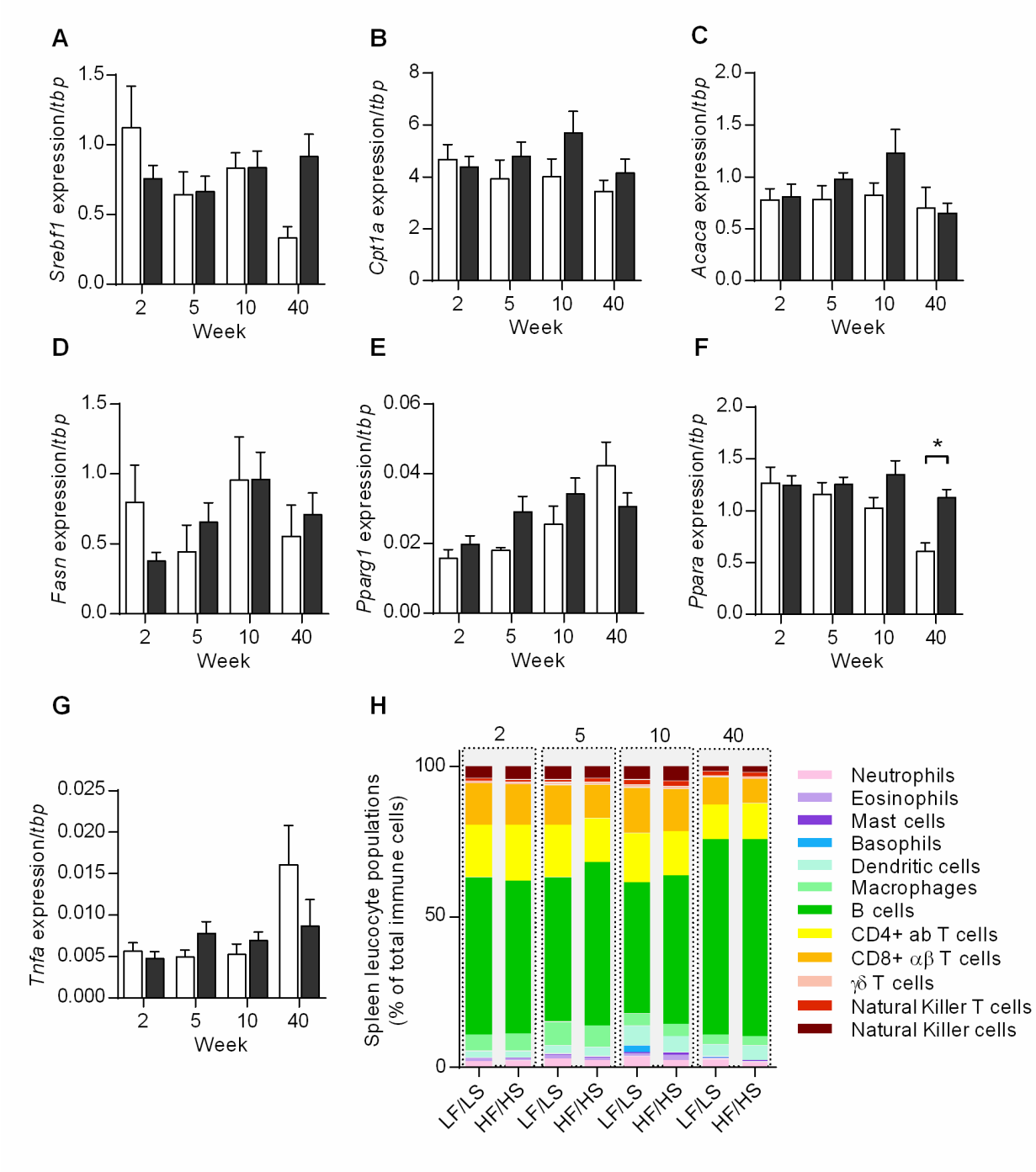

Supplementary figure 5. Hepatic gene expression and immune cells in the spleen. (A-G) Hepatic gene expression **(A)** *Srebf1*, **(B),** *Cpt1a*, **(C)** *Acaca*, **(D)** *Fasn*, **(E)** *Pparg1*, **(F)** *Ppara*, **(G)** *Tnfa*. **(H)** Immune cells in the spleen in per cent of total leucocytes. For all data, n=6-8 from two experiments. Black squares = HF/HS-fed mice, white squares = LF/LS-fed mice.

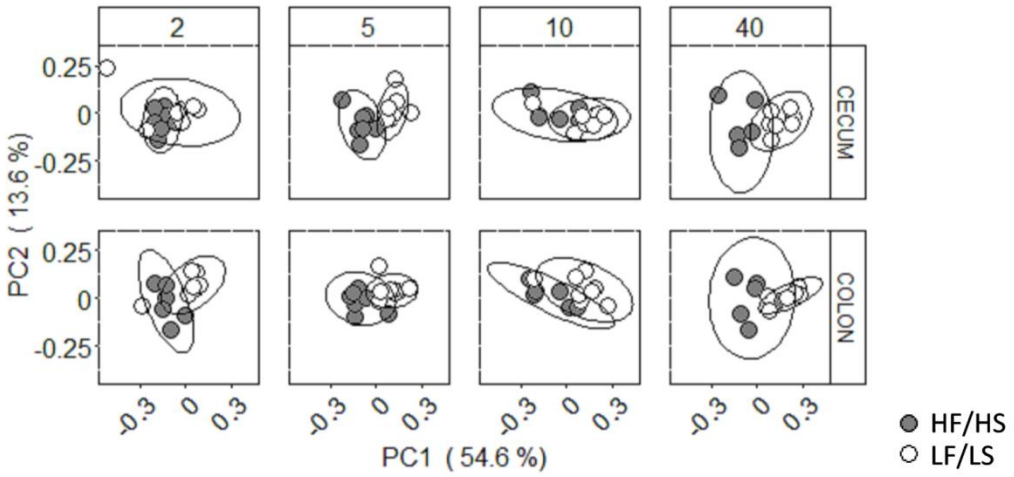

Supplementary figure 6. Microbiota composition in cecum and colon. UNIFRAC distances in cecum and colon at indicated weeks, n=6-8, experiment repeated once. Grey circles and black squares = HF/HS-fed mice, white circles and squares = LF/LS-fed mice.

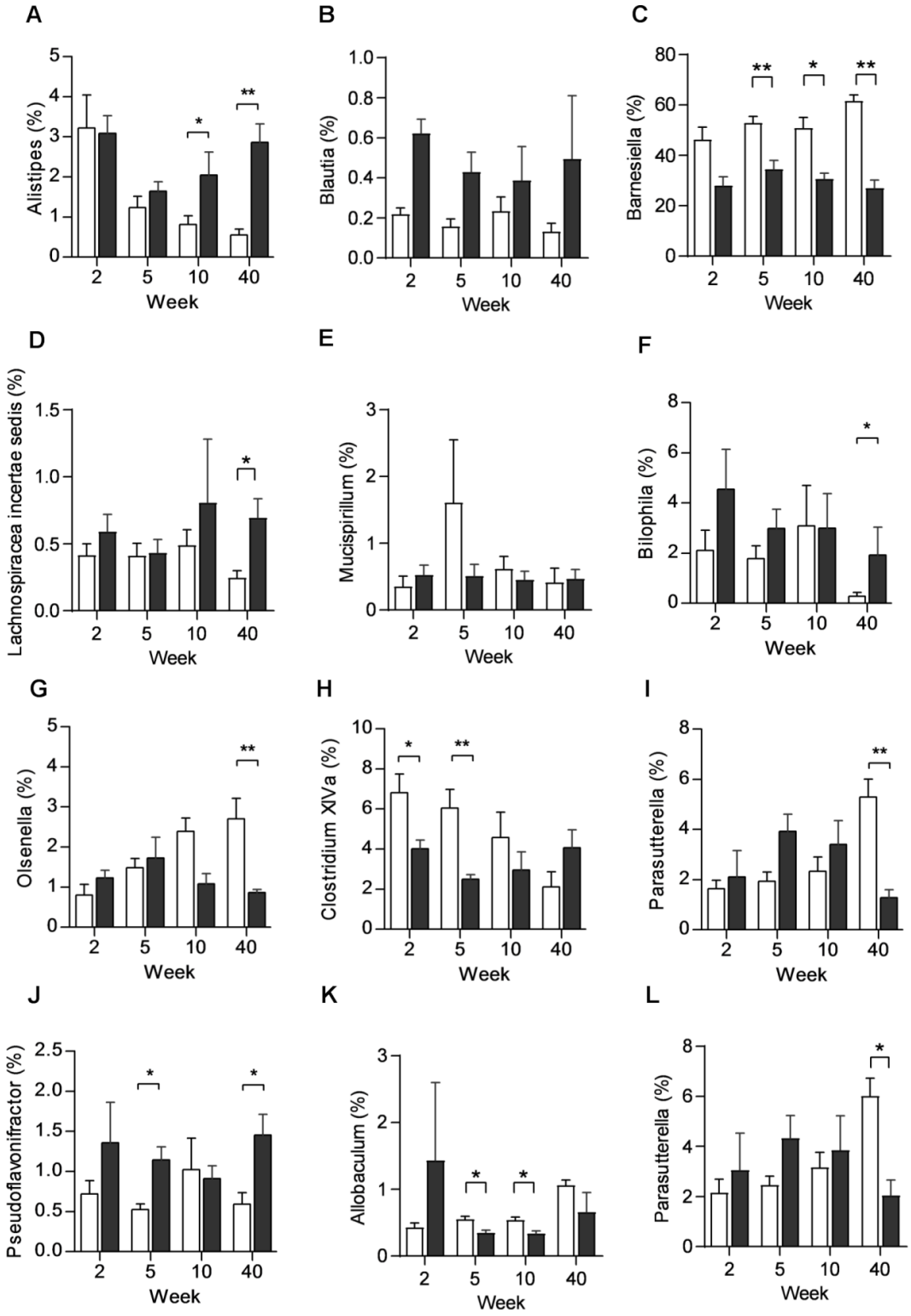

Supplementary figure 7. Microbiota composition in cecum and colon of abundant genera with at least one significant difference between HF/HS and LF/LS diets but without difference in abundance.

Genus abundance in the cecum (A and F-J). Genus abundance in the colon (B-E and K-L). For all data, n=6-8 from two experiments. Black squares = HF/HS-fed mice, white squares = LF/LS-fed mice.

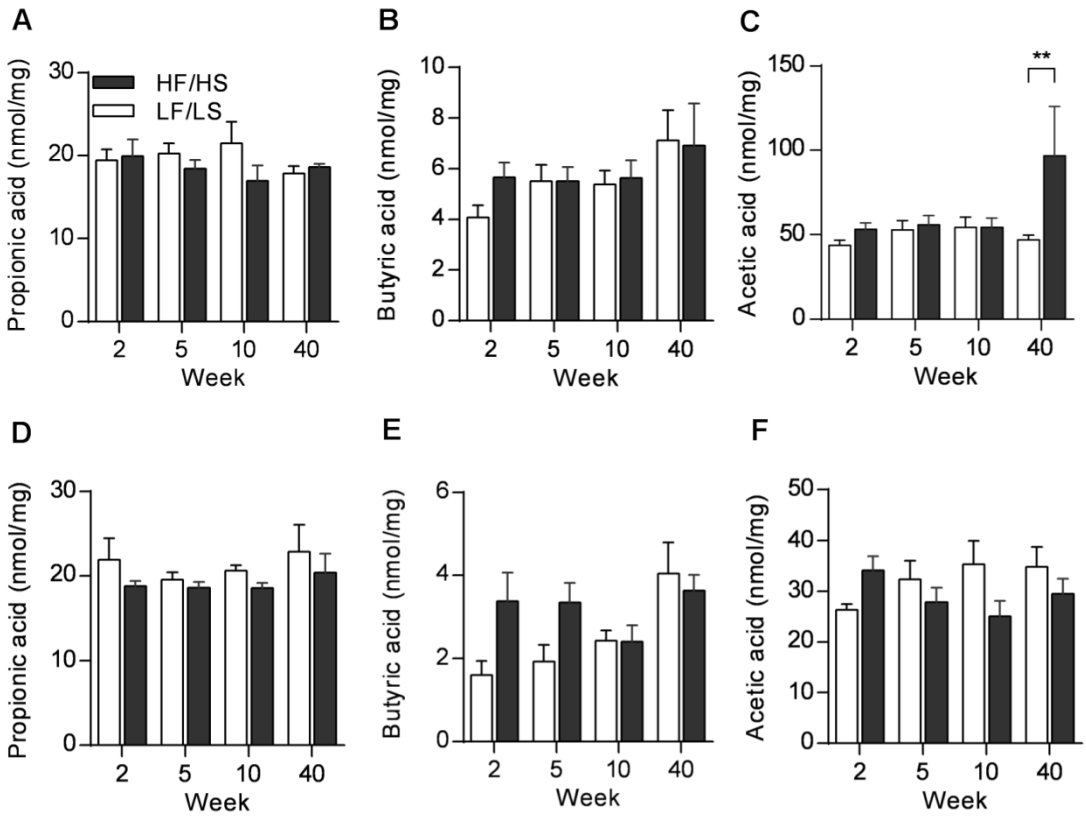

Supplementary figure 8. SCFAs in cecum and colon. Concentrations of **(A)** propionic acid, **(B)** butyric acid and, **(C)** acetic acid in the cecum. Concentrations of **(D)** propionic acid, **(E)** butyric acid and, **(F)** acetic acid in the colon. For all data, n=6-8 from two experiments. Black squares = HF/HS-fed mice, white squares = LF/LS-fed mice.

Project III: Fasting study

Introduction and objectives

Abundant clinical evidence show that increased caloric intake, such as from high fat diets, leads to metabolic, inflammatory and cardiovascular complications. Besides from the increased attention on dietary composition, there is increased awareness that the most important factor in the control of metabolic regulation is caloric intake. This has led to nutrient reduction strategies such as intermittent fasting and caloric restriction. Although the host response to fasting in rodents and humans is well-characterized, the physiological response of obese individuals to fasting following intake of a high-fat diet has not been described. We therefore aimed at describing the host metabolic response in the intestine, epididymal adipose tissue and liver to short-term fasting (8.3 to 11.6 hours), while also integrating the gut microbiome, urine metabolome and liver lipids.

Experimental setup

This study exploited the available data on fasted and fed mice from the gliadin study (Project I), only supplemented with few additional qPCR targets.

Specific aims

This study aimed to

- Identify the metabolic and immunological effects of short-term fasting of obese mice following intake of a high-fat diet
- Describe the intestinal gut microbiome of fed and fasted mice, and integrate this with the fasting host phenotype
- Integrate the urine metabolome in an effort to characterize important microbiota-host interactions

Key findings

- Short-term fasting results in higher cecal butyric acid concentrations, but lower cecal concentrations of branched-chain fatty acids iso-butyric acid, iso-valeric acid and valeric acid
- Fasting results in multiple changes in gene expression in epididymal adipose tissue, liver, ileum and colon. The most prominent is a switch towards a beige phenotype (higher *Ucp1* and *Il33* in eWAT)
- Fasting results in dramatic changes in the gut microbiome
- The higher butyric acid is possibly related to the higher colonic abundance of *Porphyromonadaceae* (which is able to produce butyric acid)
- Applying a co-abundance clustering method on metabolites and microbiome, identifies metabolites that associate with the gut bacteria, and may be involved in manifestation of the butyric acid phenotype

Manuscript III

Systems level analysis connects intestinal *Porphyromonadaceae*, *Il33* and butyric acid to *Ucp1* induction in visceral adipose tissue during short-term fasting

Daniel Andersen[1], Li Zhang[2], Henrik Munch Roager[2], Janne Marie Laursen[1], Niels Banhos Danneskiold-Samsøe[1], Karsten Kristiansen[3], Lars I. Hellgren[1], Tine Rask Licht[2], Susanne Brix[1*]

[1]Department of Biotechnology and Biomedicine, Technical University of Denmark, 2800 Kgs. Lyngby, Denmark

[2]National Food Institute, Technical University of Denmark, 2860 Søborg, Denmark

[3]Laboratory of Genomics and Molecular Biomedicine, Department of Biology, University of Copenhagen, Universitetsparken 13, DK-2100 Copenhagen, Denmark

*Corresponding author: sbp@bio.dtu.dk

ABSTRACT

Short-term fasting is increasingly used in various dietary programs as a means to regulate caloric intake and reduce weight gain. Here we aimed to study the connections between fasting-induced whole body changes, involving measures of bacterial, inflammatory and metabolic parameters determined in the intestine (ileum, cecum and colon), liver, visceral adipose tissue, blood and urine in mice fed an obesogenic diet and fasted for up to 12 hours before final examination. Cecal butyric acid, ileum *Il33*, liver *Pck1* and *Cpt1a*, blood IL-6, and eWAT *Ucp1* were all positively linked with duration of fasting while the cecal branched chain fatty acids iso-butyric acid and iso-valeric acid as well as liver *Lipc* and eWAT *Mcp1* were negatively correlated. These factors were co-regulated with specific intestinal bacteria, liver lipids and urinary metabolites, and the most prominent co-regulation cluster was based on increased cecal bytyric acid, ileal *Il33* and eWAT *Ucp1* expression correlating to

bacteria of the *Porphyromonadaceae* family with butyrate-producing potential and a urinary valeric acid-O-sulphate metabolite. The cluster of interlinked factors was supported by a fasting-induced concomitant decrease in cecal levels of the branched chain fatty acids iso-butyric acid and iso-valeric acid linked to reduced cecal abundances of members of the *Lachnospiraceae* familiy.

Our systems-level analysis reveals a connection between intestinal butyric acid production, ileal *Il33* and *Porphyromonadaceae* abundances to visceral adipose expression of the uncoupling protein *Ucp1* during short-term fasting in obese mice. This finding is suggestive of a three-tiered interlinked fasting-induced regulation in obese mice based on cecal butyric acid being connected to an intestinal homeostatic conversion towards a type 2 immune profile, which is coupled to a potentially energy-burning phenotypic switch within visceral adipose tissue. We propose that the fasting-induced nutrient restriction in the gut may exert a selection pressure that allows for increased butyric acid production by colonic *Porphyromonadaceae* mediating the phenotypic adipose tissue switch.

INTRODUCTION

Control of metabolic health by means of balancing caloric intake with energy expenditure is of paramount importance for human health, as long-term surplus energy intake leads to metabolic, inflammatory and cardiovascular complications (Moller and Kaufman, 2005). Besides exercise, caloric balancing can be mediated by implementation of weight regulation programs based on reduced caloric intake as seen with dieting, intermittent fasting and caloric restriction strategies that may result in protective effects by reprogramming an ongoing obesity-induced metabolic and inflammatory response pattern (Brandhorst et al., 2015; Fontana et al., 2004; Longo and Mattson, 2014). It has been documented that fasting induces pronounced shifts in host metabolism, such as a heightened cellular stress resistance (Longo and Mattson, 2014), increased hepatic gluconeogenesis, ketogenesis and β-oxidation accompanied by an increased efflux of free fatty acids from adipose tissue stores to sustain metabolic demands of other tissues (Geisler et al., 2016). Intake of an energy dense obesogenic diet and ensuing development of obesity also modulate several aspects of host homeostasis such as lipid and glucose metabolism, and tissue and peripheral inflammation (Glass and Olefsky, 2012; Lumeng and Saltiel, 2011) associated with marked shifts in the gut microbiome (Thaiss et al., 2016; Turnbaugh et al., 2009). Thus, the obese host and its obesity-associated gut microbiome might have adapted for an environment of nutrient-excess (Turnbaugh et al., 2006). Therefore, fasting of obese, high-fat diet fed individuals may induce a drastic metabolic shift away from the fed state. Although the host response to fasting in rodents and humans is well-characterized, the physiological response of obese individuals to short-term fasting has not been described at a system-wide level.

This study aimed at examining the metabolic effects of a short-term fasting period in diet-induced obese mice. In order to obtain a systems-wide view of interlinked fasting-induced changes in the metabolic and inflammatory profile, we conducted a comprehensive analysis of intestinal bacteria, liver lipids and urinary metabolites in fed and fasted obese mice, and compared these to cecal and colonic production of short-chain (SCFA) and branched chain fatty acids (BCFA), to gene expression

data from the intestine (ileum and colon), liver, visceral adipose tissue as well as to systemic cytokines in blood. We identified a fasting-induced phenotype which is characterized by higher levels of cecal butyric acid linked to concomitant ileal *Il33* expression and *Ucp1* expression in visceral adipose tissue, suggestive of an intestinal homeostatic conversion towards a type 2 inflammatory profile which is supportive of a beige-like phenotypic switch within the white adipose tissue of obese mice.

RESULTS

Fasting induces specific systems-level changes in obese mice

To examine the influence of short-term fasting on inflammatory and metabolically regulated factors in obese animals, we performed a comparative systems level analysis of multiple tissue and systemic parameters in C57BL/6J mice fed an obesogenic diet for 22 weeks. Before sacrifice, half of the mice were subjected to fasting for 8.3 to 11.6 hours, while the remaining fed mice had *ad libitum* access to feed throughout the study period. After 22 weeks on an obesogenic diet but before fasting, all mice were markedly obese with no differences in body weight (Fig. S1A). Following the fasting period no changes were observed in the weight of liver and adipose tissue between fasted and fed animals (Fig. S1B-C). The measured metabolic and inflammatory markers included liver triglycerides and phospholipids, gene expression of metabolic and inflammatory markers of liver, epididymal adipose tissue (eWAT), ileum and colon, SCFA and BCFA in cecum and feces, and systemic cytokines in blood (Fig. 1A, colored boxes). Additionally, a metabolic profiling of urine by Ultra Performance Liquid Chromatography Mass Spectrometry (UPLC-MS) was performed, resulting in the quantification of 1609 different urine metabolites. To reduce the 1609 urine metabolites into modules of co-regulated metabolites, we used a co-abundance clustering approach similar to Pedersen et al. (Pedersen et al., 2016), which binned the metabolites into 83 different co-abundance metabolite clusters. Based on eigengene values from all samples, 13 clusters (Me-1 to Me-13), containing a total of 375 metabolites, showed a statistically significant difference between fed and fasted mice (Student's t

test, FDR < 0.1) (Fig. S2A, Fig. 1A (urine metabolome)). In addition, we characterized the ileal, cecal and colonic gut microbiome of fed and fasted mice by 16S rRNA sequencing to examine if the gut bacterial composition in obese animals changed during short-term fasting. To identify community relationships of the gut microbiota at the operational taxonomic units (OTUs) level, OTUs were binned into tissue-specific clusters in a similar manner as for the metabolites, thus identifying one cluster in ileum (Ileum-OTU-1), one in cecum (Cecum-OTU-1) and four in colon (Colon-OTU-1 to Colon-OTU-4) that showed statistically significant differences in eigengene values between fed and fasted mice (Student's t test, FDR < 0.1) (Fig. S2B-D, Fig. 1A (Ileum-OTU, Cecum-OTU and Colon-OTU)). Finally, the same approach was applied to the liver lipids from triglyceride and phospholipid fractions, resulting in binning of liver lipids into five different clusters, of which one (Lipids-1) showed significantly different eigengene values between fed and fasted mice (Student's t test, FDR < 0.1) (Fig. S2E, Fig. 1A (Liver lipids)).

To gain an overview of the correlation between the fasting-regulated clusters of urinary metabolites, intestinal bacteria and liver lipids (grey boxes of Fig. 1A), and the measured metabolic and inflammatory markers, comprising intestinal short chain fatty acids, gene expression and blood protein levels (colored boxes of Fig. 1A), we performed multivariate correlation analysis based on the eigengenes of the clusters and the parameter groups (indicated by color-coded boxes). Since the fasted mice were subjected to different duration of fasting, we also included hours of fasting as a parameter into the multivariate analysis (emphasized by a dashed outline in Fig. 1B). The correlation matrix in Fig. 1B revealed two overarching groups of tissue genes, blood cytokines and intestinal short and branched chain fatty acids that were either co-up- or downregulated with the identified fasting-regulated clusters. Especially, we showed that Me-1, Lipids-1, and Colon-OTU-2inversely correlated with fasting duration and several markers including liver *Pck1* and *Cpt1a*, cecal butyric acid, blood IL-6, ileum *Il33* and eWAT *Il33* and *Ucp1*. These same markers were found to positively correlate with especially Colon-OTU-4, Me-9 to -13 and Ileum-OTU-1. Additionally, the same clusters were identified to essentially co-regulate in an inverse manner with the cecal-derived branched chain

fatty acids iso-butyric acid and iso-valeric acid, hence illustrating a noticeable connection between fasting-regulated intestinal bacteria, liver lipids, urine metabolites, bacterial-derived cecal fermentation products and host parameters of the small intestine, liver, blood and visceral adipose tissue. Focusing on which of these latter factors that also correlated with fasting duration, it was not surprising to observe that liver *Pck1* and *Cpt1a*, cecal butyric acid, blood IL-6, ileum *Il-33* and eWAT *Ucp1* were all positively linked with duration of fasting, while cecal iso-butyric acid and iso-valeric acid as well as liver *Lipc* and eWAT *Mcp1* were negatively correlated with fasting (Fig. S3). All of these parameters were also found to be statistically significantly different in fasted versus fed mice by univariate analysis (Fig. S4A-E).

Fasting-induced shifts in cecal SCFA and BCFA composition coincides with specific changes in the gut microbiota and visceral adipose tissue expression of *Ucp1* in obese mice

Production of SCFA and BCFA by intestinal bacteria constitutes a rapid and important gut-to-host signaling mechanism, reflecting diet availability and activity of the gut microbiome (Koh et al., 2016; Sonnenburg and Backhed, 2016), but currently it is not yet reported how fasting influences production of SCFA and BCFA. It was therefore notable that we found a fasting-related inverse regulation of cecal bacterial production of the SCFA butyric acid at the one side and the BCFAs iso-butyric and iso–valeric acid at the other side, while colonic levels were unaffected (Fig. S4A, B).

To get a more comprehensive view of the origin of the altered cecal SCFA and BCFA signature we examined the correlation between all SCFAs and BCFAs and the individual OTUs in the clusters that were dependent on fasting status. This approach identified OTUs belonging to the families of *Porphyromonadaceae* and *Lachnospiraceae* as bacteria that correlate with butyric acid (Fig. 2A). Positive correlations were mainly seen between butyric acid and bacteria belonging to *Porphyromonadaceae* or to bacteria within the phylum *Bacteroidetes* (these specific OTUs were not assigned at a lower taxonomic level), while negative correlations were uniquely observed among OTUs belonging to *Lachnospiraceae* (Spearman's correlation coefficient (SCC), FDR < 0.05) (Fig. 2A).

Abundance of *Alistipes* OTUs was inversely correlated with cecal iso-valeric and iso-butyric acid levels (Fig. 2A).

As butyric acid production by intestinal bacteria may vary even among bacteria at the same family level, all OTUs previously assigned to the fasting-dependent microbiome clusters were evaluated for their genomic potential for production of butyric acid. This was based on alignment of the *de novo* picked OTUs to the Green Genes 13.5 database, and subsequent identification of the presence of genes necessary for the butyrate kinase pathway (KEGG orthologs K00634 and K00929) or butyrate transferase pathway (KEGG orthologs K01034 and K01035). This approach identified all *Porphyromonadaceae* that could not be assigned at a taxonomical level lower than the family level as butyrate producers, while the *Porphyromonadaceae* belonging to *Parabacteroides* did not contain all necessary genes for butyric acid synthesis pathways. Bacteria of the *Lachnospiraceae* family were identified as having a mixed butyric acid biosynthesis potential, as 11 OTUs within this family had butyrate kinase or transferase potential, while 13 OTUs did not (Table S1). In support of the biosynthetic capacity for butyric acid production by *Porphyromonadaceae*, we also identified a significant correlation between the collective abundance of *Porphyromonadaceae* and cecal butyric acid levels (Fig. 2B).

Adipose tissue express receptors for SCFAs, and butyric acid supplementation has been associated with the induction of beiging of white adipose tissue which involves UCP1 expression (Lu et al., 2016). In line with this, we identified significant positive correlations between cecal fasting-induced butyric acid production and expression of *Ucp1*, in eWAT (Fig. 2C). On the contrary, we found no strong direct link between cecal butyric acid and the fasting-regulated *Il33* expression in eWAT (Fig. 2D).

Moreover, fasting mediated pronounced differences in the relative abundance several bacteria at family and genus level in cecum and colon (Fig S5). For the cecal microbiota, *Deferribacteraceae* and *Rikenellaceae* and its genus member *Alistipes* were more abundant; the latter reflected in the high abundance of OTUs assigned to *Alistipes* in the single cecum OTU cluster (Cecum OTU-1) (Fig. S5C-D).

For the colon, *Bacteroidaceae*, *Rikenellaceae* and *Porphyromonadaceae*, and consequently their respective genus members *Bacteroides*, *Alistipes* and *Parabacteroides,* were more abundant, while the low-abundance genera *Anaerotruncus* and *Ruminococcus2* were less abundant among fasted mice. Similarly, OTUs belonging to *Bacteroidaceae*, *Rikenellaceae* and *Porphyromonadaceae* were abundant among the OTU clusters in the colon (Colon-OTU-1 to Colon-OTU-4) (Fig. S5E-F).

Network analysis identifies systems level factors inter-linked with phenotypic changes in short-term fasted obese mice

To identify inter-connected links between the identified changes in individual metabolic and inflammatory factors within the intestine, liver, blood, adipose tissue and urine, we conducted a network analysis aiming to integrate all factors at the molecular level (Fig. 3). Initially, we identified the fasting-regulated metabolites that correlated with changes in the intestinal bacteria, thus being potential candidates as systemic mediators of the fasting-induced bacterial changes or byproducts of the microbiota-induced changes in host metabolism. The first reduction resulted in identification of 210 metabolites from the individual urine metabolome clusters that associated with duration of fasting (SCC, FDR < 0.05) (Fig. 3A). The following correlation of the 210 metabolites with the intestinal bacterial OTUs present in fasting-dependent OTU-clusters identified 10 metabolites that correlated with 21 bacterial OTUs (Fig. 3A, SCC, FDR < 0.05). Co-abundant metabolites and OTUs were then correlated with liver lipids (Fig. 3A, SCC, FDR < 0.01), resulting in identification of four co-regulated lipids from the triglyceride fraction (C15:0 and C20:0, both higher in fasted mice; and C18:3 n-3 and C20:1 n-9, both lower in fasted mice). To extract details on their inter-linked structure, the co-correlated intestinal bacteria, liver lipids and urine metabolites were subjected to a network analysis (Fig. 3B). The resulting network comprised three major hubs that were mainly differentiated by OTU location (ileum, cecum and colon). The ileum OTUs that increased in abundances in response to fasting comprising the genera *Staphylococcus* and *Enterococcus* correlated with increased levels of a cortisol-derived metabolite (#13), two dipeptide fragments (#235, 278), and with an unclassified

urine metabolite (#37). These dipeptide fragments also correlated with enhanced levels of C20:0 in liver triglycerides, further associated to enhanced cecal abundances of *Alistipes*. The intermediate part of the network comprised factors that were all reduced during fasting, involving a cecal *Lachnospiraceae* that correlated with 2,5-furandicarboxylic acid (#1833), and C18:3 *n*-3 and C20:1 *n*-9 in liver triglycerides. The liver C20:1 *n*-9 triglyceride also correlated with two colonic *Lachnospiraceae* which were likewise reduced by fasting. These two latter bacteria were inversely correlated to C15:0 in liver triglycerides – a saturated fatty acid produced after α-oxidation. The last hub of co-regulated molecules mainly involved the colonic bacteria of the *Porphyromonodaceae* family which were increased in abundance during fasting and correlated with cecal butyric acid levels (Fig. 2). These species correlated negatively to the urine metabolite γ-glutamyl-3-aminopropiononitrile or N-α-acetyl-L-arginine (#1796), hence indicating that 1796 may be a marker to be further explored for its relation to cecal butyric acid production and fasting. Other fasting-enriched members of this hub were the homovanillic acid sulphate (#145), the valeric acid-O-sulphate analog (#272), the nicotinic/nicotinamide analog (#391), and an unclassified metabolite (#468), of which the two first were found to inversely correlate with a colonic *Lachnospiraceae* (OTU365) that was reduced by fasting. Thus, the apparent structure of the fasting-induced network was dominated by increased abundances of ileal *Staphylococcaceae* and a cecal *Alistipes* that linked with a cortisol analog and dipeptide metabolites, with the butyric acid-associated colonic *Porphyromonadaceae* correlating with reduced levels of γ-glutamyl-3-aminopropiononitrile or N-α-acetyl-L-arginine, and with reduced abundances of cecal and colonic *Lachnospiraceae* that associated with reduced 2,5-furandicarboxylic acid and C18:3 *n*-3 and C20:1 *n*-9 from liver triglycerides.

Since these inter-related hubs were of specific importance in relation to the host phenotypic changes during short-term fasting, we performed an additional multivariate correlation analysis to identify the links between the three interlinked hubs and the major fasting-induced phenotypic factors (Fig. 3C). From this analysis it appeared that the same intestinal bacteria and metabolites showed a similar and strong correlation to cecal butyric acid levels, ileal *Il33* and eWAT *Ucp1* expression.

Besides the strong link to colonic *Porphyromonadaceae*, we also found a positive association between the three factors and urinary valeric acid-O-sulphate metabolites (#272) as well as to an unclassified urinary metabolite (#468). Moreover, ileal *Il33* and ewat *Ucp1* were found to co-correlate with urinary homovanillic acid sulphate (#145) and the nicotinic/nicotinamide analog (#391), and additionally, we also found a strong correlation between ileal *Il33* expression and specific urinary cortisol analogs (#13) and the unclassified urinary metabolite (#37), whereas no significant associations were identified for the ileal bacteria (*Staphylococcaceae* and *Enterococcaceae*) that clustered with #13 and 37 (Fig. 3B). The factors that specifically interlinked with fasting-induced increases in expression of liver *Pck1* and *Cpt1a* were increased levels of the urinary valeric acid-O-sulphate metabolites (#272) and the unclassified metabolite (#37). For *Pck1*, it also involved correlations to cecal *Alistipes*, and the dipeptide metabolite (#278), whereas *Cpt1a* correlated to certain colonic *Porphyromonadaceae*. Systemic IL-6 levels were distinctly positively correlated to C20:0 liver triglycerides, as well as to the nicotinic/nicotinamide analog (#391). We found an additional positive influence on these fasting-induced parameters by factors that were reduced during fasting; involving the parameters within the intermediate hub of Fig. 3B comprised of reduced cecal *Lachnospiraceae*, C18:3 *n*-3 and C20:1 *n*-9 from liver triglycerides, and the metabolite γ-glutamyl-3-aminopropiononitrile or N-a-acetyl-L-arginine (#1796).

The cecal BCFAs iso-butyric and iso-valeric acid that were reduced during short-term fasting showed a specific counter-regulated pattern; parameters like the intermediate hub liver lipids C18:3 *n*-3 and C20:1 *n*-9, cecal *Lachnospiraceae* and 2,5-furandicarboxylic acid (#1833) correlated positively with BCFA production, while a big cluster comprised of cecal *Alistipes*, ileal *Enterococcus*, dipeptide fragments, C20:0 liver triglyceride, cortisol analogs and two unclassified metabolites all were regulated oppositely to these cecal BCFA. Apart from the cortisol analog, the fasting-induced reduction in liver *Lipc* expression was mainly counter-associated to yet other urinary metabolites (#468, 391, 145, and also 272), as well as two colonic Bacteroidetes species (OTU 705, 628). The correlation pattern for eWAT *Mcp1* expression appeared to be similar to that of *Lipc,* although the

Mcp1 expression was positively associated with the factors that also correlated positively with the cecal BCFAs iso-butyric and iso-valeric acid. Thus, a collective systems-wide network of fasting-induced and reduced variables is in play, most prominently geared by the interlinked phenotypes of increased cecal bytyric acid, ileal *Il33* and eWAT *Ucp1* expression correlated to colonic *Porphyromonadaceae*, the urinary valeric acid-O-sulphate metabolites (#272), and an unclassified metabolite (#468), and concomitantly decreased cecal levels of the BCFAs iso-butyric and iso-valeric acid as well as cecal *Lachnospiraceae*.

DISCUSSION

The mammalian body and its symbiosis with the gut microbiome constitute a highly flexible holo-organism, permitting a rapid adaptation to changes in nutrient availability. In this study, we report drastic changes in host metabolic regulation following short-term fasting in obese animals; a change that was defined as an interlinked connection between specific intestinal bacteria and their fermentation products, gene expression in ileum, liver and visceral adipose tissue, and certain urinary metabolites. Especially the gut microbial composition and activity were found to be markedly changed in the nutrient deficient state with a reduction in cecal branched-chain fatty acids and an increase in butyric acid concentration. Several ecological aspects define fiber fermentation capacity in the gut including gut microbiome composition, gut transit time, and substrate availability to carbohydrate-fermenting bacteria. In the fasted state, competition between host and microbe for dietary nutrients is heightened and consequently the host may respond by increasing intestinal uptake of lipids, simple carbohydrates and amino acids. Whereas the absolute levels of microbiota-accessible carbohydrates are lower in the fasted state, the relative levels and their accessibility to the gut bacteria are potentially increased (Sonnenburg and Backhed, 2016). The most significant alterations in bacterial abundances were seen for the higher relative abundances of *Porphyromonadaceae*, which correlated robustly with cecal butyric acid concentrations and were identified as having butyric acid production capabilities by KEGG ortholog analysis.

Butyric acid is involved in the maintenance of colonic epithelial homeostasis and the regulation of intestinal inflammation (Kelly et al., 2015; Vieira et al., 2012). Low abundance of butyric acid producing bacteria has been associated with increased risk for the development of type 2 diabetes (Qin et al., 2012) and the addition of sodium butyrate to a high-fat diet results in the prevention of diet-induced obesity via a butyrate-induced stabilization of body weight and adiposity and increase in energy expenditure and the expression of the prothermogenic regulators PGC-1α and UCP1 of brown adipose tissue (Gao et al., 2009). Similarly, several studies have identified a link between SCFAs and energy expenditure. The addition of acetate, propionate or butyrate to a high-fat diet prevents diet-induced body weight gain and increase energy expenditure (den Besten et al., 2015), and the expression of beige adipocyte markers in epididymal adipose tissue (Lu et al., 2016). In addition, intraperitoneal injection of sodium butyrate in *db*/*db* mice lowers inflammation in subcutaneous and epididymal adipose tissue via the inhibition of NLRP3 activation (Wang et al., 2015). These findings are in line with the observation that a fasting-induced increase in cecal butyric acid concentration is associated with the transcriptional induction of a brown-like phenotype marked by increased expression of *Ucp1*, and decreased expression of *Mcp1* in visceral adipose tissue.

In the present study, fasting was associated with an intestinal reprogramming mirroring the response in the adipose tissue, as higher ileal *Il33* is connected with *Ucp1* expression in eWAT. IL-33 is linked with propagation of an innate and adaptive type 2 immune response which is in play in the homeostatic intestinal environment (Monticelli et al., 2015). First of all, IL-33 is involved in activation of type 2 innate lymphoid cells (Monticelli et al., 2015) which produces IL-5 and IL-13. IL-5 recruits and activates eosinophils to produce IL-4 which is essential for insulin regulation. IL-13 on the other hand is essential for mucus production by goblet cells to decrease microbe-intestinal barrier interplays. IL-33 is also reported to expand regulatory T cells (Schiering et al., 2014; Vasanthakumar et al., 2015), and to favor a classical adaptive Th2 polarization resulting in increased IL-4, IL-5, and IL-13 (Yang et al., 2013). Moreover, it is reported that IL-33 promotes the differentiation of intestinal epithelial cells towards a secretory phenotype (Mahapatro et al., 2016). Cleavage of IL-33 by

inflammasome activated caspases will inactivate the IL-33 protein. However, since inflammasome activation via NLRP3 is reduced by butyric acid (Wang et al., 2015),the identified ileal *Il33* gene expression may in fact be translated to functional bioactive protein during the fasting conditions in obese animals. Further support for this has been reported in fasted humans, where activation of the inflammasome component NLRP3 was reduced (Traba et al., 2015).

A connection between local IL-33 and browning of white adipose tissue with induction of *Ucp1* expression has previously been reported (Brestoff and Artis, 2015; Lee et al., 2015). In the current study, we observed a correlation of r=0.68 between eWAT *Il33* and *Ucp1* expression (Fig. S3), but since the threshold used for identifying significant correlations was just below that obtained for the correlation between eWAT *Il33* and fasting duration, we did not pick up eWAT *Il33* to be significantly changed by the current fasting-focused approach. However, due to the tight connection between eWAT *Il33* and *Ucp1* it is likely that a type 2 immune response was induced in visceral fat by short-term fasting, and that this might be involved in promotion of a brown/beige-like phenotype in white adipose tissue. Such notion is in accordance with a previous report of type 2 mediated browning of adipose tissue during caloric restriction (Fabbiano et al 2016). Apart from higher *Ucp1* expression, the fasted obese mice also showed lower relative expression of the gene encoding the pro-inflammatory type 1 immunity-linked chemokine *Mcp1* in eWAT, but without notable changes in the pro-inflammatory cytokines *Tnfa* or *Il6*. Likewise, there were no connection between our focus on fasting duration and expression of the adipogenic regulator *Pparg*, the transcription factor *Cebpa* required for white adipocyte differentiation but not for brown-like differentiation (Linhart et al 2001, PNAS), the lipogenic regulators *Fasn* and *Dgat1*, and the fibrogenic marker *Col6a3*. In the liver, the interlinked fasting-induced expression of the carnitine palmitoyltransferase 1A, *Cpt1a* and the gluconeogenic enzyme PEPCK, *Pck1* was not surprising, since CPT1a stimulates β-oxidation (likely of adipose-released FFAs) and thus promotes acetyl-CoA generation, which in turn increases PEPCK/gluconeogenesis and function as a substrate in ketogenesis (Geisler et al., 2016). Of the measured liver lipids, only C20:1 *n*-9 and C18:3 *n*-3 were found to correlate with liver gene

expression, showing that lower levels of C20:1 *n*-9 and C18:3 *n*-3 correlated with higher *Cpt1a* and *Pck1* expression, but otherwise the links between the fasting-regulated hepatic gene expression and liver lipids were sparse.

The insight into fasting-induced changes in the abundances of *Porphyromonadaceae* are also quite sparse, but in one previous study by Zhang et al. *Porphyromonadaceae* were identified as being more abundant in calorie-restricted rather than *ad libitum* high-fat fed mice (Wang et al., 2015). At the current stage, it can only be speculated if *Porphyromonodaceae* may be more robust in handling nutrient unavailability than other bacteria. Zhang et al. propose that calorie-restriction limits nutrients for the gut microbiota and the host and that the host acts to increase protein and lipid absorption, thus increasing the relative proportion of fiber in the gut (Zhang et al., 2013). This explanation could also be likely during the similar nutrient-scarce condition of short-term fasting, and might even give a probable explanation for the observed increase in cecal butyric acid production at the expense of cecal BCFA. In this regard, the reduction in BCFAs could be speculated to be due to their ketogenic properties, allowing them to be used as substrates for ketone body production. Such a role would explain the "missing" cecal BCFAs in fasted mice, as in this instance, the BCFAs would not be kept as fermentation products in the gut but rather be taken up for transport to and further metabolism in the liver. If this situation is in play, it also highlights a possible difference between the cecum and colonic BCFA as storage depot for delivery to the liver, as we only found variations in BCFA levels in the cecum, and not the colon.

Several urinary metabolites showed consistent correlations with the fasting-induced changes in metabolic and inflammatory properties within the obese mice. The valeric acid-O-sulphate metabolite (#272) and the unclassified urinary metabolite (#468) correlated with *Il33, Ucp1* and butyric acid, while homovanillic acid sulphate (#145), and the nicotinic/nicotinamide analog (#391) correlated with ileum *Il33* and *Ucp1*, and several of these metabolites are related to dietary intake. The nicotinic compound nicotinamide N-oxide (#391), is a precursor of nicotinamide-adenine dinucleotide (NAD+) (Murray and Chaykin, 1966). NAD+ is depleted in the liver during fasting due to

increased β-oxidation, but NAD+ is regenerated from NADH as a part of the conversion of acetoacetate to β-hydroxy-butyrate or, alternatively, via mitochondrial uncoupling through UCP2 (Geisler et al 2016). Interestingly, NAD+ acts as an indispensable cofactor for the activation of all the sirtuins (SIRT1-7), nutrient-sensing histone deacetylases. In the context of fasting and calorie restriction, SIRT1 is the best described as it orchestrates liver metabolism in the fasted state (Hayashida et al., 2010) and have been implicated in the life-span extension associated with calorie restriction in several organisms (Michan, 2014; Rehan et al., 2014). The valeric acid-O-sulphate metabolite (#272) and homovanillic acid sulphate (#145) are likely diet-derived flavanols formed by colonic fermentation (Rechner et al, Manach et al, Sanchez-Patan et al) and are thus indicative of an altered gut microbiota activity in fasted mice. Whether or not they play a direct role in modifying the adipose tissue phenotype will need further investigations. We also found a strong correlation between ileal *Il33* expression and specific urinary cortisol analogs (#13) and the unclassified urinary metabolite (#37). Cortisol and cortisol derivatives are well-characterized fasting-dependent host metabolites, as cortisol stimulates gluconeogenesis, suppresses the immune system, and modifies fat and carbohydrate metabolism (ref.).

Altogether, our systems-level analysis revealed a novel connection between intestinal butyric acid production, ileal *Il33* and *Porphyromonadaceae* to visceral adipose expression of the uncoupling protein *Ucp1* during short-term fasting in obese mice. The fasting-induced nutrient restriction in the intestine is suggested to exert a selection pressure that may allow for increased butyric acid production by colonic *Porphyromonadaceae.* Collectively, the identified changes in inflammatory and metabolic parameters in short-term fasted obese mice point to a positive effect of short-term fasting involving propagation of a tissue-sustaining type 2 immune profile in intestinal tissue and visceral fat being coupled to a fat-burning phenotype that suggests for short-term improvement of inflammatory and metabolic health.

MATERIALS AND METHODS

Animal experiments

Twenty male C57BL/6NTac mice (Taconic, Lille Skensved, Denmark) aged four weeks at arrival were housed two by two and fed *ad libitum* a standard rodent diet Altromin 1324 (Altromin, Lage, Germany) at Week 0. From Week 1, all mice (n = 20) were fed a synthetic D12492 high-fat diet containing 60% of the energy from fat (54.4% from lard and 5.6% from soybean oil), for 22 weeks. All mice were caged two-by-two with a fasted and a fed mouse in each cage. Temperature at 20-24 °C, humidity 55% ± 10% with a strict 12 h light cycle. One mouse died during cheek blood sampling at Week 9.

Sampling

The mice were transferred to clean cages and fecal pellets were collected immediately after defecation for short chain fatty acid (SCFA) analysis.
Urine samples were collected at the terminal week (Week 22) and kept on ice until transfer to -80 °C. All mice were weighed prior to the fasting, to validate the presence of a similarly obese phenotype.
One mouse from each cage was fasted for 8.3 to 11.6 hours when the light was switched on, while the other one was fed *ad libitum*. All mice were anesthetized with a Hypnorm/Dormicum mixture (0.315 mg/mL Fentanyl, 10 mg/mL Fluanisone and 5 mg/mL Midazolam) injected subcutaneously as a 1:1:2 water solution (0.006 mL/g body weight). Blood was sampled from the periorbital plexus into EDTA-coated tubes and centrifuged (2000 g, 5 min) to obtain plasma for cytokine and alanine aminotransferase measurements. The mice were then euthanized by cervical dislocation and dissected. Liver and epididymal white adipose tissue (eWAT) were weighed. Samples from ileum, colon and liver were placed in the RNA*later* RNA stabilization reagent (QIAGEN, Hilden, Germany) overnight; liver samples were flash-frozen in liquid nitrogen for triglyceride and phospholipid analysis and eWAT samples were flash-frozen for RNA extraction. Luminal contents from ileum, cecum and colon were flash-frozen. All samples except the paraformaldehyde fixed tissues were stored at -80 °C until further analyses.

Biochemical Measurements in blood and plasma

Plasma alanine aminotransferase was measured with an ELISA kit (MyBioSource, San Diego, CA, USA). Plasma cytokines, IL-1β, IL-6, IFN-γ, TNF-α and IL-10, were measured using a custom V-PLEX Mouse Biomarkers ELISA Kit (Meso Scale Discovery, Rockville, MD, USA).

SCFA and BCFA analysis

SCFAs were analyzed in cecal samples and feces by Gas Chromatography Mass Spectrometry essentially as previously described (Zhao *et al.*, 2006; Nejrup *et al.*, 2015).
Frozen cecum content and fecal pellets were thawed on ice. Cecum contents (5-25 mg) were homogenized in 250 µl methanol, 250 µL Milli-Q water and 10 µL internal standard (100 mM 2-ethylbutyric acid in 12% formic acid, Sigma-Aldrich, St.Louis, MO, USA) using a micro-homogenizer. Similarly, one or two fecal pellets per sample were homogenized in 1.5 mL water and 100 µl internal standard using a bead-beater, and incubated for 10 min at room-temperature with slow shaking. Acidity of samples was adjusted to pH = 2-3 using 3M HCl. The samples were then centrifuged at 10,000 g for 10 min, and supernatants were filtered through 0.45 µm Phenex-NY syringe filters (Phenomenex, Værløse, Denmark). External calibration was performed using standard solution mixtures of acetic acid, propionic acid, butyric acid, iso-butyric acid, valeric acid, iso-valeric acid, caproic acid and 2-ethylbutyric acid (Sigma-Aldrich) in the concentrations 10, 20, 50, 100, 250, 500 and 1,000 mM with extra acetic acid, propionic acid and butyric acid in the concentrations 2000 and 5000 mM.
Aliquots (3 µL) of each sample were injected into a HP 6890 GC system (Agilent Technologies, Santa Clara, CA, USA) with a CP-FFA WCOT fused silica capillary column (25 m x 0.53 mm i.d. coated with 1

µm film thickness, Chrompack, EA Middelburg, The Netherlands). The carrier gas was helium at a flow rate of 20 mL/min. The initial oven temperature of 60 °C was maintained for 0.25 min, raised to 180 °C at 8 °C/min and held for 3 min, then increased to 215 °C at 20 °C/min, and finally held at 215 °C for 5 min. The temperature of the front inlet detector and the injector was 250 °C. The flow rates of hydrogen, air and helium as makeup gas were 40, 450, and 45 mL/min, respectively. The run time for each analysis was 22 min. Data handling was performed using the OpenLAB Chromatography Data System ChemStation Edition software (Rev.A.10.02). The concentration of SCFA in the samples was calculated against the individual external standards, and adjusted according to the loss of internal standard.

Urine metabolome profiling with Ultra Performance Liquid Chromatography Mass Spectrometry (UPLC-MS)

Frozen urine samples were thawed on ice and centrifuged at 10,000 g for 10 min at 4 °C to remove particles. Subsequently, samples were diluted 1:100 with Milli-Q water, mixed by vortexing, and pipetted into LC vials. Pooled quality control (QC) samples were prepared by mixing aliquots of all urine samples, thereby ensuring the QC sample represented the whole sample set. The samples were kept on ice during preparation.

The column was conditioned by running a couple of blank samples (water) followed by five injections of the QC sample before urine samples were injected. The QC sample was analysed once for every ten urine samples throughout the LC-MS analysis to provide data from which the reproducibility could be assessed. For each sample, 2 µL of diluted urine (1:100 in water) was analysed in both negative and positive mode by a UPLC-QTOF-MS system consisting of Dionex Ultimate 3000 RS liquid chromatograph (Thermo Scientific, Sunnyvale, CA, USA) coupled to a Bruker maXis time of flight mass spectrometer equipped with an electrospray interphase (Bruker Daltonics, Bremen, Germany). The analytes were separated on a Poroshell 120 SB-C18 column with a dimension of 2.1 x 100 mm and 2.7 µm particle size (Agilent Technologies, CA, USA) based on the settings according to Want et al. (Want *et al.*, 2010). Shortly, the column was held at 40 °C and the sampler at 4 °C. The UPLC mobile phases consisted of 0.1% formic acid in water (solution A) and 0.1% of formic acid in acetonitrile (solution B). While containing a constant flow rate of 0.4 mL/min, the analytes were eluted using the following gradient. Solvent programming was isocratic 1% B for 1 min followed by a linear gradient up to 15% at 3 min, then a linear gradient up to 50% B at 6 min, and finally a linear gradient up to 95% B at 9 min. The final gradient composition, 95% B, was held constant until 10 min, followed by a return of the solvent composition to initial conditions at 10.1 min and equilibration until 13 min. Mass spectrometry data were collected in full scan mode at 2 Hz with a scan range of 50-1000 mass/charge (m/z). The following electrospray interphase settings were used: nebulizer pressure 2 bar, drying gas 10 L/min, 200 °C, capillary voltage 4500 V. For MS/MS analyses, a ramp collision energy ranging from 10 to 30 eV was applied on a scheduled precursor list. To improve the measurement accuracy, external and internal calibrations were done using sodium formate clusters (Sigma-Aldrich) and in addition a lock-mass calibration was applied (hexakis(1H,1H,2H-perfluoroetoxy)phosphazene, Apollo Scientific, Manchester, UK).

The raw LC-MS data were converted to mzXML files using Bruker Compass DataAnalysis 4.2 software (Bruker Daltonics) and were then pre-processed through noise filtering, peak detection, and alignment using the open-source R package XCMS (v1.38.0) (Smith *et al.*, 2006). Noise filtering settings included that features should be detected in minimum 50 % of samples within a group. Data tables were generated comprising m/z, retention time, and intensity (peak area) for each variable in every sample. For each sample, the urinary features were normalized to the total intensity of the given sample. Subsequently, the data were filtered using the pooled QC samples: features with coefficient of variation above 30% in the QC samples were excluded, and features with a retention time above 8 min were also excluded. Metabolite candidates were identified by searching the accurate masses of parent ions and fragments (from MS/MS), against the METLIN (Smith *et al.*, 2005) and HMDB databases (Wishart *et al.*, 2013). The metabolites were identified according to the four different levels described by the Metabolomics Standard Initiative (Sumner *et al.*, 2007).

16S rRNA gene sequencing

Bacterial DNA was extracted from feces and luminal contents using the PowerLyzer PowerSoil DNA Isolation Kit (Mo Bio Laboratories, Carlsbad, CA, USA). Around 10-20 fecal pellets (100 mg) per sample were used to make sure that both mice in the cage were represented. DNA concentrations were measured using the Nanodrop Spectrophotometer ND-1000 (Thermo Scientific, Wilmington, DE, USA). Variable Region 3 (V3) of the 16S rRNA gene was amplified using a universal forward primer with a unique 10-12 bp barcode (IonXpress barcode, Ion Torrent) for each bacterial community (PBU 5'-A-adapter-TCAG-barcode-GAT-CCTACGGGAGGCAGCAG-3') and a universal reverse primer (PBR 5'-trP1-adapter-ATTACCGCGGCTGCTGG-3'). The PCR reactions were conducted with 5 ng template DNA, 10 mmol/L dNTP, 1 µmol/L forward/reverse primer, 4 µL HF-buffer and 0.2 µL Phusion High-Fidelity DNA polymerase (Thermo Scientific, Vilnius, Lithuania) in a total reaction volume of 20 µL. PCR conditions were 30 s at 98 °C, 24 cycles of 15 s at 98 °C, 30 s at 72 °C, followed by 5 min at 72 °C. For a few samples that did not yield sufficient PCR products, an initial PCR was performed with universal primers without barcodes or adaptors (30 cycles) followed by a second round of PCR (15 cycles) with barcoded primers using a 10-fold dilution of the first PCR product as template. PCR products were separated on a 1.5% agarose gel at 3.5 V/cm for 90 minutes, and bands of the expected size (approximately 260 bp) were excised from the gel. DNA was purified from the excised gel using the MinElute Gel Extraction Kit (Qiagen, Germany) according to the instructions of the manufacturer. DNA concentrations were determined using the Qubit 2.0 fluorometer (Invitrogen, Carlsbad, CA, USA) with the dsDNA HS assay (Invitrogen, Eugene, OR, USA), and equal amounts of PCR products from each community were pooled to construct a library. Sequencing was performed using the Ion PGM Template OT2 200 Kit and the Ion PGM Sequencing 200 Kit v2 with the 318-chip (Ion Torrent).

Sequencing data analysis

Sequences were de-multiplexed, trimmed to eliminate primers, and filtered with a length range of 125-180 bp using the CLC Genomic Workbench v7.0.3 (Qiagen, Aarhus, Denmark). Each sequence was classified to the lowest possible taxonomic rank (assignment confidence ≥ 50%) using the Ribosomal Database Project (RDP) Classifier v2.10.1 (Wang *et al.*, 2007), and collapsed at genus, family, phylum and domain levels. The depths (range, median) of the resulting phylotype data table were: 35,156-95,090, 59,500 for fecal samples, 35,672-93,032, 73,251 for ileal samples, 23,216-57,266, 42,276 for cecal samples and 25,066-52,617, 42,754 for colonic samples.

Operational taxonomic units (OTUs) were generated *de novo* using UPARSE v8.0.1623 (Edgar, 2013). All sequences were subjected to quality filtering with a cut-off of maxee of 3.5 (discard reads with > 3.5 total expected errors for all bases in the read). Unique sequences except singletons were clustered at 97% sequence homology. Chimeras were first filtered by the UPARSE-OTU algorithm and then by the UCHIME algorithm (Edgar *et al.*, 2011) using the RDP classifier training database v9 and the default threshold. Taxonomies of OTU representative sequences were also assigned using the RDP classifier. The depths (range, median) of the resulting OTU data table were: 28,606-74,454, 47230 for fecal samples, 30,421-89,534, 67,731 for ileal samples, 14,542-41,654, 29,559 for cecal samples and 15,495-37,974, 29,731 for colonic samples.

OTU representative sequences were pooled with a 16S rRNA gene sequence assigned as *Methanosarcina* within the Archaea, and aligned to the Greengenes core set (Greengenes 13_5 PyNAST aligned 85% OTU representative sequences) (McDonald *et al.*, 2012) using PyNAST (Caporaso, Bittinger, *et al.*, 2010). A phylogenetic tree was created using FastTree. Using Dendroscope v3.3.2, the tree was re-rooted with the Archaea outgroup, and then the outgroup was pruned from the tree, thereby generating a phylogenetic tree for downstream analyses.

To discover features, i.e. OTUs and bacterial groups at genus/family/phylum levels (based on the phylotype data table), that were differentially abundant in the Fed and Fasted mice, features that were less abundant than 0.02% of average numbers of total bacteria in both groups and features that presented in less than 50% of samples in both groups were filtered out. The matrices of relative abundances were permutated 10,000 times, and p values represent fraction of times that permuted

differences assessed by Welch's t test were greater than or equal to real differences, followed by the FDR correction (FDR < 0.05).
Butyrate production potential in OTUs was identified using GreenGenes KEGG orthology mapping and defined as OTUs possessing either all genes for the butyrate kinase (*buk)* pathway or both subunits of the butyryl-CoA transferase enzyme needed for the *but* pathway.

Gene expression analysis using real time RT-PCR
Total RNA from liver, ileal and colonic tissues was extracted using the RNeasy Plus Mini Kit (Qiagen, Germany) according to the product protocol, while for adipose tissue, total RNA was harvested by trizol and chloroform based purification followed by kit extraction. For gut barrier function related genes, RNA concentration and purity were determined using the Nanodrop Spectrophotometer ND-1000, and cDNA was synthesized from 1.4 µg RNA in 20 µL reactions using the SuperScript VILO cDNA Synthesis Kit (Invitrogen, Carlsbad, CA, USA), and diluted 20-fold for further use. Quantitative real time RT-PCR was performed with a SYBR Green I Master (Roche Diagnostics GmbH, Mannheim, Germany) and a LightCycler 480 system (Roche Diagnostics GmbH) using the described primer sets (S5 Table), and the PCR reactions were run under the following conditions: 95 °C for 5 min; 40 cycles of 95 °C for 10 sec, 55 °C for 10 sec, and 72 °C for 30 sec; melting curve generation with preparation with 95 °C for 5 sec, 65 °C for 1min and increasing the temperature to 98 °C with a rate of 0.11 °C/sec with continuous fluorescence detection. The amplification efficiency of each primer was assessed by a standard curve. The amount of each mRNA was normalized to the geometric mean of expression levels of phosphoglycerate kinase 1 gene (*Pgk1*), actin beta gene (*Actb*) and glyceraldehyde 3-phosphate dehydrogenase gene (*Gapdh*). For the remaining analyses, RNA concentrations were measured using a Qbit 2.0 fluorometer, and cDNA was synthesized by a High Capacity cDNA Reverse Transcription Kit (Applied Biosystems) from 2 µg RNA. Real time PCR of the cDNA was performed with a TaqMan Fast Universal PCR Master Mix (Applied Biosystems, Foster city, CA, USA) and a 7900HT Fast Real-time PCR system (Applied Biosystems) using primers and probes (S6 Table) purchased from Integrated DNA Technologies (Leuven, Belgium). The PCR reactions were run under the following conditions: 95 °C for 20 sec; 40 cycles of 95 °C for 1 sec and 60 °C for 20 sec. Normalization was done with the beta-2 microglobulin gene (*B2m*) and *Gapdh*, and subsequently gene expression of fasted mice were normalized to that of fed mice.

Statistical analysis
Unless specified, two-sided Student's t test (if normally distributed) or Mann-Whitney test (if non-continuous data or not normally distributed) were performed using GraphPad Prism 6.02. Maximally one outlier from each group detected by Grubbs' test (http://www.graphpad.com/quickcalcs/Grubbs1.cfm, alpha = 0.05) was excluded before the statistical tests. Spearman's rank correlation was used for the calculation of correlation coefficients. Networks based on Spearman correlations were built using Cytoscape v3.3.0.
Co-abundance clustering was performed using R v. 3.1.2 (R_Core_Team, 2015) and the R package WGCNA (Langfelder and Horvath, 2008). Signed weighted co-abundance correlations were obtained by bi-weight mid-correlations of co-abundant metabolites (log-transformed), the relative abundance of bacterial OTUs and the relative concentration of the identified liver lipids from the phospholipid and triglyceride fractions. Scale free topology criteria, β, were used: β = 8 for metabolites, β=6 for lipids, β=14 for ileum, β=7 for cecum, β=9 for colon. To detect clusters using the dynamic hybrid tree-cutting algorithm, minimum cluster sizes were set at 5 (except for the lipids, which were at 3) using deepSplit of 2 for OTUs and 4 for both metabolites and lipids.

References

Brandhorst, S., Choi, I.Y., Wei, M., Cheng, C.W., Sedrakyan, S., Navarrete, G., Dubeau, L., Yap, L.P., Park, R., Vinciguerra, M.*, et al.* (2015). A Periodic Diet that Mimics Fasting Promotes Multi-System Regeneration, Enhanced Cognitive Performance, and Healthspan. Cell metabolism *22*, 86-99.

Brestoff, J.R., and Artis, D. (2015). Immune regulation of metabolic homeostasis in health and disease. Cell *161*, 146-160.

den Besten, G., Bleeker, A., Gerding, A., van Eunen, K., Havinga, R., van Dijk, T.H., Oosterveer, M.H., Jonker, J.W., Groen, A.K., Reijngoud, D.J.*, et al.* (2015). Short-Chain Fatty Acids Protect Against High-Fat Diet-Induced Obesity via a PPARgamma-Dependent Switch From Lipogenesis to Fat Oxidation. Diabetes *64*, 2398-2408.

Fontana, L., Meyer, T.E., Klein, S., and Holloszy, J.O. (2004). Long-term calorie restriction is highly effective in reducing the risk for atherosclerosis in humans. Proceedings of the National Academy of Sciences of the United States of America *101*, 6659-6663.

Gao, Z., Yin, J., Zhang, J., Ward, R.E., Martin, R.J., Lefevre, M., Cefalu, W.T., and Ye, J. (2009). Butyrate improves insulin sensitivity and increases energy expenditure in mice. Diabetes *58*, 1509-1517.

Geisler, C.E., Hepler, C., Higgins, M.R., and Renquist, B.J. (2016). Hepatic adaptations to maintain metabolic homeostasis in response to fasting and refeeding in mice. Nutrition & metabolism *13*, 62.

Glass, Christopher K., and Olefsky, Jerrold M. (2012). Inflammation and Lipid Signaling in the Etiology of Insulin Resistance. Cell Metabolism *15*, 635-645.

Hayashida, S., Arimoto, A., Kuramoto, Y., Kozako, T., Honda, S., Shimeno, H., and Soeda, S. (2010). Fasting promotes the expression of SIRT1, an NAD+ -dependent protein deacetylase, via activation of PPARalpha in mice. Molecular and cellular biochemistry *339*, 285-292.

Kelly, C.J., Zheng, L., Campbell, E.L., Saeedi, B., Scholz, C.C., Bayless, A.J., Wilson, K.E., Glover, L.E., Kominsky, D.J., Magnuson, A.*, et al.* (2015). Crosstalk between Microbiota-Derived Short-Chain Fatty Acids and Intestinal Epithelial HIF Augments Tissue Barrier Function. Cell host & microbe *17*, 662-671.

Koh, A., De Vadder, F., Kovatcheva-Datchary, P., and Backhed, F. (2016). From Dietary Fiber to Host Physiology: Short-Chain Fatty Acids as Key Bacterial Metabolites. Cell *165*, 1332-1345.

Langfelder, P., and Horvath, S. (2008). WGCNA: an R package for weighted correlation network analysis. BMC bioinformatics *9*, 559.

Lee, M.W., Odegaard, J.I., Mukundan, L., Qiu, Y., Molofsky, A.B., Nussbaum, J.C., Yun, K., Locksley, R.M., and Chawla, A. (2015). Activated type 2 innate lymphoid cells regulate beige fat biogenesis. Cell *160*, 74-87.

Longo, V.D., and Mattson, M.P. (2014). Fasting: molecular mechanisms and clinical applications. Cell metabolism *19*, 181-192.

Lu, Y., Fan, C., Li, P., Lu, Y., Chang, X., and Qi, K. (2016). Short Chain Fatty Acids Prevent High-fat-diet-induced Obesity in Mice by Regulating G Protein-coupled Receptors and Gut Microbiota. Scientific reports *6*, 37589.

Lumeng, C.N., and Saltiel, A.R. (2011). Inflammatory links between obesity and metabolic disease. J Clin Invest *121*, 2111-2117.

Mahapatro, M., Foersch, S., Hefele, M., He, G.W., Giner-Ventura, E., McHedlidze, T., Kindermann, M., Vetrano, S., Danese, S., Gunther, C.*, et al.* (2016). Programming of Intestinal Epithelial Differentiation by IL-33 Derived from Pericryptal Fibroblasts in Response to Systemic Infection. Cell reports *15*, 1743-1756.

Michan, S. (2014). Calorie restriction and NAD(+)/sirtuin counteract the hallmarks of aging. Frontiers in bioscience *19*, 1300-1319.

Moller, D.E., and Kaufman, K.D. (2005). Metabolic syndrome: a clinical and molecular perspective. Annual review of medicine *56*, 45-62.

Monticelli, L.A., Osborne, L.C., Noti, M., Tran, S.V., Zaiss, D.M., and Artis, D. (2015). IL-33 promotes an innate immune pathway of intestinal tissue protection dependent on amphiregulin-EGFR interactions. Proceedings of the National Academy of Sciences of the United States of America *112*, 10762-10767.

Murray, K.N., and Chaykin, S. (1966). The reduction of nicotinamide N-oxide by xanthine oxidase. The Journal of biological chemistry *241*, 3468-3473.

Pedersen, H.K., Gudmundsdottir, V., Nielsen, H.B., Hyotylainen, T., Nielsen, T., Jensen, B.A., Forslund, K., Hildebrand, F., Prifti, E., Falony, G.*, et al.* (2016). Human gut microbes impact host serum metabolome and insulin sensitivity. Nature *535*, 376-381.

Qin, J., Li, Y., Cai, Z., Li, S., Zhu, J., Zhang, F., Liang, S., Zhang, W., Guan, Y., Shen, D.*, et al.* (2012). A metagenome-wide association study of gut microbiota in type 2 diabetes. Nature *490*, 55-60.

R_Core_Team (2015). R: A language and environment for statistical computing. https://www.R-project.org/.

Rehan, L., Laszki-Szczachor, K., Sobieszczanska, M., and Polak-Jonkisz, D. (2014). SIRT1 and NAD as regulators of ageing. Life sciences *105*, 1-6.

Schiering, C., Krausgruber, T., Chomka, A., Frohlich, A., Adelmann, K., Wohlfert, E.A., Pott, J., Griseri, T., Bollrath, J., Hegazy, A.N.*, et al.* (2014). The alarmin IL-33 promotes regulatory T-cell function in the intestine. Nature *513*, 564-568.

Sonnenburg, J.L., and Backhed, F. (2016). Diet-microbiota interactions as moderators of human metabolism. Nature *535*, 56-64.

Thaiss, C.A., Zmora, N., Levy, M., and Elinav, E. (2016). The microbiome and innate immunity. Nature *535*, 65-74.

Traba, J., Kwarteng-Siaw, M., Okoli, T.C., Li, J., Huffstutler, R.D., Bray, A., Waclawiw, M.A., Han, K., Pelletier, M., Sauve, A.A.*, et al.* (2015). Fasting and refeeding differentially regulate NLRP3 inflammasome activation in human subjects. The Journal of clinical investigation *125*, 4592-4600.

Turnbaugh, P.J., Hamady, M., Yatsunenko, T., Cantarel, B.L., Duncan, A., Ley, R.E., Sogin, M.L., Jones, W.J., Roe, B.A., Affourtit, J.P.*, et al.* (2009). A core gut microbiome in obese and lean twins. Nature *457*, 480-484.

Turnbaugh, P.J., Ley, R.E., Mahowald, M.A., Magrini, V., Mardis, E.R., and Gordon, J.I. (2006). An obesity-associated gut microbiome with increased capacity for energy harvest. Nature *444*, 1027-1031.

Vasanthakumar, A., Moro, K., Xin, A., Liao, Y., Gloury, R., Kawamoto, S., Fagarasan, S., Mielke, L.A., Afshar-Sterle, S., Masters, S.L.*, et al.* (2015). The transcriptional regulators IRF4, BATF and IL-33 orchestrate development and maintenance of adipose tissue-resident regulatory T cells. Nature immunology *16*, 276-285.

Vieira, E.L., Leonel, A.J., Sad, A.P., Beltrao, N.R., Costa, T.F., Ferreira, T.M., Gomes-Santos, A.C., Faria, A.M., Peluzio, M.C., Cara, D.C.*, et al.* (2012). Oral administration of sodium butyrate attenuates inflammation and mucosal lesion in experimental acute ulcerative colitis. The Journal of nutritional biochemistry *23*, 430-436.

Wang, X., He, G., Peng, Y., Zhong, W., Wang, Y., and Zhang, B. (2015). Sodium butyrate alleviates adipocyte inflammation by inhibiting NLRP3 pathway. Scientific reports *5*, 12676.

Yang, Z., Sun, R., Grinchuk, V., Fernandez-Blanco, J.A., Notari, L., Bohl, J.A., McLean, L.P., Ramalingam, T.R., Wynn, T.A., Urban, J.F., Jr.*, et al.* (2013). IL-33-induced alterations in murine intestinal function and cytokine responses are MyD88, STAT6, and IL-13 dependent. American journal of physiology Gastrointestinal and liver physiology *304*, G381-389.

Zhang, C., Li, S., Yang, L., Huang, P., Li, W., Wang, S., Zhao, G., Zhang, M., Pang, X., Yan, Z.*, et al.* (2013). Structural modulation of gut microbiota in life-long calorie-restricted mice. Nature communications *4*, 2163.

Figure legends

Figure 1: Integration of bacterial fermentation and host parameters with fasting-associated gut microbiota, liver lipid, and urine metabolite clusters.

(**a**) Metabolic and inflammatory host responses parameters were determined in fed (n= 10) and fasted (n= 8) mice along with gut microbiota composition and fermentation products. Host parameters included quantification of gene expression of liver (dark red color-coded box), epididymal white adipose tissue (eWAT, orange), ileum (light green) and colon (dark green) by quantitative RT-PCR, and plasma-derived cytokines and alanine aminotransferase (ALT) (pink) by ELISA. Short-chain fatty acids from cecum (turquoise) and fecal pellets (blue) and liver lipid species from the triglyceride and phospholipid fractions were determined by gas chromatography. The lipid species were binned into six co-abundance clusters of which one was associated with fasting (Lipids-1, grey liver lipids box). Similarly, 1609 urine metabolites quantified by UPLC-MS were binned into 83 co-abundance clusters of which 13 (Me-1 to Me-13, grey urine metabolome box) showed fasting-dependency. 16s rRNA sequencing-generated OTUs from the ileal, cecal and colonic compartments were binned into co-abundance clusters tissue-wise, identifying a total of six fasting-dependent clusters (Ileum-OTU-1, Cecum-OTU-1, Colon-OTU-1 to Colon-OTU-4, grey intestinal-located boxes). (**b**) Correlation heatmap of z-score-normalized host parameters (y-axis) against the fasting-dependent lipid, metabolite and OTU clusters (x-axis). Duration of fasting is included as a host parameter (8.3 to 11.6 hours for fasted mice). The coloring of host parameters correspond to tissue origin as indicated in the legend. Heatmap color represents Spearman's r-values (red, positive r-values; blue, negative r-values). Asterisks mark significant correlations (*, $p < 0.05$; †, $p < 0.01$; ‡, $p < 0.001$; #, $p < 0.0001$).

Figure 2: Fasting-induced cecal butyric acid production link to colonic Porphyromonadaceae and adipose tissue expression of *Ucp1*.

(**a**) Heatmap representation of correlations between fasting-associated bacterial OTU clusters and SCFA and BCFA levels determined in cecum and feces. The heatmap color represents Spearman's r-values (red, positive r-values; blue, negative r-values). Asterisks mark significant correlations (Spearman; FDR < 0.05; •, $q < 0.1$; *, $q < 0.05$). (**b-d**) Selected correlations related to the cecal butyric acid phenotype. Correlations of butyric acid (µg/mol) and the sum of the relative abundance of all *Porphyromonadaceae* belonging to Colon-OTU-1 to -4 (**b**), butyric acid (µg/mol) and eWAT *Ucp1* (relative expression) (**c**), butyric acid and eWAT *Il33* (relative expression) (**d**). Red line indicates the linear regression line; grey area is the 95 % confidence interval.

Figure 3: Combined network and multivariate correlation analysis to interlink fasting-induced whole body parameters.

(**a**) Step-wise approach to integrate the fasting-associated urine metabolome with the bacterial OTUs and liver lipids. All metabolites (348 in total) belonging to either of the metabolite clusters (Me-1, and Me-9 to Me-13) were initially reduced to 210 metabolites based on correlation with fasting duration (Spearman, FDR < 0.05). This subpopulation of metabolites was subsequently correlated with all OTUs belonging to any of the six fasting-associated bacterial OTU clusters (Ileum-OTU-1, Cecum-OTU-1, and Colon-OTU-1 to -4) (Spearman, FDR < 0.05). The OTUs and metabolites present in the OTU-metabolite correlations were then correlated with the five liver-derived lipids present in the fasting-dependent Lipids-1 cluster (Spearman, FDR < 0.01). The inserted table displays the names for each of the interlinked fasting-associated factors. (**b**) Network analysis representing the resulting correlations from (**a**). The line color between nodes defines the correlational direction (red lines, positive correlations; blue lines, negative correlations). The color of the edge of nodes

defines the fasting-induced response (red edges, higher in fasted mice; blue edges, lower in fasted mice). Identifiers for the metabolites, OTUs and lipids are shown in the table in (**a**). (**c**) Heatmap of the correlations between the resulting bacterial OTUs, liver lipids and urine metabolites and the major fasting-associated bacterial fermentation products and metabolic and inflammatory host factors (Spearman; FDR < 0.05; *, q < 0.05; †, q < 0.01). Solid red lines indicate factors that are enhanced by fasting duration, and solid blue lines those that are reduced by fasting.

Figure S1: Weight of animals at termination.
C57BL/6J mice were fed a high-fat diet for 22 weeks. Before sacrifice, half of the mice were subjected to fasting for 8.3 to 11.6 hours, while the remaining fed mice were provided *ad libitum* access to diet throughout the study period. Whole body weight prior to fasting (**a**), and liver (**b**) and epididymal adipose tissue (**c**) weights were registered after termination. Fasted, n=8, and fed mice, n= 10.

Figure S2: Eigengene values of all urine metabolite, gut microbiota and liver lipid clusters.
(**a**) Co-abundance clusters from the urine metabolome, (**b**) ileum, (**c**) cecum and (**d**) colon microbiome at the OTU level, (**e**) and liver lipids. For (**a-e**), asterisks mark the significant differences in eigengene values between fed and fasted mice (t test; FDR < 0.1; *, q < 0.05; **, q < 0.01).

Figure S3: Co-correlation analysis of fasting-associated bacterial fermentation products and metabolic and inflammatory host factors.
Co-correlation analysis of the z-score of fasting-associated host parameters (colored boxed in Fig. 1A) based on Spearman's r-values. Spearman; FDR < 0.05; *, q < 0.05; †, q < 0.01; ‡, q < 0.001; #, q < 0.0001, $, q < 0.00001, X, q < 0.000001.

Figure S4: Univariate display of measured bacterial fermentation products and metabolic and inflammatory host factors.
Tissues were harvested from fed (n=10) and fasted (n=8) obese mice for the following analysis: (**a**) cecal and (**b**) fecal SCFAs, liver lipids from the triglyceride fraction (**c**) and phospholipid fraction (**d**). Quantitative RT-PCR of (**e**) ileum, (**f**) colon, (**g**) liver and (**h**) epididymal white adipose tissue (eWAT), and plasma protein levels of (**i**) cytokines (**j**) alanine aminotransferase. (**a-d**) shown as boxplots of the mean with error bars marking the 5^{th}-95^{th} percentiles, (**e-i**) boxplots showing the mean with standard deviation. For all statistics: t test; FDR < 0.05; *, q < 0.05; **, q < 0.01; ***, q < 0.001; ****, q < 0.0001.

Figure S5: Relative abundance at family and genus level of the ileal, cecal and colonic microbiota.
Samples from fed (n=10) and fasted (n=8) obese mice were subjected to 16s rDNA-based sequencing. Identified OTUs within ileum, cecum and colon were color-coded according to family (**a**, **c**, **e**), and genera (**b**, **d**, **f**). Statistical comparison of the two groups was done by permutation test (10,000 times). Asterisks represent fraction of times that permuted differences assessed by Welch's t-test were greater than or equal to real differences, (FDR < 0.05) (*, q < 0.05).

Table S1:
The presence or absence of enzymes of the butyrate kinase (buk) or butyrate transferase (but) pathway of OTUs belonging to fasting-dependent clusters. The 98 de novo picked OTUs were aligned to 44 different GreenGenes OTUs. X represents the presence of *But* or *Buk* pathways or either pathway.

Figures

Fig. 1

A

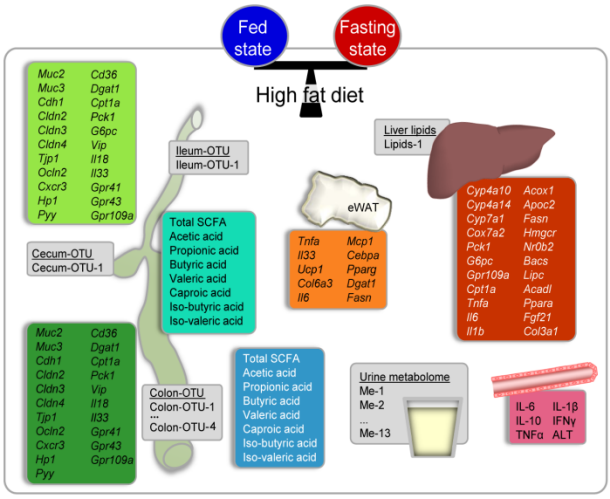

B

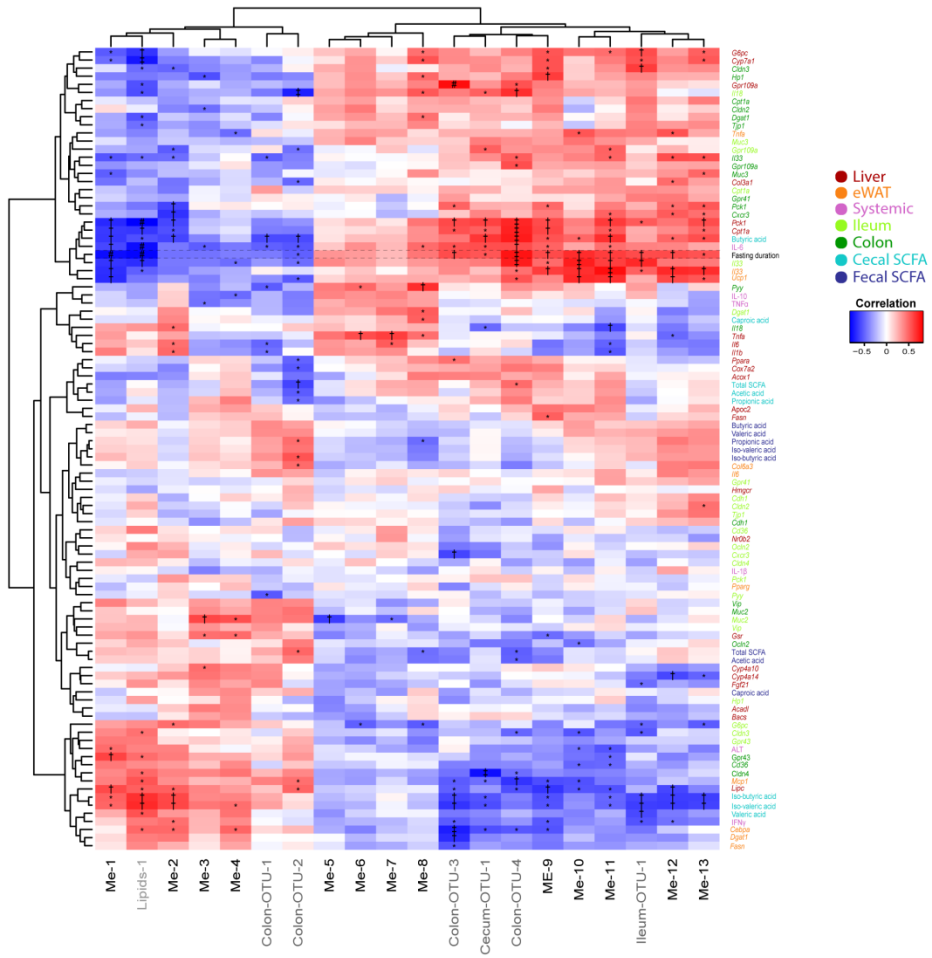

Fig. 2

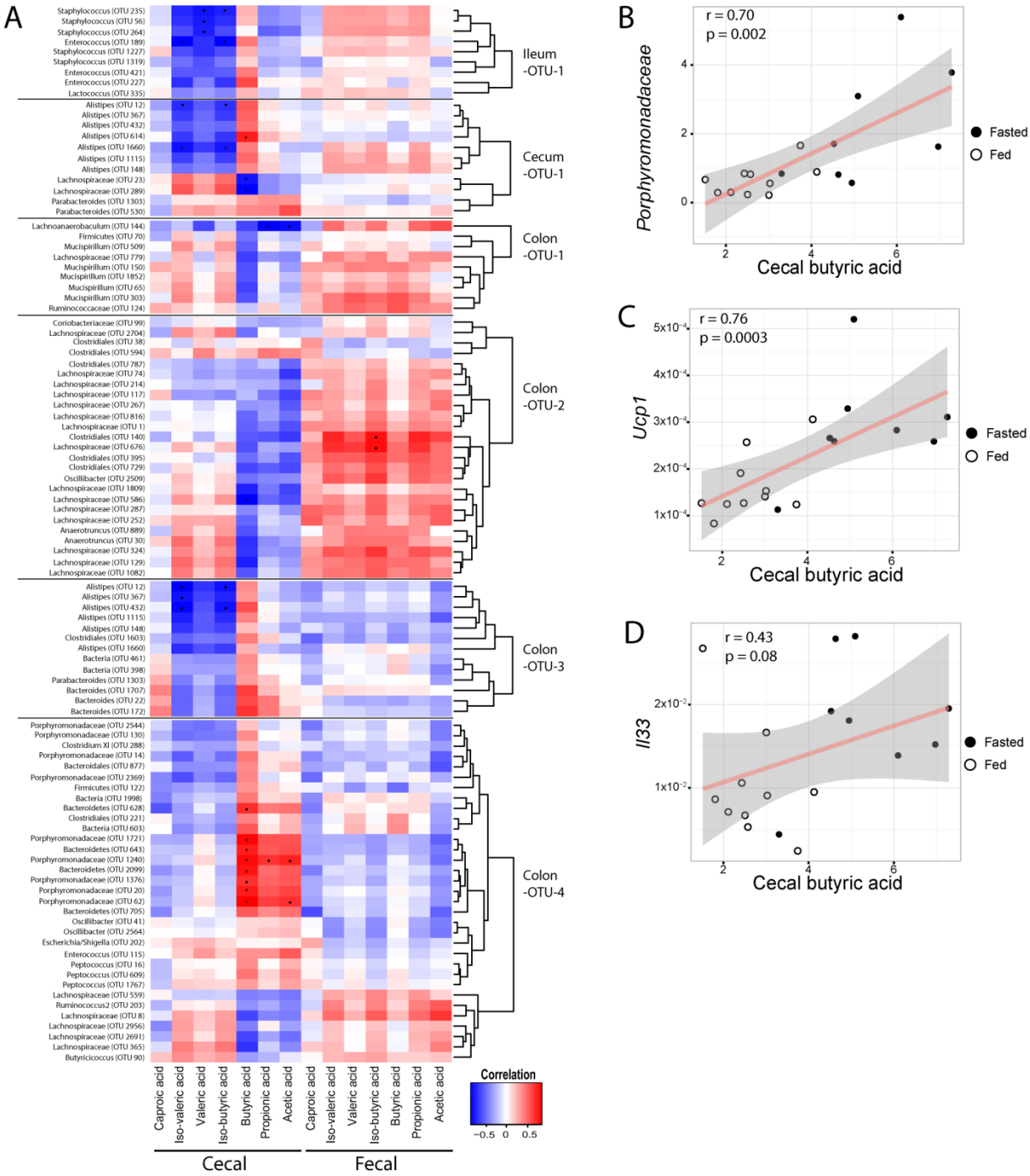
A
Staphylococcus (OTU 235)
Staphylococcus (OTU 56)
Staphylococcus (OTU 264)
Enterococcus (OTU 189)
Staphylococcus (OTU 1227)
Staphylococcus (OTU 1319)
Enterococcus (OTU 421)
Enterococcus (OTU 227)
Lactococcus (OTU 335)
Alistipes (OTU 12)
Alistipes (OTU 367)
Alistipes (OTU 432)
Alistipes (OTU 614)
Alistipes (OTU 1660)
Alistipes (OTU 1115)
Alistipes (OTU 148)
Lachnospiraceae (OTU 23)
Lachnospiraceae (OTU 289)
Parabacteroides (OTU 1303)
Parabacteroides (OTU 530)
Lachnoanaerobaculum (OTU 144)
Firmicutes (OTU 70)
Mucispirillum (OTU 509)
Lachnospiraceae (OTU 779)
Mucispirillum (OTU 150)
Mucispirillum (OTU 1852)
Mucispirillum (OTU 65)
Mucispirillum (OTU 303)
Ruminococcaceae (OTU 124)
Coriobacteriaceae (OTU 99)
Lachnospiraceae (OTU 2704)
Clostridiales (OTU 38)
Clostridiales (OTU 594)
Clostridiales (OTU 787)
Lachnospiraceae (OTU 74)
Lachnospiraceae (OTU 214)
Lachnospiraceae (OTU 117)
Lachnospiraceae (OTU 267)
Lachnospiraceae (OTU 816)
Lachnospiraceae (OTU 1)
Clostridiales (OTU 140)
Lachnospiraceae (OTU 676)
Clostridiales (OTU 395)
Clostridiales (OTU 729)
Oscillibacter (OTU 2509)
Lachnospiraceae (OTU 1809)
Lachnospiraceae (OTU 586)
Lachnospiraceae (OTU 287)
Lachnospiraceae (OTU 252)
Anaerotruncus (OTU 889)
Anaerotruncus (OTU 30)
Lachnospiraceae (OTU 324)
Lachnospiraceae (OTU 129)
Lachnospiraceae (OTU 1082)
Alistipes (OTU 12)
Alistipes (OTU 367)
Alistipes (OTU 432)
Alistipes (OTU 1115)
Alistipes (OTU 148)
Clostridiales (OTU 1603)
Alistipes (OTU 1660)
Bacteria (OTU 461)
Bacteria (OTU 398)
Parabacteroides (OTU 1303)
Bacteroides (OTU 1707)
Bacteroides (OTU 22)
Bacteroides (OTU 172)
Porphyromonadaceae (OTU 2544)
Porphyromonadaceae (OTU 130)
Clostridium XI (OTU 288)
Porphyromonadaceae (OTU 14)
Bacteroidales (OTU 877)
Porphyromonadaceae (OTU 2369)
Firmicutes (OTU 122)
Bacteria (OTU 1998)
Bacteroidetes (OTU 628)
Clostridiales (OTU 221)
Bacteria (OTU 603)
Porphyromonadaceae (OTU 1721)
Bacteroidetes (OTU 643)
Porphyromonadaceae (OTU 1240)
Bacteroidetes (OTU 2099)
Porphyromonadaceae (OTU 1376)
Porphyromonadaceae (OTU 20)
Porphyromonadaceae (OTU 62)
Bacteroidetes (OTU 705)
Oscillibacter (OTU 41)
Oscillibacter (OTU 2564)
Escherichia/Shigella (OTU 202)
Enterococcus (OTU 115)
Peptococcus (OTU 16)
Peptococcus (OTU 609)
Peptococcus (OTU 1767)
Lachnospiraceae (OTU 559)
Ruminococcus2 (OTU 203)
Lachnospiraceae (OTU 8)
Lachnospiraceae (OTU 2956)
Lachnospiraceae (OTU 2691)
Lachnospiraceae (OTU 365)
Butyricicoccus (OTU 90)
Ileum -OTU-1
Cecum -OTU-1
Colon -OTU-1
Colon -OTU-2
Colon -OTU-3
Colon -OTU-4
Caproic acid
Iso-valeric acid
Valeric acid
Iso-butyric acid
Butyric acid
Propionic acid
Acetic acid
Cecal
Fecal
Correlation
−0.5 0 0.5
B
r = 0.70
p = 0.002
Porphyromonadaceae
Cecal butyric acid
Fasted
Fed
C
r = 0.76
p = 0.0003
Ucp1
Cecal butyric acid
Fasted
Fed
D
r = 0.43
p = 0.08
Il33
Cecal butyric acid
Fasted
Fed

Fig. 3

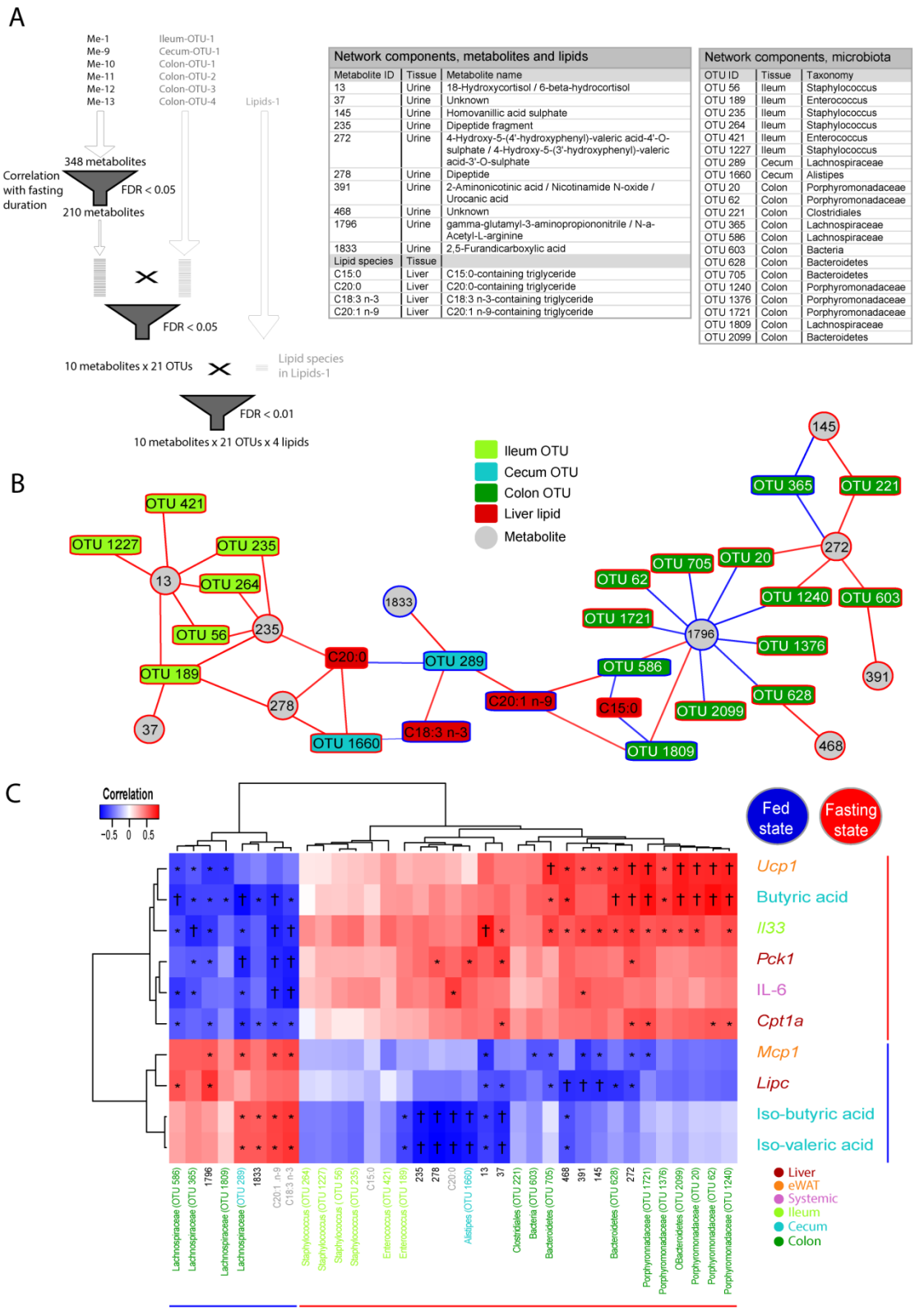

Network components, metabolites and lipids		
Metabolite ID	Tissue	Metabolite name
13	Urine	18-Hydroxycortisol / 6-beta-hydrocortisol
37	Urine	Unknown
145	Urine	Homovanillic acid sulphate
235	Urine	Dipeptide fragment
272	Urine	4-Hydroxy-5-(4'-hydroxyphenyl)-valeric acid-4'-O-sulphate / 4-Hydroxy-5-(3'-hydroxyphenyl)-valeric acid-3'-O-sulphate
278	Urine	Dipeptide
391	Urine	2-Aminonicotinic acid / Nicotinamide N-oxide / Urocanic acid
468	Urine	Unknown
1796	Urine	gamma-glutamyl-3-aminopropiononitrile / N-a-Acetyl-L-arginine
1833	Urine	2,5-Furandicarboxylic acid
Lipid species	Tissue	
C15:0	Liver	C15:0-containing triglyceride
C20:0	Liver	C20:0-containing triglyceride
C18:3 n-3	Liver	C18:3 n-3-containing triglyceride
C20:1 n-9	Liver	C20:1 n-9-containing triglyceride

Network components, microbiota		
OTU ID	Tissue	Taxonomy
OTU 56	Ileum	Staphylococcus
OTU 189	Ileum	Enterococcus
OTU 235	Ileum	Staphylococcus
OTU 264	Ileum	Staphylococcus
OTU 421	Ileum	Enterococcus
OTU 1227	Ileum	Staphylococcus
OTU 289	Cecum	Lachnospiraceae
OTU 1660	Cecum	Alistipes
OTU 20	Colon	Porphyromonadaceae
OTU 62	Colon	Porphyromonadaceae
OTU 221	Colon	Clostridiales
OTU 365	Colon	Lachnospiraceae
OTU 586	Colon	Lachnospiraceae
OTU 603	Colon	Bacteria
OTU 628	Colon	Bacteroidetes
OTU 705	Colon	Bacteroidetes
OTU 1240	Colon	Porphyromonadaceae
OTU 1376	Colon	Porphyromonadaceae
OTU 1721	Colon	Porphyromonadaceae
OTU 1809	Colon	Lachnospiraceae
OTU 2099	Colon	Bacteroidetes

Supplementary figures and tables

Fig. S1

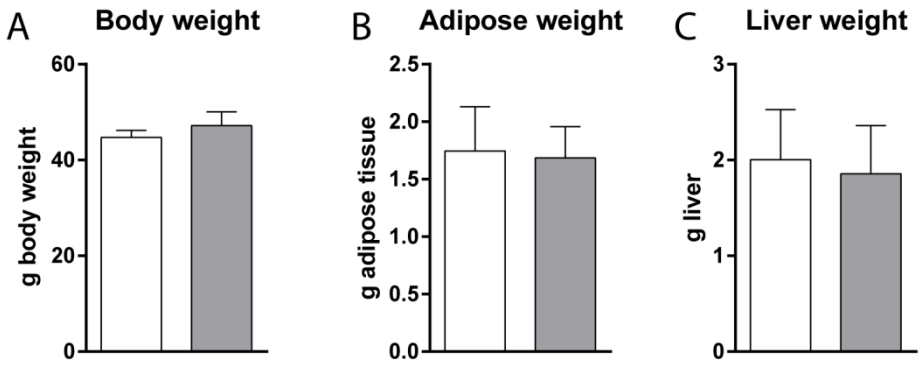

Fig. S2

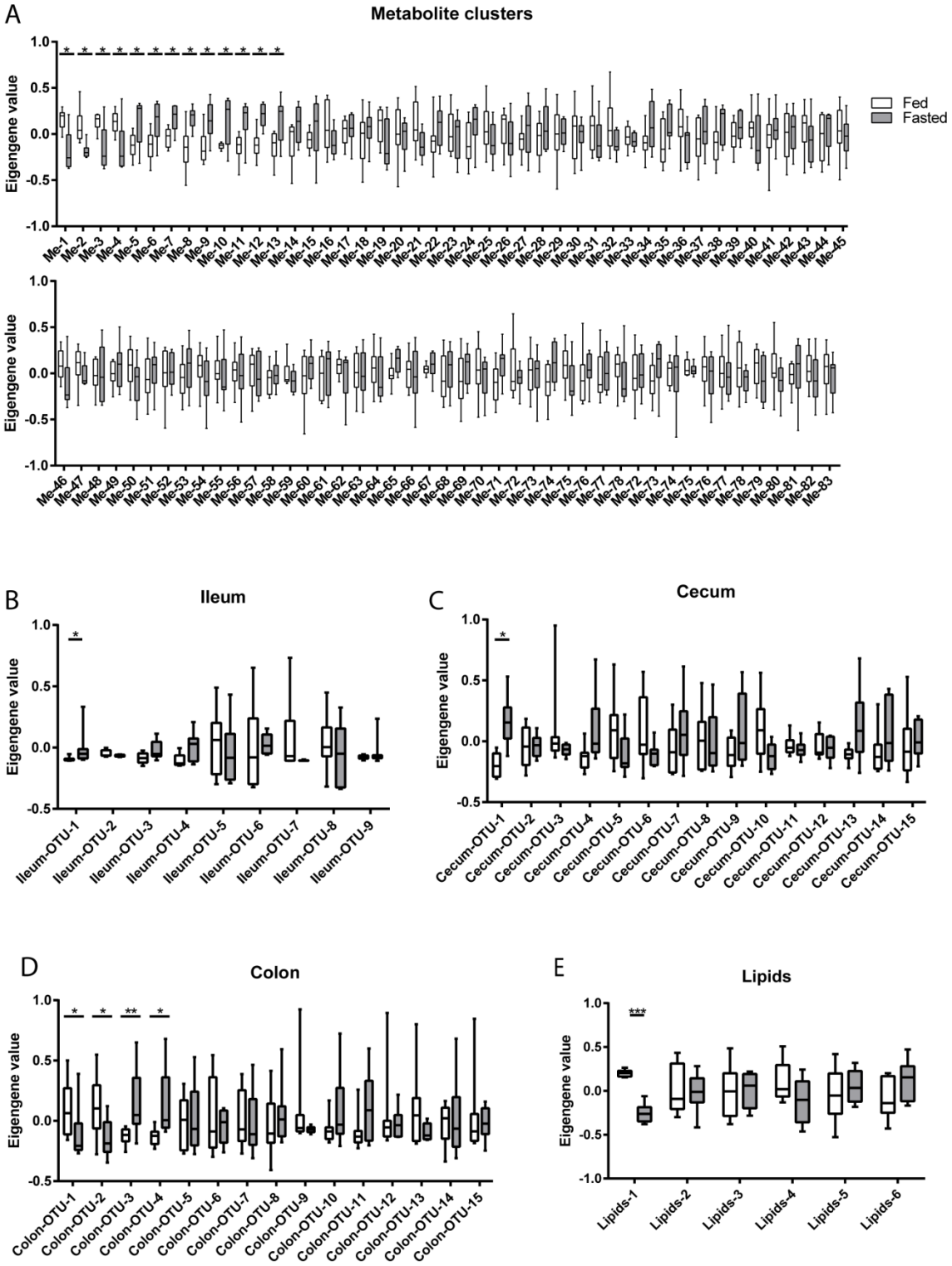
A
Metabolite clusters
Eigengene value
Fed
Fasted
B
Ileum
Ileum-OTU-1
Ileum-OTU-2
Ileum-OTU-3
Ileum-OTU-4
Ileum-OTU-5
Ileum-OTU-6
Ileum-OTU-7
Ileum-OTU-8
Ileum-OTU-9
C
Cecum
Cecum-OTU-1
Cecum-OTU-2
Cecum-OTU-3
Cecum-OTU-4
Cecum-OTU-5
Cecum-OTU-6
Cecum-OTU-7
Cecum-OTU-8
Cecum-OTU-9
Cecum-OTU-10
Cecum-OTU-11
Cecum-OTU-12
Cecum-OTU-13
Cecum-OTU-14
Cecum-OTU-15
D
Colon
Colon-OTU-1
Colon-OTU-2
Colon-OTU-3
Colon-OTU-4
Colon-OTU-5
Colon-OTU-6
Colon-OTU-7
Colon-OTU-8
Colon-OTU-9
Colon-OTU-10
Colon-OTU-11
Colon-OTU-12
Colon-OTU-13
Colon-OTU-14
Colon-OTU-15
E
Lipids
Lipids-1
Lipids-2
Lipids-3
Lipids-4
Lipids-5
Lipids-6

Fig. S3

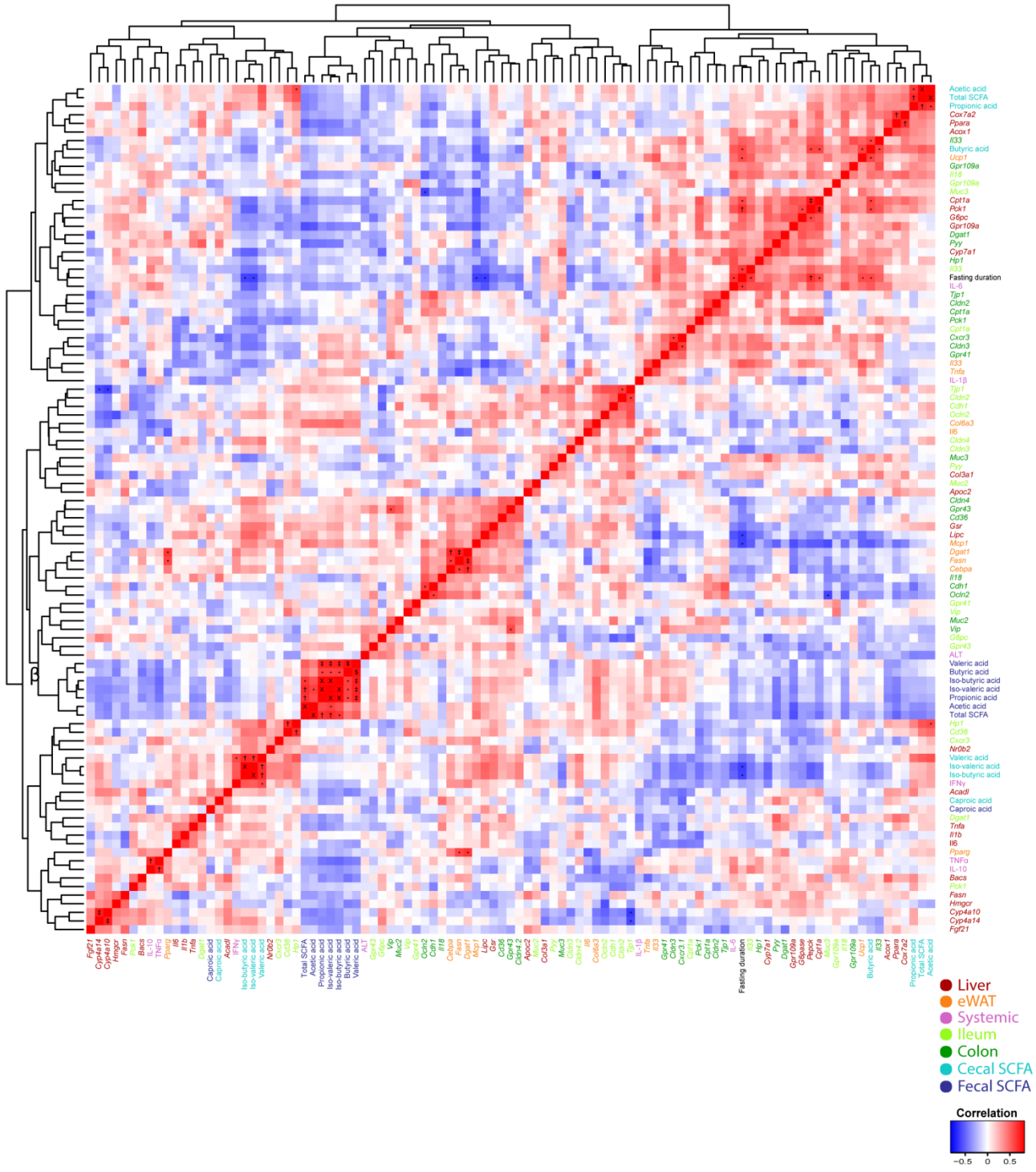
Liver
eWAT
Systemic
Ileum
Colon
Cecal SCFA
Fecal SCFA
Correlation
−0.5
0
0.5

Fig. S4

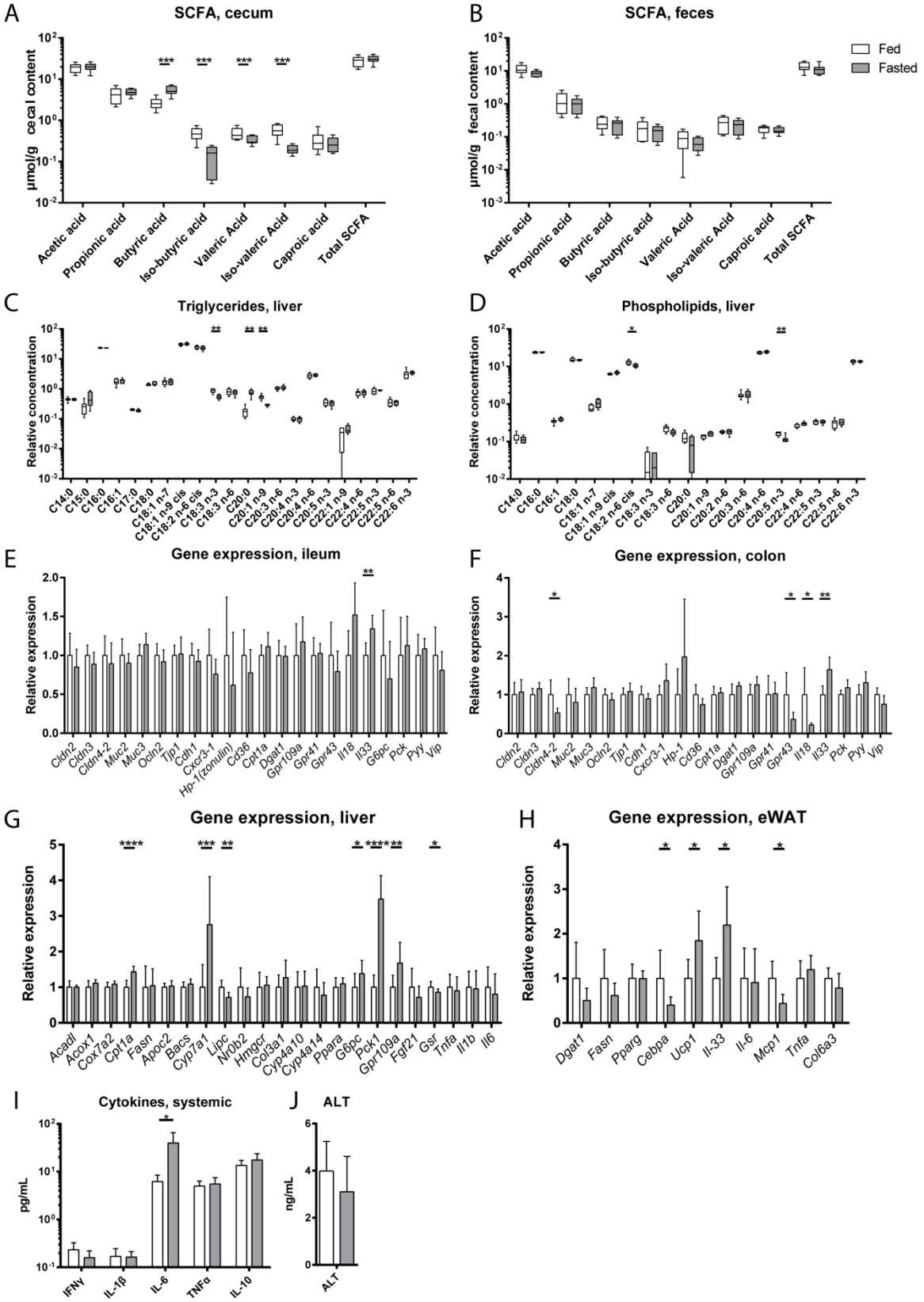
A
SCFA, cecum
µmol/g cecal content
Acetic acid
Propionic acid
Butyric acid
Iso-butyric acid
Valeric Acid
Iso-valeric Acid
Caproic acid
Total SCFA
B
SCFA, feces
µmol/g fecal content
Fed
Fasted
C
Triglycerides, liver
Relative concentration
D
Phospholipids, liver
E
Gene expression, ileum
Relative expression
F
Gene expression, colon
G
Gene expression, liver
H
Gene expression, eWAT
I
Cytokines, systemic
pg/mL
IFNγ
IL-1β
IL-6
TNFα
IL-10
J
ALT
ng/mL

Fig. S5

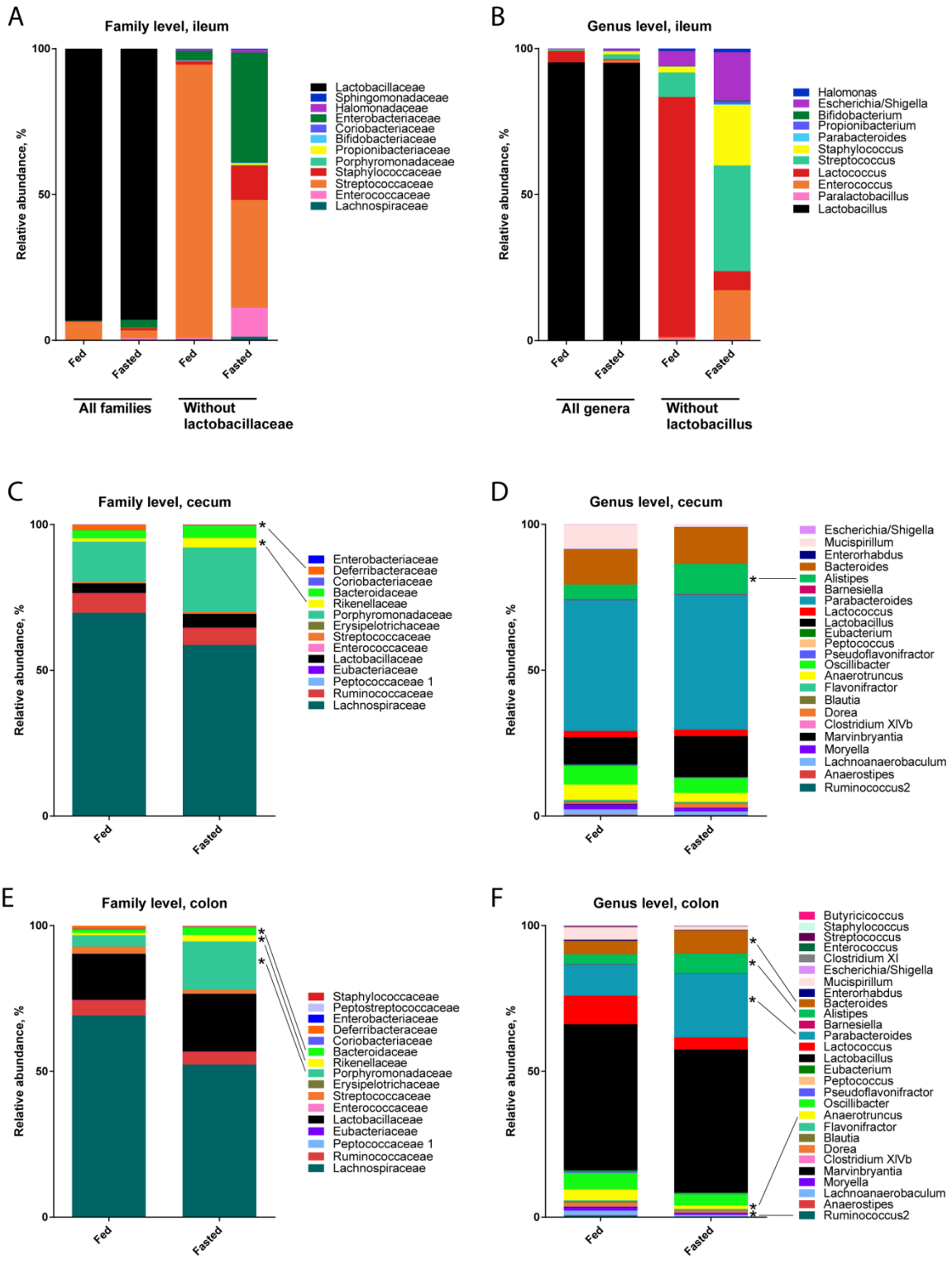
A
Family level, ileum
Relative abundance, %
100
50
0
Fed
Fasted
Fed
Fasted
All families
Without lactobacillaceae
Lactobacillaceae
Sphingomonadaceae
Halomonadaceae
Enterobacteriaceae
Coriobacteriaceae
Bifidobacteriaceae
Propionibacteriaceae
Porphyromonadaceae
Staphylococcaceae
Streptococcaceae
Enterococcaceae
Lachnospiraceae
B
Genus level, ileum
Relative abundance, %
All genera
Without lactobacillus
Halomonas
Escherichia/Shigella
Bifidobacterium
Propionibacterium
Parabacteroides
Staphylococcus
Streptococcus
Lactococcus
Enterococcus
Paralactobacillus
Lactobacillus
C
Family level, cecum
Relative abundance, %
Enterobacteriaceae
Deferribacteraceae
Coriobacteriaceae
Bacteroidaceae
Rikenellaceae
Porphyromonadaceae
Erysipelotrichaceae
Streptococcaceae
Enterococcaceae
Lactobacillaceae
Eubacteriaceae
Peptococcaceae 1
Ruminococcaceae
Lachnospiraceae
D
Genus level, cecum
Relative abundance, %
Escherichia/Shigella
Mucispirillum
Enterorhabdus
Bacteroides
Alistipes
Barnesiella
Parabacteroides
Lactococcus
Lactobacillus
Eubacterium
Peptococcus
Pseudoflavonifractor
Oscillibacter
Anaerotruncus
Flavonifractor
Blautia
Dorea
Clostridium XlVb
Marvinbryantia
Moryella
Lachnoanaerobaculum
Anaerostipes
Ruminococcus2
E
Family level, colon
Relative abundance, %
Staphylococcaceae
Peptostreptococcaceae
Enterobacteriaceae
Deferribacteraceae
Coriobacteriaceae
Bacteroidaceae
Rikenellaceae
Porphyromonadaceae
Erysipelotrichaceae
Streptococcaceae
Enterococcaceae
Lactobacillaceae
Eubacteriaceae
Peptococcaceae 1
Ruminococcaceae
Lachnospiraceae
F
Genus level, colon
Relative abundance, %
Butyricicoccus
Staphylococcus
Streptococcus
Enterococcus
Clostridium XI
Escherichia/Shigella
Mucispirillum
Enterorhabdus
Bacteroides
Alistipes
Barnesiella
Parabacteroides
Lactococcus
Lactobacillus
Eubacterium
Peptococcus
Pseudoflavonifractor
Oscillibacter
Anaerotruncus
Flavonifractor
Blautia
Dorea
Clostridium XlVb
Marvinbryantia
Moryella
Lachnoanaerobaculum
Anaerostipes
Ruminococcus2

Table S1

Green Genes OTU IDs	De novo OTU IDs	But pathway	Buk pathway	Either pathway
13031	603	X		X
110020	335	X		X
174924	221			
182420	2509, 41			
182893	1240	X		X
183870	172, 628, 20, 643, 2099	X		X
185258	586, 22, 1707			
194286	1303, 816, 2691	X		X
195985	129, 1303, 530			
221240	150, 1809, 676, 729, 1, 140, 117			
261016	8, 1852, 65			
261623	1721, 2956, 203			
267411	324, 62, 1376, 705			
270890	144, 2704			
272428	1998			
297390	288			
301717	303			
310215	877	X		X
311952	252, 130, 2369	X		X
325539	2564, 365			
330118	287			
340276	398, 395, 267			
341823	70, 461			
354920	38	X		X
455130	235, 594	X		X
512191	214, 1227	X		X
522549	14, 779	X		X
526963	1082, 2544	X		X
529442	432	X		X
529506	559, 12, 1115, 1660, 148, 61, 12, 1660, 432, 1115, 148	X	X	X
541079	122, 289, 23			
555076	1603			
555844	264	X		X
559954	202			
667312	99	X		X
773586	56	X		X
1523543	227, 1319	X		X
2594571	367, 189, 421			
3268451	609, 367			
4341816	115, 16, 1767	X		X
4364418	124	X		X
4406624	509	X		X
4426962	30	X	X	X
4483633	90, 889			

Discussion and perspectives

Diet constitutes one of the most important factors defining metabolic capacity, which is the major focus in these studies. Therefore, the three studies included in this PhD thesis are all based on long-term dietary challenges of C57BL/6 mice in order to increase our understanding of the impact of specific dietary components on host metabolism and sub-clinical inflammation.

Although mice and humans do show some differences in terms of immune and metabolic regulation, rodent models of metabolic dysregulation constitute a reliable model in which to perform exploratory studies.

Dietary components

In Project I (the gliadin study), we aimed to identify the role of a single dietary component, gliadin, in the regulation of host homeostasis when mice are fed a high-fat diet. The putative negative impacts of gliadin on intestinal inflammation allowed us to design a synthetic diet composed of 4 % gliadin, as this would permit the specific evaluation of this protein. Conversely, the use of gluten-rich diets or even more loosely defined diets (e.g. western, high fiber, high fat diets, etc.) potentially introduce confounding factors that limits the interpretation of the studies.

The combination of gliadin and a high-fat diet allows for the characterization of gliadin when mice are obese, which is physiologically relevant due to the increased consumption of bread-based and high-fat diets. However, since a high-fat diet introduces multiple phenotypic changes (microbiome, intestinal integrity, tissue and systemic sub-clinical inflammation, glucose and lipid dysregulation, etc.), this study does not allow the identification of specific high-fat diet-associated factors that drive the observed difference between HFD and HFD+gliadin animals.

In addition, the extensive experimental characterization did not permit an identification of the role of gliadin in mice that are not metabolically stressed by a high-fat diet. Therefore, further studies are needed to discern whether it is primarily the gliadin that reshapes the host and microbiome or that gliadin-induced pathology depends on a high-fat diet and/or obesity.

In a similar manner, in Project II (the safflower study), we aimed at characterizing the obesogenic effect of not just a generic HFD, but rather a HFD based on safflower oil, and thus rich in the n-6 PUFA linoleic acid. Diet-induced obesity studies are primarily based on lard-derived fatty acids, and thus the addition of a more classical HFD rich in saturated fats would have allowed us to justify that the limited obesity associated with a safflower oil diet was due to the diet composition (and not affected by the animal provider, housing conditions, etc.) (Muller et al., 2016).

Project III (the fasting study) exploited the fact that mice had been either fasted or fed for the gliadin study. However, the study was not set up for the analysis of the fasting response, and therefore some challenges exist. For example were the mice fasted when the light cycle was on, and consequently the mice were feed deprived only during their usually inactive period. Still, the effect of fasting is clearly visible. Also, tissues were harvested at three different days (first 10 fed animals, then 20 fasted, and finally 10 fed). This can potentially introduce a technical bias. However, our extensive analyses of the fed animals did not identify any sampling day-dependent differences.

Evaluation of immune cell populations

The markers used for the in-depth flow cytometry-based characterization of immune cell populations was primarily defined using the current literature (*anno* 2012) on immune cell populations associated with high-fat diet-induced obesity. In light of this and the finding that gliadin induces a higher *Il33* expression in epididymal adipose tissue, an updated version could have included the identification of innate lymphoid cells (ILCs). This would have been of relevance due to the now well-characterized insulin-sensitizing effects of the ILC2-eosinophil-alternatively activated macrophage axis. Similarly, the addition of ILC2 markers such as IL-5 and Il-13 would allow us to speculate if the IL-33 changes observed are mediated by ILC2 activation (Brestoff and Artis, 2015). Our setup did not permit a flow cytometric analysis of the potential immune cell changes upon fasting (such as ILC2s in eWAT), although this could have been relevant due to our finding that fasting induce a beige-like IL-33 mediated switch (Lee et al., 2015).

Complex interplay between host metabolism and immune regulation

Project I (the gliadin study) is marked by a considerable baseline morbidity, independently of gliadin status due to the extremely obesogenic HFD. Thus, one should take into account that the exacerbation of host metabolism and inflammation of gliadin fed mice are based on a highly dysregulated starting point. The immune cell characterization identified few gliadin-dependent changes. However, through the analysis of multiple immune cell subsets, we identified more overall changes such as the higher concentration of liver myeloid dendritic cells, NKT and γδ T cells suggestive of the presence of diet-derived or microbial ligands in the liver.

Contrastingly, the n-6 PUFA rich HFD in Project II (the safflower study) confers a much more subtle phenotypic change than expected. This is manifested in the relative lack of immune cell markers in liver and adipose tissue. Although the altered M1/M2 ratio and TNFα expression of M1 macrophages are potentially induced by the n-6 PUFA rich diet (Teng et al., 2014), overall, the HFD is much less obesogenic and pro-inflammatory than expected. The higher concentration of substrates for pro-inflammatory lipid mediators (namely linoleic acid and arachidonic acid, which indeed are increased in liver phospholipids) does not manifest as a typical HFD-induced adipose tissue inflammation or adipogenesis as previously reported (Naughton et al., 2016). Several lines of data suggest that the pro-inflammatory and pro-adipogenic properties of n-6 PUFAs are dependent on pre-existing adiposity or circulating cytokines (Teng et al., 2014). Thus, the limited adiposity may itself protect

against n-6 PUFA-induced inflammation. Exactly why intake of the safflower diet does not result in obesity is still not clear, but could be explained by a different baseline microbiota composition prior to the intervention. Obviously this deserves more attention.

Concluding remarks

The studies included in this PhD thesis rely on distinct approaches, yet they share the overall focus of employing large exploratory experimental setups to investigate the effects of dietary composition on host metabolism in C57BL/6 mice. In order to understand the observed metabolic phenotypes, we aimed at quantifying immune cell subsets that have previously been defined as key in the establishment of metabolic dysfunction using an in-depth flow cytometric characterization method. To further approach the mechanisms involved in the manifestation of the diet-induced phenotypes, we applied various multidimensional analyses that would allow for the association of metabolic, immunological and microbial traits.

Through our dietary intervention studies and various systems-level analyses applied, we have identified interesting associations between diet, the gut microbiota and the host response, allowing us to suggest several biological mechanisms mediating the observed phenotypes. Further validation of these hypotheses will require a more focused experimental approach to elucidate the molecular mechanisms governing the complex interplay between diet, gut microbiome and host regulation.

References

Akira, S., and Takeda, K. (2004). Toll-like receptor signalling. Nat Rev Immunol *4*, 499-511.

Altintas, M.M., Azad, A., Nayer, B., Contreras, G., Zaias, J., Faul, C., Reiser, J., and Nayer, A. (2011). Mast cells, macrophages, and crown-like structures distinguish subcutaneous from visceral fat in mice. Journal of lipid research *52*, 480-488.

Amar, J., Chabo, C., Waget, A., Klopp, P., Vachoux, C., Bermudez-Humaran, L.G., Smirnova, N., Berge, M., Sulpice, T., Lahtinen, S*., et al.* (2011). Intestinal mucosal adherence and translocation of commensal bacteria at the early onset of type 2 diabetes: molecular mechanisms and probiotic treatment. EMBO molecular medicine *3*, 559-572.

Ang, Z., and Ding, J.L. (2016). GPR41 and GPR43 in Obesity and Inflammation - Protective or Causative? Frontiers in immunology *7*, 28.

Backhed, F., Ding, H., Wang, T., Hooper, L.V., Koh, G.Y., Nagy, A., Semenkovich, C.F., and Gordon, J.I. (2004). The gut microbiota as an environmental factor that regulates fat storage. Proc Natl Acad Sci U S A *101*, 15718-15723.

Backhed, F., Manchester, J.K., Semenkovich, C.F., and Gordon, J.I. (2007). Mechanisms underlying the resistance to diet-induced obesity in germ-free mice. Proc Natl Acad Sci U S A *104*, 979-984.

Bandyopadhyay, K., Marrero, I., and Kumar, V. (2016). NKT cell subsets as key participants in liver physiology and pathology. Cellular & molecular immunology *13*, 337-346.

Bardella, M.T., Elli, L., and Ferretti, F. (2016). Non Celiac Gluten Sensitivity. Current gastroenterology reports *18*, 63.

Bellahcene, M., O'Dowd, J.F., Wargent, E.T., Zaibi, M.S., Hislop, D.C., Ngala, R.A., Smith, D.M., Cawthorne, M.A., Stocker, C.J., and Arch, J.R. (2013). Male mice that lack the G-protein-coupled receptor GPR41 have low energy expenditure and increased body fat content. The British journal of nutrition *109*, 1755-1764.

Bergstrom, K.S., Kissoon-Singh, V., Gibson, D.L., Ma, C., Montero, M., Sham, H.P., Ryz, N., Huang, T., Velcich, A., Finlay, B.B*., et al.* (2010). Muc2 protects against lethal infectious colitis by disassociating pathogenic and commensal bacteria from the colonic mucosa. PLoS pathogens *6*, e1000902.

Bertola, A., Ciucci, T., Rousseau, D., Bourlier, V., Duffaut, C., Bonnafous, S., Blin-Wakkach, C., Anty, R., Iannelli, A., Gugenheim, J*., et al.* (2012). Identification of adipose tissue dendritic cells correlated with obesity-associated insulin-resistance and inducing Th17 responses in mice and patients. Diabetes *61*, 2238-2247.

Bieghs, V., and Trautwein, C. (2013). The innate immune response during liver inflammation and metabolic disease. Trends in immunology *34*, 446-452.

Bjursell, M., Admyre, T., Goransson, M., Marley, A.E., Smith, D.M., Oscarsson, J., and Bohlooly, Y.M. (2011). Improved glucose control and reduced body fat mass in free fatty acid receptor 2-deficient mice fed a high-fat diet. Am J Physiol Endocrinol Metab *300*, E211-220.

Brestoff, J.R., and Artis, D. (2015). Immune regulation of metabolic homeostasis in health and disease. Cell *161*, 146-160.

Brigl, M., and Brenner, M.B. (2010). How invariant natural killer T cells respond to infection by recognizing microbial or endogenous lipid antigens. Seminars in immunology *22*, 79-86.

Brown, M.S., and Goldstein, J.L. (2008). Selective versus total insulin resistance: a pathogenic paradox. Cell Metab *7*, 95-96.

Burcelin, R., Garidou, L., and Pomie, C. (2012). Immuno-microbiota cross and talk: the new paradigm of metabolic diseases. Seminars in immunology *24*, 67-74.

Caesar, R., Nygren, H., Oresic, M., and Backhed, F. (2016). Interaction between dietary lipids and gut microbiota regulates hepatic cholesterol metabolism. Journal of lipid research *57*, 474-481.

Caesar, R., Reigstad, C.S., Backhed, H.K., Reinhardt, C., Ketonen, M., Lunden, G.O., Cani, P.D., and Backhed, F. (2012). Gut-derived lipopolysaccharide augments adipose macrophage accumulation but is not essential for impaired glucose or insulin tolerance in mice. Gut *61*, 1701-1707.

Cani, P.D., Amar, J., Iglesias, M.A., Poggi, M., Knauf, C., Bastelica, D., Neyrinck, A.M., Fava, F., Tuohy, K.M., Chabo, C*., et al.* (2007). Metabolic endotoxemia initiates obesity and insulin resistance. Diabetes *56*, 1761-1772.

Cani, P.D., Bibiloni, R., Knauf, C., Waget, A., Neyrinck, A.M., Delzenne, N.M., and Burcelin, R. (2008). Changes in gut microbiota control metabolic endotoxemia-induced inflammation in high-fat diet-induced obesity and diabetes in mice. Diabetes *57*, 1470-1481.

Cani, P.D., Plovier, H., Van Hul, M., Geurts, L., Delzenne, N.M., Druart, C., and Everard, A. (2016). Endocannabinoids--at the crossroads between the gut microbiota and host metabolism. Nature reviews Endocrinology *12*, 133-143.

Caspar-Bauguil, S., Cousin, B., Galinier, A., Segafredo, C., Nibbelink, M., Andre, M., Casteilla, L., and Penicaud, L. (2005). Adipose tissues as an ancestral immune organ: site-specific change in obesity. FEBS letters *579*, 3487-3492.

Castoldi, A., Naffah de Souza, C., Camara, N.O., and Moraes-Vieira, P.M. (2015). The Macrophage Switch in Obesity Development. Frontiers in immunology *6*, 637.

Chawla, A., Nguyen, K.D., and Goh, Y.P. (2011). Macrophage-mediated inflammation in metabolic disease. Nat Rev Immunol *11*, 738-749.

Chen, Y., Tian, J., Tian, X., Tang, X., Rui, K., Tong, J., Lu, L., Xu, H., and Wang, S. (2014). Adipose tissue dendritic cells enhances inflammation by prompting the generation of Th17 cells. PLoS One *9*, e92450.

Chladkova, B., Kamanova, J., Palova-Jelinkova, L., Cinova, J., Sebo, P., and Tuckova, L. (2011). Gliadin fragments promote migration of dendritic cells. Journal of cellular and molecular medicine *15*, 938-948.

Choe, S.S., Huh, J.Y., Hwang, I.J., Kim, J.I., and Kim, J.B. (2016). Adipose Tissue Remodeling: Its Role in Energy Metabolism and Metabolic Disorders. Frontiers in endocrinology *7*, 30.

Clementi, A.H., Gaudy, A.M., van Rooijen, N., Pierce, R.H., and Mooney, R.A. (2009). Loss of Kupffer cells in diet-induced obesity is associated with increased hepatic steatosis, STAT3 signaling, and further decreases in insulin signaling. Biochim Biophys Acta *1792*, 1062-1072.

Coquet, J.M., Chakravarti, S., Kyparissoudis, K., McNab, F.W., Pitt, L.A., McKenzie, B.S., Berzins, S.P., Smyth, M.J., and Godfrey, D.I. (2008). Diverse cytokine production by NKT cell subsets and identification of an IL-17-producing CD4-NK1.1- NKT cell population. Proc Natl Acad Sci U S A *105*, 11287-11292.

Cotillard, A., Kennedy, S.P., Kong, L.C., Prifti, E., Pons, N., Le Chatelier, E., Almeida, M., Quinquis, B., Levenez, F., Galleron, N*., et al.* (2013). Dietary intervention impact on gut microbial gene richness. Nature *500*, 585-588.

Csak, T., Ganz, M., Pespisa, J., Kodys, K., Dolganiuc, A., and Szabo, G. (2011). Fatty acid and endotoxin activate inflammasomes in mouse hepatocytes that release danger signals to stimulate immune cells. Hepatology *54*, 133-144.

David, L.A., Maurice, C.F., Carmody, R.N., Gootenberg, D.B., Button, J.E., Wolfe, B.E., Ling, A.V., Devlin, A.S., Varma, Y., Fischbach, M.A*., et al.* (2014). Diet rapidly and reproducibly alters the human gut microbiome. Nature *505*, 559-563.

Davis, J.E., Gabler, N.K., Walker-Daniels, J., and Spurlock, M.E. (2008). Tlr-4 deficiency selectively protects against obesity induced by diets high in saturated fat. Obesity (Silver Spring) *16*, 1248-1255.

De Vadder, F., Kovatcheva-Datchary, P., Goncalves, D., Vinera, J., Zitoun, C., Duchampt, A., Backhed, F., and Mithieux, G. (2014). Microbiota-generated metabolites promote metabolic benefits via gut-brain neural circuits. Cell *156*, 84-96.

DeFuria, J., Belkina, A.C., Jagannathan-Bogdan, M., Snyder-Cappione, J., Carr, J.D., Nersesova, Y.R., Markham, D., Strissel, K.J., Watkins, A.A., Zhu, M*., et al.* (2013). B cells promote inflammation in obesity and type 2 diabetes through regulation of T-cell function and an inflammatory cytokine profile. Proc Natl Acad Sci U S A *110*, 5133-5138.

den Besten, G., Bleeker, A., Gerding, A., van Eunen, K., Havinga, R., van Dijk, T.H., Oosterveer, M.H., Jonker, J.W., Groen, A.K., Reijngoud, D.J*., et al.* (2015). Short-Chain Fatty Acids Protect Against High-Fat Diet-Induced Obesity via a PPARgamma-Dependent Switch From Lipogenesis to Fat Oxidation. Diabetes *64*, 2398-2408.

den Besten, G., Lange, K., Havinga, R., van Dijk, T.H., Gerding, A., van Eunen, K., Muller, M., Groen, A.K., Hooiveld, G.J., Bakker, B.M*., et al.* (2013). Gut-derived short-chain fatty acids are vividly assimilated into host carbohydrates and lipids. American journal of physiology Gastrointestinal and liver physiology *305*, G900-910.

Deng, Z.B., Liu, Y., Liu, C., Xiang, X., Wang, J., Cheng, Z., Shah, S.V., Zhang, S., Zhang, L., Zhuang, X*., et al.* (2009). Immature myeloid cells induced by a high-fat diet contribute to liver inflammation. Hepatology *50*, 1412-1420.

Ding, S., Chi, M.M., Scull, B.P., Rigby, R., Schwerbrock, N.M., Magness, S., Jobin, C., and Lund, P.K. (2010). High-fat diet: bacteria interactions promote intestinal inflammation which precedes and correlates with obesity and insulin resistance in mouse. PLoS One *5*, e12191.

Dixon, L.J., Flask, C.A., Papouchado, B.G., Feldstein, A.E., and Nagy, L.E. (2013). Caspase-1 as a central regulator of high fat diet-induced non-alcoholic steatohepatitis. PLoS One *8*, e56100.

Donohoe, D.R., Garge, N., Zhang, X., Sun, W., O'Connell, T.M., Bunger, M.K., and Bultman, S.J. (2011). The microbiome and butyrate regulate energy metabolism and autophagy in the mammalian colon. Cell Metab *13*, 517-526.

Elgazar-Carmon, V., Rudich, A., Hadad, N., and Levy, R. (2008). Neutrophils transiently infiltrate intra-abdominal fat early in the course of high-fat feeding. Journal of lipid research *49*, 1894-1903.

Esposito, K., Pontillo, A., Ciotola, M., Di Palo, C., Grella, E., Nicoletti, G., and Giugliano, D. (2002). Weight loss reduces interleukin-18 levels in obese women. The Journal of clinical endocrinology and metabolism *87*, 3864-3866.

Everard, A., Belzer, C., Geurts, L., Ouwerkerk, J.P., Druart, C., Bindels, L.B., Guiot, Y., Derrien, M., Muccioli, G.G., Delzenne, N.M*., et al.* (2013). Cross-talk between Akkermansia muciniphila and intestinal epithelium controls diet-induced obesity. Proc Natl Acad Sci U S A *110*, 9066-9071.

Everard, A., Geurts, L., Caesar, R., Van Hul, M., Matamoros, S., Duparc, T., Denis, R.G., Cochez, P., Pierard, F., Castel, J*., et al.* (2014). Intestinal epithelial MyD88 is a sensor switching host metabolism towards obesity according to nutritional status. Nature communications *5*, 5648.

Ferramosca, A., and Zara, V. (2014). Modulation of hepatic steatosis by dietary fatty acids. World journal of gastroenterology *20*, 1746-1755.

Ferrante, A.W., Jr. (2013). The immune cells in adipose tissue. Diabetes Obes Metab *15 Suppl 3*, 34-38.

Feuerer, M., Herrero, L., Cipolletta, D., Naaz, A., Wong, J., Nayer, A., Lee, J., Goldfine, A.B., Benoist, C., Shoelson, S*., et al.* (2009). Lean, but not obese, fat is enriched for a unique population of regulatory T cells that affect metabolic parameters. Nature medicine *15*, 930-939.

Flegal, K.M., Kruszon-Moran, D., Carroll, M.D., Fryar, C.D., and Ogden, C.L. (2016). Trends in Obesity Among Adults in the United States, 2005 to 2014. JAMA : the journal of the American Medical Association *315*, 2284-2291.

Forbes, J.M., and Cooper, M.E. (2013). Mechanisms of diabetic complications. Physiological reviews *93*, 137-188.

Freire, R.H., Fernandes, L.R., Silva, R.B., Coelho, B.S., de Araujo, L.P., Ribeiro, L.S., Andrade, J.M., Lima, P.M., Araujo, R.S., Santos, S.H*., et al.* (2016). Wheat gluten intake increases weight gain and adiposity associated with reduced thermogenesis and energy expenditure in an animal model of obesity. International journal of obesity *40*, 479-486.

Fukuda, S., Toh, H., Hase, K., Oshima, K., Nakanishi, Y., Yoshimura, K., Tobe, T., Clarke, J.M., Topping, D.L., Suzuki, T*., et al.* (2011). Bifidobacteria can protect from enteropathogenic infection through production of acetate. Nature *469*, 543-547.

Funda, D.P., Kaas, A., Bock, T., Tlaskalova-Hogenova, H., and Buschard, K. (1999). Gluten-free diet prevents diabetes in NOD mice. Diabetes/metabolism research and reviews *15*, 323-327.

Ganeshan, K., and Chawla, A. (2014). Metabolic regulation of immune responses. Annual review of immunology *32*, 609-634.

Ganz, M., Csak, T., Nath, B., and Szabo, G. (2011). Lipopolysaccharide induces and activates the Nalp3 inflammasome in the liver. World journal of gastroenterology *17*, 4772-4778.

Gao, Z., Yin, J., Zhang, J., Ward, R.E., Martin, R.J., Lefevre, M., Cefalu, W.T., and Ye, J. (2009). Butyrate improves insulin sensitivity and increases energy expenditure in mice. Diabetes *58*, 1509-1517.

Ghoshal, S., Witta, J., Zhong, J., de Villiers, W., and Eckhardt, E. (2009). Chylomicrons promote intestinal absorption of lipopolysaccharides. Journal of lipid research *50*, 90-97.

Gordon, S., and Taylor, P.R. (2005). Monocyte and macrophage heterogeneity. Nat Rev Immunol *5*, 953-964.

Guebre-Xabier, M., Yang, S., Lin, H.Z., Schwenk, R., Krzych, U., and Diehl, A.M. (2000). Altered hepatic lymphocyte subpopulations in obesity-related murine fatty livers: potential mechanism for sensitization to liver damage. Hepatology *31*, 633-640.

Guo, S. (2014). Insulin signaling, resistance, and the metabolic syndrome: insights from mouse models into disease mechanisms. The Journal of endocrinology *220*, T1-T23.

Halder, R.C., Aguilera, C., Maricic, I., and Kumar, V. (2007). Type II NKT cell-mediated anergy induction in type I NKT cells prevents inflammatory liver disease. J Clin Invest *117*, 2302-2312.

Hams, E., Locksley, R.M., McKenzie, A.N., and Fallon, P.G. (2013). Cutting edge: IL-25 elicits innate lymphoid type 2 and type II NKT cells that regulate obesity in mice. Journal of immunology *191*, 5349-5353.

Hashimoto, D., Miller, J., and Merad, M. (2011). Dendritic Cell and Macrophage Heterogeneity In Vivo. Immunity *35*, 323-335.

Haupt-Jorgensen, M., Buschard, K., Hansen, A.K., Josefsen, K., and Antvorskov, J.C. (2016). Gluten-free diet increases beta-cell volume and improves glucose tolerance in an animal model of type 2 diabetes. Diabetes/metabolism research and reviews *32*, 675-684.

Henao-Mejia, J., Elinav, E., Jin, C., Hao, L., Mehal, W.Z., Strowig, T., Thaiss, C.A., Kau, A.L., Eisenbarth, S.C., Jurczak, M.J*., et al.* (2012). Inflammasome-mediated dysbiosis regulates progression of NAFLD and obesity. Nature *482*, 179-185.

Hirai, S., Ohyane, C., Kim, Y.I., Lin, S., Goto, T., Takahashi, N., Kim, C.S., Kang, J., Yu, R., and Kawada, T. (2014). Involvement of mast cells in adipose tissue fibrosis. Am J Physiol Endocrinol Metab *306*, E247-255.

Hotamisligil, G.S. (2010). Endoplasmic reticulum stress and the inflammatory basis of metabolic disease. Cell *140*, 900-917.

Hotamisligil, G.S., Peraldi, P., Budavari, A., Ellis, R., White, M.F., and Spiegelman, B.M. (1996). IRS-1-mediated inhibition of insulin receptor tyrosine kinase activity in TNF-alpha- and obesity-induced insulin resistance. Science *271*, 665-668.

Hotamisligil, G.S., Shargill, N.S., and Spiegelman, B.M. (1993). Adipose expression of tumor necrosis factor-alpha: direct role in obesity-linked insulin resistance. Science *259*, 87-91.

Hubler, M.J., and Kennedy, A.J. (2016). Role of lipids in the metabolism and activation of immune cells. The Journal of nutritional biochemistry *34*, 1-7.

Hung, J., McQuillan, B.M., Chapman, C.M., Thompson, P.L., and Beilby, J.P. (2005). Elevated interleukin-18 levels are associated with the metabolic syndrome independent of obesity and insulin resistance. Arterioscler Thromb Vasc Biol *25*, 1268-1273.

Ishijima, Y., Ohmori, S., and Ohneda, K. (2013). Mast cell deficiency results in the accumulation of preadipocytes in adipose tissue in both obese and non-obese mice. FEBS open bio *4*, 18-24.

Italiani, P., and Boraschi, D. (2014). From Monocytes to M1/M2 Macrophages: Phenotypical vs. Functional Differentiation. Frontiers in immunology *5*, 514.

Ji, Y., Sun, S., Xia, S., Yang, L., Li, X., and Qi, L. (2012). Short term high fat diet challenge promotes alternative macrophage polarization in adipose tissue via natural killer T cells and interleukin-4. J Biol Chem *287*, 24378-24386.

Johansson, M.E., Phillipson, M., Petersson, J., Velcich, A., Holm, L., and Hansson, G.C. (2008). The inner of the two Muc2 mucin-dependent mucus layers in colon is devoid of bacteria. Proc Natl Acad Sci U S A *105*, 15064-15069.

Johnson, A.M., and Olefsky, J.M. (2013). The origins and drivers of insulin resistance. Cell *152*, 673-684.

Jornayvaz, F.R., and Shulman, G.I. (2012). Diacylglycerol activation of protein kinase Cepsilon and hepatic insulin resistance. Cell Metab *15*, 574-584.

Jung, T.H., Park, J.H., Jeon, W.M., and Han, K.S. (2015). Butyrate modulates bacterial adherence on LS174T human colorectal cells by stimulating mucin secretion and MAPK signaling pathway. Nutrition research and practice *9*, 343-349.

Kahn, S.E. (2001). Clinical review 135: The importance of beta-cell failure in the development and progression of type 2 diabetes. The Journal of clinical endocrinology and metabolism *86*, 4047-4058.

Kahn, S.E., Hull, R.L., and Utzschneider, K.M. (2006). Mechanisms linking obesity to insulin resistance and type 2 diabetes. Nature *444*, 840-846.

Kamei, N., Tobe, K., Suzuki, R., Ohsugi, M., Watanabe, T., Kubota, N., Ohtsuka-Kowatari, N., Kumagai, K., Sakamoto, K., Kobayashi, M*., et al.* (2006). Overexpression of monocyte chemoattractant protein-1 in adipose tissues causes macrophage recruitment and insulin resistance. J Biol Chem *281*, 26602-26614.

Kang, K., Reilly, S.M., Karabacak, V., Gangl, M.R., Fitzgerald, K., Hatano, B., and Lee, C.H. (2008). Adipocyte-derived Th2 cytokines and myeloid PPARdelta regulate macrophage polarization and insulin sensitivity. Cell Metab *7*, 485-495.

Karlmark, K.R., Weiskirchen, R., Zimmermann, H.W., Gassler, N., Ginhoux, F., Weber, C., Merad, M., Luedde, T., Trautwein, C., and Tacke, F. (2009). Hepatic recruitment of the inflammatory Gr1+ monocyte subset upon liver injury promotes hepatic fibrosis. Hepatology *50*, 261-274.

Karlmark, K.R., Zimmermann, H.W., Roderburg, C., Gassler, N., Wasmuth, H.E., Luedde, T., Trautwein, C., and Tacke, F. (2010). The fractalkine receptor CX(3)CR1 protects against liver fibrosis by controlling differentiation and survival of infiltrating hepatic monocytes. Hepatology *52*, 1769-1782.

Kassi, E., Pervanidou, P., Kaltsas, G., and Chrousos, G. (2011). Metabolic syndrome: definitions and controversies. BMC medicine *9*, 48.

Kelly, C.J., Zheng, L., Campbell, E.L., Saeedi, B., Scholz, C.C., Bayless, A.J., Wilson, K.E., Glover, L.E., Kominsky, D.J., Magnuson, A.*, et al.* (2015). Crosstalk between Microbiota-Derived Short-Chain Fatty Acids and Intestinal Epithelial HIF Augments Tissue Barrier Function. Cell host & microbe *17*, 662-671.

Kim, J., Li, Y., and Watkins, B.A. (2013). Fat to treat fat: emerging relationship between dietary PUFA, endocannabinoids, and obesity. Prostaglandins & other lipid mediators *104-105*, 32-41.

Kimura, I., Ozawa, K., Inoue, D., Imamura, T., Kimura, K., Maeda, T., Terasawa, K., Kashihara, D., Hirano, K., Tani, T.*, et al.* (2013). The gut microbiota suppresses insulin-mediated fat accumulation via the short-chain fatty acid receptor GPR43. Nature communications *4*, 1829.

Kirpich, I.A., Marsano, L.S., and McClain, C.J. (2015). Gut-liver axis, nutrition, and non-alcoholic fatty liver disease. Clinical biochemistry *48*, 923-930.

Klein, I., Cornejo, J.C., Polakos, N.K., John, B., Wuensch, S.A., Topham, D.J., Pierce, R.H., and Crispe, I.N. (2007). Kupffer cell heterogeneity: functional properties of bone marrow derived and sessile hepatic macrophages. Blood *110*, 4077-4085.

Kloting, N., Fasshauer, M., Dietrich, A., Kovacs, P., Schon, M.R., Kern, M., Stumvoll, M., and Bluher, M. (2010). Insulin-sensitive obesity. Am J Physiol Endocrinol Metab *299*, E506-515.

Kogelman, L.J., Fu, J., Franke, L., Greve, J.W., Hofker, M., Rensen, S.S., and Kadarmideen, H.N. (2016). Inter-Tissue Gene Co-Expression Networks between Metabolically Healthy and Unhealthy Obese Individuals. PLoS One *11*, e0167519.

Koh, A., De Vadder, F., Kovatcheva-Datchary, P., and Backhed, F. (2016). From Dietary Fiber to Host Physiology: Short-Chain Fatty Acids as Key Bacterial Metabolites. Cell *165*, 1332-1345.

Kolodin, D., van Panhuys, N., Li, C., Magnuson, A.M., Cipolletta, D., Miller, C.M., Wagers, A., Germain, R.N., Benoist, C., and Mathis, D. (2015). Antigen- and cytokine-driven accumulation of regulatory T cells in visceral adipose tissue of lean mice. Cell Metab *21*, 543-557.

Kremer, M., Thomas, E., Milton, R.J., Perry, A.W., van Rooijen, N., Wheeler, M.D., Zacks, S., Fried, M., Rippe, R.A., and Hines, I.N. (2010). Kupffer cell and interleukin-12-dependent loss of natural killer T cells in hepatosteatosis. Hepatology *51*, 130-141.

Lam, Y.Y., Ha, C.W., Hoffmann, J.M., Oscarsson, J., Dinudom, A., Mather, T.J., Cook, D.I., Hunt, N.H., Caterson, I.D., Holmes, A.J.*, et al.* (2015). Effects of dietary fat profile on gut permeability and microbiota and their relationships with metabolic changes in mice. Obesity (Silver Spring) *23*, 1429-1439.

Lammers, K.M., Chieppa, M., Liu, L., Liu, S., Omatsu, T., Janka-Junttila, M., Casolaro, V., Reinecker, H.C., Parent, C.A., and Fasano, A. (2015). Gliadin Induces Neutrophil Migration via Engagement of the Formyl Peptide Receptor, FPR1. PLoS One *10*, e0138338.

Lammers, K.M., Lu, R., Brownley, J., Lu, B., Gerard, C., Thomas, K., Rallabhandi, P., Shea-Donohue, T., Tamiz, A., Alkan, S.*, et al.* (2008). Gliadin induces an increase in intestinal permeability and zonulin release by binding to the chemokine receptor CXCR3. Gastroenterology *135*, 194-204 e193.

Lanthier, N., Molendi-Coste, O., Horsmans, Y., van Rooijen, N., Cani, P.D., and Leclercq, I.A. (2010). Kupffer cell activation is a causal factor for hepatic insulin resistance. American Journal of Physiology-Gastrointestinal and Liver Physiology *298*, G107-G116.

Le Chatelier, E., Nielsen, T., Qin, J., Prifti, E., Hildebrand, F., Falony, G., Almeida, M., Arumugam, M., Batto, J.M., Kennedy, S.*, et al.* (2013). Richness of human gut microbiome correlates with metabolic markers. Nature *500*, 541-546.

Lee, M.W., Odegaard, J.I., Mukundan, L., Qiu, Y., Molofsky, A.B., Nussbaum, J.C., Yun, K., Locksley, R.M., and Chawla, A. (2015). Activated type 2 innate lymphoid cells regulate beige fat biogenesis. Cell *160*, 74-87.

Lee, Y., Hirose, H., Ohneda, M., Johnson, J.H., McGarry, J.D., and Unger, R.H. (1994). Beta-cell lipotoxicity in the pathogenesis of non-insulin-dependent diabetes mellitus of obese rats: impairment in adipocyte-beta-cell relationships. Proc Natl Acad Sci U S A *91*, 10878-10882.

Ley, R.E., Backhed, F., Turnbaugh, P., Lozupone, C.A., Knight, R.D., and Gordon, J.I. (2005). Obesity alters gut microbial ecology. Proc Natl Acad Sci U S A *102*, 11070-11075.

Li, Z., Soloski, M.J., and Diehl, A.M. (2005). Dietary factors alter hepatic innate immune system in mice with nonalcoholic fatty liver disease. Hepatology *42*, 880-885.

Liu, J., Divoux, A., Sun, J., Zhang, J., Clement, K., Glickman, J.N., Sukhova, G.K., Wolters, P.J., Du, J., Gorgun, C.Z.*, et al.* (2009). Genetic deficiency and pharmacological stabilization of mast cells reduce diet-induced obesity and diabetes in mice. Nature medicine *15*, 940-U144.

Lotta, L.A., Gulati, P., Day, F.R., Payne, F., Ongen, H., van de Bunt, M., Gaulton, K.J., Eicher, J.D., Sharp, S.J., Luan, J.*, et al.* (2016). Integrative genomic analysis implicates limited peripheral adipose storage capacity in the pathogenesis of human insulin resistance. Nature genetics.

Lu, Y., Fan, C., Li, P., Lu, Y., Chang, X., and Qi, K. (2016). Short Chain Fatty Acids Prevent High-fat-diet-induced Obesity in Mice by Regulating G Protein-coupled Receptors and Gut Microbiota. Scientific reports *6*, 37589.

Lumeng, C.N., Bodzin, J.L., and Saltiel, A.R. (2007a). Obesity induces a phenotypic switch in adipose tissue macrophage polarization. J Clin Invest *117*, 175-184.

Lumeng, C.N., Deyoung, S.M., Bodzin, J.L., and Saltiel, A.R. (2007b). Increased inflammatory properties of adipose tissue macrophages recruited during diet-induced obesity. Diabetes *56*, 16-23.

Lynch, L., Nowak, M., Varghese, B., Clark, J., Hogan, A.E., Toxavidis, V., Balk, S.P., O'Shea, D., O'Farrelly, C., and Exley, M.A. (2012). Adipose tissue invariant NKT cells protect against diet-induced obesity and metabolic disorder through regulatory cytokine production. Immunity *37*, 574-587.

Macia, L., Tan, J., Vieira, A.T., Leach, K., Stanley, D., Luong, S., Maruya, M., Ian McKenzie, C., Hijikata, A., Wong, C.*, et al.* (2015). Metabolite-sensing receptors GPR43 and GPR109A facilitate dietary fibre-induced gut homeostasis through regulation of the inflammasome. Nature communications *6*, 6734.

Mantell, B.S., Stefanovic-Racic, M., Yang, X., Dedousis, N., Sipula, I.J., and O'Doherty, R.M. (2011). Mice lacking NKT cells but with a complete complement of CD8+ T-cells are not protected against the metabolic abnormalities of diet-induced obesity. PLoS One *6*, e19831.

Martinez-Fernandez, L., Laiglesia, L.M., Huerta, A.E., Martinez, J.A., and Moreno-Aliaga, M.J. (2015). Omega-3 fatty acids and adipose tissue function in obesity and metabolic syndrome. Prostaglandins & other lipid mediators *121*, 24-41.

Mathis, D. (2013). Immunological goings-on in visceral adipose tissue. Cell Metab *17*, 851-859.

McNelis, J.C., Lee, Y.S., Mayoral, R., van der Kant, R., Johnson, A.M., Wollam, J., and Olefsky, J.M. (2015). GPR43 Potentiates beta-Cell Function in Obesity. Diabetes *64*, 3203-3217.

Mehta, P., Nuotio-Antar, A.M., and Smith, C.W. (2015). gammadelta T cells promote inflammation and insulin resistance during high fat diet-induced obesity in mice. J Leukoc Biol *97*, 121-134.

Meli, R., Mattace Raso, G., and Calignano, A. (2014). Role of innate immune response in non-alcoholic Fatty liver disease: metabolic complications and therapeutic tools. Frontiers in immunology *5*, 177.

Miele, L., Valenza, V., La Torre, G., Montalto, M., Cammarota, G., Ricci, R., Masciana, R., Forgione, A., Gabrieli, M.L., Perotti, G.*, et al.* (2009). Increased intestinal permeability and tight junction alterations in nonalcoholic fatty liver disease. Hepatology *49*, 1877-1887.

Mildner, A., and Jung, S. (2014). Development and function of dendritic cell subsets. Immunity *40*, 642-656.

Moller, D.E., and Kaufman, K.D. (2005). Metabolic syndrome: a clinical and molecular perspective. Annual review of medicine *56*, 45-62.

Molofsky, A.B., Nussbaum, J.C., Liang, H.E., Van Dyken, S.J., Cheng, L.E., Mohapatra, A., Chawla, A., and Locksley, R.M. (2013). Innate lymphoid type 2 cells sustain visceral adipose tissue eosinophils and alternatively activated macrophages. The Journal of experimental medicine *210*, 535-549.

Morris, D.L., Cho, K.W., Delproposto, J.L., Oatmen, K.E., Geletka, L.M., Martinez-Santibanez, G., Singer, K., and Lumeng, C.N. (2013). Adipose tissue macrophages function as antigen-presenting cells and regulate adipose tissue CD4+ T cells in mice. Diabetes *62*, 2762-2772.

Muller, V.M., Zietek, T., Rohm, F., Fiamoncini, J., Lagkouvardos, I., Haller, D., Clavel, T., and Daniel, H. (2016). Gut barrier impairment by high-fat diet in mice depends on housing conditions. Molecular nutrition & food research *60*, 897-908.

Murphy, A.J., Kraakman, M.J., Kammoun, H.L., Dragoljevic, D., Lee, M.K., Lawlor, K.E., Wentworth, J.M., Vasanthakumar, A., Gerlic, M., Whitehead, L.W.*, et al.* (2016). IL-18 Production from the NLRP1 Inflammasome Prevents Obesity and Metabolic Syndrome. Cell Metab *23*, 155-164.

Murray, C.J., Atkinson, C., Bhalla, K., Birbeck, G., Burstein, R., Chou, D., Dellavalle, R., Danaei, G., Ezzati, M., Fahimi, A.*, et al.* (2013). The state of US health, 1990-2010: burden of diseases, injuries, and risk factors. JAMA : the journal of the American Medical Association *310*, 591-608.

Naughton, S.S., Mathai, M.L., Hryciw, D.H., and McAinch, A.J. (2016). Linoleic acid and the pathogenesis of obesity. Prostaglandins & other lipid mediators *125*, 90-99.

Neis, E.P., Dejong, C.H., and Rensen, S.S. (2015). The role of microbial amino acid metabolism in host metabolism. Nutrients *7*, 2930-2946.

Newgard, C.B., An, J., Bain, J.R., Muehlbauer, M.J., Stevens, R.D., Lien, L.F., Haqq, A.M., Shah, S.H., Arlotto, M., Slentz, C.A*., et al.* (2009). A branched-chain amino acid-related metabolic signature that differentiates obese and lean humans and contributes to insulin resistance. Cell Metab *9*, 311-326.

Neyrinck, A.M., Cani, P.D., Dewulf, E.M., De Backer, F., Bindels, L.B., and Delzenne, N.M. (2009). Critical role of Kupffer cells in the management of diet-induced diabetes and obesity. Biochemical and biophysical research communications *385*, 351-356.

Nishimura, S., Manabe, I., Nagasaki, M., Eto, K., Yamashita, H., Ohsugi, M., Otsu, M., Hara, K., Ueki, K., Sugiura, S*., et al.* (2009). CD8+ effector T cells contribute to macrophage recruitment and adipose tissue inflammation in obesity. Nature medicine *15*, 914-920.

Obstfeld, A.E., Sugaru, E., Thearle, M., Francisco, A.M., Gayet, C., Ginsberg, H.N., Ables, E.V., and Ferrante, A.W., Jr. (2010). C-C chemokine receptor 2 (CCR2) regulates the hepatic recruitment of myeloid cells that promote obesity-induced hepatic steatosis. Diabetes *59*, 916-925.

Odegaard, J.I., and Chawla, A. (2013a). The immune system as a sensor of the metabolic state. Immunity *38*, 644-654.

Odegaard, J.I., and Chawla, A. (2013b). Pleiotropic actions of insulin resistance and inflammation in metabolic homeostasis. Science *339*, 172-177.

Odegaard, J.I., Ricardo-Gonzalez, R.R., Red Eagle, A., Vats, D., Morel, C.R., Goforth, M.H., Subramanian, V., Mukundan, L., Ferrante, A.W., and Chawla, A. (2008). Alternative M2 activation of Kupffer cells by PPARdelta ameliorates obesity-induced insulin resistance. Cell Metab *7*, 496-507.

Oh, D.Y., Talukdar, S., Bae, E.J., Imamura, T., Morinaga, H., Fan, W., Li, P., Lu, W.J., Watkins, S.M., and Olefsky, J.M. (2010). GPR120 is an omega-3 fatty acid receptor mediating potent anti-inflammatory and insulin-sensitizing effects. Cell *142*, 687-698.

Ohmura, K., Ishimori, N., Ohmura, Y., Tokuhara, S., Nozawa, A., Horii, S., Andoh, Y., Fujii, S., Iwabuchi, K., Onoe, K*., et al.* (2010). Natural killer T cells are involved in adipose tissues inflammation and glucose intolerance in diet-induced obese mice. Arterioscler Thromb Vasc Biol *30*, 193-199.

Park, B.S., and Lee, J.O. (2013). Recognition of lipopolysaccharide pattern by TLR4 complexes. Experimental & molecular medicine *45*, e66.

Park, B.S., Song, D.H., Kim, H.M., Choi, B.S., Lee, H., and Lee, J.O. (2009). The structural basis of lipopolysaccharide recognition by the TLR4-MD-2 complex. Nature *458*, 1191-1195.

Patsouris, D., Li, P.-P., Thapar, D., Chapman, J., Olefsky, J.M., and Neels, J.G. (2008). Ablation of CD11c-Positive Cells Normalizes Insulin Sensitivity in Obese Insulin Resistant Animals. Cell Metabolism *8*, 301-309.

Peng, L., Li, Z.R., Green, R.S., Holzman, I.R., and Lin, J. (2009). Butyrate enhances the intestinal barrier by facilitating tight junction assembly via activation of AMP-activated protein kinase in Caco-2 cell monolayers. The Journal of nutrition *139*, 1619-1625.

Perry, R.J., Samuel, V.T., Petersen, K.F., and Shulman, G.I. (2014). The role of hepatic lipids in hepatic insulin resistance and type 2 diabetes. Nature *510*, 84-91.

Petersson, J., Schreiber, O., Hansson, G.C., Gendler, S.J., Velcich, A., Lundberg, J.O., Roos, S., Holm, L., and Phillipson, M. (2011). Importance and regulation of the colonic mucus barrier in a mouse model of colitis. American journal of physiology Gastrointestinal and liver physiology *300*, G327-333.

Popkin, B.M. (2006). Global nutrition dynamics: the world is shifting rapidly toward a diet linked with noncommunicable diseases. Am J Clin Nutr *84*, 289-298.

Popkin, B.M., Adair, L.S., and Ng, S.W. (2012). Global nutrition transition and the pandemic of obesity in developing countries. Nutrition reviews *70*, 3-21.

Priyadarshini, M., Villa, S.R., Fuller, M., Wicksteed, B., Mackay, C.R., Alquier, T., Poitout, V., Mancebo, H., Mirmira, R.G., Gilchrist, A.*, et al.* (2015). An Acetate-Specific GPCR, FFAR2, Regulates Insulin Secretion. Mol Endocrinol *29*, 1055-1066.

Rahat-Rozenbloom, S., Fernandes, J., Gloor, G.B., and Wolever, T.M. (2014). Evidence for greater production of colonic short-chain fatty acids in overweight than lean humans. International journal of obesity *38*, 1525-1531.

Ridlon, J.M., Kang, D.J., Hylemon, P.B., and Bajaj, J.S. (2014). Bile acids and the gut microbiome. Current opinion in gastroenterology *30*, 332-338.

Rios-Covian, D., Ruas-Madiedo, P., Margolles, A., Gueimonde, M., de Los Reyes-Gavilan, C.G., and Salazar, N. (2016). Intestinal Short Chain Fatty Acids and their Link with Diet and Human Health. Frontiers in microbiology *7*, 185.

Rivera, C.A., Adegboyega, P., van Rooijen, N., Tagalicud, A., Allman, M., and Wallace, M. (2007). Toll-like receptor-4 signaling and Kupffer cells play pivotal roles in the pathogenesis of non-alcoholic steatohepatitis. J Hepatol *47*, 571-579.

Sahuri-Arisoylu, M., Brody, L.P., Parkinson, J.R., Parkes, H., Navaratnam, N., Miller, A.D., Thomas, E.L., Frost, G., and Bell, J.D. (2016). Reprogramming of hepatic fat accumulation and 'browning' of adipose tissue by the short-chain fatty acid acetate. International journal of obesity *40*, 955-963.

Saltiel, A.R., and Kahn, C.R. (2001). Insulin signalling and the regulation of glucose and lipid metabolism. Nature *414*, 799-806.

Samuel, B.S., Shaito, A., Motoike, T., Rey, F.E., Backhed, F., Manchester, J.K., Hammer, R.E., Williams, S.C., Crowley, J., Yanagisawa, M.*, et al.* (2008). Effects of the gut microbiota on host adiposity are modulated by the short-chain fatty-acid binding G protein-coupled receptor, Gpr41. Proc Natl Acad Sci U S A *105*, 16767-16772.

Samuel, V.T., and Shulman, G.I. (2012). Mechanisms for insulin resistance: common threads and missing links. Cell *148*, 852-871.

Sander, G.R., Cummins, A.G., Henshall, T., and Powell, B.C. (2005). Rapid disruption of intestinal barrier function by gliadin involves altered expression of apical junctional proteins. FEBS letters *579*, 4851-4855.

Sapone, A., Bai, J.C., Ciacci, C., Dolinsek, J., Green, P.H., Hadjivassiliou, M., Kaukinen, K., Rostami, K., Sanders, D.S., Schumann, M.*, et al.* (2012). Spectrum of gluten-related disorders: consensus on new nomenclature and classification. BMC medicine *10*, 13.

Satoh, M., Andoh, Y., Clingan, C.S., Ogura, H., Fujii, S., Eshima, K., Nakayama, T., Taniguchi, M., Hirata, N., Ishimori, N.*, et al.* (2012). Type II NKT cells stimulate diet-induced obesity by mediating adipose tissue inflammation, steatohepatitis and insulin resistance. PLoS One *7*, e30568.

Satpathy, A.T., Wu, X., Albring, J.C., and Murphy, K.M. (2012). Re(de)fining the dendritic cell lineage. Nat Immunol *13*, 1145-1154.

Schipper, H.S., Prakken, B., Kalkhoven, E., and Boes, M. (2012). Adipose tissue-resident immune cells: key players in immunometabolism. Trends in endocrinology and metabolism: TEM *23*, 407-415.

Serhan, C.N. (2014). Pro-resolving lipid mediators are leads for resolution physiology. Nature *510*, 92-101.

Serviddio, G., Sastre, J., Bellanti, F., Vina, J., Vendemiale, G., and Altomare, E. (2008). Mitochondrial involvement in non-alcoholic steatohepatitis. Molecular aspects of medicine *29*, 22-35.

Shaul, M.E., Bennett, G., Strissel, K.J., Greenberg, A.S., and Obin, M.S. (2010). Dynamic, M2-like remodeling phenotypes of CD11c+ adipose tissue macrophages during high-fat diet--induced obesity in mice. Diabetes *59*, 1171-1181.

Shaw, J.E., Sicree, R.A., and Zimmet, P.Z. (2010). Global estimates of the prevalence of diabetes for 2010 and 2030. Diabetes research and clinical practice *87*, 4-14.

Simopoulos, A.P. (2002). The importance of the ratio of omega-6/omega-3 essential fatty acids. Biomedicine & pharmacotherapy = Biomedecine & pharmacotherapie *56*, 365-379.

Soares, F.L., de Oliveira Matoso, R., Teixeira, L.G., Menezes, Z., Pereira, S.S., Alves, A.C., Batista, N.V., de Faria, A.M., Cara, D.C., Ferreira, A.V.*, et al.* (2013). Gluten-free diet reduces adiposity, inflammation and insulin resistance associated with the induction of PPAR-alpha and PPAR-gamma expression. The Journal of nutritional biochemistry *24*, 1105-1111.

Soeters, M.R., and Soeters, P.B. (2012). The evolutionary benefit of insulin resistance. Clinical nutrition *31*, 1002-1007.

Sonnenburg, J.L., and Backhed, F. (2016). Diet-microbiota interactions as moderators of human metabolism. Nature *535*, 56-64.

Spruss, A., Kanuri, G., Wagnerberger, S., Haub, S., Bischoff, S.C., and Bergheim, I. (2009). Toll-like receptor 4 is involved in the development of fructose-induced hepatic steatosis in mice. Hepatology *50*, 1094-1104.

St-Onge, M.P., Janssen, I., and Heymsfield, S.B. (2004). Metabolic syndrome in normal-weight Americans: new definition of the metabolically obese, normal-weight individual. Diabetes care *27*, 2222-2228.

Stanton, M.C., Chen, S.C., Jackson, J.V., Rojas-Triana, A., Kinsley, D., Cui, L., Fine, J.S., Greenfeder, S., Bober, L.A., and Jenh, C.H. (2011). Inflammatory Signals shift from adipose to liver during high fat feeding and influence the development of steatohepatitis in mice. Journal of inflammation *8*, 8.

Stefan, N., Kantartzis, K., Machann, J., Schick, F., Thamer, C., Rittig, K., Balletshofer, B., Machicao, F., Fritsche, A., and Haring, H.U. (2008). Identification and characterization of metabolically benign obesity in humans. Archives of internal medicine *168*, 1609-1616.

Stefanovic-Racic, M., Yang, X., Turner, M.S., Mantell, B.S., Stolz, D.B., Sumpter, T.L., Sipula, I.J., Dedousis, N., Scott, D.K., Morel, P.A.*, et al.* (2012). Dendritic cells promote macrophage infiltration and comprise a substantial proportion of obesity-associated increases in CD11c+ cells in adipose tissue and liver. Diabetes *61*, 2330-2339.

Stienstra, R., van Diepen, J.A., Tack, C.J., Zaki, M.H., van de Veerdonk, F.L., Perera, D., Neale, G.A., Hooiveld, G.J., Hijmans, A., Vroegrijk, I.*, et al.* (2011). Inflammasome is a central player in the induction of obesity and insulin resistance. Proc Natl Acad Sci U S A *108*, 15324-15329.

Strissel, K.J., DeFuria, J., Shaul, M.E., Bennett, G., Greenberg, A.S., and Obin, M.S. (2010). T-cell recruitment and Th1 polarization in adipose tissue during diet-induced obesity in C57BL/6 mice. Obesity (Silver Spring) *18*, 1918-1925.

Sunderkötter, C., Nikolic, T., Dillon, M.J., van Rooijen, N., Stehling, M., Drevets, D.A., and Leenen, P.J.M. (2004). Subpopulations of Mouse Blood Monocytes Differ in Maturation Stage and Inflammatory Response. The Journal of Immunology *172*, 4410-4417.

Swann, J.R., Want, E.J., Geier, F.M., Spagou, K., Wilson, I.D., Sidaway, J.E., Nicholson, J.K., and Holmes, E. (2011). Systemic gut microbial modulation of bile acid metabolism in host tissue compartments. Proc Natl Acad Sci U S A *108 Suppl 1*, 4523-4530.

Takahashi, K., Mizuarai, S., Araki, H., Mashiko, S., Ishihara, A., Kanatani, A., Itadani, H., and Kotani, H. (2003). Adiposity elevates plasma MCP-1 levels leading to the increased CD11b-positive monocytes in mice. J Biol Chem *278*, 46654-46660.

Talukdar, S., Oh da, Y., Bandyopadhyay, G., Li, D., Xu, J., McNelis, J., Lu, M., Li, P., Yan, Q., Zhu, Y.*, et al.* (2012). Neutrophils mediate insulin resistance in mice fed a high-fat diet through secreted elastase. Nature medicine *18*, 1407-1412.

Taoka, H., Yokoyama, Y., Morimoto, K., Kitamura, N., Tanigaki, T., Takashina, Y., Tsubota, K., and Watanabe, M. (2016). Role of bile acids in the regulation of the metabolic pathways. World journal of diabetes *7*, 260-270.

Teghanemt, A., Zhang, D., Levis, E.N., Weiss, J.P., and Gioannini, T.L. (2005). Molecular basis of reduced potency of underacylated endotoxins. Journal of immunology *175*, 4669-4676.

Teng, K.T., Chang, C.Y., Chang, L.F., and Nesaretnam, K. (2014). Modulation of obesity-induced inflammation by dietary fats: mechanisms and clinical evidence. Nutrition journal *13*, 12.

Thaiss, C.A., Zmora, N., Levy, M., and Elinav, E. (2016). The microbiome and innate immunity. Nature *535*, 65-74.

Thomas, C., Gioiello, A., Noriega, L., Strehle, A., Oury, J., Rizzo, G., Macchiarulo, A., Yamamoto, H., Mataki, C., Pruzanski, M.*, et al.* (2009). TGR5-mediated bile acid sensing controls glucose homeostasis. Cell Metab *10*, 167-177.

Tilg, H., and Moschen, A.R. (2010). Evolution of inflammation in nonalcoholic fatty liver disease: the multiple parallel hits hypothesis. Hepatology *52*, 1836-1846.

Turnbaugh, P.J., Hamady, M., Yatsunenko, T., Cantarel, B.L., Duncan, A., Ley, R.E., Sogin, M.L., Jones, W.J., Roe, B.A., Affourtit, J.P.*, et al.* (2009). A core gut microbiome in obese and lean twins. Nature *457*, 480-484.

Turnbaugh, P.J., Ley, R.E., Mahowald, M.A., Magrini, V., Mardis, E.R., and Gordon, J.I. (2006). An obesity-associated gut microbiome with increased capacity for energy harvest. Nature *444*, 1027-1031.

Vandanmagsar, B., Youm, Y.H., Ravussin, A., Galgani, J.E., Stadler, K., Mynatt, R.L., Ravussin, E., Stephens, J.M., and Dixit, V.D. (2011). The NLRP3 inflammasome instigates obesity-induced inflammation and insulin resistance. Nature medicine *17*, 179-188.

Vavassori, P., Mencarelli, A., Renga, B., Distrutti, E., and Fiorucci, S. (2009). The bile acid receptor FXR is a modulator of intestinal innate immunity. Journal of immunology *183*, 6251-6261.

Velagapudi, V.R., Hezaveh, R., Reigstad, C.S., Gopalacharyulu, P., Yetukuri, L., Islam, S., Felin, J., Perkins, R., Boren, J., Oresic, M.*, et al.* (2010). The gut microbiota modulates host energy and lipid metabolism in mice. Journal of lipid research *51*, 1101-1112.

Vijay-Kumar, M., Aitken, J.D., Carvalho, F.A., Cullender, T.C., Mwangi, S., Srinivasan, S., Sitaraman, S.V., Knight, R., Ley, R.E., and Gewirtz, A.T. (2010). Metabolic syndrome and altered gut microbiota in mice lacking Toll-like receptor 5. Science *328*, 228-231.

Virtue, S., and Vidal-Puig, A. (2010). Adipose tissue expandability, lipotoxicity and the Metabolic Syndrome--an allostatic perspective. Biochim Biophys Acta *1801*, 338-349.

Vrieze, A., Holleman, F., Zoetendal, E.G., de Vos, W.M., Hoekstra, J.B., and Nieuwdorp, M. (2010). The environment within: how gut microbiota may influence metabolism and body composition. Diabetologia *53*, 606-613.

Wang, Q., Xie, Z., Zhang, W., Zhou, J., Wu, Y., Zhang, M., Zhu, H., and Zou, M.H. (2014a). Myeloperoxidase deletion prevents high-fat diet-induced obesity and insulin resistance. Diabetes *63*, 4172-4185.

Wang, X., Ota, N., Manzanillo, P., Kates, L., Zavala-Solorio, J., Eidenschenk, C., Zhang, J., Lesch, J., Lee, W.P., Ross, J.*, et al.* (2014b). Interleukin-22 alleviates metabolic disorders and restores mucosal immunity in diabetes. Nature *514*, 237-241.

Watanabe, M., Houten, S.M., Wang, L., Moschetta, A., Mangelsdorf, D.J., Heyman, R.A., Moore, D.D., and Auwerx, J. (2004). Bile acids lower triglyceride levels via a pathway involving FXR, SHP, and SREBP-1c. J Clin Invest *113*, 1408-1418.

Weisberg, S., Hunter, D., Huber, R., Lemieux, J., Slaymaker, S., Vaddi, K., Charo, I., Leibel, R., and Ferrante, A. (2006). CCR2 modulates inflammatory and metabolic effects of high-fat feeding. J Clin Invest *116*, 115 - 124.

Weisberg, S.P., McCann, D., Desai, M., Rosenbaum, M., Leibel, R.L., and Ferrante, A.W., Jr. (2003). Obesity is associated with macrophage accumulation in adipose tissue. J Clin Invest *112*, 1796-1808.

Wernersson, S., and Pejler, G. (2014). Mast cell secretory granules: armed for battle. Nat Rev Immunol *14*, 478-494.

Winer, D.A., Winer, S., Shen, L., Wadia, P.P., Yantha, J., Paltser, G., Tsui, H., Wu, P., Davidson, M.G., Alonso, M.N.*, et al.* (2011). B cells promote insulin resistance through modulation of T cells and production of pathogenic IgG antibodies. Nature medicine *17*, 610-617.

Winer, S., Chan, Y., Paltser, G., Truong, D., Tsui, H., Bahrami, J., Dorfman, R., Wang, Y., Zielenski, J., Mastronardi, F*., et al.* (2009). Normalization of obesity-associated insulin resistance through immunotherapy. Nature medicine *15*, 921-929.

Wu, D., Molofsky, A.B., Liang, H.E., Ricardo-Gonzalez, R.R., Jouihan, H.A., Bando, J.K., Chawla, A., and Locksley, R.M. (2011a). Eosinophils Sustain Adipose Alternatively Activated Macrophages Associated with Glucose Homeostasis. Science *332*, 243-247.

Wu, G.D., Chen, J., Hoffmann, C., Bittinger, K., Chen, Y.Y., Keilbaugh, S.A., Bewtra, M., Knights, D., Walters, W.A., Knight, R*., et al.* (2011b). Linking long-term dietary patterns with gut microbial enterotypes. Science *334*, 105-108.

Xu, H., Barnes, G.T., Yang, Q., Tan, G., Yang, D., Chou, C.J., Sole, J., Nichols, A., Ross, J.S., Tartaglia, L.A*., et al.* (2003). Chronic inflammation in fat plays a crucial role in the development of obesity-related insulin resistance. J Clin Invest *112*, 1821-1830.

Xu, X., Grijalva, A., Skowronski, A., van Eijk, M., Serlie, M.J., and Ferrante, A.W., Jr. (2013). Obesity activates a program of lysosomal-dependent lipid metabolism in adipose tissue macrophages independently of classic activation. Cell Metab *18*, 816-830.

Xue, J., Schmidt, S.V., Sander, J., Draffehn, A., Krebs, W., Quester, I., De Nardo, D., Gohel, T.D., Emde, M., Schmidleithner, L*., et al.* (2014). Transcriptome-based network analysis reveals a spectrum model of human macrophage activation. Immunity *40*, 274-288.

Yamashita, H., Fujisawa, K., Ito, E., Idei, S., Kawaguchi, N., Kimoto, M., Hiemori, M., and Tsuji, H. (2007). Improvement of obesity and glucose tolerance by acetate in Type 2 diabetic Otsuka Long-Evans Tokushima Fatty (OLETF) rats. Bioscience, biotechnology, and biochemistry *71*, 1236-1243.

Zaibi, M.S., Stocker, C.J., O'Dowd, J., Davies, A., Bellahcene, M., Cawthorne, M.A., Brown, A.J., Smith, D.M., and Arch, J.R. (2010). Roles of GPR41 and GPR43 in leptin secretory responses of murine adipocytes to short chain fatty acids. FEBS letters *584*, 2381-2386.

Zajonc, D.M., and Girardi, E. (2014). A gammadelta T-cell glimpse of glycolipids. Immunology and cell biology *92*, 99-100.

Zuniga, L.A., Shen, W.J., Joyce-Shaikh, B., Pyatnova, E.A., Richards, A.G., Thom, C., Andrade, S.M., Cua, D.J., Kraemer, F.B., and Butcher, E.C. (2010). IL-17 regulates adipogenesis, glucose homeostasis, and obesity. Journal of immunology *185*, 6947-6959.